Republic of Iraq
Ministry of Higher Education
and Scientific Research
University of Babylon
College of Engineering
Civil Engineering Department

Soil Structure Interaction of Mechanically Stabilized Earth Wall for Bridge Abutments

A Thesis

Submitted to the College of Engineering at the University of Babylon in Partial Fulfilment of the Requirements for the Degree of Doctor of Philosophy in Engineering/ Civil Engineering/Structures

By

Mayadah Waheed Falah Kuthaib

Supervised by

Prof. Dr. Haitham H. Muteb

2023 A.D **1445 A.H**

بِسْمِ اللَّهِ الرَّحْمَنِ الرَّحِيمِ ﴿١﴾

الْحَمْدُ لِلَّهِ رَبِّ الْعَالَمِينَ ﴿٢﴾ الرَّحْمَنِ الرَّحِيمِ ﴿٣﴾ مَالِكِ يَوْمِ الدِّينِ ﴿٤﴾ إِيَّاكَ نَعْبُدُ وَإِيَّاكَ نَسْتَعِينُ ﴿٥﴾ اهْدِنَا الصِّرَاطَ الْمُسْتَقِيمَ ﴿٦﴾ صِرَاطَ الَّذِينَ أَنْعَمْتَ عَلَيْهِمْ غَيْرِ الْمَغْضُوبِ عَلَيْهِمْ وَلَا الضَّالِّينَ ﴿٧﴾

صدق الله العليُ العظيم

سورة الفاتحة

Supervisor's Certification

I certify that this dissertation **" Soil Structure Interaction of Mechanically Stabilized Earth Wall for Bridge Abutments" ,** submitted by the student **" Mayadah Waheed Falah"** was prepared under my supervision at the Department of Civil Engineering/ College of Engineering/ University of Babylon as a part of requirements for the degree of Doctor of Philosophy in Engineering/ Civil Engineering / Structures.

Signature:

Supervisor: ***Prof. Dr. Haitham H. Muteb***

Date: / / 2023

I certify that this dissertation mentioned above has been completed in Civil Engineering in the College of Engineering / University of Babylon.

Signature:

Head of Department: **Asst.Prof. Dr.** ***Zaid H. Majeed Al-Hasoon***

Date: / / 2023

Examining Committee Certificate

We certify that we have read this thesis entitled " **Soil Structure Interaction of Mechanically Stabilized Earth Wall for Bridge Abutments** " and, as an examining cee, examined that student "**Mayadah Waheed Falah**" in its content and that, in our opinion, it meets the standard of a thesis for the degree of Doctor of Philosophy in Engineering/ Civil Engineering / Structures.

Signature:
Name: **Prof. Dr. Ammar Yasir Ali**
(Chairman)
Date: / / 2023

Signature:
Name: **Prof.Dr. Nabeel Hassan Ali**
(Member)
Date: / / 2023

Signature:
Name: **Asst.Prof.Dr.Hussein Talab Nhabih Al-wetaefi**
(Member)
Date: / / 2023

Signature:
Name: **Prof.Dr.Thaar S. Al-Gasham**
(Member)
Date: / / 2023

Signature:
Name: **Asst. Prof. Dr. Muhammad Jawad**
(Member)
Date: / / 2023

Signature:
Name: **Prof. Dr. Haitham H. Muteb**
(Member and supervisor)
Date: / / 2023

Approval of Head of Civil Engineering Department

Signature:
Name: **Asst.Prof. Dr.** ***Zaid H. Majeed Al-Hasoon***
(Head of Civil Engineering Department)
Date: / / 2023

Approve of the Dean of the College of Engineering

Signature:
Name: **Prof. Dr. Laith Ali Abdul-Rahaim**
(Dean of the College of Engineering)
Date: / / 2023

Acknowledgments

“In the Name of Allah, the Most Gracious, the Most Merciful”

First, thank **Allah**, who gave me the willingness and strength to complete this research.

I would like to express sincere appreciation and deepest gratitude to my supervisor **Prof. Dr Haitham H. Muteb**, for his advice, guidance, and encouragement throughout this work.

Special thanks and gratitude are due to **my lovely mother** for her care, patience, and encouragement throughout the research period. I also wish to thank **my brothers** and **my sisters** for their encouragement and assistance.

Thanks to the staff of Building and Construction Techniques Engineering Department /College of the Engineering /Al-Mustaqbal University for their appreciable support.

I would like to thank my friends for supporting me spiritually and practically and helping me throughout preparing the experimental work. Special thanks go to Eng. Emad (Manager of AL-Danube Company), Zainab S. Al-Khafaji, Abdul Al-Reda Shaker Majdi, Wisam Nadir and Mustafa Salah to whom I am so grateful.

Thanks to the College of Engineering and the Civil Engineering Department staff at the University of Babylon for their appreciable support.

Finally, thanks to all who participated in providing help and assistance to complete this work.

Mayadah Waheed Falah

/ / 2023

Dedication

Great thank to Almighty Allah for His blessings and all the achievements in my life. I am grateful to my family for their support and patience throughout my studies and provided me with motivation and financial support. Without them, none of this achievement would be possible.

To:

My father's soul

My lovely mother

My supervisor Prof. Dr Haitham H. Muteb

My brothers and my sisters.

Every person supported me during my entire life.

Mayadah Waheed Falah

/ / 2023

ABSTRACT

Recently, civil engineering projects have increasingly used **M**echanically **S**tabilized **E**arth (MSE) retaining walls as an effective alternative to reinforced concrete ones. The reinforced soil structure's internal stability depends on mechanical interactions between the fill material, reinforcement, and facing.

Accordingly, the current research aims to study the behavior of MSE wall under static load. The working methodology of the study consists of three parts: the first one focus on the field study to measure the lateral pressure distribution of the MSE used as the retaining walls of AL-Um intersection in Hillah-Iraq.

For Al-Um intersection bridge the working methodology consists of two parts first one during construction and the second one during operation. The number of sensors is 4, the distance between one sensor and the second is 50 cm. They were installed during construction, but the readings were taken in two stages, the first stage during the construction of the bridge, and readings were taken under the influence of static load, and then readings were taken during the operation period of the bridge under the influence of car traffic. The results showed that the pressure effect laterally on MSE wall decreased with the wall depth increase.

The second part is to simulate the MSE wall simplified model approximately. The model enables the investigation of many parameters; Zigzag shape and Straight shape, for that Two specimens are built and tested approximately. The experimental findings show that using of zigzag strips reinforcement give better resistance for both lateral and vertical pressure than straight strips reinforcement. And the zigzag shape gives better results than straight shape by 19% in lateral pressure. While the zigzag shape gives better results than straight shape by 60% in vertical pressure.

Also, using of zigzag strips reinforcement give lower displacement in MSE wall than straight strips. In addition to that using both kinds of soil strips reinforcement led to decrease later displacement with depth. And the straight shape gives better results than zigzag shape by 50% in reducing the displacement.

The Third part is a finite element model using ABAQUS Standard/Explicit 2019 software to investigate the nonlinear behavior of MSE wall. FEM findings indicated good compatibility with the experimental findings. The program's ability to extend the study gives more results in understanding the actual behavior of MSE wall. In this thesis, a parametric analysis is performed to investigate a wide range of the main variables (Width of strip and location of applied load). To sum up, the parametric investigation showed that the used strip with width **W** decreased the displacement effect laterally, and the place of load affected the behavior on the MSE. The relationship between the place of the applied load and the displacement effect laterally, lateral pressure, stresses in strips is negative one when the load is near to the wall the displacement effect laterally, lateral pressure and stresses in strips increase.

Contents

List of Figures

List of Tables

Notation

The following are the major symbols used in this dissertation:

Symbol	Description	Units
A	Area	mm^2
cm	centimeter	----
f_{cu}	Concrete cube compressive strength.	MPa
f'_c	Concrete cylinder compressive strength	MPa
φ	Diameter of the reinforced bar	mm
H	Hight of MSE wall	m
S_h	Horizontal Spacing	m, cm,mm
M	Mass	Kg
m	meter	----
mm	millimeter	----
E_c	Modulus of elasticity of concrete	MPa
E_s	Modulus of elasticity of steel	GPa
f_r	Modulus of rupture, MPa	MPa
υ	Poisson ratio	----
f_t	Splitting tensile strength, MPa	MPa
Ko	The at-rest earth pressure coefficient	----
Kr	The coefficient for lateral earth pressure	----
Fu	Ultimate strength	MPa
Vs	velocity	m/Sec
S_v	Vertical Spacing	m, cm,mm
W1	Weight	Kg
W	width	mm
fy	Yielding stress	MPa

Abbreviation

Abbreviation	Description
AASHTO	**A**merican **A**ssociation of **S**tate **H**ighway and **T**ransportation **O**fficials
ASD	**A**llowable **S**tress **D**esign
ASTM	**A**merican **S**ociety for **T**esting and **M**aterials
CDOT	The **C**olorado **D**epartment **O**f **T**ransportation
DOTs	**S**tate **D**epartments of **T**ransportation
Exp.	**E**xperimental
FEM	**F**inite **E**lement **M**ethod
FEN	**F**inite **E**lement **A**nalysis
FHWA	**F**ederal **H**igh**W**ay **A**dministration
FLAC	**F**ast **L**agrangian **A**nalysis of **C**ontinua
FSR	**F**orce-**S**ensitive **R**esistors
GRWs	**G**ravity **R**etaining **W**alls
IABs	**I**ntegral **A**butment **B**ridges
IQS	**I**raqi **S**pecification
ITD	The **I**daho **T**ransportation **D**epartment
kg	**k**ilo**g**ram
L.L.	The **L**iquid **L**imit
LA	**L**imit **A**nalysis
LRFD	**L**oad **R**esisting **F**actor **D**esign
LVDT	**L**inear **V**ariable **D**ifferential **T**ransducer
m	**m**eter
Max.	**M**aximum
MDD	**M**ax. **D**ry **D**ensity
Min.	**M**inimum
MLR	**M**ultiple **L**inear **R**egression analysis
MPa	**M**ega **P**ascal (MN/m2)
MSE	**M**echanically **S**tabilized **E**arth

Abbreviation	Description
No.	**N**umber
NPP	**N**uclear **P**ower **P**lants
Num.	**N**umerical
OMC	**O**ptimum **M**oisture **C**ontent
OPC	**O**rdinary **P**ortland **C**ement
P.I.	**P**lasticity **I**ndex
P.L.	**P**lastic **L**imit
RBD	**R**eliability-**B**ased **D**esign
Rc	The **C**overage **R**atio
RI	**R**esistivity **I**maging
SC	**C**layey **S**and
SERA	**S**eismology and **E**arthquake Engineering **R**esearch Infrastructure **A**lliance for Europe
SSI	**S**oil-**S**tructure **I**nteraction
TDMS	**T**echnical **D**ata **M**anagement **S**treaming
$\mathbf{T_{max}}$	The max allowable reinforcing tension
UPRR	The **U**nion **P**acific **R**ailroad
USCS	**U**nified **S**oil **C**lassification **S**ystem

CHAPTER ONE

INTRODUCTION

CHAPTER ONE

INTRODUCTION

1.1. Introduction

Most civil engineering constructions have a structural component that is in direct contact with the ground. The structural and ground displacements are not independent of one another once external forces, like earthquakes, impinge on these systems. **S**oil-**S**tructure **I**nteraction (**SSI**) refers to the phenomenon whereby the displacement of a structure is influenced by the reaction of the underlying soil, and conversely, the response of the soil is influenced by the motion of the structure **(Naji et al., 2020).**

A composite solid construction called a **M**echanically **S**tabilized **E**arth (**MSE**) wall is made up of facing components, soil mass, and reinforcement. Since their development in the 1960s, several of the older strengthening techniques have been employed primarily as abutments, seawalls, berms, and bridge retaining walls. The concept of reinforced earth structures was introduced by Henri Vidal (1969) in France, and in 1971 it was brought to the U.S (Toufigh, 2012).

Structural and geotechnical engineering are used to create mechanically stabilized ground. A variety of partial load parameter that have been applied to loads in design blends and material parameter that are applied to the structural parts have been defined as a result of the development of limit state design in structural engineering (Scholzen et al., 2015).

In a conventional MSE Wall (MSEW), horizontal layers of geosynthetic materials or steel strips support compacted granular soil. The system's strength

is greatly increased by the usage of reinforced parts (Palmeira et al., 2008). Facing elements seem to be relatively thin parts that are often built of shotcrete, welded wire mesh panels, or pre-cast concrete (Kulczykowski et al., 2017). Holding the soil in place between the strengthening layers is their structural goal. A facing system makes it possible to build an MSE wall that is steep or even vertical. In addition, soil is positioned without reinforcement between the ground's natural surface and the stabilized region called retained backfill (Muteb & Falah, 2021).

A full MSE wall is a construction that relies on gravity. The applied forces, such as seismic loads, water pressures, lateral earth pressures, or loads resulting from human activities, are supported by the object's mass (D. G. Anderson, 2008).

Compared to concrete barriers, MSEW are affordable constructions that can sustain greater total and differential settlements. They can also be built more easily and faster since they don't need curing time or support structures like scaffolding. Additionally, they demonstrate remarkable tolerance to ongoing and dynamic stresses (for example, earthquakes) (Tourse et al., 2018).

One drawback of MSE construction is that a minimum width is required for the wall to be stable enough. Furthermore, the granular material that makes up the reinforced soil mass should be easily accessible; otherwise, it might also be expensive (Bhandari, 2021; Muteb & Falah, 2021). Finally, the reinforced component has to be built to survive processes like corrosion and erosion that may seriously impair the mechanical behavior of the composite structure (Bagherpour, 2012).

However, the main application of MSE wall as following:

- The first attempt to build such structures was documented in 1850s in Europe, which were military structures.

- Technique rediscovered for retaining walls by Vidal in France in the early 1960s as shown in Figure 1.1.
- First mechanically stabilized earth (MSE) structure in united states in 1972 along Highway 39 in the San Gabriel Mountains, California.
- Geosynthetics have greatly accelerated use of soil reinforcement over the past 30 years as shown in Figure 1.2.(Suidan & Schnobrich, 1973)

Figure 1.1: First Highway Use of Modern MSE Earth Wall (France Between Nice and the Italian Border (Fitzpatrick, n.d.).

Figure 1.2: MSE Structure for supporting the soft soil (A. M. Hulagabali et al., 2018).

1.2. Retaining Walls Types

Retaining wall constructions come in a variety of forms and are employed for a variety of purposes:

1.2.1. Gravity Retaining Wall

Gravity **R**etaining **W**alls (**GRWs**) rely exclusively on their self-weight to counteract the lateral pressure exerted by the surrounding soil. GRWs typically exhibit significant dimensions due to the necessity of counterbalancing soil pressure with a considerable amount of gravitational force. The construction of this type of retaining wall necessitates meticulous attention to the forces of bearing, overturning, and sliding. The construction of the object can be accomplished through the utilization of diverse materials, such as concrete, stone, and brick as shown in figure 1.3. The cost is within a reasonable range for structures that are no more than 3 meters in height. Gravity retaining walls encompass various types of structures, such as crib retaining walls, bin retaining walls, and gabions (Sayeed & Reddy, 2014).

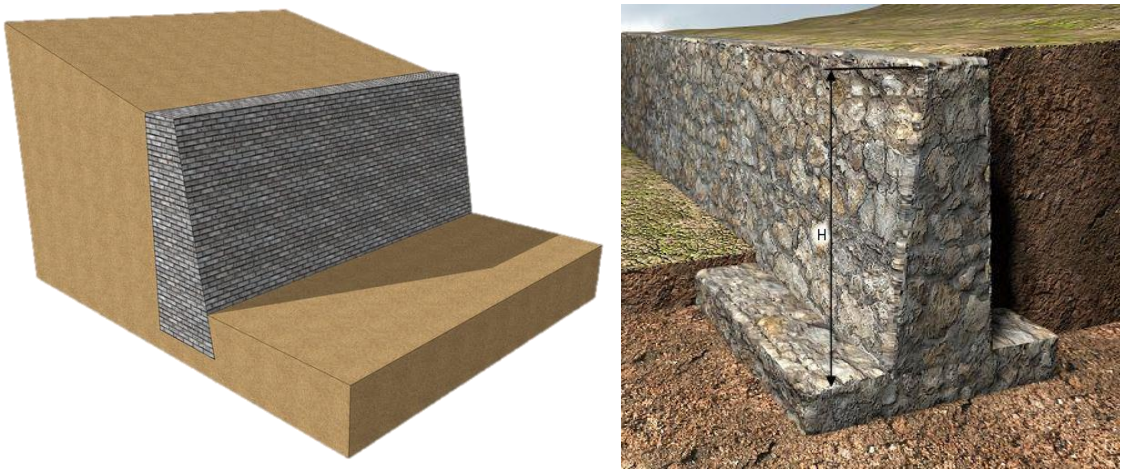

Figure 1.3: Gravity retaining wall (Sayeed & Reddy, 2014).

1.2.2. Crib Retaining Wall

Crib retaining walls are among the gravity barriers. The structures were constructed using interlocking pre-cast concrete or wooden modules. In order to create a structure that allows for efficient drainage, it is necessary to fill the boxes with coarse granular materials such as crushed stone Figure 1.4 shows the concrete crib retaining wall. Crib retaining walls are frequently constructed using reinforced precast and wood materials. The material in question is deemed appropriate for providing reinforcement to planting regions, albeit not recommended for bolstering structures or inclines (Greenway et al., 2012; Tsinker, 1997).

Figure 1.4: Concrete Crib Retaining Wall Gold Coast City Council (Greenway et al., 2012; Tsinker, 1997).

1.2.3. Gabion Retaining Walls

Gabion retaining walls are constructed by filling rectangular wire mesh boxes with rocks or other suitable materials as shown in figure 1.5. This material has the potential to be utilized in the construction of edifices that serve as a barrier against erosion. Furthermore, it has been reported that the stabilization of steep slopes is achieved through its utilization (Chalisgaonkar, 2021; RANJAN,

2020). Retaining walls are classified into six types: cantilever, counterfort/buttressed (as depicted in Figure 1.6), anchored, piled, mechanically stabilized earth (MSE), and hybrid systems.

Figure 1.5: Gabion retaining wall (Ramli et al., 2013).

Figure 1.6: Buttressed retaining wall (Molina-Moreno et al., 2017).

1.3. Mechanically Stabilized Earth Components

The mechanically stabilized earth components consist of many components as showed below (Morsy & Thakeb, 2022; Weldu et al., 2015):

- Soil.
- Geosynthetic Reinforcement (Geotextile or Geogrid).
- Masonry Block Facing Units.

- Drainage System.
- Leveling Pad.

Figure 1.7 shows the components of MSE wall.

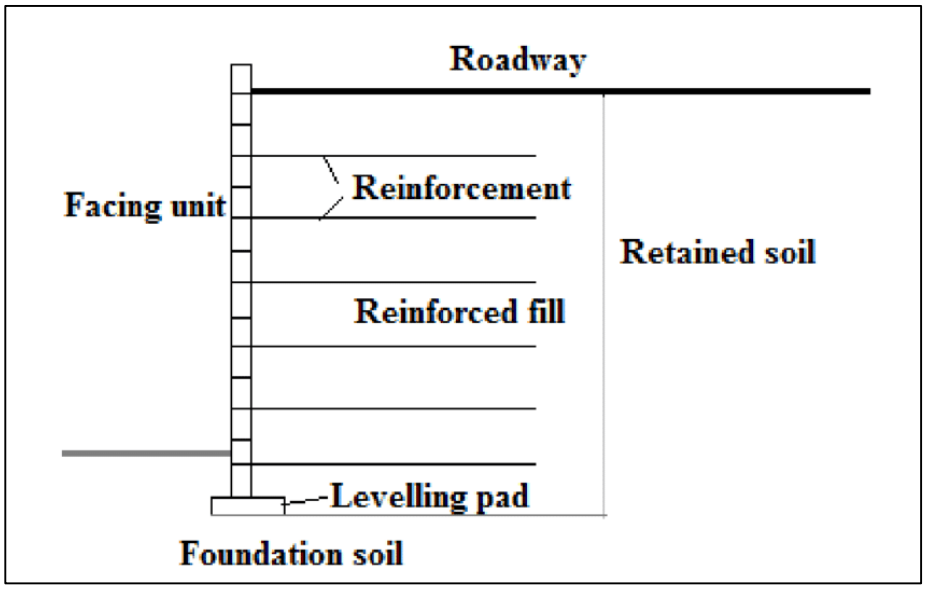

Figure 1.7: MSEW components (Bathurst, 2020).

1.4. Advantages of MSE walls

Advantages in terms of economy, ease of construction and rapid and speedy construction with minimum disturbances to traffic and other services makes MSE walls one of the most favorites and preferred retaining wall system. A variety of materials and customization options in terms of design and construction made it one of the most popular earth retaining system (Khan, 2014). The fascia elements, the back-fill, and the reinforcing system combine to form a gravity retaining structure that relies on the self-weight of the reinforced soil mass. This self-weight resists the lateral pressure from the earth and the service loads, seismic loads, and hydro static pressure (Lamis, n.d.; Morsy & Thakeb, 2022). The main advantages of MSE wall including:

- They can be designed to take extremely heavy loads like bridge abutment footings, crane loads, service loads, etc.

- MSE walls can resist seismic and dynamic forces and transfers the bearing pressure to a wide area.
- Faster construction than conventional retaining walls.
- Less site preparation is required and can be constructed in confined areas where other retaining walls are impossible to construct.
- There are no supports, finishes and curing time.
- The fascia walls are lightweight and are precast and conveyed to the site and lifted using simple lifting equipment. These walls can be made to any height and can resist unequal settlements.
- They can be customized to any geometry and the construction process is very simple. They do not need any heavy types of machinery and specialized workers.
- The fascia can be customized for designs and logos and gives superior and elegant finished and aligned walls.
- Any obstructions inside the back filled areas can be managed by adjusting the angle of the reinforcing elements.
- They possess a very good service life in extreme loading and complex applications.

1.5. Disadvantages of MSE retaining walls.

- MSE retaining walls require granular material in huge quantities. Areas where there is a scarcity of granular material the construction cost increase and make the structure uneconomical.
- The corrosion of reinforcement and deterioration of geo-grids on exposed to sunlight has to be addressed. The reinforced component must be designed to withstand erosion and corrosion processes which can highly deteriorate the mechanical behavior of the composite structure.

- The granular back filling enables free drainage of water through the exposed panel joints and reduces hydro static pressure.
- A proper drainage system should be provided.
- The wall must obtain a minimum width in order to acquire adequate stability.

1.6. Applications of Mechanically Stabilized Earth Walls

Mechanically stabilized earth barriers may be employed in a variety of scenarios, depending on the location, including (Balunaini et al., 2009; Elias et al., 2001; Sankey & Soliman, 2004):

- Abutments for bridges.
- Creating storage space.
- At building locations with problematic soil.
- In regions with a lot of earthquake activity.
- Along the wings.
- As temporary buildings during road construction.
- Use as dams or structures for soil retention.
- Around oil tanks as containment structures.
- Walls of containment surrounding gas storage tanks.
- Adding height to levees and building dams increases storage capacity.

1.7. Retaining Wall Failure

There are two main ways that retaining walls might collapse. The wall may fall if it advances too far and encroaches on the area it was intended to secure. Additionally, it may collapse by flipping over and falling on its face. (Yoo & Jung, 2006).

1.7.1. Sliding-Failure

Once the horizontal forces that tend to produce sliding are larger than the lateral loads that resist sliding, sliding failure takes place and the wall slides

forward as a result. This often happens once the driving force or the opposing force are overestimated as shown in Figure 1.8. The most frequent error is underestimating the driving power, which often stems from (Voight & Elsworth, 1997; Yoon et al., 2002):

1. The omission of surcharge forces from adjacent walls has been observed.
2. The design has been found to incorporate level backfill despite the presence of sloping backfill.
3. The utilization of cohesive soils as backfill material has been noted.

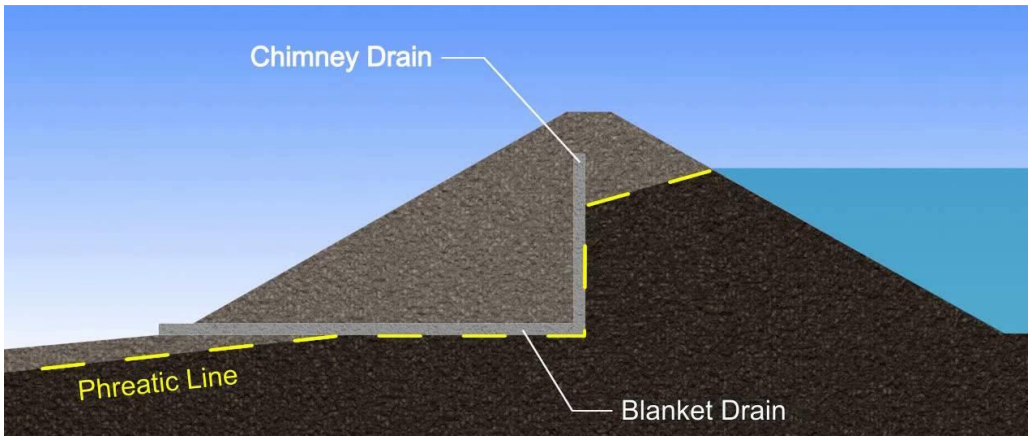

Figure 1.8: Slide Failure at Dam (Alonso et al., 2010)

1.7.2. Overturning Failure

The wall rotating around its bottom front edge indicates overturning failure (also recognized the wall's toe). Once there are more moments likely to produce overturning than times trying to prevent overturning, this happens as shown in Figure 1.9. Overturning failures often originate from underestimating the driving forces, much as with sliding problems. (Brooks & Nielsen, 2010; Walls, n.d.).

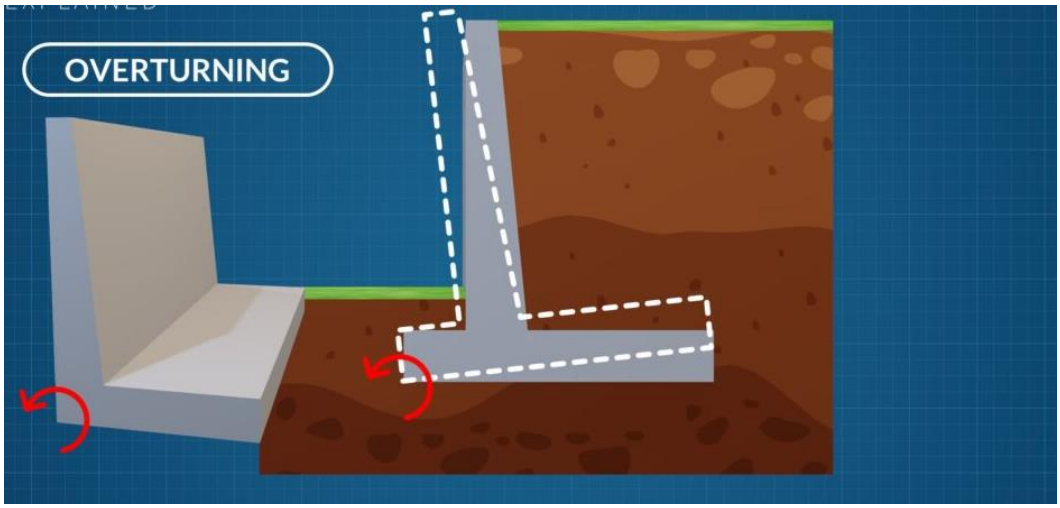

Figure 1.9: Overturning Failure (Zhu et al., 2021).

1.8. Bridge Abutment

An abutment is an important component of a bridge and serves the purpose of providing vertical support for the bridge's structure while also acting as a load distribution point for the bridge. A bridge's abutments are what link the span of the bridge to the embankments on each side as shown in Figure 1.10 (Zhou et al., 2017).

Figure 1.10: Bridge Abutment (Zhou et al., 2017)

The abutments of the bridge are often built directly into the ground. They provide a connection between the ground and the bridge deck. The bridge's abutments take the load and weight that are placed on the bridge deck. A large and weighty foundation is used to support abutments, which are then vertically positioned inside the water or obstruction (Keller & Devin, 2003). Because of their tremendous weight, the abutments can withstand the force that is applied by the combined weight of the water and the earth. When building shorter bridges, abutments are placed solely beneath the two bridge's sides that are directly opposite one another at each embankment (Liu et al., 2020). However, when building longer bridges, additional abutments are placed at certain distances under the bridge's long span. The length of the bridge span determines the abutments' number that are required for the structure. The following is a list of the many structural components that make up an abutment (Briaud, 1997; Lan, 2012):

1. **Bridge Seat:** The term "Bridge Seat" refers to the abutment top that has a broader span than the rest of the abutment and is where the bridge's deck is situated.
2. **Wing Wall:** This section of the abutment is exclusive to the abutments that are used to link the bridge to an embankment. These are temporary walls that are built to hold back soil and prevent erosion on the embankment.
3. **Back Wall:** This component is unique to embankment walls and is only present in them. Most bridges have back walls that are built up vertically at the ends of the spans. The expansion joints found in the bridge span and deck are supported by the rear walls.
4. **The Abutment's Pile:** The abutment's pile is the filament that links the ground foundations of the abutment with the seat of the bridge. The bridge's height and the extent of the obstruction both have a role in determining the length of the pile (canal, river, and stream).

5. **The Bridge's Foundation:** Also Known as the Footing of the Abutment The foundation of the bridge is also known as the footing of the abutment. The footing is what establishes the pile's connection to the earth. The footing is far more extensive and weightier. The abutment shouldn't be allowed to collapse into the ground; thus, the footing is there to stop that from happening.

1.8.1. Types of Abutments

The following is a list of the most essential kinds of abutments (Tatsuoka et al., 2005):

1.8.1.1. Gravity Abutments

The object in question exhibits resistance to the lateral forces of the earth and water through its inertial mass. The abutments are founded on a substantial base that is both broad and weighty. The abutment structure is designed to be placed directly on the ground, relying on the force of gravity to maintain its stability (X. Yu et al., 2005).

1.8.1.2. U-shaped Gravity Abutments

The U-shaped Gravity Abutments bridge abutment design features perpendicular wings that serve as counterforts. These abutments exhibit a high degree of stability. The wing walls of the abutment are oriented orthogonally to the seat of the bridge. The U-shaped abutment is comprised of a set of two piles that are positioned at a distance equivalent to the width of the bridges. The abutments are fabricated utilizing reinforced cement concrete. The foundation serves to connect the piles of the abutment at their base as shown in Figure 1.11. Both piles share a common base (Qin & Liu, 2009).

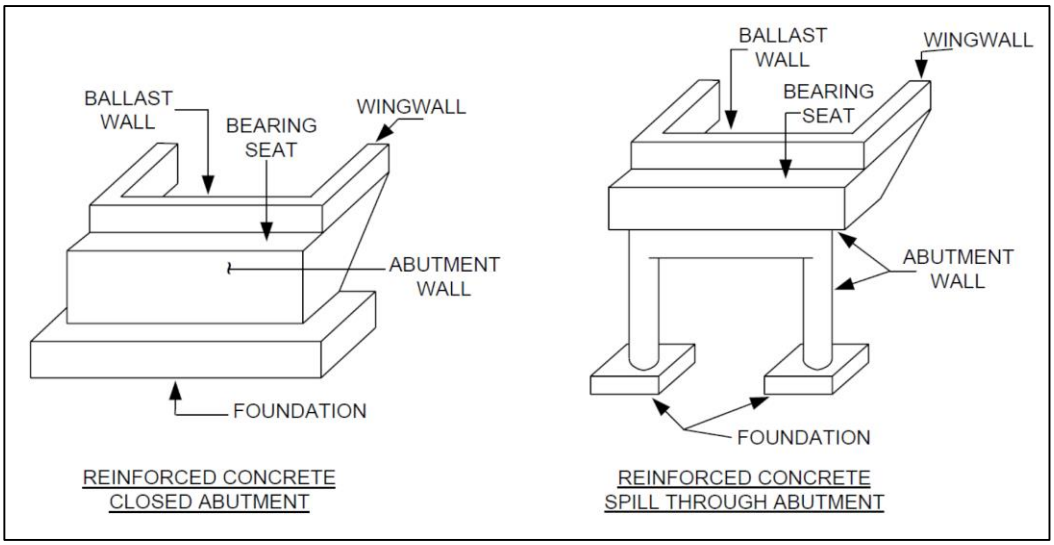

Figure 1.11: U-shaped Gravity Abutments (Qin & Liu, 2009).

1.8.1.3. Cantilever Wall Abutments

The Cantilever Abutment serves two primary functions: firstly, to retain the soil situated behind the bridge ends, and secondly, to provide support to the bridge superstructure. Certain types of wall abutments are commonly known as stub abutments (Lan, 2012). The abutments are designed to be of minimal length and are situated at the summit of the fill embankments. Typically, stub abutments are designed to retain soils that have a marginal elevation compared to the thickness of the superstructure as shown in Figure 1.12. Although stub abutments can offer cost savings, they tend to elongate the end spans. Additional wall abutments may possess greater height and are frequently built to the complete altitude of the crossing. The construction of full height abutments presents a greater level of complexity, yet they have the potential to decrease the span length of end sections (Olson et al., 2013).

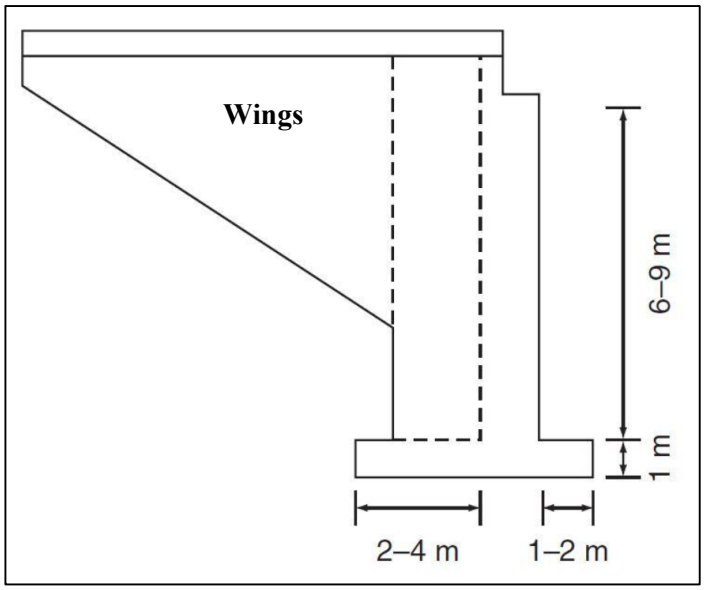

Figure 1.12: Side view of Cantilever Wall Abutments (Olson et al., 2013)

1.8.1.4. Full Height Abutments

It is an abutment of considerable height that has been built at the lower-level highway and is intended to provide support for the whole embankment. This abutment is expensive; however, it is frequently utilized in densely populated urban and metropolitan regions that place a premium on the structure's depth as shown in Figure 1.13 (Tatsuoka et al., 2007).

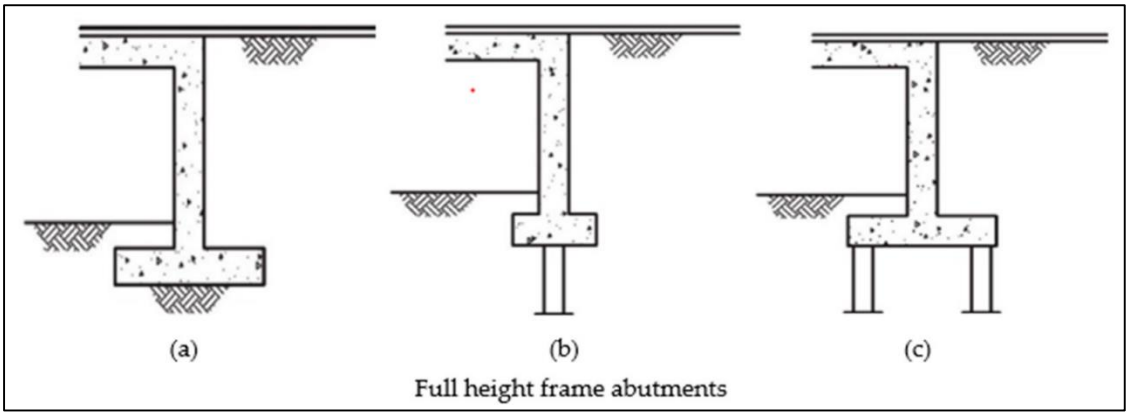

Figure 1.13: Full Height Abutments (Tatsuoka et al., 2007).

1.8.1.5. Stub Abutments

They are relatively short abutments that are often supported on piles and are built at the embankment's top or on the embankment's slope. They are incredibly low, and one cannot see them from a higher elevation as shown in Figure 1.14 (Kumar & Roy, 2022).

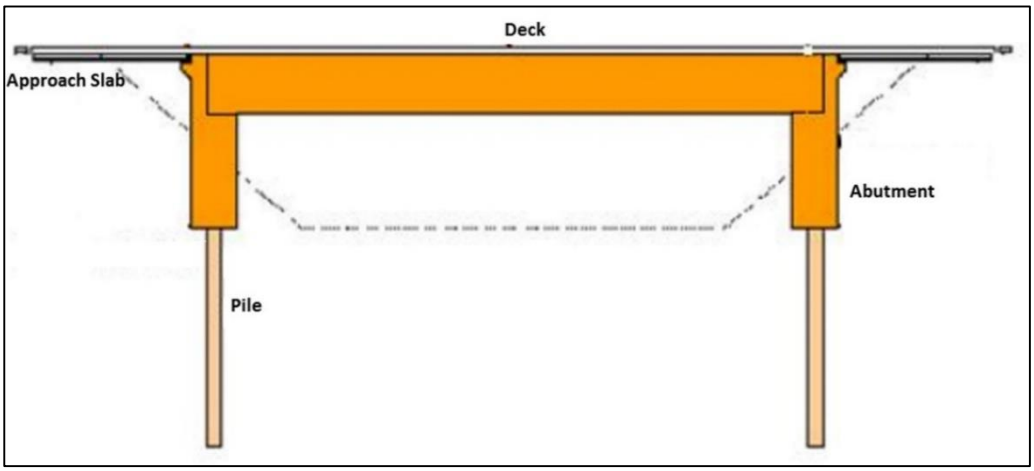

Figure 1.14: Stub Abutments (Kumar & Roy, 2022).

1.8.1.6. Semi-stub Abutments

A semi-stub abutment has a height that falls somewhere in the middle of a full-height abutment and a stub abutment. In contrast to stub abutments, which are built on the top or somewhere close the embankment's top, full-height abutments are built at the embankment's bottom, and semi-stub abutments are built anywhere in the middle of the embankment, between the top and the bottom as shown in Figure 1.15 (Silva et al., 2023). Because of their height, which places them above that of stub abutments but below that of full-height abutments, they are referred to as semi-stub abutments.

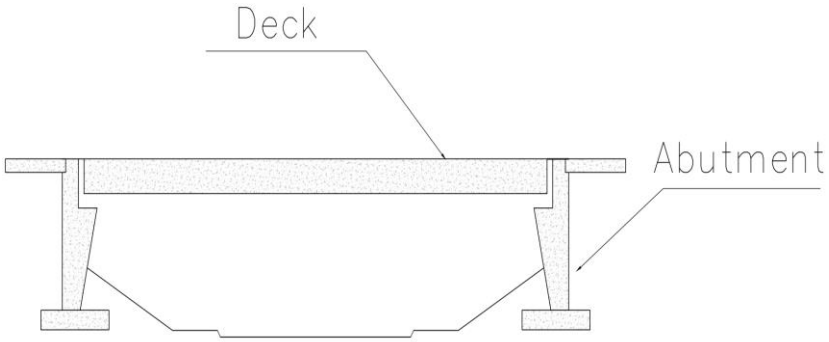

Figure 1.15: Semi-stub Abutments (Silva et al., 2023).

1.8.1.7. Counterfort Abutments

It is comparable to the retaining wall that was built against the counterfort. In an abutment known as a counterfort, the breast wall and the footing are connected by a thin wall known as the counterfort. These counterforts were constructed at regular intervals in order to make the breast wall seem more like a supported slab instead of a cantilevered structure (Churilla & Diviney, 1979).

1.8.1.8. Spill-Through Abutments

The installation of wide gaps in the stem of spill-thru abutments is done with the intention of lowering the amount of soil pressure that is exerted on the abutment. The difference between piers and spill-thru abutments is that the latter have the bulk of their construction below ground (Melville et al., 2006).

1.8.1.9. MSE System

Mechanically Stabilized Earth is the abbreviation for MSE. True MSE abutments (which do not include piles) have a lower overall cost compared to composite abutments (piles under the bridge seat). Both are cost-effective alternatives to traditional concrete abutments, and they save a substantial amount of money when used in lieu of concrete abutments on piles (Khan, 2010).

1.8.1.10. Pile Bent Abutments

The pile bent abutment seems to be a variation on the spill-thru abutment that substitutes the wall-like support with a sequence of piles, also known as columns, to hold the support beam. This abutment type is also known as a pile bent abutment as shown in Figure 1.16 (Wilhelmi, n.d.).

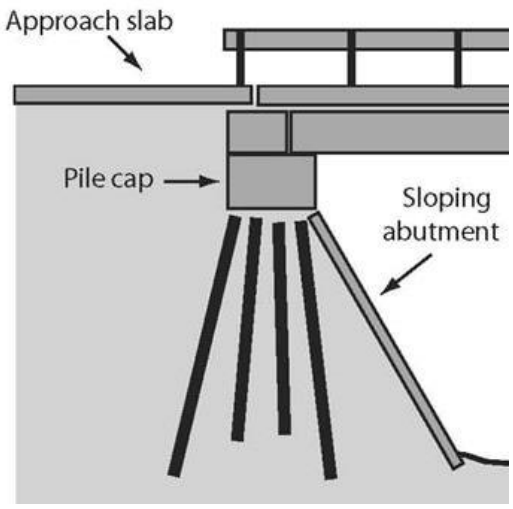

Figure 1.16: Pile Bent Abutments (Thakkar et al., 2023).

1.9. Problem statement

Since becoming a common engineering practice, mechanically stabilized earth (MSE) walls have attracted many research attentions. Building an earth-retaining structure using dirt and little strengthening is efficient in terms of cost and effectiveness. To be competitive in the market, the MSEW industry is always looking for ways to improve effectiveness and save costs. This improvement results from novel soil strengthening techniques being created and a better knowledge of wall performance compared to existing conventional design approaches.

MSEW' simplicity of installation and speedy construction are significant benefits over traditional reinforced concrete barriers. Every layer is extremely durable as it is set down and does not need formwork or curing, which reduces

the need for cranes, scaffolding, or support. Additionally, they don't need the face to be worked on anymore.

In addition to the flexibility of MSEW during their design and construction, seismic testing conducted at the Japan National Institute of Agricultural Engineering in Tsukuba City, utilizing a large-scale shaking table the lab, has demonstrated that modular block reinforced walls and geocell retention walls exhibit sufficient flexibility to withstand substantial deformations without compromising their structural integrity, thereby exhibiting high earthquakes load resistance. The INTER-LOK System is frequently employed for the construction of overpasses spanning highways and interstates.

1.10. Project novelty

The novelty of this study is adopting a field and experimental work for a specific type of return wall (MSE wall), which is considered a new supporting method for structural engineering in Iraq specially in Babylon governorate. The project consists of applying MSE wall on constructing bridge abutments for the first time in Al-Um Bridge in Hilla city and spreading a load cell sensor in this bridge to identify both static and dynamic load reactions. As well as creating a small model like the real bridge case in order to investigate the effect of changing strips width and shape on and the sensor location on the load reaction.

1.11. Aim and Objectives of the Research

This project will focus on the using of Mechanically Stabilized Earth MSE structures in constructing bridge abutments in Al-Um Bridge in Hilla city/ Iraq. The present study focuses on the following major points:

2. The effect of static load location on the MSEW was experimentally investigated.
3. The effect of the shape of geosynthetics reinforcement on the MSEW's stability was investigated.

4. Creating a full-scale section model compatible with Al-Um Bridge intersection to identify the relationship between the lateral pressure of soil with MSE depth, vertical pressure with time, lateral displacement with MSE wall depth.
5. Created three-dimensional model by the finite element method to simulate the nonlinear behavior of MSEW under static load by using the ABAQUS Standard/Explicit 2019 computer program.
6. Determine the effect of changing different parameters such as width of strips, and location of load with respect to the panel on lateral pressure, vertical pressure of soil and lateral deformation of MSEW.
7. Installing four force sensors in the real Bridge in Hilla city to find the lateral pressure of soil on MSEW.

1.12. Thesis Layout

This thesis consists of six chapters:

Chapter One (Introduction): includes a brief introduction, type of retained wall, application of MSE wall, advantage, and disadvantage of MSE wall, Bridge Abutment, and the objectives of the present study.

Chapter Two (Literature Review): Present brief information about Mechanically stabilized earth (MSE) walls, case studies related to MSE, and finally previous research works related to MSE wall and literature review about enhancing soft soils and the applications of (MSE) walls.

Chapter Three (experimental work): covers the experimental program, including the materials utilized, the MSE wall models' features and manufacturing method, and testing.

Chapter Four (results and discussions): The results of the selected tests on the real mode are presented and discussed in this chapter. Pressure, stress, and deformation are presented in the results in addition to case study for Al-Um intersection Bridge.

Chapter Five (Finite Element Modeling By ABAQUS): Recommendations for choosing the optimum three-dimensional wire panel for the unique circumstances described in the thesis are provided based on the findings from the previous chapter. The main conclusions of this study are presented and discussed.

Chapter Six (Conclusion and Recommendations): This chapter includes a thorough overview, the primary finding from the investigation, and suggestions for next research.

CHAPTER TWO

LITERATURE REVIEW

CHAPTER TWO

LITERATURE REVIEW

2.1. Introduction

Most of the time, the soil that is employed in MSE constructions is a granular material that is known as "Select Granular Backfill." This material has a max of 15 percent fines and a max size of (10 cm). There is a wide variety of configurations available for extensible geosynthetic reinforcing (Brabant, 2001). The primary categories consist of geogrids, biaxial, uniaxial, and non-woven and woven geotextiles. Tensile reinforcing stretches, and frequently to the point where the strain in the reinforcing is higher than or equal to the strain in the soil mass. As a result, there is a significant amount of lateral forces that occurs once extensible soil reinforcing is utilized (Das, 2005).

2.2. Soil-Structure Interaction (SSI)

Soil–**S**tructure **I**nteraction (**SSI**) is basically an exchange of mutual stress, in which the moving of the ground-structure system is impacted by both the kind of ground and the structure's kind (Jain & Sepate, n.d.). This exchange of mutual stress seems to be the primary cause of the phenomenon. This is particularly relevant to regions that experience frequent earthquakes. Different relationships between soil and buildings may either magnify or lessen the movement and damage that results from earthquakes (Datta, 2010). A structure that is situated on stiff ground, as opposed to malleable ground, is more likely to sustain severe damage. The sinking of foundations is a second interaction influence that is connected to the mechanical qualities of the soil and is exacerbated when a seismic event occurs. The term for this kind of event is "soil liquefaction." (Raghu Kanth & Dash, 2010).

Most constructions that are the result of civil engineering include some kind of structural element that is in direct contact with the ground. The structural displacements and the ground displacements are not independent of one another when these systems are subjected to the action of external forces including earthquakes (Sextos et al., 2003). Traditional techniques of structural design do not consider the consequences of SSI. For light structures on relatively stiff soil, including low-rise buildings and simple rigid retaining walls, it is fair to disregard SSI as an important consideration. The influence of SSI, on the other hand, becomes more noticeable for large structures that are sitting on relatively soft soils. For instance, nuclear power plants, high-rise skyscrapers, and elevated roadways on soft soil are all examples of constructions that are susceptible to the influence of SSI (Tadesse et al., 2022). Recent earthquakes, such as the one that occurred in Kobe in 1995, have brought to light the fact that the earthquake behavior of a structure has been heavily impacted not only by the reaction of the superstructure, however also by the reaction of the foundations and the grounds as well. This was brought to light as a result of the damage that was caused by these earthquakes (MIWA & IKEDA, 2006). Because of this, the most recent seismic design codes, such as the Implementing Regulations for Building Structures: Seismic Performance Verification JSCE 2005 (Usami et al., 2005), stipulate that the response analysis must be carried out by considering a whole structural system such as the ground, foundation, and superstructure.

Once those forces have a considerable influence on the movement of the basement in comparison to the movement of the free-field ground, a research and engineering committee will focus its attention on the study of SSI. The movement that is observed on the soil's surface is known as the free-field ground movement. This motion occurs even when there is no structure present to influence it. The reaction of structures to earthquakes is heavily reliant on

the interactions of three connected systems, which are as follows (Cakir, 2013):

1. The structure
2. The Foundation
3. The underlying soil

The study of SSI is the procedure that is used to evaluate the collective reaction of the three connected systems that were discussed before in response to a particular ground movement. The reaction from the soil may be said to impact the movement of the structure, and the movement of the structure could be said to affect the response from the soil. This process is referred to as the SSI, and it could be characterized as follows (Alisawi et al., 2023).

The displacements of structure and the ground are not related to one another in any way during these phenomena. Most soil-structure forces are interactions that may take place between the soil and any construction. However, these are not able to alter the movement of the soil in all circumstances (Cakir, 2013).

2.3. Analysis in SSI

Two different approaches of analysis may be used to quantify the interactions. They are (Hattori et al., 2003):

1. Direct Analysis
2. Substructure Approach

2.3.1. Direct Analysis in SSI

In this kind of investigation, both the ground and the building itself are included in the same analytical model. They are evaluated as a system. A continuum is used to illustrate the soil system in Figure 2.1, which may be found below. One illustration of this kind is provided using finite elements. Included in this are the foundation, the structural components, the load

transmitting boundaries, and the elements at the interface positioned on the borders of the foundation (Mulligan & Wainwright, 2013).

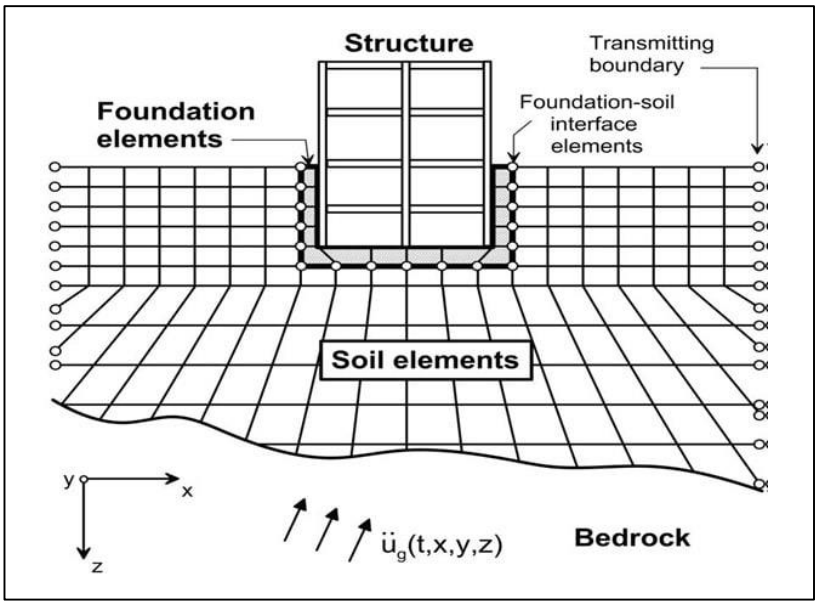

Figure 2.1: Analysis of SSI by the Finite elements' aids sketch (Van Nguyen et al., 2021).

Since it requires a lot of work and is quite difficult to understand, this approach is seldom ever utilized in actual life.

2.3.2. Substructure Approach in SSI

The activity known as SSI is broken up into two distinct sections. After then, these elements are integrated to provide a comprehensive answer to the issue. Within the scope of this technique, a model is developed with the following requirements (Nyamabo et al., 2021):

- An analysis of the free-field movements and the soil qualities that correlate to those motions.
- An analysis of the transfer functions that are used to transform the free-field motion to the foundation input motion.
- The dashpots and springs are included in the design. At the contact between the earth and the foundation, the springs are representative of the stiffness, and the dashpots are representative of the damping.

- An investigation on the combined structure's responses

The evaluation of generic issue A is shown below in Figure 2.2, which may be found below. It is broken up into two issues, which we will refer to as A1 and A2, in such a manner that A=A1 + A2. This is performed using the superposition principle as the guiding concept. Each issue is examined on its own, and the aggregated findings are what constitutes the ultimate answer (Stengel, 1994).

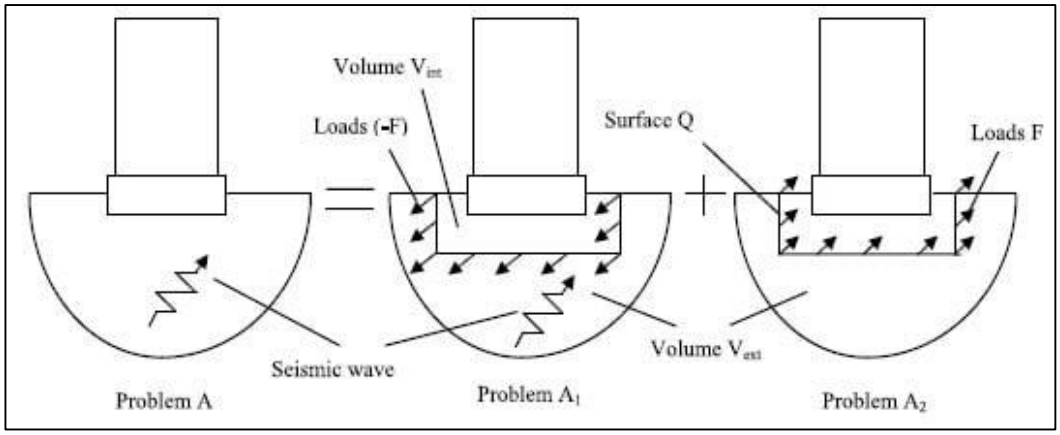

Figure 2.2: Issue Splitting A by Superposition-Substructure Approaches (Stengel, 1994).

2.4. Basic Mechanics of Mechanically Stabilized Earth

The fundamental physics of Reinforced Earth were well known by Vidal and were detailed in depth in his early books," as cited in McKittrick, (McKittrick & DP, 1979) Figure 2.3 provides an illustration of a simplified version of these fundamental mechanical principles. An axial force applied to a sample of granular material would lead to lateral expansion in dense materials, as illustrated in Figure 2.3a. This is the case for materials with higher densities. As a direct result of dilatation, the lateral strain seems to be more than one-half of what the axial strain is. Nevertheless, when inextensible horizontal reinforcing elements objects are placed inside the soil mass, as illustrated in Figure 2.3, these reinforcing will prevent lateral strain due to friction between the soil and reinforcing elements, and the behavior will be like when a lateral restraining pressure or load was already implemented on the element. Figure

2.3: Unless inextensible horizontal reinforcing components are arranged within the soil mass. This corresponding lateral load that is being placed on the soil element is the same as the earth pressure that is being exerted when it is at rest (Kov). Every component of the soil mass is subject to the same lateral stress, denoted by the symbol Kov. Because of this, the horizontal restraining stresses, also known as lateral forces, would likewise grow in direct proportion to the increase in the vertical stresses (Amadei & Stephansson, 1997).

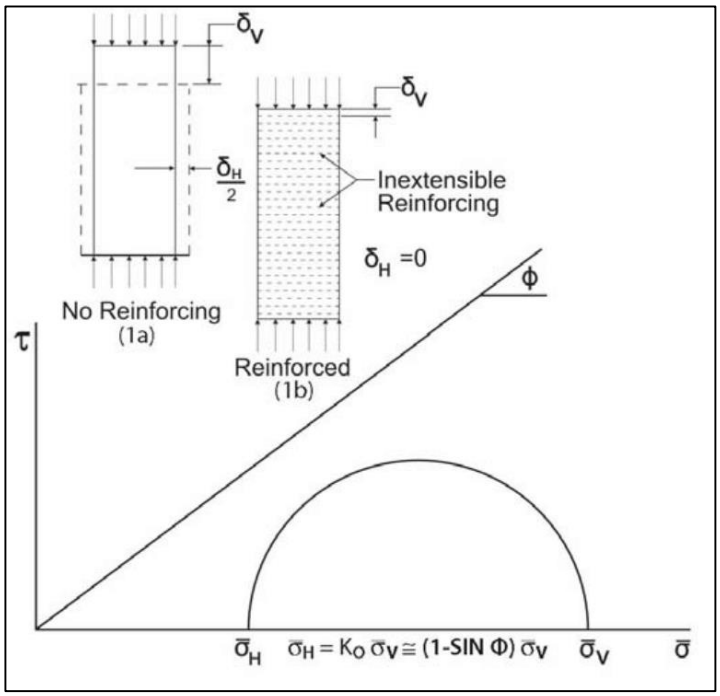

Figure 2.3: Fundamental Reinforced Earth Mechanics (Amadei & Stephansson, 1997).

The AASHTO Requirements handled this core idea by implementing a change that was first suggested in 2008 and then published in the Interim Specifications in 2009 (Officials, 2009). The justification provided by AASHTO for this modification is quite clear: "There has been a lot of confusion over the use of live load surcharge in relation to pullout calculations for the internal stability of MSE walls (Dobie, 2001). Therefore, there have been a lot of different interpretations of the specifications addressing this problem. After going back and looking at how this standard was developed in the past, it has become clear that the purpose of this requirement is to make

the recommendation which live load surcharge should not be included for pullout computations. This applies to the calculation of reinforcing load (T_{max}) for the assessment of pullout stability and the computation of vertical stress for the computation of pullout resistance. Both of these calculations are necessary to determine pullout stability and resistance (Nowak & Iatsko, 2017). Because of this, two independent estimates of the max allowable reinforcing tension (T_{max}) are necessary, and the following should be taught to engineers:

- Apply the surcharge to the MSE reinforced soil once calculating T_{max} as part of conducting computations for reinforcing and connection rupture.
- Do not apply the surcharge to the MSE reinforcing soil once calculating T_{max} as part of performing computations for pullout.

The performance of MSE structures is directly impacted by the backfill that is employed in such structures. Granular material with a max size of 100 millimeters and less than 15 percent fines is the kind of MSE structure backfill that is required by AASHTO specifications to achieve performance standards (Table 2.1).

Table 2.1: Gradation Limits per AASHTO (Sivan & Mathew, 2010)

U.S. Sieve Size	Percent Passing
100 mm	100
420 μm	0-60
75 μm	0-15

AASHTO additionally specifies additional standards for soundness, plasticity index, and internal friction angle, in addition to specifications for electrochemical characteristics. Depending on the local characteristics of the

material, several DOTs adjust the gradation restrictions or lower the percentage of penalties that are permissible.

2.4.1. Design Techniques

It should come as no surprise that MSE wall designers sometimes feel perplexed by the options they must choose from. Both inextensible (steel) and extendable (geosynthetic) MSE wall reinforcing operate differently. Steel is inextensible, whereas geosynthetics are extensible (Lee, 1993). It is necessary for designers to understand the behavior of the reinforcing in order to choose the design technique that is most suitable for each kind of reinforcing and achieve the requisite levels of performance and service life for the structure. In the following paragraphs, we will talk about design techniques and reinforcing behaviors, complement the technique logical approach to the reinforcing, and demonstrate unequivocally that the Coherent Gravity Technique must be utilized for the design of MSE walls with inextensible reinforcing, whereas the Simplified Technique must be utilized for the design of MSE walls with expandable reinforcing. The status of the practice is as described above, with the appropriate choice of the MSE design approach being important to the effective design of MSE walls for road constructions (Olkowski, 2021).

2.4.1.1. Coherent Gravity Technique

The Coherent Gravity technique development (P. L. Anderson et al., 2010) was a result of postulating the behavior of MSE structures, observing actual structures, and interpreting data based on the fundamental principles of statics and soil mechanics. The Coherent Gravity Technique was established for the design of MSE structures subsequent to the delivery of a substantial amount of information at three global conferences on soil reinforcing in 1978 and 1979

(Kempton et al., 2008). The following is a list of the design features of the Coherent Gravity technique, which can be found illustrated in Figure 2.4.

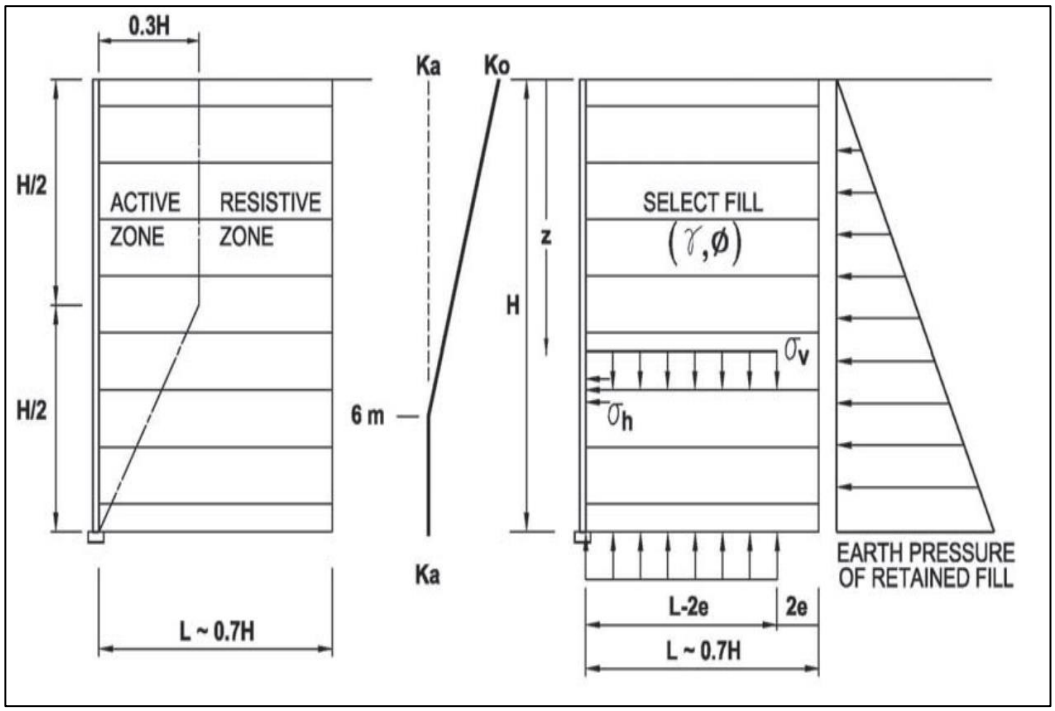

Figure 2.4: Properties of the Coherent Gravity Technique (Lin, 2023).

2.4.1.2. Tieback Wedge Technique

The Tieback Wedge Technique was formulated by Bell, et al. (Bell et al., 1975) as a continuation of the trial wedge technique from classical soil mechanics (Huntington, 1957). It has consistently been deemed as the suitable approach for the design of geosynthetic-reinforced MSE walls. It is postulated that in a MSE wall featuring geosynthetic reinforcing, the failure plane will manifest along the Rankine rupture surface. Figure 2.5 shows the Tieback Wedge Technique.

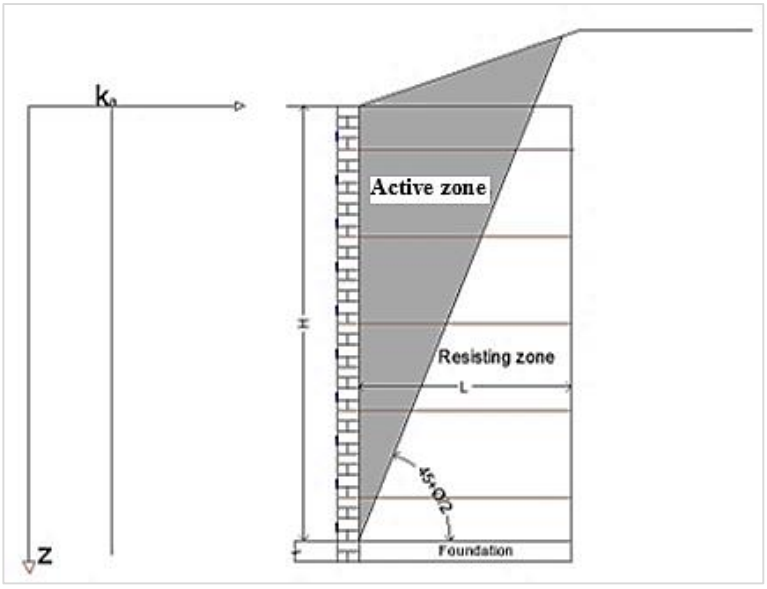

Figure 2.5: Tieback Wedge Technique (Kakrasul, 2018).

2.4.1.3. Structure Stiffness Technique

The Structure Stiffness Technique was formulated by Christopher, et al. (Christopher et al., 1990) through the utilization of instrumentation on test walls of full-scale and examination of data documented in the literature from instrumented walls that are in-service. The Structure Stiffness Technique bears resemblance to the Tieback Wedge Technique, albeit with a distinction in the assumption of a bilinear envelope of max reinforcing tension for inextensible (steel) reinforcing and a Rankine failure plane angled at 45+ ϕ /2 from the horizontal for extensible (geosynthetic) reinforcing. The coefficient for lateral earth pressure, denoted as Kr, is determined by a sophisticated equation that considers the overall rigidity of the reinforcing (P. L. Anderson et al., 2010).

2.4.1.4. Simplified Technique

The Simplified Technique was formulated as a unifying design approach for MSE walls that utilize either extensible or inextensible reinforcing. This approach was derived from the Tieback Wedge Technique (T. Allen et al., 2001). The Simplified Technique offers an approximation of the increase in

internal vertical stress caused by overturning at each inextensible reinforcing level. This approximation involves adding 0.2 z (z = internal vertical stress) to the soil overburden, rather than performing individual calculations for each level of reinforcing. Nevertheless, extensible reinforcing is utilized without inducing any increment in stress. The Simplified Technique, as described in reference (Shrestha, 2013), employs the bilinear envelope of max reinforcing tension from the Coherent Gravity Technique for walls that are reinforced with inextensible reinforcing. For walls reinforced with extensible reinforcing, the technique utilizes the Rankine failure plane, which is inclined at an angle of 45+ ϕ /2 from the horizontal. The Simplified Technique is a variant of the Tieback Wedge Technique that incorporates Kr/Ka proportions derived from the Structure Stiffness Technique.

2.4.1.5. Ko-Stiffness Technique

The Ko-Stiffness Technique, as proposed by Allen, et al. (T. M. Allen & Bathurst, 2001), is a technique aimed at facilitating the design of MSE structures featuring either inextensible or extensible reinforcing. The Ko-stiffness Technique, akin to the structure stiffness technique, necessitates the utilization of a multifaceted equation for the computation of the max tension in every reinforcing layer (Maw, 2009). The equation comprises various factors, namely a global reinforcing stiffness parameter, a facing stiffness parameter, a facing batter parameter, a local stiffness parameter, and distribution parameter. These factors act as variations to the at-rest earth pressure coefficient, Ko (T. M. Allen & Bathurst, 2002).

2.5. REINFORCED SOIL CONCEPTS

The concept of a reinforced soil mass bears resemblance to that of reinforced concrete, whereby the mechanical characteristics of the mass are enhanced through the incorporation of reinforcing that is aligned with the principal strain direction. This serves to counteract the limited tensile resistance of soil. The

enhanced tensile characteristics are an outcome of the interplay between the reinforcing and soil. The composite material exhibits the following properties:

- The transfer of stress between the reinforcing and soil occurs in a continuous manner along the length of the reinforcing.
- The distribution of reinforcing during the soil region is characterized by a certain degree of regularity.

2.5.1. Stress Transfer Mechanisms

The transfer of stresses between reinforcing and soil is accomplished through either friction (as depicted in Figure 2.6a) or passive resistance (as depicted in Figure 2.6b), with the specific mechanism being dependent on the geometry of the reinforcing (Zhang et al., 2017).

Friction arises in areas where there is a relative shear displacement and a corresponding shear stress between the surface of the soil and the reinforcing. It is recommended that friction-dependent reinforcing elements be oriented in accordance with the direction of movement of soil reinforcing. Various types of reinforcing elements, such as geosynthetic straps, geotextile, steel strips, longitudinal bars in grids, and certain geogrid layers, can serve as instances of such strengthening components (Van Der Steen, 2007).

Passive resistance is generated by the emergence of stresses of a bearing nature on surfaces of "transverse" reinforcing that are perpendicular to the direction of movement of soil reinforcing (Jones, 2013). The predominant mode of interaction for bar mat, wire mesh reinforcing, and geogrids featuring rigid cross machine direction ribs is commonly acknowledged to be passive resistance. The transverse ridges present on the "ribbed" strip reinforcing offer a degree of passive resistance (Wei, 1990).

The relative significance of individual transfer mechanisms pertaining to a specific reinforcing is contingent upon several factors, including the surface

roughness (i.e., skin friction), the normal effective stress, the dimensions of the grid opening, the thickness of the transverse members, and the elongation properties of the reinforcing. Soil characteristics such as stiffness, cohesion, amount of water, density, particle shape, grain size distribution, and grain size, are of equal importance in the development of interactions (Norris & Norris, 1992).

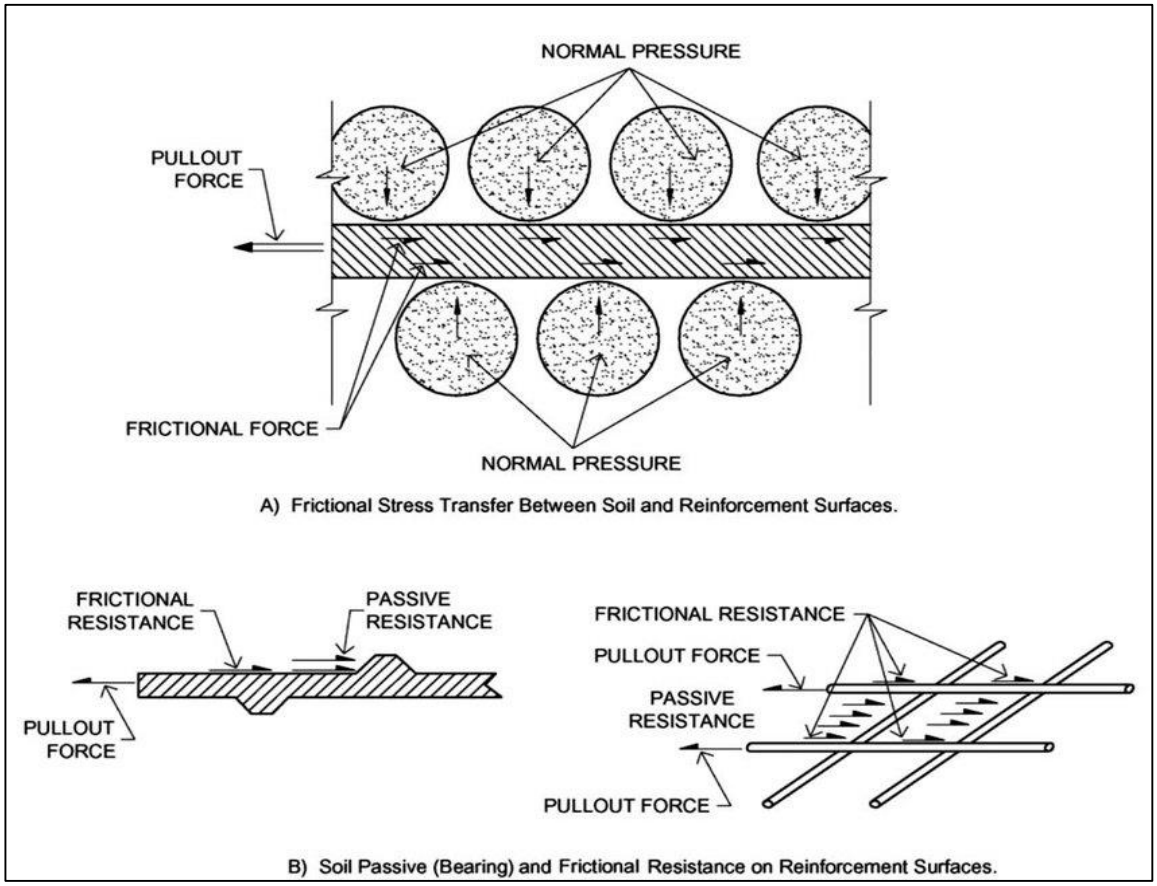

Figure 2.6: Stress transfer mechanisms for soil reinforcing (Sieira et al., 2009).

2.5.2. Geometric Characteristics

There are two distinct categories that can be identified:

- **Steel grids, bars, and strips.** The physical attributes of a steel layer comprising of strips, bars, or grids are defined by the cross-sectional area, thickness, and perimeter of the reinforcing element. Additionally, the center-to-center horizontal distance between elements is also a

significant parameter to consider. In the case of steel grids, an element is identified as a longitudinal member of the grid that extends into the wall (Sharbatdar, 2003).

- **Geogrids and Geotextiles** are materials commonly used in civil engineering and construction projects. The dimensions of a geosynthetic layer are defined by the width of the strips and the horizontal center-to-center spacing between them. The utilization of cross-sectional area is deemed unnecessary in the evaluation of geosynthetic strip strength, as it is represented by the tensile force per unit width, rather than stress. The challenges associated with determining the thickness of thin and compressible materials hinder the ability to accurately determine stress levels (Sommers & Viswanadham, 2009).

The utilization of the coverage ratio (R_c) is employed to establish a correlation between the force exerted per unit width of individual reinforcing and the force per unit width necessitated throughout the entirety of the structure. Please refer to Figure 2.7 for a visual representation of the concepts (Huber et al., 2023).

$$\mathbf{R}_c = \frac{b}{S_h} \tag{2.1}$$

Whereas:

b is the strip, sheet, or grid's gross width. As shown in Figure 2.7, for grids are calculated from the centers of the outside longitudinal bars.

S_h stands for the horizontal center-to-center distance between strips, sheets, or grids.

Keep in mind that $R_c = 1$ in the case of continuous reinforcing, meaning that each reinforcing layer completely encloses the reinforced soil zone's horizontal surface. Alternately, for planning and details, force per width may

be more readily computed per panel width, for discrete reinforcing and segmental precast concrete facing (Patel, 2019).

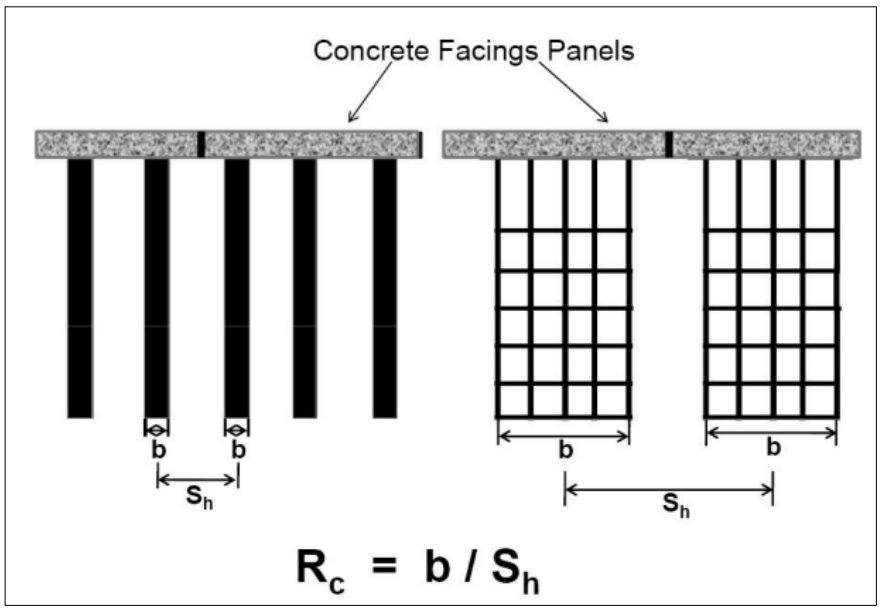

Figure 2.7: Coverage proportion Top view (Patel, 2019).

2.5.3. Reinforced Earth Abutments

Reinforced earth walls are typically composed of modular facing panels, which are commonly constructed using soil reinforcing, earth fill, and pre-cast concrete. The construction of the wall involves a repetitive execution of a set of tasks at different elevations (Nejad, 2017). These tasks include the installation of frontal panels, placement, and compaction of soil fill, laying of geotextile reinforcing, and further placement and compaction of soil fill. The procedures are reiterated until the requisite altitude is achieved (Warren, 2015).

The configuration of the facing panels facilitates the formation of nearly perpendicular walls, while the resultant wall is capable of withstanding horizontal pressure by means of the reinforcing's frictional force. Reinforced earth may serve as a viable component of the abutment once constructing a bankseat atop it (O'Shaughnessy, 1999). To mitigate potential localized impact from loading that may lead to deformations on the surface of the wall,

it is common practice to position the bankseat at a distance from the top of the wall. Reinforced earth walls are a commonly employed solution in combination with other forms of abutment structures to construct cost-effective retaining walls surrounding bridge approaches (BROUTHEN, 2022). Figure 2.8 shows the Reinforcement earth abutment.

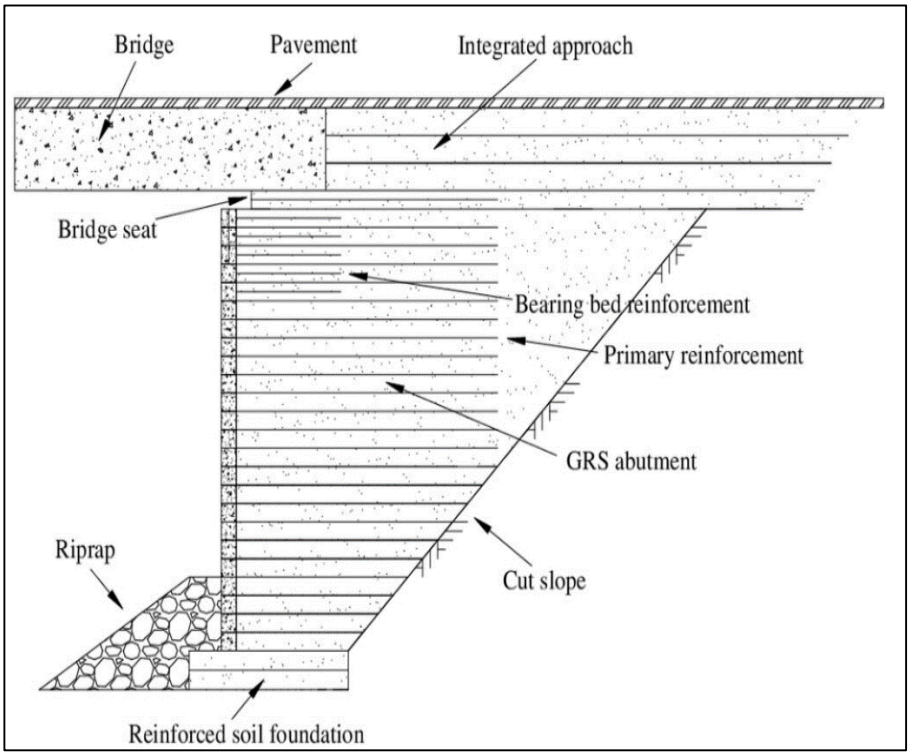

Figure 2.8: Reinforcement earth abutment (BROUTHEN, 2022).

2.6. Previous Case study

(Bathurst et al., 2000) describe the test program, and some instrumentation details and present selected results from the first four walls completed to date. Three of the walls were constructed with a column of dry-stacked modular concrete units and one nominal identical wall was constructed with a wrapped-face as shown in Figure 2.9. All the structures were surcharge loaded to stress levels well more than working load conditions. The data gathered from this program has been useful to identify important performance features of the reinforced soil structures and to identify possible sources of conservatism in

current methods of analysis for geosynthetic reinforced soil structures in North America.

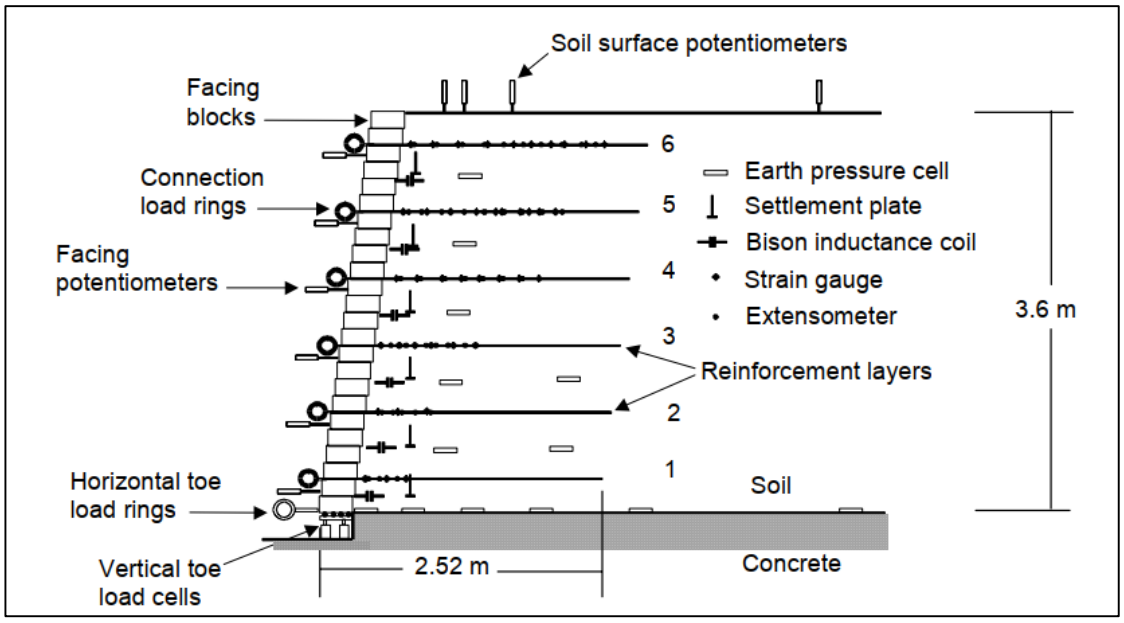

Figure 2.9. Typical instrumentation plan (Wall 1) (Bathurst et al., 2000)

(Armour et al., 2004) investigated a case history of a 25-year-old MSE wall that exhibited a catastrophic failure in Soda Springs, Idaho. Six precast panels fell out in 2002 Figure 2.10. After a wide investigation, it was determined that the cause of the failure was due to corroded steel strips that sheared at the panel connections. It was found that the lateral earth pressure applied at the facing panels exceeded the connection's tensile strength.

Figure 2.10. Failed MSE wall at Soda Springs, Idaho (Armour et al., 2004).

(Burke et al., 2004), conducted numerical simulation using finite element procedure on a full-scale model of geosynthetic-reinforced soil structure. The wall was 2.8 m high and was reinforced with reinforcement of length 73% of the wall height at a vertical spacing of 60 cm as shown in Figure 2.11. It was subjected to Kobe earthquake motions that were scaled to an acceleration amplitude of 0.4g.

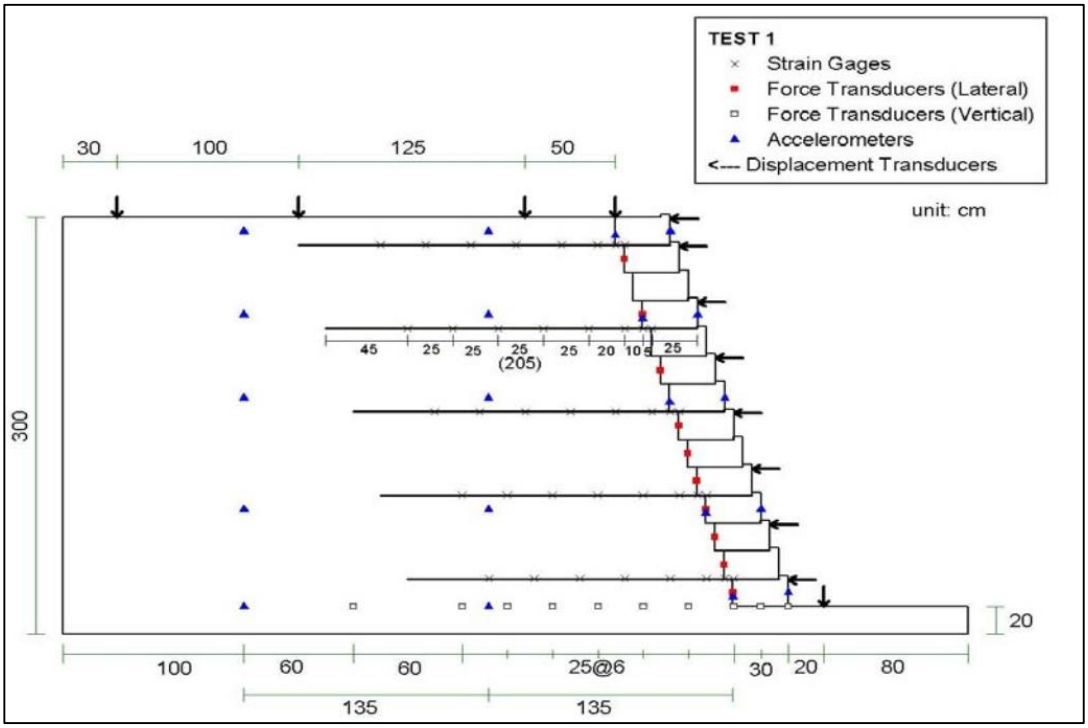

Figure 2.11: Layout of Full-Scale Shaking Table Test (Burke et al., 2004).

MSE walls are often characterized by redundancy; if the failure occurs at some of the reinforcement layers, the wall may not collapse since the rest of the reinforcement layers will be responsible for carrying increased loads. This aspect is typically ignored by previous models. A case study (Zevgolis & Bourdeau, 2008) regards this aspect by modeling a stochastic MSE wall to assess the internal stability of an MSE wall. To account for the redundancy nature, the reinforcement layers were modeled as an individual in series system. This means when a layer fails due to pullout or rupture, it will no longer contribute to resisting the internal forces. The results show that most of the failure modes occur due to pullout of reinforcements.

(Han & Leshchinsky, 2010) adopted finite difference numerical methods based on Fast Lagrangian Analysis of Continua FLAC software for the study, as well as limit-equilibrium approaches. The objective was to investigate the effect of the wall width to height ratio (W/H) and the quality of the backfill material (friction angle ϕ) on the behavior of back-to-back reinforced soil walls under self-weight Figure 2.12. The critical failure surface, the maximum required tensile force in the reinforcement as well as the active thrust behind the reinforced zone are selected as criteria for assessing the stability of the structure.

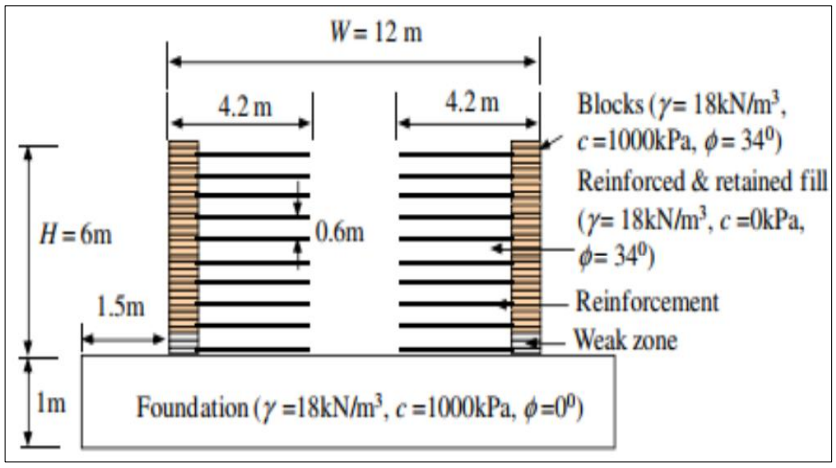

Figure 2.12: Basic model for the case W/H=2 (Han & Leshchinsky, 2010)

The following results were obtained: The analysis of the failure surface shows that the two opposite walls are treated in an independent way when they are far apart, the case W/H≥2 (D≥3.6 m), and interact with each other when they are close, The FHWA design guideline underestimates the interaction distance, When the distance between the facings becomes very small (W/H=1.4), the lateral pressure of the earth behind the reinforced zone is still existing. The required maximum tensile force in the reinforcements decreases slightly. On the other hand, when the facings are very close together, connecting the reinforcements in the middle reduces the maximum tension required at the reinforcement.

Significant wall movement may be caused by the poor quality of backfill soil and poor drainage system. (Hossain et al., 2012) investigated a case study of an MSE wall located at State Highway 342 in Lancaster, Texas, which showed a lateral movement ranged between 12-18 inches in only 5 years after construction. Several site and laboratory tests were performed to detect the cause of the movement. The results of the tested soil samples obtained from the backfill soil show that the soil contains high content of clayey sand according to the Unified Soil Classification System.

A dynamic finite element procedure, using a generalized plasticity soil model, was used to simulate the behavior of a full-scale reinforced soil retaining wall. The comparison of numerical and experimental results showed that the finite-element procedure was able to simulate the dynamic behavior very well.

(Y. Yu et al., 2017) numerical models used to predict the performance of two 3.6 m-high well-instrumented wrapped-face walls. The walls were nominally identical except that the reinforcement material in one wall was a steel welded wire mesh and in the other a biaxial polypropylene geogrid. The backfill soil was modelled using both linear and nonlinear elastic-plastic constitutive models. A general hyperbolic (nonlinear) axial load-strain-time model was used for the reinforcement as shown in Figure 2.13. The numerical results show good agreement with measured performance features for the welded wire mesh wrapped-face wall. The agreement between numerical predictions of facing displacements and maximum reinforcement loads was less accurate for the very flexible geogrid wrapped-face wall. The discrepancies are believed to be related to the unusually flexible wrapped face used in the geogrid wall construction. Numerically predicted and measured maximum reinforcement loads are compared to loads using the AASHTO reinforcement strength-based design approach (Simplified Method) and the Simplified Stiffness Method which is an empirical reinforcement stiffness-based method.

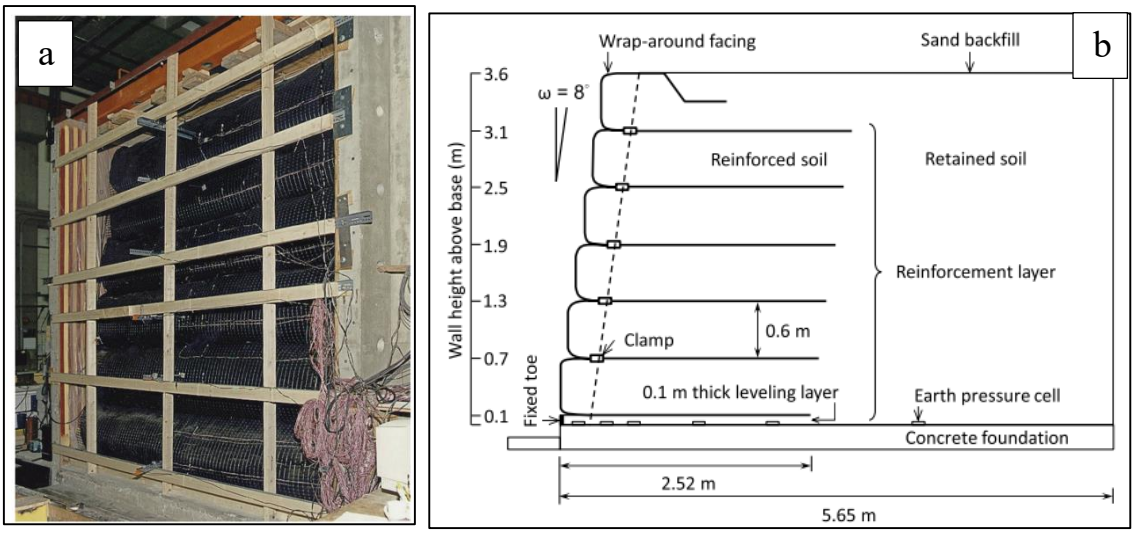

Figure 2.13: Wrapped-face wall constructed in the RMCC Retaining Wall Test Facility: (a) photograph of geogrid wall face at end of construction, and (b) cross-section view (Y. Yu et al., 2017).

(A. Hulagabali et al., 2018) studied, reinforced wall had been analyzed using finite element numerical tool PLAXIS 2D. Different types of reinforcements such as HDPE Geogrid, PET Geogrid and Ribbed steel strip were used for wall. Also, backfill and foundation soil varied with different types such as, sand, gravel, silt, clay. Walls deformations, ground settlement behind the wall and facing panel deformations were observed for different types of reinforcements, backfill and foundation soil. Ground settlements are found to be lesser for steel reinforcements behind the wall along the horizontal profile. HDPE and steel reinforcements are found to be more reliable because deformations and settlements are found to be less compared with PET Geogrid as shown in Figure 2.14. Gravel found to exert lesser wall deformation because of its good drainage property. Even the settlements behind the wall were found to be lesser for gravel material. Hence it is adopted as good backfill and foundation material. Also, the effect of surcharge loads on behavior of MSE wall was studied. It was observed that, for smaller magnitude surcharge loads, deformations observed were less.

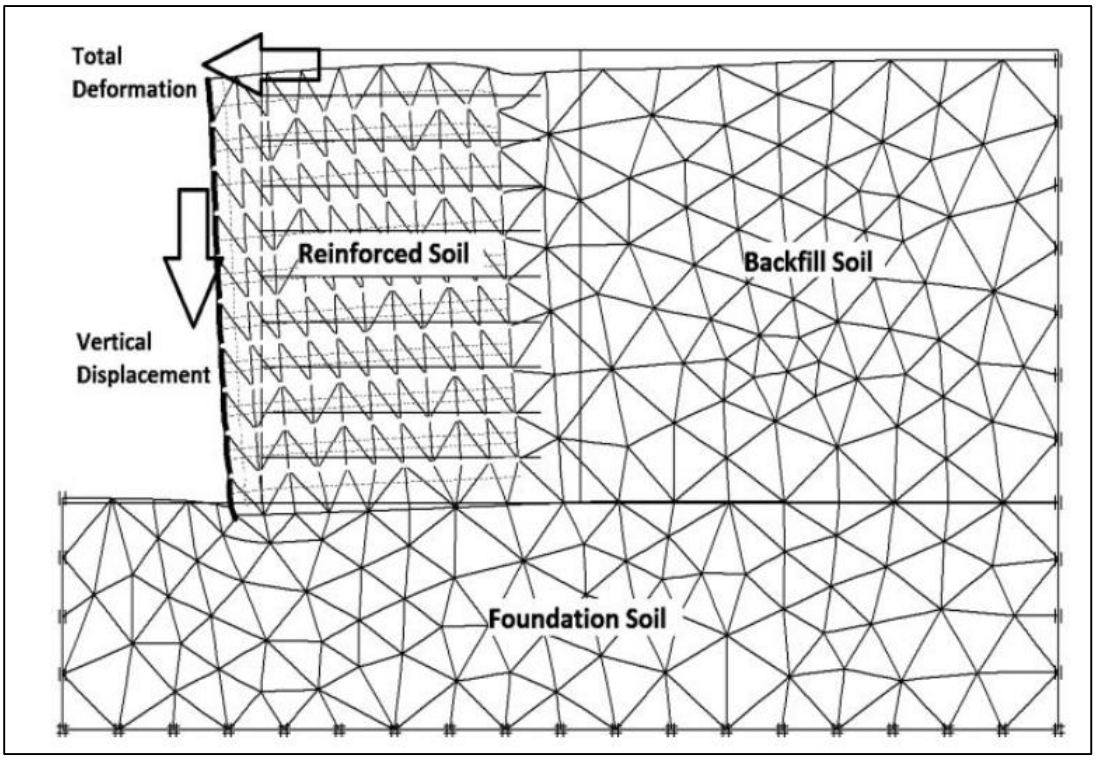

Figure 2.14: Deformations for different types of reinforcements (A. Hulagabali et al., 2018).

(Won & Langcuyan, 2020) studied a series of numerical analyses performed to investigate the compaction effect on the behavior of the MSE walls. The results showed that the horizontal displacement of the MSE wall significantly increased during construction and decreased because of surcharge load application after the construction. In addition, the strains of reinforcement increased significantly during the construction and decreased slightly because of surcharge load application after the construction as shown in Figure 2.15. Therefore, it is important to consider the compaction loads when modeling the MSE walls as shown in Figure 2.16, so that the lateral displacement at the wall facing will not be underestimated during construction and will not be overestimated because of surcharge load application after the construction.

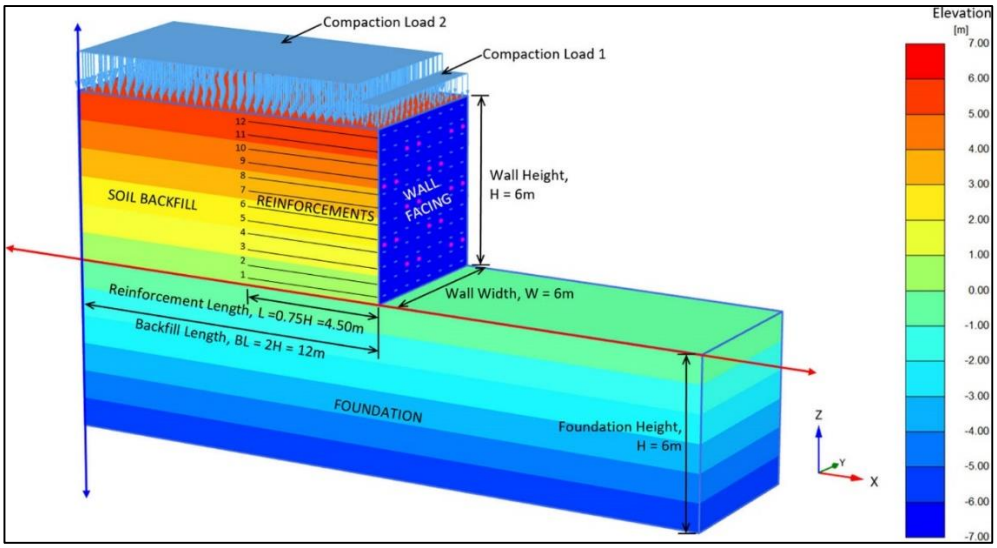

Figure 2.15: Plaxis 3D geometry model and components of MSE wall (Won & Langcuyan, 2020).

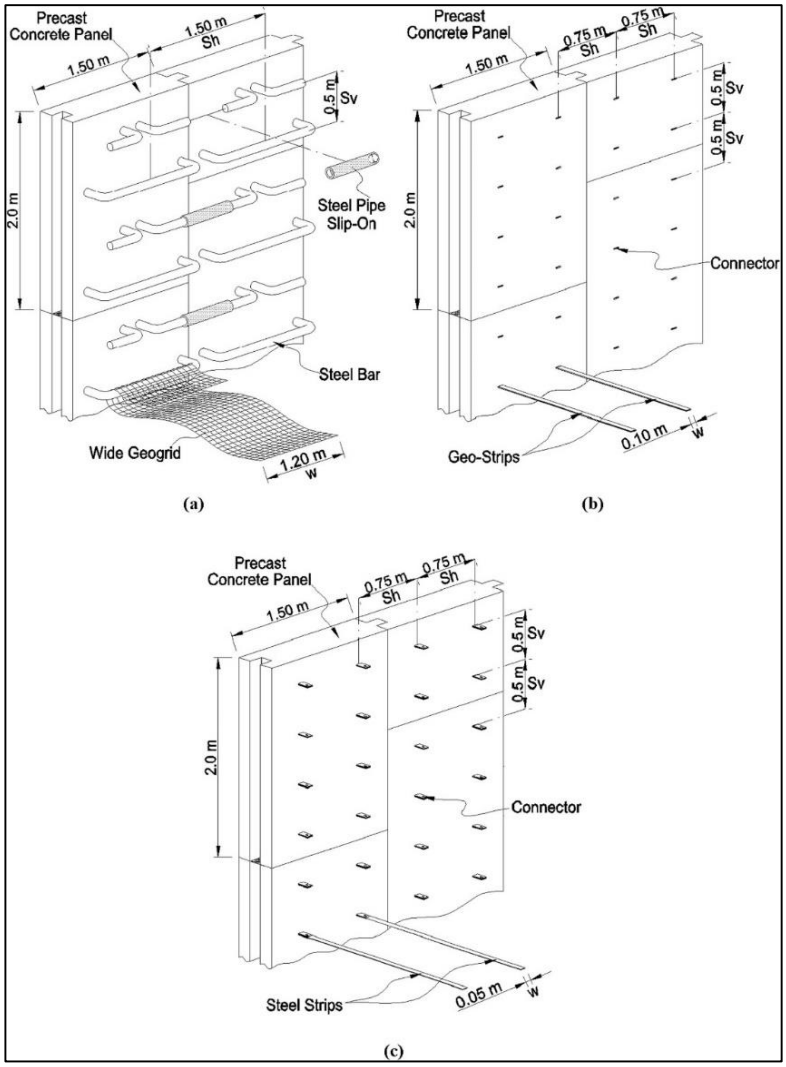

Figure 2.16: Details on reinforcement type and arrangement using precast concrete panel type wall facing: (a) Case 1, (b) Case 2, and (c) Case 3 (Won & Langcuyan, 2020).

(System & Won, 2021) GRS-IB and GRS-IBS are examined. The former uses a GRS bridge abutment with a staged-construction full height rigid (FHR) facing integrated to a continuous girder on top of the FHR facings. The latter uses a block-faced GRS bridge abutment that supports the girders without bearings. In addition, a conventional integral bridge (IB) is considered for comparison. The numerical analyses of the three bridges using Plaxis 2D under static and dynamic loadings are present as shown in Figure 2.17. The results showed that the GRS-IB exhibited the least lateral displacement (almost zero) at wall facing and vertical displacements increments at the top of the abutment compared to those of the GRS-IBS and IB. The presence of the reinforcements (GRS-IB) reduced the vertical displacement increments by 4.7 and 1.3 times (max) compared to IB after the applied general traffic and railway loads, respectively.

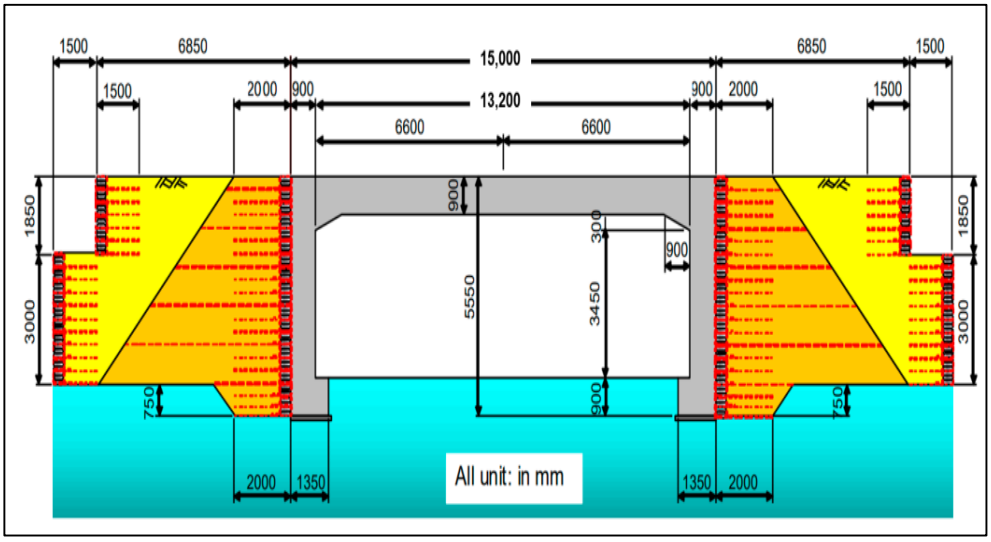

Figure 2.17: Full model scale that utilized by System and Won (System & Won, 2021).

(Hai et al., 2022) presented a series of PLAXIS numerical simulations to investigate the influences of MSE wall dimensions and geocomposite drainage capacity on seepage responses inside the protected zone of the wall. The research results indicate that the distance from the upstream water source to the drainage face (L) influences most to the maximum steady-state phreatic level (h_o) variation inside the protected zone. In comparison, the horizontal

wall dimension has more effects on (h_o) drops than vertical wall dimension as shown in Figure 2.18 and Figure 2.19.

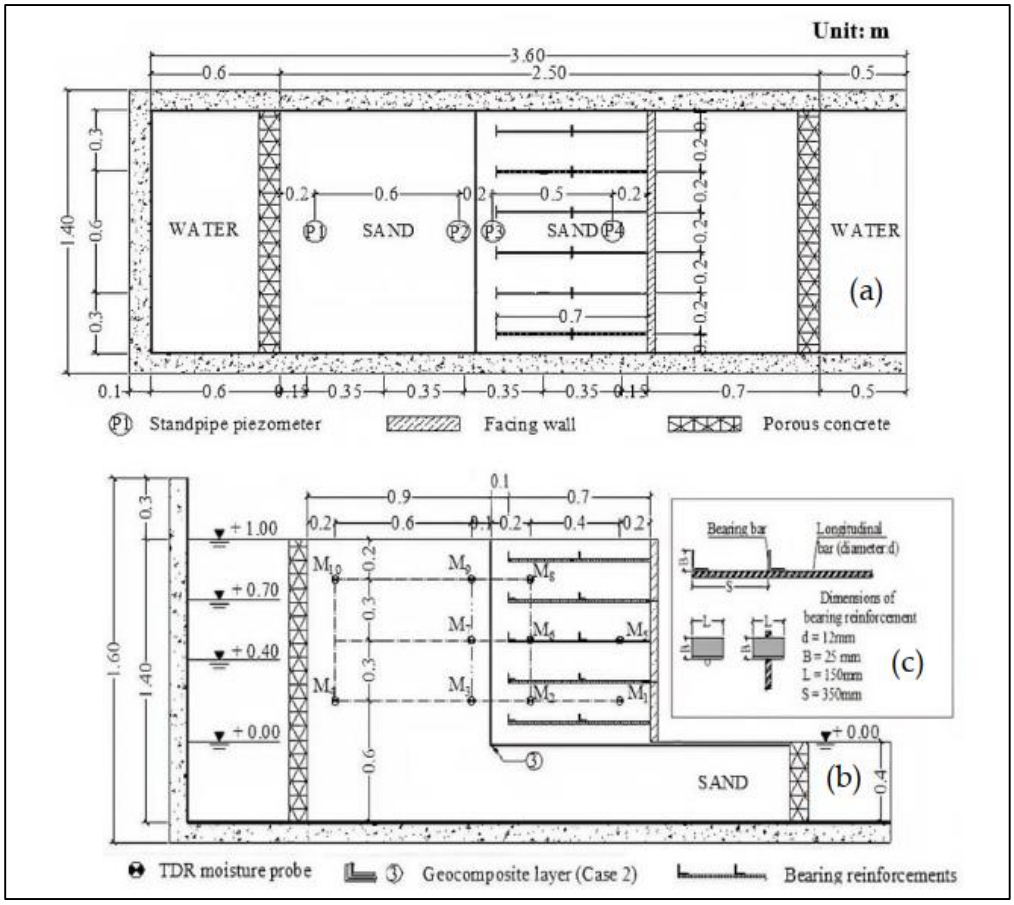

Figure 2.18: Sketch of the physical test model and its instrumentation (Hai et al., 2022).

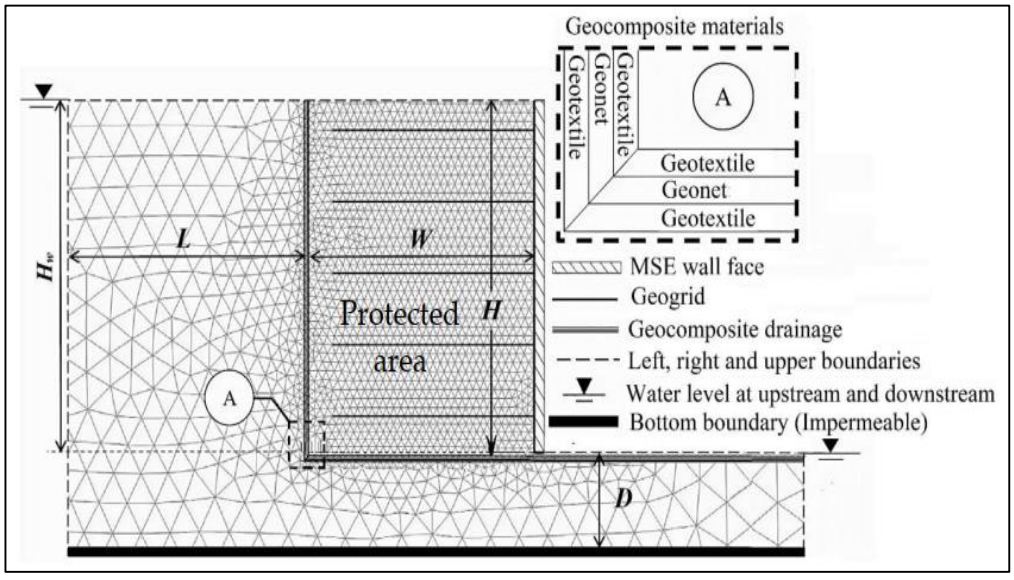

Figure 2.19: Plaxis model of mesh discretization with ho and conceptual assigned MSE wall (Hai et al., 2022).

There are many other articles that deal with MSE wall from different sides, which are not all covered in literature review part, therefore, Table 2.2. will be summarized these articles as shown blow.

Table 2.2: Summary of another related research

Ref.	Parameter investigated	Results and Observations	Conclusion
(Ng et al., 1998)	Centrifuge model tests were conducted on spread-base integral bridge abutments to simulate these temperature effects on the soil-structure interaction. Thermal expansion and contraction of the deck were modelled by imposing controlled cyclic displacements at the top of the abutment wall.	Substantial horizontal sliding and the rocking of the abutment due to soil densification and "strain" ratchetting were observed. The measured lateral earth pressure increased with the amplitude of the displacements into the fill (in the passive sense) and the number of cycles, but at a decreasing rate. For the ultimate limit state and the 1 in 120 years return event, the measured lateral earth pressure coefficient was 3.7 and 4.2 for the abutment backfilled with dense and loose sand respectively.	The measured bending moments varied fairly linearly with depth, rather than varying as a cubic function with depth as would be expected for a relatively flexible wall subjected to a triangular distribution of lateral pressure. The measured value appeared to reach the design bending capacity of the reinforced concrete wall and base for the 1 in 120 years return event.
(Sankey & Anderson, 1999)	It is noted that galvanized steel reinforcements without a cathodic protection system have been the predominant choice since 1990.	The discrete metallic reinforcements used in Reinforced Earth structures lack electrical continuity, so the reinforcements act as individual short length conductors instead of part of a continuous network.	Select backfill that conforms to the standard mechanical and electrochemical requirements for Reinforced Earth structures provides additional resistance to the flow of stray currents.

Table 2.2: Summary of another related research (continued)

(Brabant , 2001)	The use of MSE walls for direct support (Abutment resting on a spread footing atop the MSE structure) and indirect support (Abutment on piles with the MSE structure supporting the fill) of bridge structures is well documented.	Pile Supported Abutments are designed as a simple MSE retaining wall, with the vertical loads from the bridge being imparted to the piles. Horizontal bridge loads may be resisted by additional earth reinforcement added to the pile cap. MSE structure.	Nearly thirty years of experience in the implementation of MSE walls and abutments successfully demonstrates the applicability and performance of this technology.
(Ellis & Springman, 2001)	Full-height piled bridge abutments constructed on soft clay are prone to soil–structure interaction effects. A series of geotechnical centrifuge tests of this type of structure has been undertaken, and an accompanying series of plane strain finite element analyses are reported.	Some aspects of the structure do not conform to a plane strain analysis (most notably the piles), and the methods used to incorporate this soil–structure interaction are described. Success of the methods is illustrated by good comparison with the centrifuge test results, and the numerical analyses revealed interaction effects which could not be specifically identified in the centrifuge tests.	The soil–structure interaction between the embankment and retaining structure was of greatest interest, and this aspect of behaviour is more readily analysed in plane strain. Thus plane strain FEM analyses were undertaken, and the results were compared with data from corresponding geotechnical centrifuge tests.

Table 2.2: Summary of another related research (continued)

(Stulgis, 2005)	Develop selection guidelines, soil parameters, testing methods, and construction specifications that will allow the use of a wider range of reinforced fill materials within the reinforced zone of mechanically stabilized earth (MSE) walls than is currently practiced.	State transportation agency and private industry responses to a "survey of the current practice" for MSE backfill are discussed. New guidelines for MSE backfill are recommended, and economic incentive to relax current MSE wall reinforced fill specifications is presented.	The field test walls will be fully instrumented, to provide answers to a wide range of technical questions
(Leshchinsky, 2005)	Failures of MSE wall and slope structures are frequently attributed to poor drainage and the presence of water within or behind the reinforced zone.	The water combined with low permeability backfill may, and often does, lead to poor performance (excessive deformation or actual collapse) of MSE structures. It also indicates that it is possible to use such low quality backfill provided that a properly designed drainage system is installed.	Prefabricated composite sheet drains can provide a solution enabling rapid drainage while keeping costs down. This research should produce a computerized design to enable a rational incorporation of such drains in MSE structures.
(Hatami & Witthoeft, 2008)	The potential benefit of placing a panel of compressible (i.e. expanded polystyrene) geofoam behind the reinforced zone of MSE walls is investigated using a numerical modeling approach. A panel of geofoam is placed immediately behind the reinforced zone during the construction phase of an idealized plane-strain reinforced soil segmental wall model.	It is shown that placing geofoam behind the reinforced zone can reduce the maximum lateral earth pressure behind this zone by as much as 50% depending on the geofoam thickness and stiffness values. The magnitudes of total lateral earth force (i.e. the resultant force of the lateral earth pressure distribution) behind the reinforced mass and overturning moment about the wall toe are shown to decrease by 31% and 26%, respectively.	The findings point to a significant potential for using geofoam to reduce the lateral earth pressure demand on MSE walls (i.e. as opposed to rigid retaining walls examined previously) and thereby increase their serviceability and their factors of safety against external instability.

Table 2.2: Summary of another related research (continued)			
(Tavakolian & Sankey, 2009)	(1) a standalone conventional MSE design for the narrow wall section, (2) a direct attachment design with anchors from new wall fascia to an existing stabilized face (3) a "Sandwich Connection" design concept using overlapping reinforcements between the new wall fascia and existing stabilized face.	The Sandwich Connection concept is a preferable design alternative for construction of a narrow wall section when space is available between new and existing wall facings.	It is noted that although the design cases in this paper were modeled for an original MSE wall face, it is possible to consider a similar connection type for other stable retaining wall or anchored facings
(Rafalko et al., 2010)	Describes a life cycle assessment (LCA)	The assessed impact categories are energy consumption, abiotic depletion, climate change, photo-oxidant formation and acidification. For comparison purposes, the environmental impact of a gravity wall is also evaluated using similar methods developed from the LCA study.	MSE wall solutions have long since proven to hold major advantages over other solutions for retaining wall applications such as less cost, quick construction and reduced labor and construction equipment needs.

Table 2.2: Summary of another related research (continued)			
(David & Forth, 2011)	Integral Abutment Bridges (IAB) Various soil constitutive models have been used in studies of soil-structure interaction in this kind of structures by researchers.	This paper is an effort to review the implementation of various finite elements model which explicitly incorporates the nonlinear soil and linear structural response considering various soil constitutive models and finite element mesh.	For instance, the need to study the behaviour of the structural elements of integral abutment bridge under environmental loading has been highlighted by Jimin Huang et.al, 2008. Youseff Dehne and Sophia Hassiotis also stated that provisions for accurate soil-structure interaction are needed.
(Kibria et al., 2012),	The performance of MSE wall strongly depends on the backfill soil condition. MSE wall located at state highway 342, Lancaster, Texas. The top of the wall has moved as much as 300 mm to 450 mm at some locations.	The soil samples collected from backfill zone were classified as clayey sand (SC) according to Unified Soil Classification System (USCS). Laboratory testing conducted on the collected soil samples showed 29% to 39% of fine content in backfill soil. RI was performed twice during the investigation period to monitor the moisture condition within the backfill soil.	Increase in moisture content along profiles was observed during investigation period. The rate of wall movement also increased from 1 mm/month to 4 mm/month during this period.

Table 2.2: Summary of another related research (continued)

(Hossain et al., 2012)	An extensive site and laboratory investigation testing program was conducted to determine the possible causes of the MSE wall movement. The site investigation included soil test boring and resistivity imaging (RI). Perched water zones were identified at a few locations in the backfill area using RI.	The bulging of the MSE wall facings was observed where the perched water zones were located. The test results indicated the backfill soil was clayey sand according to the Unified Soil Classification System. Based on the test results and analyses, it was determined that the presence of high fine content may have caused the excessive movement of the MSE wall.	The actual movement of the MSE wall and the obtained movement from the model were in good agreement.
(Hardian to et al., 2013)	Increase the water storage capacity of a reservoir. Evaluation of the wall was performed using a conventional AASHTO Allowable Strength Design method and considers fully submerged and rapid drawdown conditions, as well as high seismic acceleration.	The use of gravel backfill, while effective in minimizing the hydrostatic pressure applied to the MSE wall, has caused backfill compaction and wall alignment challenges during construction.	The presence of a rock backface behind the wall and the non-uniform lengths of soil reinforcement contributed to the challenges to maintain a vertical wall facing. Despite some construction challenges, once fully erected, the MSE walls are stable.

Table 2.2: Summary of another related research (continued)

(Zheng et al., 2014)	In the numerical simulations, soil-block, block-block, and soil-abutment interactions were simulated using interface elements, and soil-geogrid interactions were simulated using cable elements.	The MSE bridge abutment has a max lateral displacement of 36.4 mm for the lower wall and an average settlement of 37.6 mm for the abutment structure. Application of the bridge load significantly increased lateral earth pressures on the lower wall and vertical pressures at soil foundation level and under the abutment structure. The max tensile force in the reinforcement is 8.2 kN/m for the lower wall, which is well below the tensile yield strength.	The static behavior of a realistic MSE wall-supported bridge abutment was simulated using the finite difference program FLAC. The abutment structure was subjected to a vertical pressure of 200 kPa to simulate the load transmitted from bridge superstructure to the reinforced soil mass for the lower wall.
(Kibria et al., 2014)	As a part of the forensic investigation, two inclinometers were installed at the site to monitor any additional movement of the MSE wall. The inclinometer results suggested that the wall continued to move at an average rate of 4.5 mm/month during the investigation period. A finite-element (FE) program was used to simulate horizontal displacement and stability of the MSE wall.	It was observed that the numerical modeling results were in good agreement with inclinometer results. A parametric study was conducted to identify the effects of soil reinforcement on horizontal movement at varied wall heights and backfill conditions. Numerical analyses results indicated that the effect of reinforcement stiffness was not significant at a wall height of 4 m compared with 8 and 12 m. The wall movement varied from 74 to 29 mm for an increase in reinforcement stiffness from 250 to 42,000 kN/m at 1.0H reinforcement length.	The variations in displacement with reinforcement lengths suggested that substantial reduction in displacement occurred for an increase in length-height (L/H) ratio from 0.5 to 0.7. FE modeling results were used for sensitivity analysis employing a statistical analysis program. Based on the analyses, reinforcement length and stiffness were identified as influential factors for the horizontal displacement of MSE walls at a specific height.

Table 2.2: Summary of another related research (continued)

(Xie & Leshchinsky, 2015)	The effects on stability are evaluated for two scenarios: (1) a "top-down" approach where reinforcement spacing density is progressively increased from the top of the wall downwards and (2) a "bottom-up" approach where the spacing density is progressively increased from the toe of the wall upwards.	Presented within this study are the results of comprehensive parametric analysis varying reinforcement spacing, reinforcement strength and footing location, highlighting the stability benefits of top-down and bottom-up reinforcement density approaches. Placement of dense reinforcements near the crest of surcharge-supporting walls had a notable benefit for stability, while placement of dense reinforcements at the toe improved stability for walls without a surcharge.	Hence, reinforcement spacing tailored to specific wall functions may provide significant economic benefits when considering reduced reinforcement needs, lessened tensile strength requirements, or shortened bridge deck length based on surcharge placement – all by concentrating reinforcement density at a specific height of a structure.
(Tarawneh et al., 2018)	In this paper, the results of a large-scale inspection program are analyzed to identify the most frequent MSE wall problems, and a new inspection rating system procedure is proposed. A risk assessment method to determine the overall rating of the MSE wall after inspection and suggests a course of action.	The annual average daily traffic (AADT) modifier (MT) is the total volume of vehicle traffic on a highway or road for a year divided by 365 days. The AADT is used to estimate how busy the road is. The MGRS is calculated by modifying the GRS using three modifiers for assessing the potential risks to public motorists' safety. The modifiers are based on the AADT of the bridge supported by the MSE wall abutment and on the age and height of the MSE wall abutment. Based on the MGRS value, the MSE wall is categorized using eight proposed categories.	This risk assessment method is proposed as a useful tool for field inspectors to propose a course of action on the basis of the MSE wall inspection results. To perform the inspection and use the risk assessment method, inspectors should have experience in the design and construction of MSE walls.

Table 2.2: Summary of another related research (continued)

(Sravanam et al., 2019)	Back-to-back geosynthetic-reinforced retaining walls are commonly used as approach embankments for bridges and flyovers. Compaction and surcharge loads should be incorporated in the model to understand the realistic behavior of mechanically stabilized earth (MSE) retaining walls through numerical modeling.	Effects of compaction and surcharge loads on back-to-back walls were analyzed. In addition, the effect of reinforcement stiffness on the behavior of these walls was evaluated. In this study, comparative study on the behavior of connected and unconnected walls was also examined. The lateral pressures mobilized were explained through occurrence of the arching phenomenon at the facing and at the end of the reinforcement zone.	Plots showing the variation of lateral earth pressure coefficients and lateral deformations versus normalized depth of wall are presented. Maximum tensile forces in the reinforcements along the depth of wall are also analyzed. The lateral pressures at the facing appear to be unaffected with W/H ratio.
(Fiorentino et al., 2021)	Integral abutment bridges (IABs) To develop a better understanding on the seismic behaviour of IABs, an extensive experimental campaign involving over 75 shaking table tests and 4800-time histories of recorded data, $\varepsilon_a = \mathrm{M_d} \cdot t_w/(2 \cdot D_W)$	(a) developing new scaling procedures for physical modelling of IABs, (b) investigating experimentally the potential benefits of adding compressible inclusions (CIs) between the abutment and the backfill (c) exploring the influence of different types of connection between the abutment and the pile foundation.	Results indicate that the CI reduces the accelerations on the bridge deck and the settlements in the backfill, while disconnecting piles from the cap decreases bending near the pile head.
(Weerasekara, n.d.)	This paper discusses the limitations of assuming that the weakest reinforcement governs the stability of the entire reinforced soil mass, particularly in relation to displacement-controlled failure mechanisms such as pullout. Other limitations of the current practice in estimating the pullout resistance are also discussed.	To overcome this limitation, the Soil Reinforcement Interaction method (Weerasekara et al. 2017) is introduced, which explicitly accounts for the interaction between the reinforcement and backfill using a non-empirical analytical model. The method allows to compute a factor of safety for the entire reinforced soil mass and not only at each reinforcement level similar to the traditional practice.	Two full-scale instrumented walls reinforced with smooth steel strips and high-strength nylon strips are discussed.

2.7. Summary and Concluding Remarks

In most of the cases that have been drawn in literature review focus on:

- The previous study mostly focuses on the soil properties and the way of improving the poor bridge backfill soil, and some of them studying the effect of soil compaction on the behavior of MSE wall. As well as the effect of changing backfill and foundation soil by different types such as (sand, gravel, silt and clay)
- Many researchers try to create a more stable MSE wall by changing the dimensions of the Walls (wall width and height ratio).
- However, most of the cases that have been studied previously used Integral abutment bridges (IABs), which are defined as simple or multiple span bridges in which the bridge deck is cast monolithically with the abutment walls.
- Also, many types of reinforcement have been investigated experimentally and numerically by using PLAXIS 2D such as (HDPE geogrid, PET geogrid, ribbed steel strips. Some of the studies investigated the effect of changing the strips length on the behavior of MSEW.
- In most of the cases, the researchers investigate the effect of surcharge load on unreinforced soil.

Based on the obtained gap for the previous research study, it has been noticed that there is no specific study that investigates the shape of strips reinforcement and the width of strips, therefore, the current study focusses on those two parameters.

The present work presents a comprehensive investigation numerically and experimentally for the effect of surcharge load and the location of the load on the behavior of reinforced soil.

CHAPTER THREE

EXPERIMENTAL MODEL FABRICATION

CHAPTER THREE

EXPERIMENTAL MODEL FABRICATION

3.1. Introduction

In this chapter, the experimental work including the details of laboratory model dimensions, reinforcement arrangement, material properties (cement, fine and coarse aggregate, steel reinforcing bar, Geosynthetics Reinforcement Strip), preparation of the specimens, testing procedure and manufacturing universal machine are presented.

3.2. Laboratory Model

3.2.1. Materials

The materials utilized in this study are readily accessible within the local vicinity and are extensively utilized for the construction of pavements in Iraq.

3.2.1.1. Cement

Resistant Cement (KAR) was used in casting all tested specimens. The chemical and mechanical properties of the cement used have been tested in Construction Material Laboratories at AL-Mustaqbal University. The mechanical and chemical properties of the used cement are given in

Table 3.1 and Table 3.2, respectively. These properties have been checked according to the Iraqi specification limits (IQ. S No.5/1984) (Iraqi Specification No.5 -1984, 2010; Specification, 1984) for resistant cement.

Table 3.1: Mechanical properties of cement.

Mechanical Properties	Test results	IQ. S No. 5/1984
Initial setting time (min) Final setting time (min)	70 255	≥ 45 min ≤ 600 min
Fineness (m^2/kg)	303	≥ 250 m2/kg
Compressive strength, MPa 3 days 7 days	 17.39 27.06	 ≥ 15 MPa ≥ 23 MPa

Table 3.2: Chemical analysis of cement.

Chemical composition		% By weight.	Limits of IQ. S No.5/1984
Lime	CaO	61.25	------
Silica	SiO_2	19.78	------
Alumina	Al_2O_3	3.41	------
Iron oxide	Fe_2O_3	4.8	------
Sulfate	SO_3	2.29	≤ 2.5 % If *C3A*< 5% ≤ 2.8 % If *C3A* > 5%
Magnesia	MgO	1.72	≤ 5%
Ratio	C_3A	0.914	≤ 3.5%
Loss on ignition	L.O. I	2.42	≤ 4%
Insoluble residue	I.R	0.85	≤ 1.5 %
Lime saturation Factor	L.S. F	0.953	(0.66–1.02) %

3.2.1.2. Fine Aggregate

In this work, natural sand was used as fine aggregate. The chemical and mechanical properties of sand are given in Table 3.3. The fine aggregate used has gradation that lies within the upper and lower limits of the ASTM C33/C33M specification (C. ASTM, 1986) and Iraqi specification (IQ.S 45/1984) zone (2), as shown in Table 3.4. Fine aggregate has been tested at Al-Mustaqbal University in the Construction Material Laboratories.

Table 3.3: Chemical and mechanical properties of fine aggregate.

Properties	Test results	IQ. S No. 45/1984 zone (2)
Specific gravity	2.6	------
Fineness modulus	3.8	≤ 5 %
Sulfate content SO_3	0.22%	≤ 0.5 %
Absorption	2%	------

Table 3.4: Grading of fine aggregate.

Sieve no.	Sieve size (mm)	Passing %		
		Fine aggregate	IQ. S No. 45 Zone (2)	ASTM C 33/C 33M
3/8 in	9.5	100	100	100
NO.4	4.75	91	90 - 100	90 - 100
NO.8	2.36	83	75 - 100	80 - 100
NO.16	1.18	74.8	55 - 90	50 - 85
NO.30	0.60	57.2	35 - 59	25 - 60
NO.50	0.30	24.2	8 - 30	5 - 30
NO.100	0.15	7.2	0 - 10	0 - 10

3.2.1.3. Coarse Aggregate (Gravel)

This work used coarse aggregate with a maximum aggregate size of 19 mm. The coarse aggregate was cleaned and washed with drinkable water, then dried before use. The mechanical and chemical properties of coarse aggregate are given in Table 3.5. The sieve analysis of coarse aggregate lies within the lower and upper limits of the Iraqi specification (IQ.S No.45/1984) (IQS, 1984), as shown in Table 3.6.

Table 3.5: Mechanical and chemical properties of coarse aggregate.

Properties	Test results	IQ. S No. 45/1984
Specific gravity	2.66	------
Sulfate content SO3	0.03%	≤ 0.1 %
Absorption	0.6%	------
Clay content	0.2%	≤ 3%

Table 3.6: Grading of coarse aggregate.

Sieve Size (mm)	Passing %	
	Coarse aggregate	IQ. S No. 45/1984
37.5	100	100
19	100	100 - 95
9.5	43	60 - 30
5.0	3	10 - 0

3.2.1.4. Water

Tap water sourced from the university lab had been employed in all concrete mixes. The water used in the curing specimens was devoid of turbidity, salts, and organic material.

3.2.1.5. Reinforcement Steel rebars

The retained wall, foundation, and precast concrete panel incorporate deformed steel bars measuring bar diameter= Ø12 mm as link reinforcement between the short and longitudinal directions. The Strength of Materials laboratory at Al-Mustaqbal University has carried out testing on steel bars. Table 3.7 presents the mechanical properties of the reinforcement bars obtained through the use of a digital computer in conjunction with the testing machine as shown in Figure 3.1 (A. ASTM, 2005).

Table 3.7: Requirements and test findings of steel bars reinforcement.

Nominal Bar Diameter (mm)	Actual bar diameter (mm)	Area (mm^2)	Yield Stress f_y (MPa)	Ultimate strength f_u (MPa)	Elongation (%)
12	11.9	113.04	677	772	14

Figure 3.1: Tested steel reinforcing bar specimens.

3.3. Mechanical Properties of Hardened Concrete

3.3.1. Compressive Strength Test

The method for determining compressive strength, illustrated in Figure 3.2, was conducted in accordance with (BS. 1881: Part 116) (B. Standard, 2009) and (ASTM C 39-21) (Committee, 2021). The study involved subjecting cubes measuring 15x15 cm and cylinders measuring 15 x 30 cm to compression testing using a hydraulic machine with a capacity of 1600 kN. For each test, the mean value of three cubes and cylinders was utilized.

$$\mathbf{F} = \frac{\boldsymbol{P}}{\boldsymbol{A}} \tag{3.1}$$

where:

F=The compressive strength (MPa)

P=Maximum load (or load until failure) to the material (N)

A=A cross section of the area of the material resisting the load (mm^2)

Figure 3.2: Photograph of compressive strength testing.

3.3.2. Splitting Tensile Strength (STS) Test

The methodology for ascertaining the STS adheres to the guidelines specified in the (ASTM C496-2017) requirements (Aggregates, 2017). Cylinders with dimensions of 10X20 cm were utilized as shown in Figure 3.3. To ensure proper testing conditions, two slender plywood strips were interposed between the sample and the lower and upper bearing blocks of a hydraulic compression machine with a capacity of 1600 kN. The mean of three cylindrical objects was computed during each trial.

$$f_{spt}\ \textbf{(Mpa)} = \frac{2F}{\pi D\ L} \qquad (3.2)$$

where:

F: is applied force (N),

D: is the diameter of a specimen (mm).

L: is the length of specimen (mm).

Figure 3.3: The test of splitting tensile strength.

3.3.3. Test of Flexural Strength

Prisms made of concrete with dimensions of 10x10x40 cm are manufactured using the procedure outlined in ASTM C 78-2018 (A. ASTM, 2018). The calculation of flexural strength, which is represented by the modulus of rupture, involves utilizing data acquired from a basic beam subjected to a two-point load, as depicted in Figure 3.4.

Figure 3.4: Test of flexural strength by two-point load.

The rupture modulus for every reading is determined by calculating the mean of the test outcomes for three samples. The determination of the flexural strength of samples is achieved with a precision of 0.05 MPa by means of the subsequent equation:

$$\boldsymbol{ft = \frac{PL}{bd^2}} \tag{3.3}$$

3.4. Soil Tests

3.4.1. Grain Size Analysis Test

Test of the volume gradient of the clay, silt and sand fractions using dry analysis using sieve analysis. The granular size analysis is intended to distribute the granules according to their size (Al-Ashw, 1991). Before proceeding with the dry sieve analysis, soil samples with all their components are taken on a sieve (No. 200) to separate the coarse granules (sand) from the mud. This method determines the exact quantity and separates the coarse and fine soil components. The method used in this American Standard (ASTM D1140-17) on the use of water or a dispersant to separate and remove fine materials from other minerals (Younas, 2017). After separating the coarse (sand) and mud soil components and drying

them, the dry analysis method with sieves is used on the coarse samples and using sieve analysis, Figure 3.5 and according to the American Standard (A. ASTM, 2017).

Figure 3.5: Particle size analysis by sieve analysis.

3.4.2. Atterberg Limits Test

The liquid limit (L.L.) test was carried out in the laboratory of soil mechanic, Al-Mustaqbal University, using the (Gassagrandi) device, which is a copper pot that can be moved electrically, and the number of strokes recorded by a counter linked to the device, as shown in Figure 3.6.

(Plastic Limit "P.L.") is determined by rolling a spherical piece of soil on a glass plate in order to reduce its German content until it reaches the required limit. This is done through several attempts until the soil wick begins to crumble, then its diameter is (3 mm), and it is calculated moisture content, which represents the limit of plasticity.

The plasticity index (P.I.) is the range of moisture content in which the soil remains in the (plastic) state, meaning that it is the difference between the highest and lowest percentage of water within which the soil remains in the state of plasticity. Therefore, the plasticity coefficient is numerically equal to the difference between the liquidity limit and the plasticity limit.

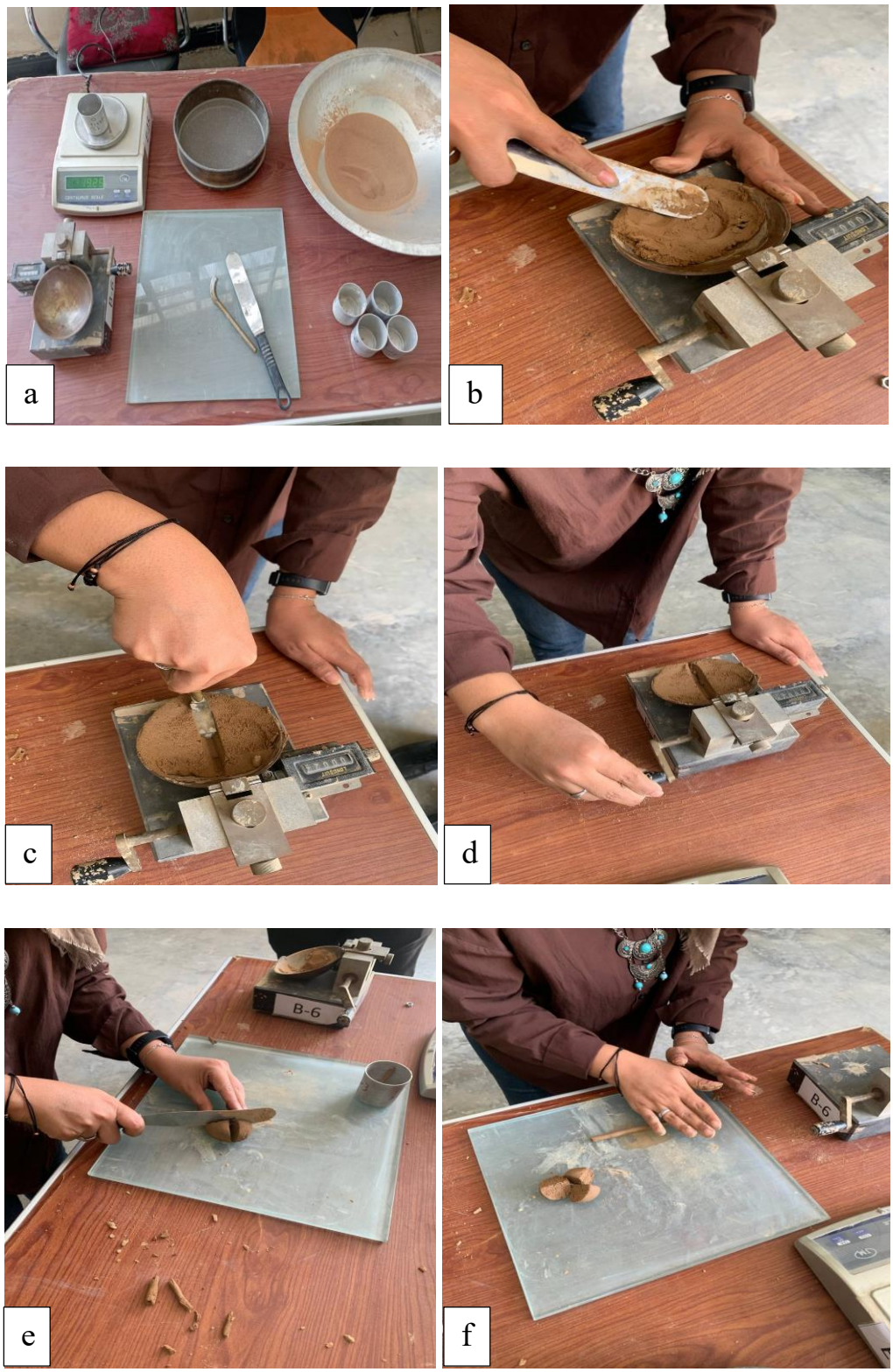

Figure 3.6: Stages of work on the Casagrande device to find (L.L.) and (P.L.).

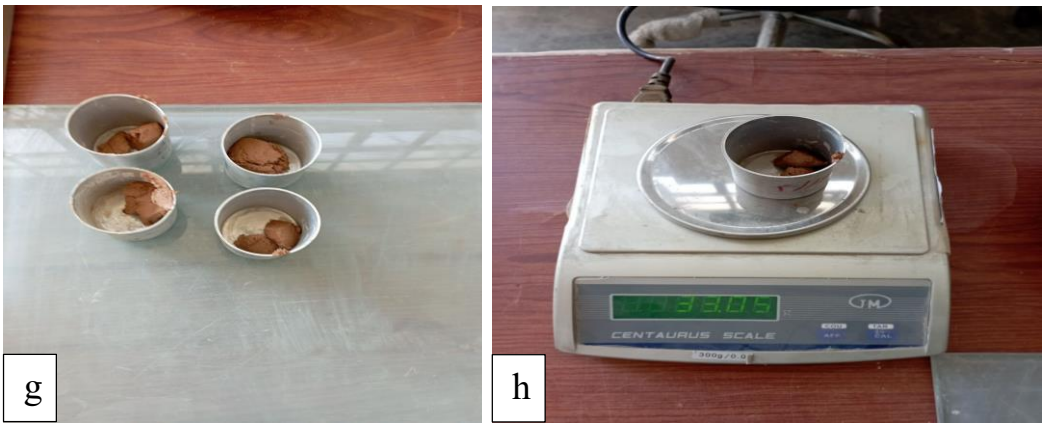

Figure 3.6: Stages of work on the Casagrande device to find (L.L.) and (P.L.) (continued).

3.4.2.1. Procedure

1. Subsequently, the vertical clamp is disengaged to facilitate the cone's insertion into the soil paste, under the weight of the cone, for a duration of 5 sec. The penetration of the cone is measured to the nearest millimeter after a duration of five seconds.
2. Remove the cone from the soil paste and meticulously cleanse it to prevent any potential abrasions.
3. Subsequently, add increments of water or soil till the test portion achieves a dense and uniform consistency. Upon the addition of water or soil, the penetration range magnitudes of roughly 15 to 25mm are achieved.
4. Obtain the weight of a diminutive aluminum bowl as W1.
5. In order to determine the amount of moisture, a 10 g specimen should be extracted from each attempt. The specimen from the penetrated area ought to be gathered using a cone and subsequently weighed to obtain (W2), which represents the combined weight of the specimen and the bowl.
6. Perform the steps a minimum of three times in succession. During these three instances, it is expected that the penetration value will remain within the approximate range of 15 to 25mm. Following each

penetration, it is recommended to eliminate the soil paste from the cup and subsequently replenish it with either soil or water. Additionally, the cup should undergo a washing and drying process.

7. The samples should be dried in an oven at a temperature of 110 degree centigrade, after which the weight of the bowl and dry the specimen should be measured to obtain (W3).

According to Barasa (2014), the amount of moisture can be calculated using the formula:

$$w=\frac{W_2-W_3}{W_3-W_1} *100\% \quad (3.4)$$

W_1: Weighing before drying.

W_2: Weight after drying.

W_3: W_1-W_2

3.4.3. Compaction Test

The purpose of this laboratory examination is to establish the correlation between the amount of moisture and the soil dry density under a particular compaction energy. The term "compaction energy" refers to the quantity of mechanical energy, which is exerted on a given soil mass. Various techniques are available for soil compaction in the field, such as static load compaction, vibration, kneading, and tamping. The lab will utilize the Proctor test, a tamping or impact compaction technique, which was originally developed by R. R. Proctor in 1933. The equipment and technique employed will be consistent with Proctor's original approach. The ASTM D698 outlines the standard testing procedures for determining the laboratory compaction properties of soil by employing a standard effort as shown in Figure 3.7.

- The process of compacting soil for engineering purposes, such as in embankments, foundation pads, and road bases, is aimed at achieving

desirable engineering characteristics including permeability, compressibility, or shear strength.

- The engineering properties of foundation soils are frequently enhanced through compaction.
- The utilization of the lab compaction tests serves as a fundamental approach to ascertain the percentage of compacting and the amount of water necessary to attain the desired engineering characteristics. Additionally, it facilitates the regulation of construction activities to ensure that the needed compaction and water amounts are attained.
- Calculate the quantity of water to incorporate by utilizing the subsequent techniques:

$$\text{Water to add (in ml)} = \frac{(\text{ Soil mass in gram }) \times 8}{100} \quad (3.5)$$

- Use the following equation to calculate the dry density utilizing the amount of water and wet density calculated in step 1:

$$\rho_d = \frac{\rho}{1+w} \quad (3.6)$$

whereas:

w = amount of water in percent split by 100, and ρ = wet density g/cm^3.

- The dry density magnitudes should be plotted on the y-axis, while the amount of moisture should be plotted on the x-axis. Construct a continuous and differentiable curve that passes through all the given data points without any abrupt changes in direction or slope.
- Please plot a curve of complete saturation, also known as the "zero air voids curve," on the same graph. The formula provided can be utilized to calculate the amount of moisture and dry density magnitudes necessary for constructing the curve:

Whereas:

$$w_{\text{sat}} = \left(\frac{\rho_w}{\rho_d} - \frac{1}{G_s}\right) \times 100$$
$$\text{or } \rho_d = \frac{\rho_w}{\left(\frac{w}{100} - \frac{1}{G_s}\right)} \quad (3.7)$$

ρ_d (g/cm^3) = dry soil density.

G_s = specific soil gravity.

ρ_w (g/cm^3) = water density (about 1)

w_{sat} = The percent of moisture amount for wholly saturation.

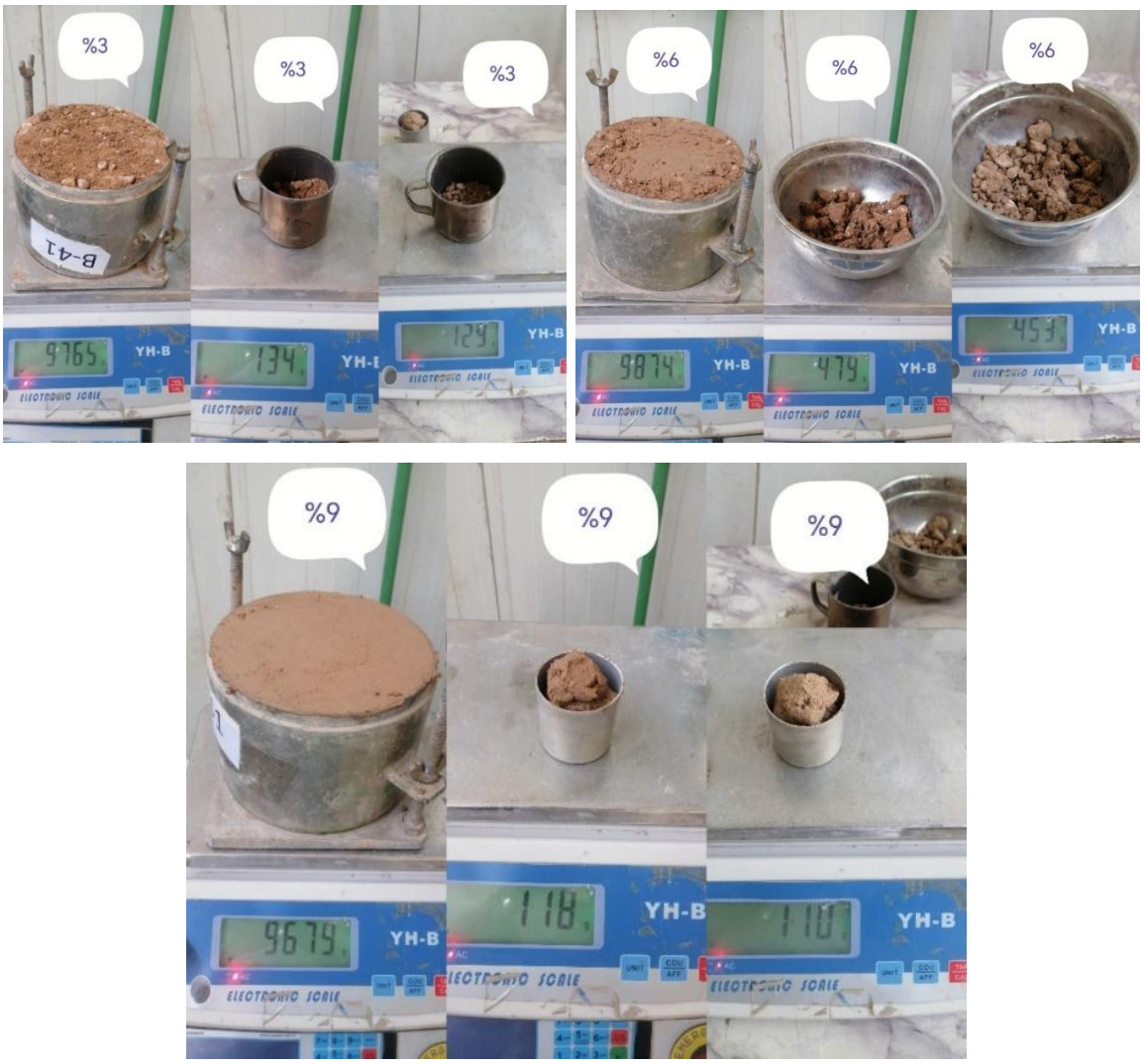

Figure 3.7: Soil compaction test for three different water ratios.

Figure 3.7: Soil compaction test for three different water ratios (continued).

3.4.5 Soil Density by Sand Cone Test

The Sand Cone Density test is a dependable and precise methodology that has been extensively employed to determine the in-situ density of soils. The methodology is explicated in the ASTM D1556 / AASHTO T 191 standard (AASHTO 2nd, 1998; D1143, 2007). At the testing location, a template in the form of a flat base plate featuring a circular aperture measuring 6.5 inches (165.1 millimeters) in diameter is employed to excavate the necessary quantity of densely packed soil material. The determination of the overall volume to be excavated is contingent upon the max particle size of the soil, which may vary and potentially reach a magnitude of 0.1 cubic feet (equivalent to 2,830 grams per cubic centimeter). Accessories for density testing, including mallets, scoops, chisels, and specimen bags, are utilized in the process of excavation. The entirety of the excavated material is meticulously gathered and preserved within a hermetically sealed receptacle.

The Sand Cone Density Apparatus, which has been pre-weighed, is placed in an inverted position onto the plate's base. Then, the metallic cone is carefully positioned into the plate of opening base. Upon opening a rotary valve, free-flow density sand testing with a predetermined density was introduced into the excavated hole testing as shown in Figure 3.8 and Figure 3.9.

Subsequently, the apparatus that contains sand to a certain extent is re-weighed, and the volume of the cavity is determined by splitting the weight of the sand that occupies the cavity by the sand's bulk density. The wet density has been determined by splitting the excavated soil weight that has been recovered by the volume of the test hole. The calculation of dry density involves the division of the weight of moist soil by its corresponding percentage of water amount. The determination of percent compaction in the field density test involves the division of the soil's dry density by the max dry density obtained from the proctor test.

Figure 3.8: Details of the two selected soil samples.

Figure 3.9: Soil density test.

3.5 MSE Wall System

The section showcases structure model that consists of precast concrete facing panels and discrete soil reinforcing strips with high adherence properties. The utilization of MSE retaining walls featuring concrete facing panels is a widely recognized approach employed internationally to facilitate and reinforce the development of infrastructure within constricted urban passageways. A small bridge sample as shown in Figure 3.10 was created in Al-Mustaqbal university with similar materials and construction method of Al-Um intersection MSE bridge to investigate the lateral pressure of soil and deflection on precast panels.

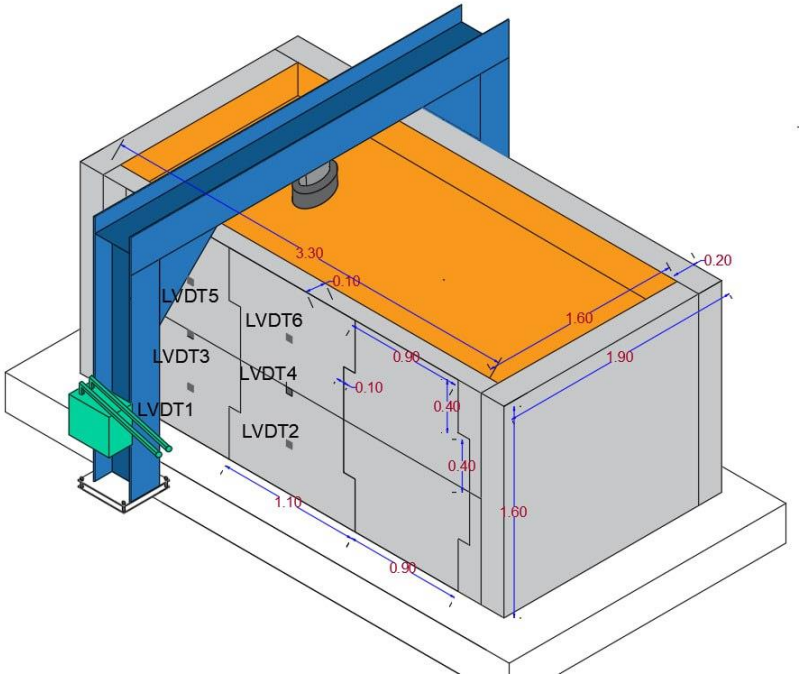

Figure 3.10: 3D model for MSE wall system.

3.5.1 Execution Sequence

3.5.1.1 Foundation Preparation

Inappropriate stuff shall be removed from the surface on which the walls are to be constructed. Such materials include organic soil, plants, waste stuff or any sort of irrelevant materials as shown in Figure 3.11. After by, the fullback soil of foundation must be compacted so that a minimum density of 90% is achieved.

Figure 3.11: Location preparation.

3.5.1.2 Placing Levelling Pad

At this stage, a layer of lean concrete with cement content of 150 kg/m^3 shall be poured over the foundation based on the specification of design MSE system. It should be noted that the purpose of such surface is merely to provide a guidance level for installing the panels and it does not function as a structural foundation. The dimensions of foundation model as following (width =2.5 m, length =4.5m and wall thickness equal to 30cm) as shown in Figure 3.12-Figure 3.14.

Figure 3.12: Placing leveling pad.

A concrete return wall has been used to give the outline shape to the model with dimensions as following (width =1.6 m, height=1.6m, length =3.3 m and wall thickness equal to 20cm). To maintain the fixed wall thickness stud bolts with washers and nuts are used as spacers.

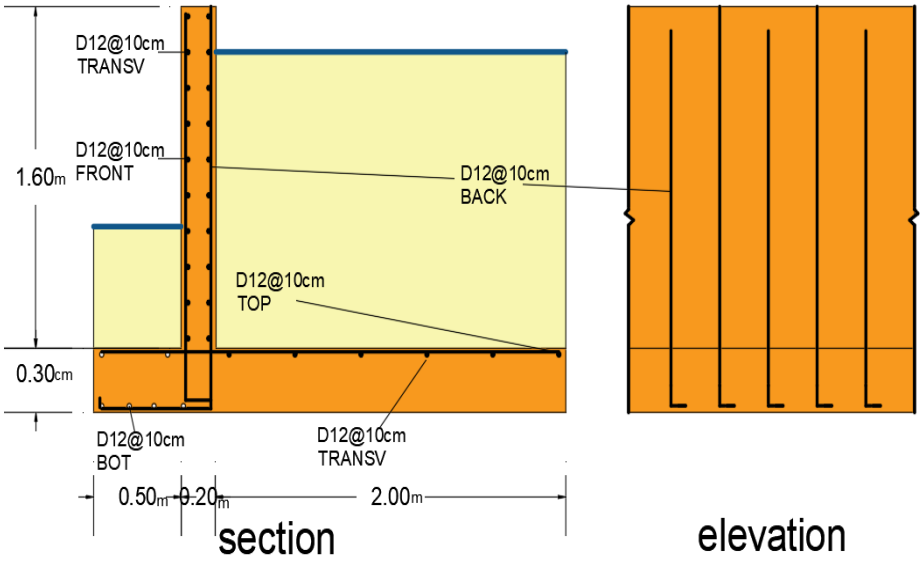

Figure 3.13: Return wall reinforcement details.

Figure 3.14: Walls frame woods.

3.5.2 Facing Precast Concrete Panel Qualification

Wall face in the shape of segmental panels was used to simulate the MSE wall. Precast concrete in the shape of a T-section has been utilized for the wall face, which has measurements of width=110 cm, height=80 cm, and thickness=10 cm. Reinforced with a thermal mesh using steel reinforcement with a diameter of 12 mm. Six sets of plywood formwork were manufactured. The formwork is made of wood edging frame and plywood Core blocks were used to obtain smooth surfaces as shown in Figure 3.15.

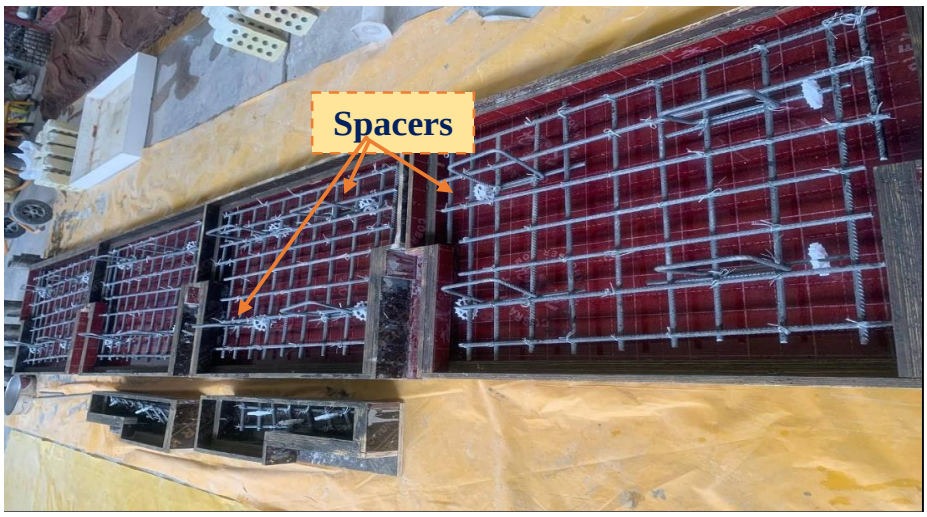

Figure 3.15: Facing mold and steel reinforcement.

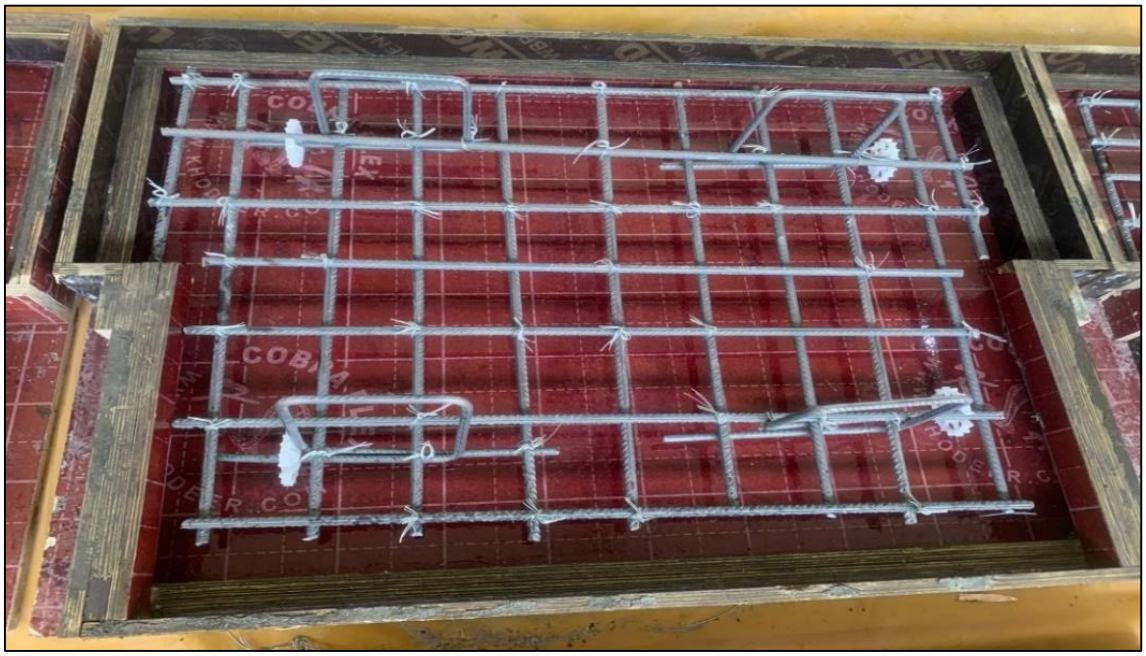

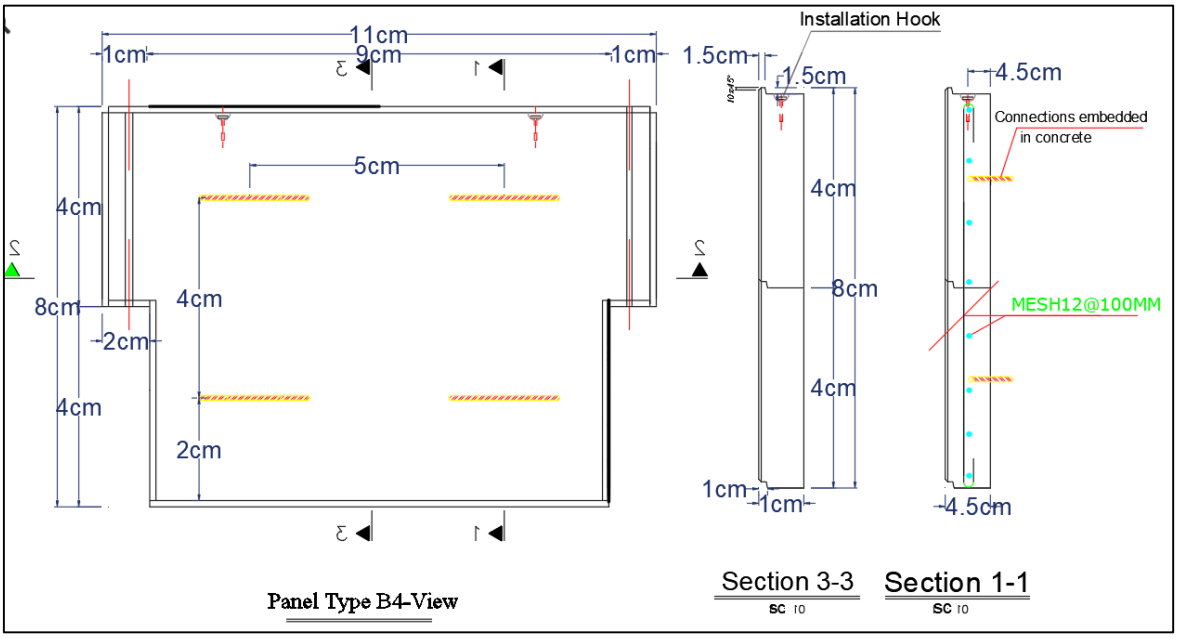

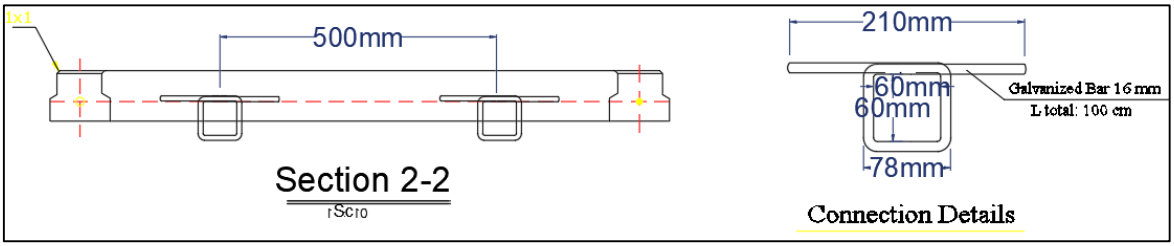

Figure 3.15: Facing mold and steel reinforcement (continued).

3.5.2.1 Mixing Procedures and Curing

After completing transporting the mixed concrete from central mixer, forms were treated with oil before putting steel reinforcement inside the form. The panels specimens are cast using the electric vibrator to ensure the concrete fills the molds.

After casting was completed, the top surface of the concrete was leveled and smoothed with a hand trowel. After 24 hours, the panels and their control specimens (cubes, cylinders, and prisms) are removed from their molds and cured by covering the specimens with burlap sacks after being moistened. A nylon sheet was draped over the moist burlap sacks to keep the water from evaporating. While the curing of the control specimens was by immersion in a water tank for 28 days, as shown in Figure 3.16 and Figure 3.17.

Figure 3.16: Molds shape and casting the panel.

Figure 3.16: Molds shape and casting the panel (continued).

Figure 3.17: Sample curing.

3.5.3 Reinforcing strips

The structural components of the system are the soil reinforcing strips that employ high tenacity coated polyester strips. The geo-strips are composed of compact clusters of high-strength polyester filaments that are closely aligned and enveloped in a resilient Linear low-density polyethylene (LLDPE) coating. The utilization of this reinforcement has been widespread across the globe in the construction of Mechanically Stabilized Earth (MSE) walls as a substitute for steel reinforcements. This is primarily because of its chemical stability and minimal creep properties. The structural connection facilitates the mechanical attachment of the strips to the facing panels. The present mechanical connection involves the utilization of polymeric reinforcing strips that are enveloped around an anchor that has been embedded into the concrete facing panel. There exist various connectivity systems that are currently available in the market. A diverse selection of tensile strengths and dimensions (width and thickness) are readily accessible for strips to accommodate distinct project needs and design prerequisites. In addition, the utilization of geosynthetic strips in environments with high alkalinity (pH levels up to 11) is made possible through the implementation of a polyethylene coating. MSE wall applications might involve the utilization of recycled concretes or lime-treated backfill materials, which can result in the creation of high alkaline environments. The determination of the max tensile strength permissible at the connection point between the panel and the reinforcement shall be accomplished through the implementation of pullout testing. It is imperative that the connection element which is anchored remains free from corrosion and effectively safeguards the polymeric soil strengthening strips against any potential harm during both the construction phase and the lifespan of the structure. The present research employed one type of geosynthetic strengthened strips PARAWED 2E/ 50 as shown in Figure 3.18 and Table 3.8.


Figure 3.18: Reinforcement Strips

Table 3.8: Mechanical and physical properties of strips (Mills, 2023).

PARAWED 2E		**Grade 30**	**Grade 40**	**Grade 50**	**Grade 75**	**Grade 100**
Mechanical Properties						
Ultimate Tensile Strength (ASTM 6637) (D. ASTM, n.d.)	Ib	6744	8992	11240	16861	22481
Creep reduced strength@100y, 20° C	Ib	4958	6611	8264	12397	16530
Long term design strength (AASHTO LRFD)	Ib	4087	5449	6812	10218	13624
Physical Properties (normal values)						
Strip width & thickness	In	3.27 / 0.06	3.27 / 0.07	3.43 / 0.08	3.54 / 0.1	3.54 / 0.12
Strip weight	Ib/328ft	19.18	24.03	27.34	39.46	53.13

3.5.3.1 Strip Types and Distribution

The distribution of strips in the created model was divided into two shapes (Z and I) shapes as shown in Figure 3.19 and Table 3.9. While the details of the strip's strength are mentioned previously in Table 3.8.

Figure 3.19: The distribution of strips

Table 3.9: Cases details.

Case No.	Type Of reinforcement		Width of strips (mm)	Length of strips (mm)	Spacing between strips (mm)
1	Z shape	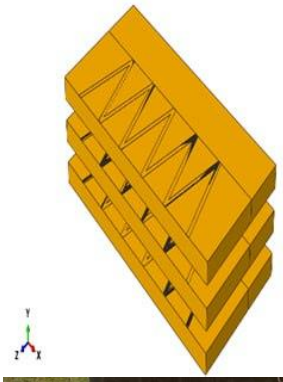 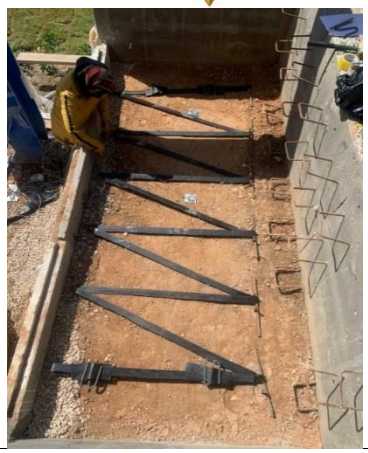	50	0.7H	500
2	I shape	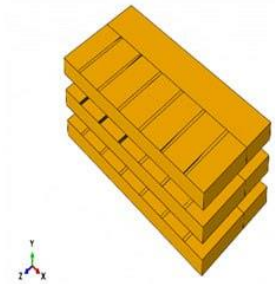 	50	0.7H	500

3.6 Soil Compaction

Diverse compaction equipment has been developed for varying purposes, yet the fundamental objective remains consistent, which is to consolidate the soil to establish a stable base. Soil compaction refers to the process of eliminating air voids within the soil through the application of external force. Soil compaction resulting in reduced air voids can enhance its load-bearing capacity as shown in Figure 3.20.

The process of mechanical soil compaction expedites the natural settling of soil and can facilitate construction activities in areas that may have otherwise been deemed unsuitable for building. To summarize, rammers are employed in restricted spaces for compacting cohesive or clayey soils. Plate compactors are commonly employed in restricted spaces to compact soils of sand and gravel composition, while trench compactors are utilized for cohesive soils in trenches or larger areas near structures. The process of selecting the appropriate machinery for a given task is contingent upon various considerations as shown in Figure 3.21.

Conversely, soils that exhibit cohesion are composed of fine-grained particles such as silts and clays. The particles exhibit a diminutive size and a tactile sensation of smoothness when subjected to manual manipulation. Cohesive soils exhibit adhesive properties when exposed to moisture, rendering them capable of being shaped or molded into a variety of forms. In its desiccated state, this variety of soil exhibits a high degree of compaction and resistance to fragmentation.

The optimal method for compacting cohesive soils is through the application of impact force. The application of force by a rammer or trench roller results in a shearing effect that eliminates air voids and excess water present between the particles.

Certain types of soil exhibit better suitability for construction purposes than others. The objective of compaction is to enhance the load-bearing capacity,

mitigate settling, minimize water seepage, and prevent damage caused by frost. Inadequate compaction of soil can lead to insufficient support for any construction erected on the foundation. Nevertheless, the utilized soil comprises a blend of 80 percent sub-base class B and 20 percent regular soil.

Figure 3.20: Compaction soil by vibration machine.

Figure 3.21: Vibration machine model 5.0 EY 2.0.

3.6.2 Conducting First Backfill Layer, Compaction up to the level of 1st reinforcement tier.

At this stage, the first soil layer is conducted with approximately 20cm thickness and then compacted. The minimum density of backfill soil is 95% based on AASHTO T-99 (AASHTO 2nd, 1998).

3.7 Sensors

3.7.1 Force Sensing

A force-sensing resistor is a type of material that exhibits a change in its electrical resistance in response to the application of mechanical stress, pressure, or force. These devices are commonly referred to as force-sensitive resistors and are occasionally denoted by the acronym FSR as shown in Figure 3.22.

It is widely known among engineers that the equation for force is the product of an object's mass and its acceleration, expressed as F=M*A. Alternatively, force can be calculated as the product of applied pressure and the contact area, expressed as F=P*Area. There exist various engineering units that can be utilized to denote the symbol "F" in the equations, including but not limited to Newtons (N), pound-force (lbf), and other such units.

Force sensing resistors lack pre-calibration to establish a correlation between force readings and recognized engineering units. The output of force measurement obtained from a force sensing resistor can be associated with the applied force by means of a calibration process.

Figure 3.22: Force sensors that used in the current investigation.

3.8Instrumentations of Static Test

3.8.1 Testing Machine

It has been manufactured a hydraulic jack testing machine with a capacity of about 60 Ton in AL-Mustaqbal university to use it for testing MSE wall specimens under static load using the load control technique, as shown in Figure 3.28.

3.8.2 Load Cell

A sensor 24-bit analog to digital converter with 60 Ton capacity was used to measure the applied load Figure 3.28.

3.8.3 Deflection

The linear variable differential transducer (LVDT) (10 cm), as shown in Figure 3.27 indicators were used to measure the lateral displacement of MSE wall (the location of the LVDT was at different cases as shown in Figure 3.28.

3.8.4 Strain Gauge

Twelve steel strain gauges and twelve concrete strain gauges with 120 Ω resistance Figure 3.23, were used to measure the strain distribution. These

gauges were distributed on the inner face of concrete and steel strain distributed on the strips in two regions the first one in the middle of strips and the second one in the edge of strip near the hook in three layers at the edge panel and middle panel. The distribution locations of the strain gauges are shown in Figure 3.23 and Figure 3.24:

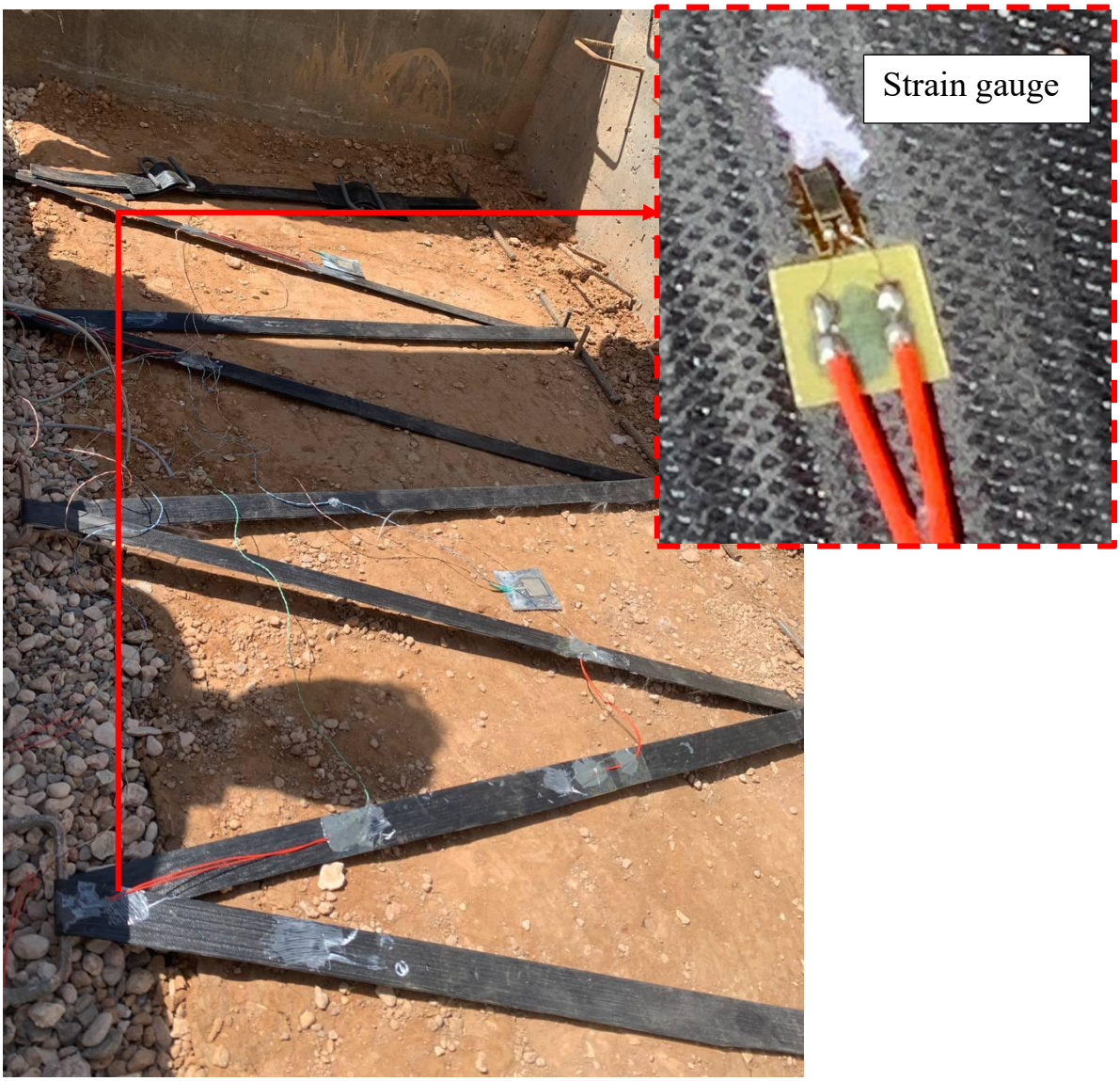

Figure 3.23: Distribution of strain gauges across width of the wall.

Figure 3.24: Distribution of force gauges across wall and earth layers.

3.8.5 Test Machine

The load frame of the rolled steel I-section has been specially designed to provide a static load. This frame consists of two separate parts; the upper part is a triple piece, i.e., three parts welded together like an inverted letter (U), while the bottom part is a single piece placed under the base of the MSE wall. At the end of this part, holes connect it with the triple report by bolts. The

function of this frame is to load the soil during the testing process by using hydraulic jacking. Figure 3.27 shows the details of the loading frame and hydraulic jacking. The steps of the manufactured frame are shown in Figure 3.25:

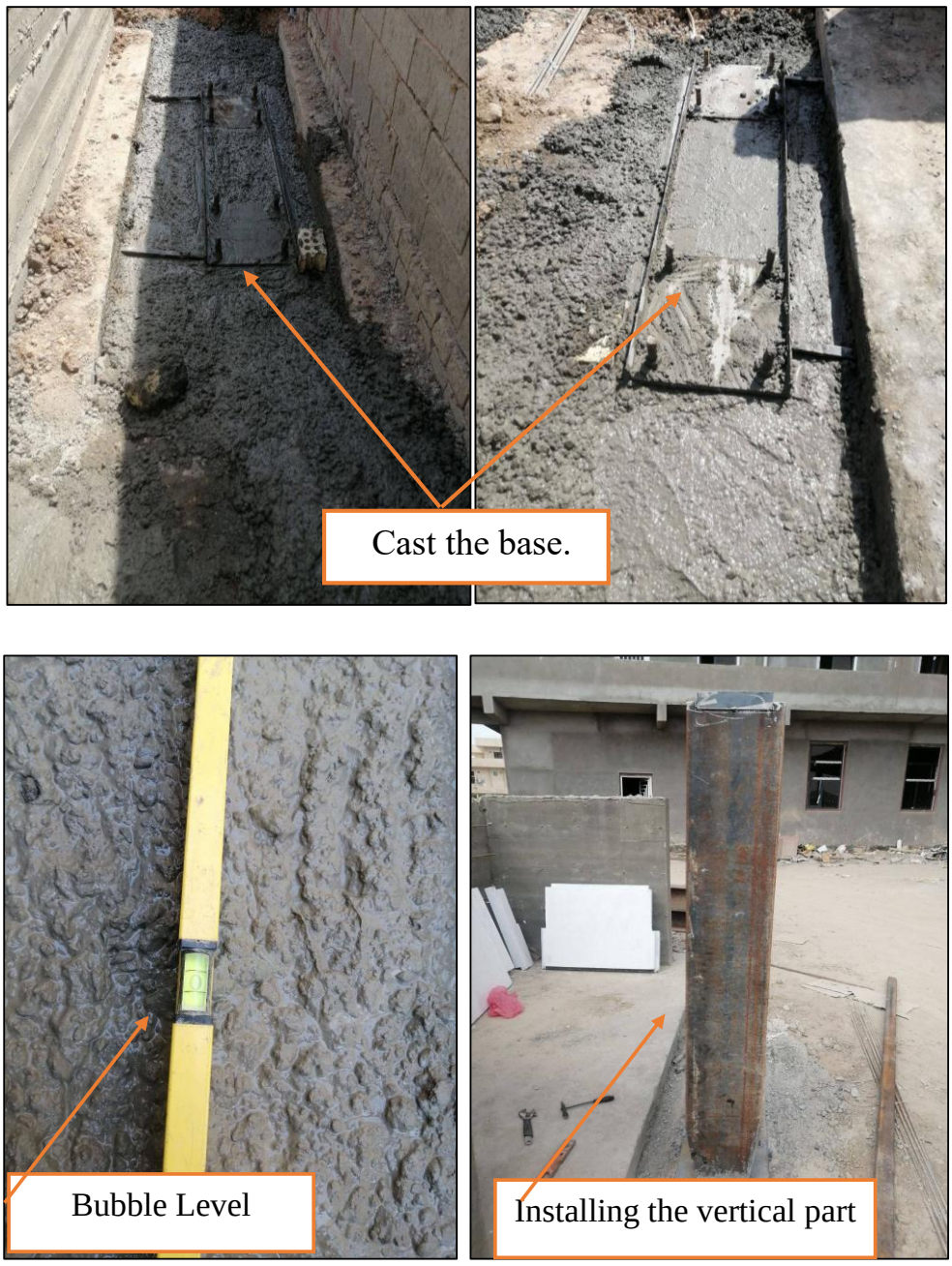

Figure 3.25: Steps of manufacturing frame.

After completing the device's manufacturing process, the model was prepared for testing, three layers of reinforced soil were used, sensors were placed to

measure the strain of concrete and strip, six LVDTs were used to measure the lateral displacement of wall and special sensors were used to measure vertical and lateral soil pressure. All sensors are connected to the Data Logger. The test began with applying a vertical load to the soil surface when applying the load, the sensors started to read.

Figure 3.25: Steps of manufacturing frame (continued).

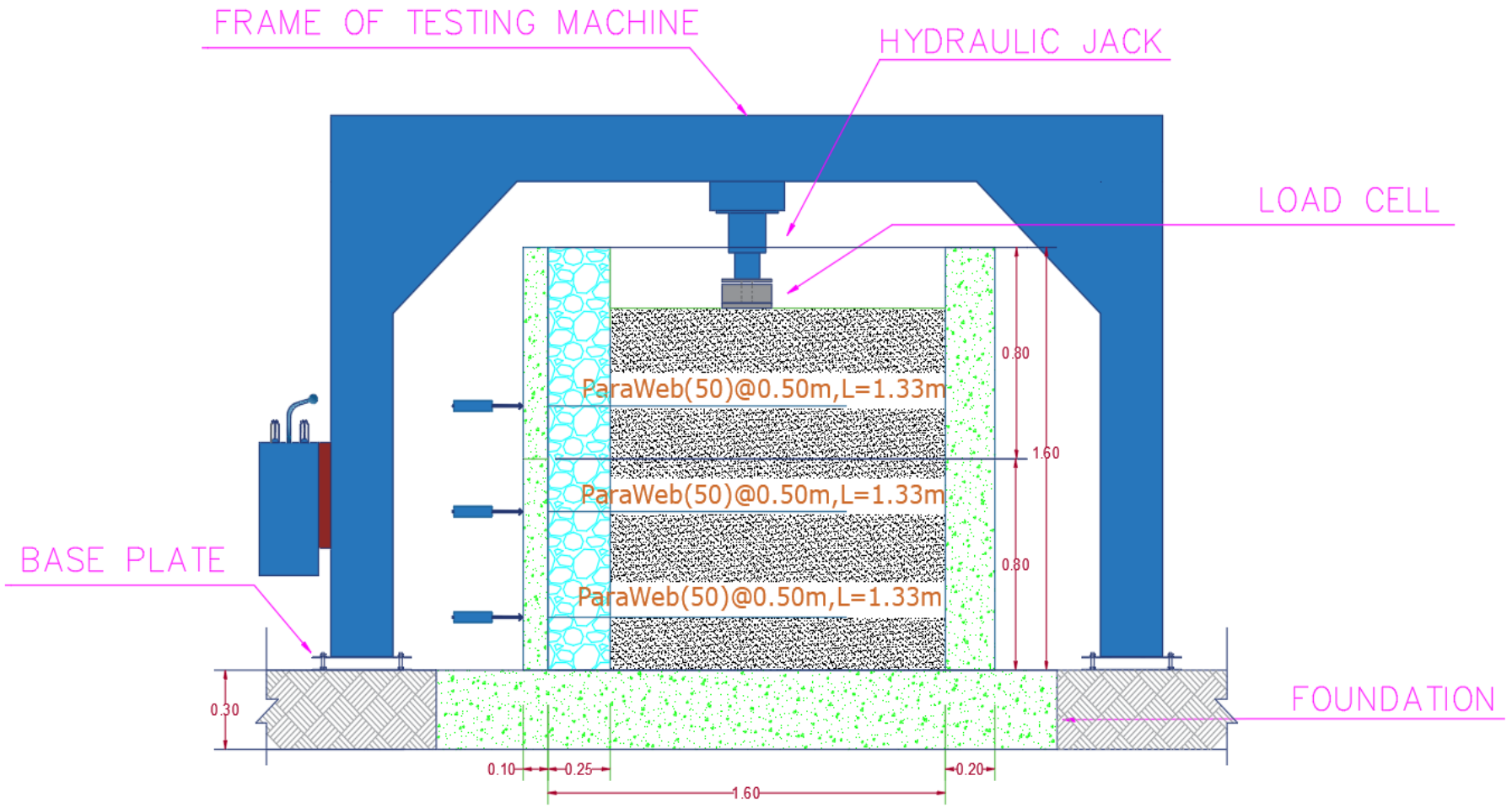

Figure 3.26. Loading system for MSE wall under static load.

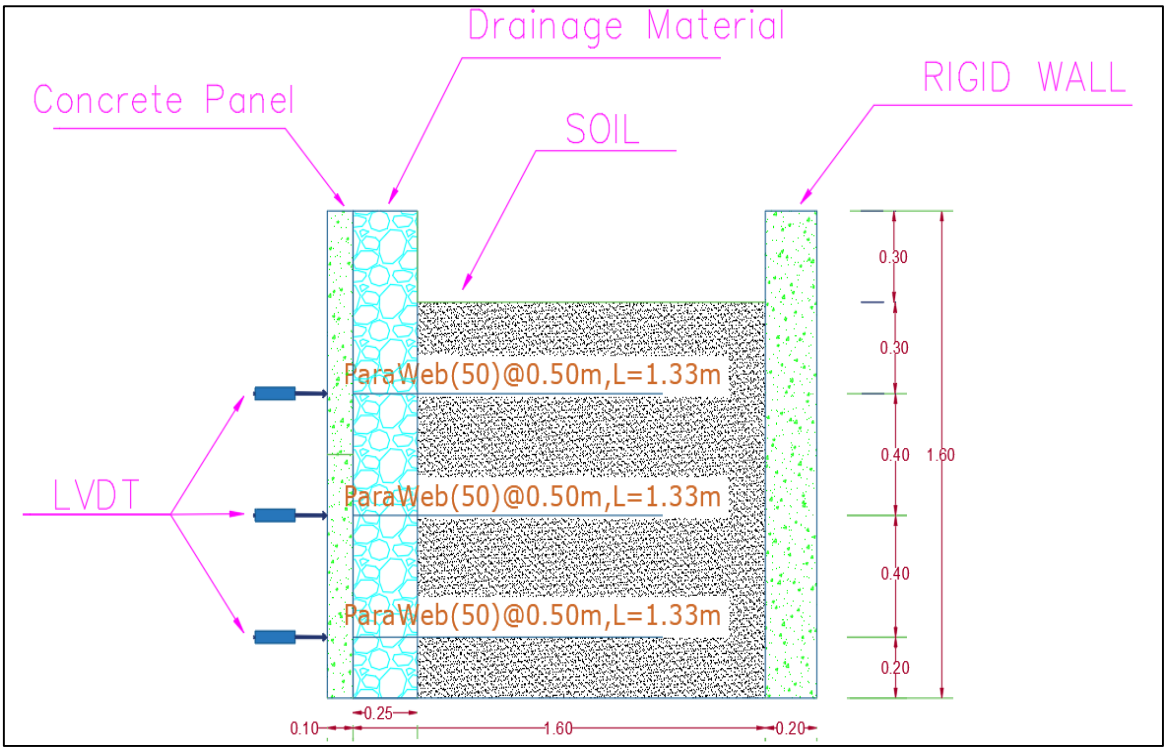

Figure 3.27: Section A-A in MSE wall.

Two digital data loggers with 36 channels had been connected to a laptop (Dell precision M4800) supplied with a specific program set up in LabVIEW 2020 to receive all the data. These data were saved as technical data management streaming (TDMS) files to be used later in various data management software like Excel or DIAdem.

a) Install frame of universal testing machine

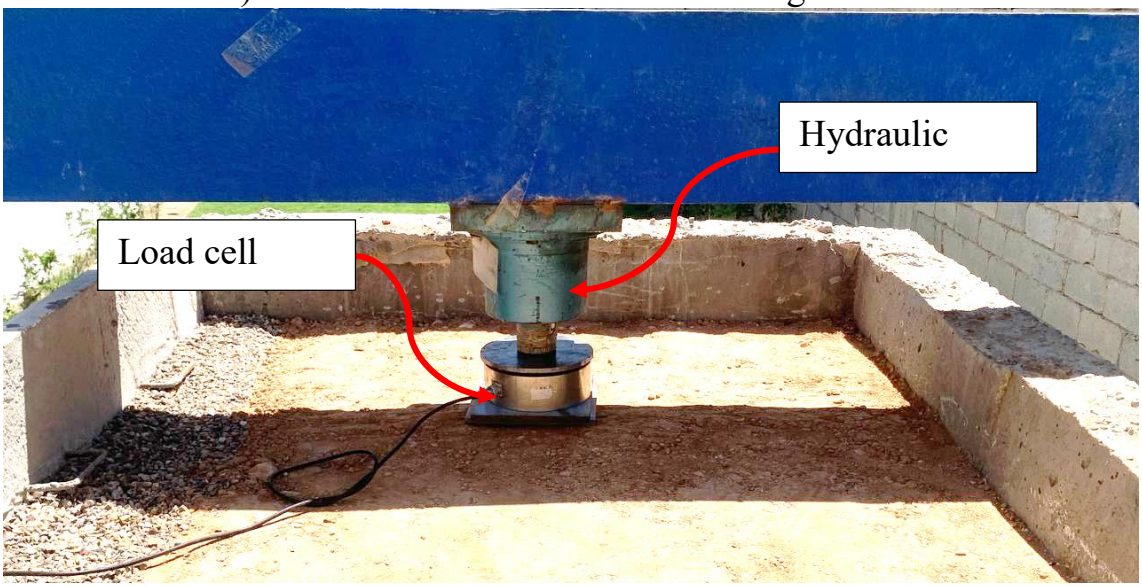

b) install load cell and applied compression load.

Figure 3.28: Instruments of testing.

c) Install LVDTs to measure the lateral displacements.

Figure 3.28: Instruments of testing (continued).

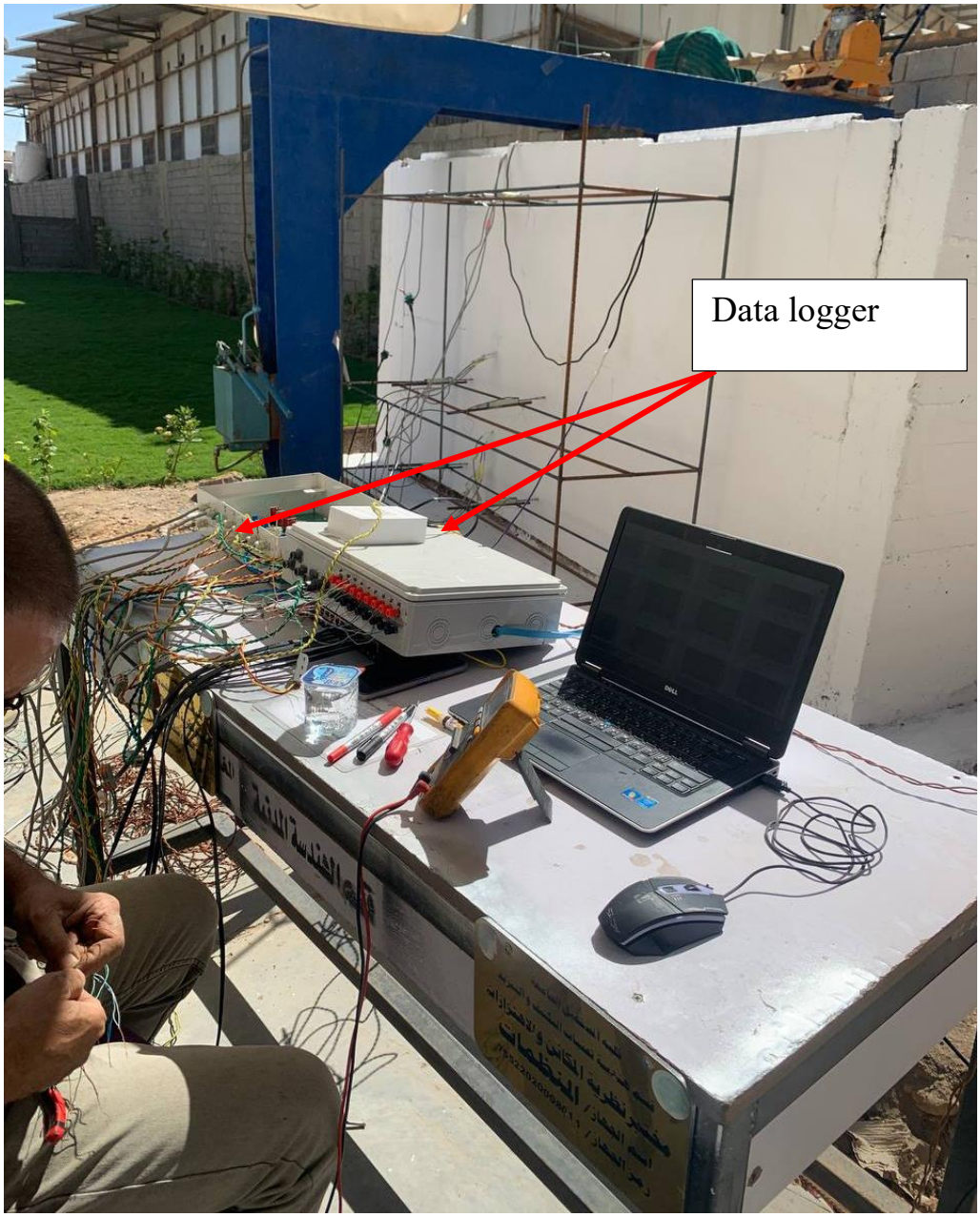

d) Receive all the data from load cell, LVDT, stain gauge, and force sensor.

Figure 3.28: Instruments of testing continued.

CHAPTER FOUR

RESULTS AND DISCUSSIONS

CHAPTER FOUR

RESULTS AND DISCUSSION

4.1. Introduction

The objective of this study is to experimentally evaluate the behavior of MSE wall under static load. This chapter consists of two parts: The first one is the laboratory test while the second one is the case study in Al-Um bridge.

The results of the experimental work which are mentioned in chapter three are discussed in this chapter. The experimental results of two case studies of soil reinforcement are discussed in this chapter. The results of testing were compared to each other to determine the significance of the considered experimental variables**.**

4.2. Concrete samples Results

Several specimens were cast and tested to find the mechanical and physical characteristics of the concrete, including compressive strength, indirect tensile strength (splitting tensile strength and modulus of rupture). For each of these mechanical characteristics, each value represents the average of three specimens.

4.2.1. Compressive Strength Test

The most important and relevant indicator for evaluating concrete is its compressive strength. It is also a significant feature of concrete. The cubes compressive strength value for average three samples was 46.2 MPa and cylinder compressive strength average value was 36 MPa at 28 curing days.

4.2.2. Splitting Tensile Strength Test

The mean value of three cylinders had been calculated during every test. The result of determining the splitting tensile strength was 3.42 MPa for three average sample at 28 curing days.

4.2.3. Test of Flexural Strength

Prisms with dimensions of (100 x 100 x 400) mm are tested according to the (C78/C78M, 2018) procedure. The average flexure tensile strength values of six tested prisms specimens are 4.64 MPa.

4.3. Soil Tests

4.3.1. Grain Size Analysis Test

The grain size analysis of the mixed soil and subbase class B are shown in Figure 4.1 and Table 4.1. Based on Figure 4.1 the highest percentage of the passed sample are located within the subbase ranges which almost 80% of the selected sample.

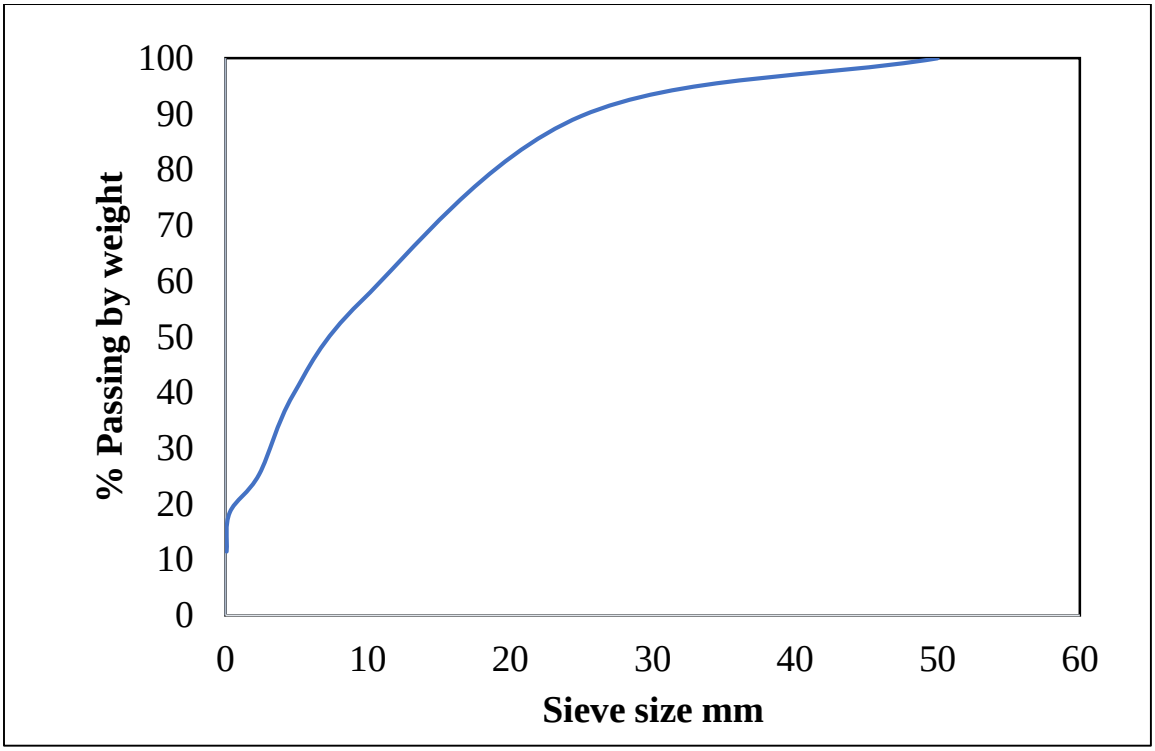

Figure 4.1: Soil sample particle size distribution.

Table 4.1: The compacted soil characteristics that are used in Alum intersection MSE.

Sieve size (mm)	% Passing by weight	Limits of the Iraqi requirement No.45/1984 (zone 2)
75	-	-
50	100	100
25	89.66	75-95
9.5	56.33	40-75
4.75	39.61	30-60
2.36	25.31	21-47
0.3	18.5	14-28
0.075	11.47	5-15

4.3.2. Atterberg Limits Test

As previously indicated in Chapter 3, a small amount of material is gathered during each fall-cone penetration test to ascertain its weight both before and after the drying process, with the aim of investigating the moisture amount.

The correlation between the depth of penetration (measured in millimeters) and the percentage of water amount is employed in determining the liquid limit of the specimen. The obtained findings of Atterberg limits test are demonstrated in Table 4.2.

Table 4.2: Atterberg limits test findings.

Properties	Test findings	Limits of the Iraqi requirement No.45/1984 (zone 2)
Liquid Limit LL %	20.36	≤ (25- 35)
Plasticity Index PI %	3.91	≤ 6 ≤ (4-9)

4.3.3. Compaction Test

As stated in chapter three, the compaction test necessitates the collection of significant data to determine the dry density and water amount for each trial. This includes information such as the measurements of the empty and full mould, as well as the weight of the specimen before and after the drying process. The determination of the dry density and amount of moisture was performed manually, as indicated in Table 4.3.

Table 4.3: Findings of compaction test.

Properties	Test findings	Limits of the Iraqi requirement No.45/1984 (zone 2)
Max. dry density (MDD) (gm/cm3)	2.214	-
Optimum moisture content (OMC) %	10.76	-
The California loading Ratio for 95%.	38.56	≥ 35 (class B)

4.4. MSE Wall Mechanism and Implementation

The model that has been created within the site uses both strain gauge, force sensor and LVDT with all nations as following:

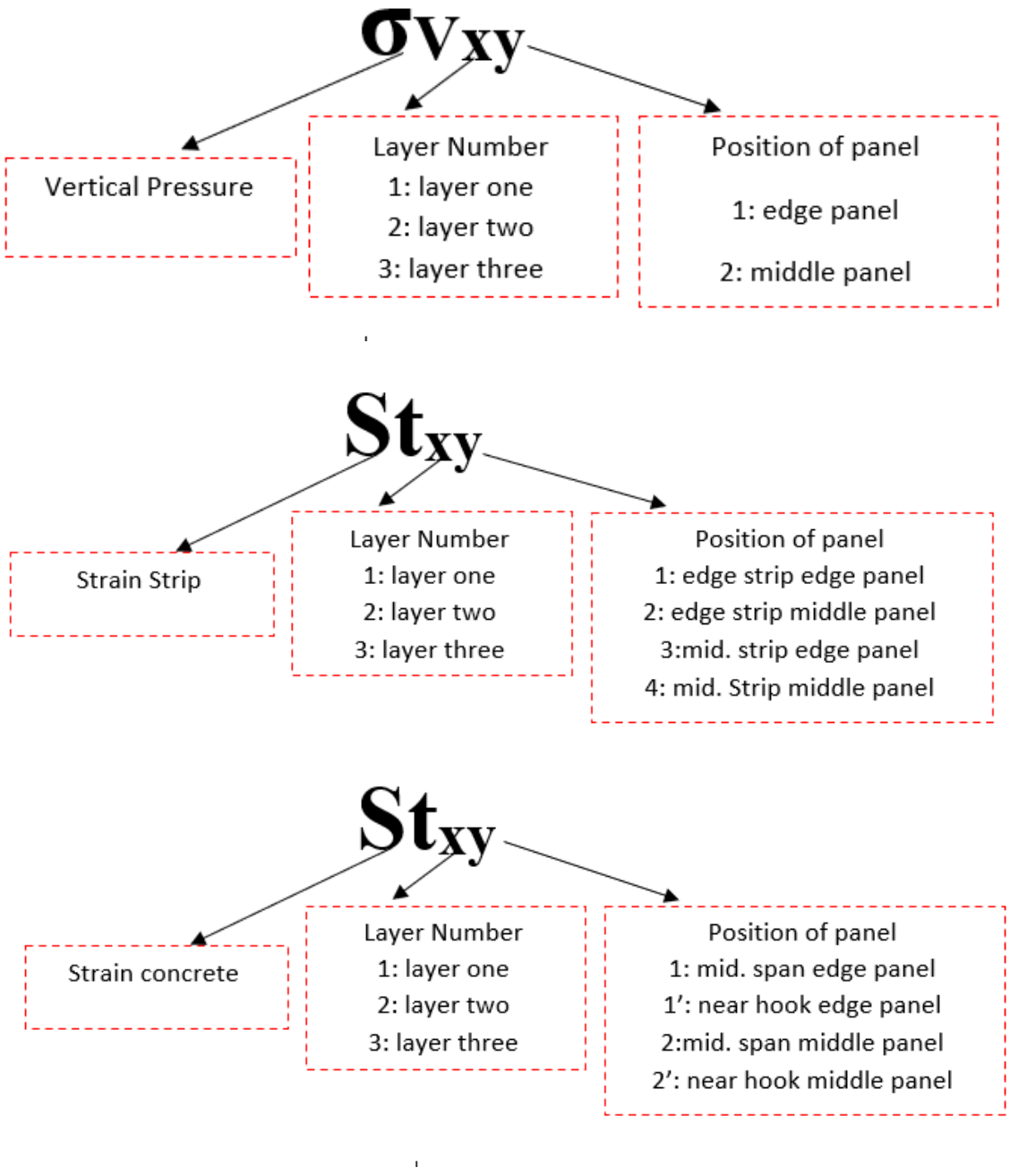

Figure 4.2: Description, location, and details of the effective parameters on MSEW behavior

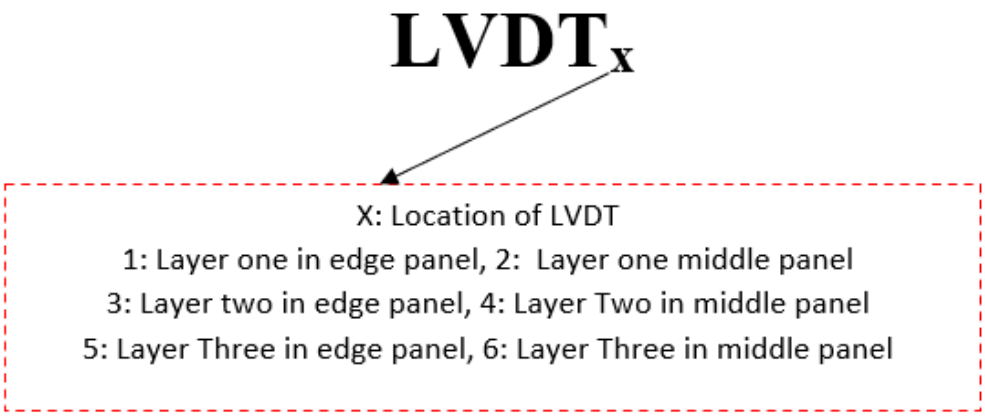

Figure 4.2: Description, location, and details of the effective parameters on MSEW behavior (continued).

4.5. Lateral Pressure

The determination of the horizontal spacing of the reinforcements is contingent upon the calculation of the maximum tension (T_{max}) experienced at each level of reinforcements. This necessitates the computation of the horizontal stress, denoted as σ_H, at every respective reinforcement level. The tensile resistance and pullout resistance of the reinforcement are subsequently compared to the maximum allowable resistance (T_{max}). And a suitable reinforcement pattern is selected, this section presents the methodology for determining the horizontal stress, denoted as σ_H, as well as the max tension, referred to as T_{max}. The determination of the horizontal stress, denoted as σ_H, at any given depth within the Mechanically Stabilized Earth (MSE) wall is solely dependent on the soil load. The horizontal soil pressure at any given level can determine through the utilization of the following formula (Berg et al., 2009):

$$\sigma_H = \sigma_{H-soil} + \sigma_{H-surcharge} \quad (4.1)$$

➢ Case One (Zigzag reinforcement shape)

In this case, the soil was strengthened with geosynthetic strips, where three layers of soil were reinforced, and sensors were placed to measure lateral pressure, where they were placed on the wall from the inner side towards the soil as shown in Figure 4.3. After completing all the layers, the test began by applied static load. Six readings were taken in three levels, three of these readings were recorded to calculate the lateral pressure of the wall near the load area, while the other three were taken in the middle wall, as in Figure 4.4. The ultimate load has been identified to be 140 kN due to appearing the punching shear failure in the upper surface soil under the applied load.

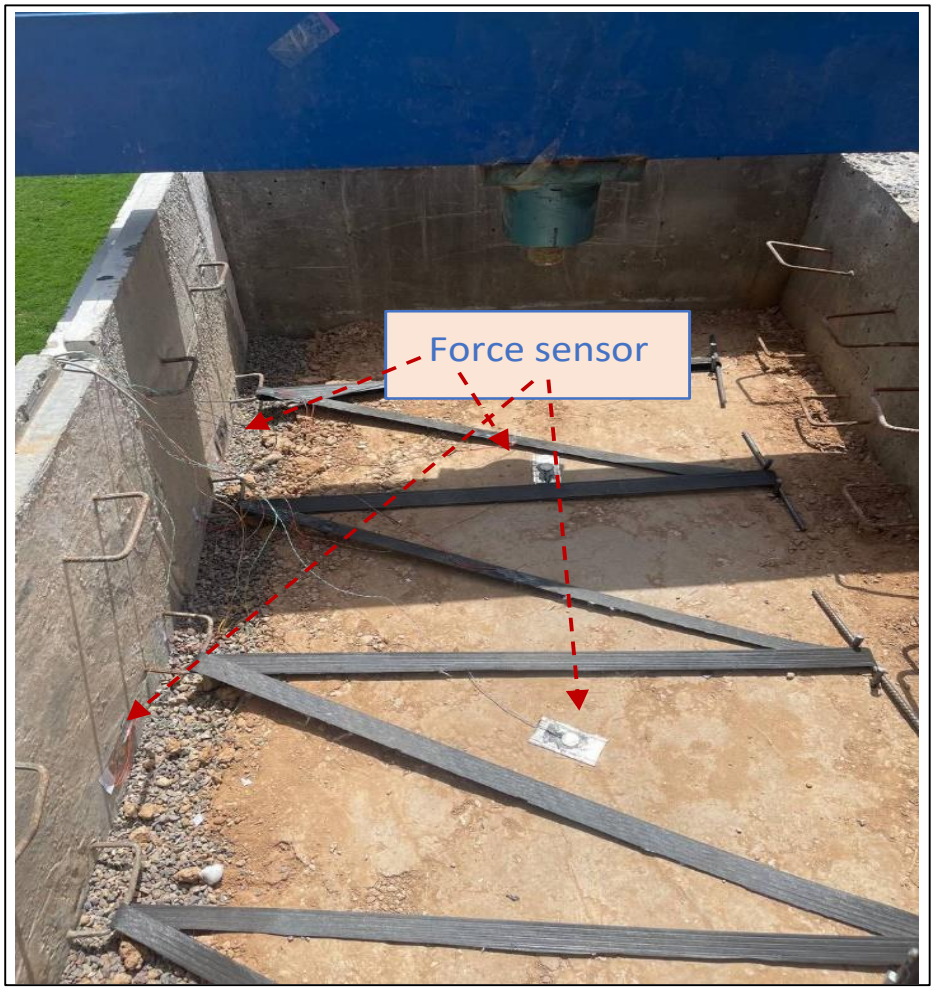

Figure 4.3: The arrangement of force sensor for strips Zigzag shape.

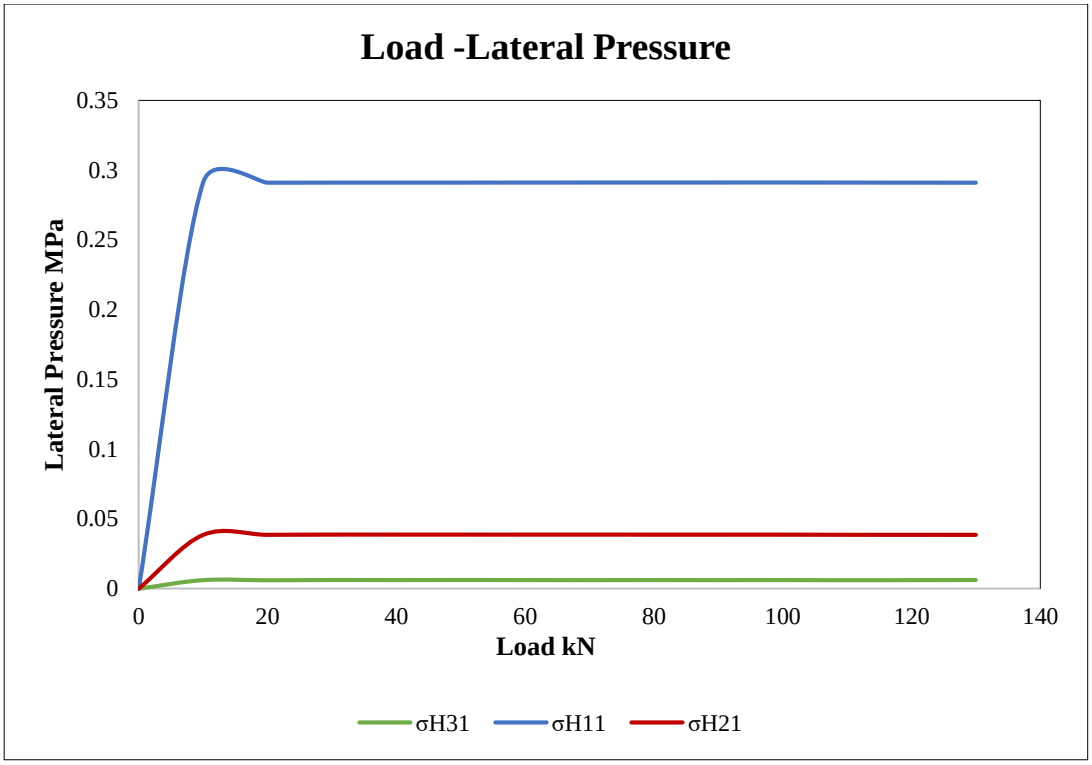

Figure 4.4: lateral pressure of soil in three levels edge panel in Zigzag strips strengthening.

➢ **Case Two (Straight reinforcement shape)**

The straight reinforcement shape was used in this case to evaluate the behavior of soil horizontal pressure. Three soil layers strengthened by these strips with length of 0.7 H where H is the height of wall. As mentioned in case one, the force sensor installed in the inner face of wall to record the lateral pressure as shown in Figure 4.5.

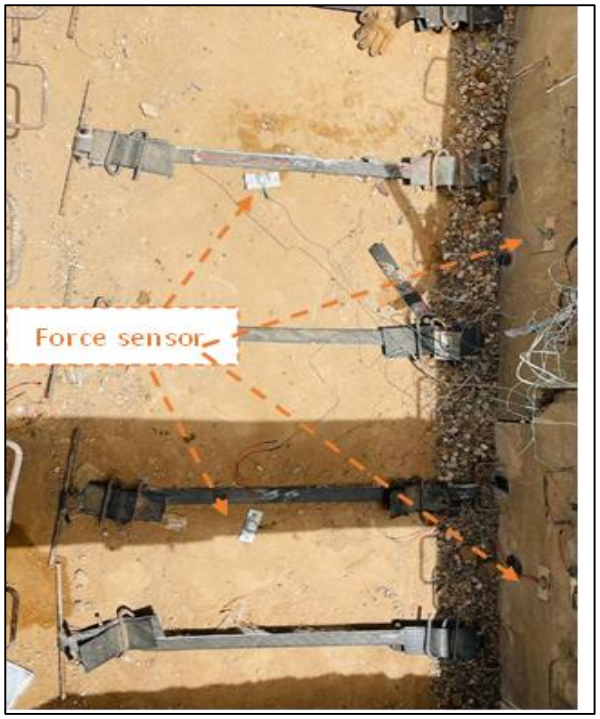

Figure 4.5: The arrangement of strips Straight shape for force sensor.

Figure 4.7 shows the relationship between load and lateral pressure for three soil layers that shown in Figure 4.6. Based on Figure 4.7 layer one carried the highest load due to direct effect of load on soil, which already reduced with increasing the soil depth (Jacobs et al., 2016). The lateral pressure of soil on MSE wall has been presented in Figure 4.7 and Figure 4.8 for straight strips shape.

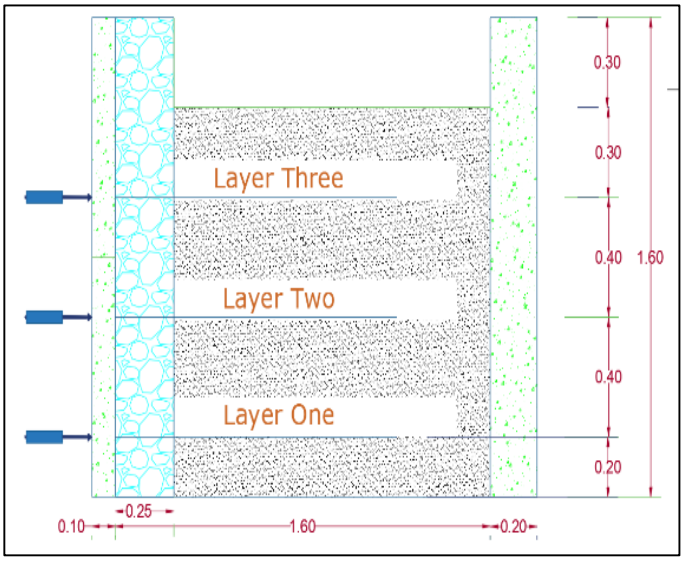

Figure 4.6: The soil layers arrangement.

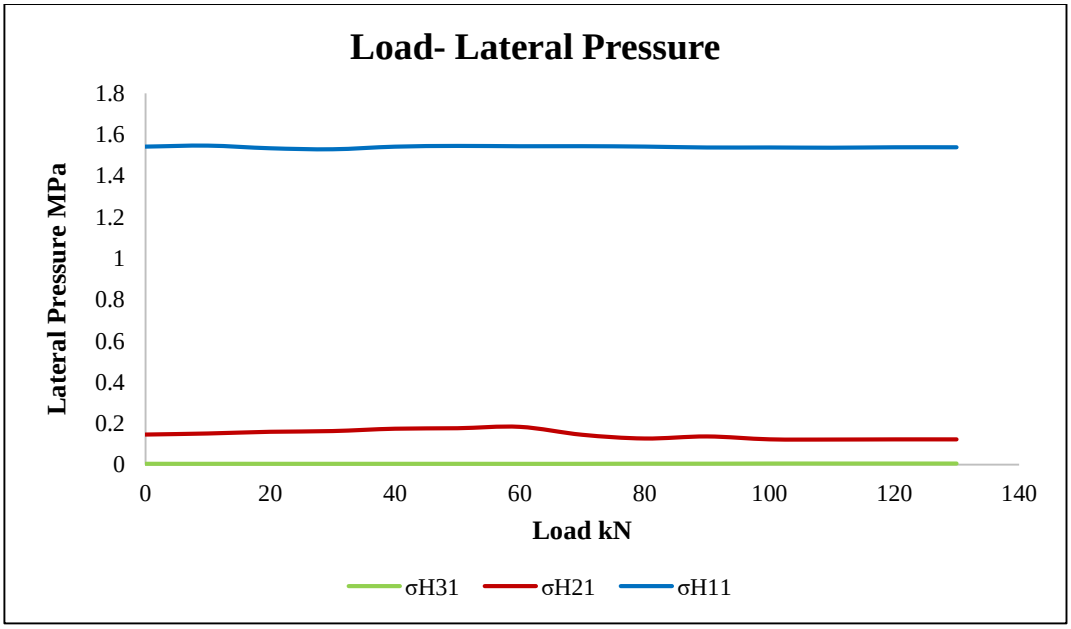

Figure 4.7: lateral pressure of soil in three levels edge panel in straight strips strengthening.

The horizontal pressure from soil on panel is shown in Figure 4.8, σ_H for the third layer with external panel due to increase the load of soil above force sensor and due to kind of support in the MSE wall model.

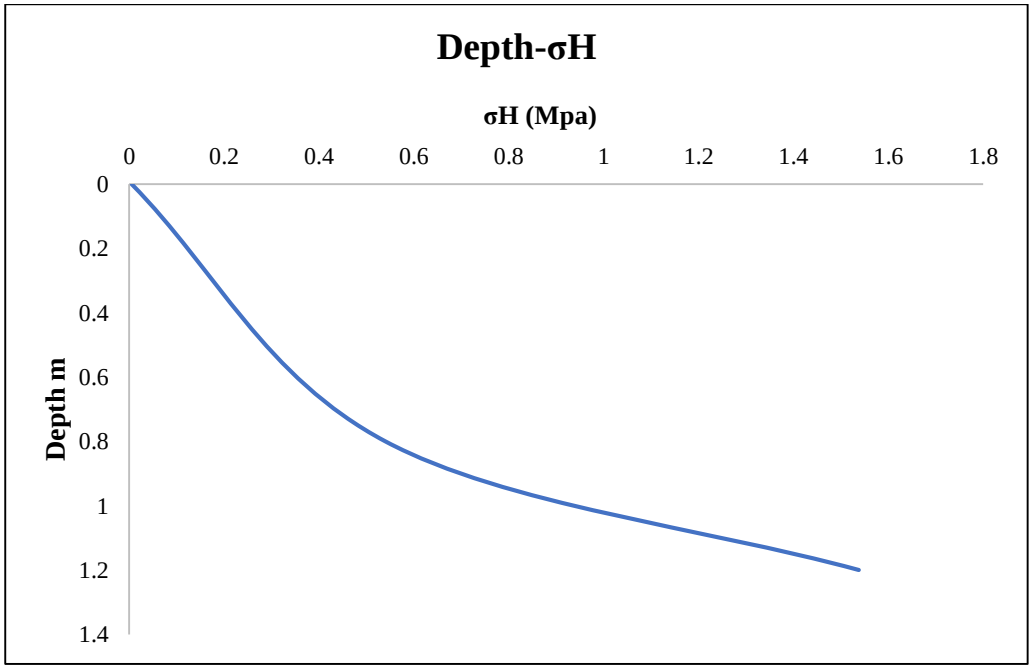

Figure 4.8: Lateral pressure vs depth in straight strips strengthening.

4.6. Vertical Pressure

The data was taken from the vertical force sensors as shown in the figures below. The force sensor was put in three levels as mentioned in chapter three. Two sensors in each layer, one of them near the applied load and the second at the mid span of MSE wall structure. During the test it has been noticed that the vertical pressure decreases with the depth.

➢ Case One (Zigzag reinforcement shape)

When using zigzag reinforcement shape, Figure 4.9 shows the relationship between load and vertical pressure for three soil layers. Based on Figure 4.9 layer one carried the highest load due to direct effect of load, which already reduced with increasing the soil depth (Jacobs et al., 2016). The sudden increase in vertical pressure of the soil surface layer resulting from reaching the compacted soil to settlement and starting the movement of particle.

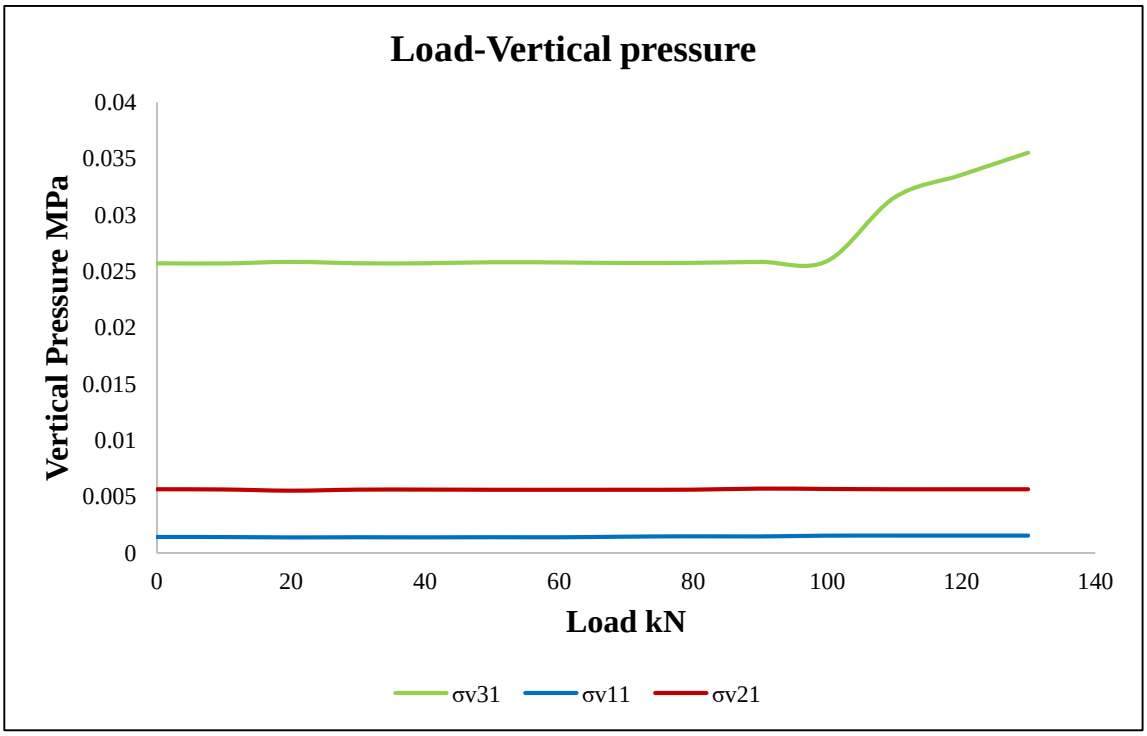

Figure 4.9: Vertical pressure of soil in three levels edge panel in Zigzag strips strengthening.

➢ Case Two (Straight reinforcement shape)

When using straight reinforcement shape, Figure 4.10 shows the relationship between load and vertical pressure for three soil layers. Based on Figure 4.10 layer three carried the highest load due to direct effect of load, which already reduced with increasing the soil depth (Jacobs et al., 2016). In comparison with Figure 4.9, zigzag strips resist vertical and horizontal pressure higher than straight one due to analysis the force into two components.

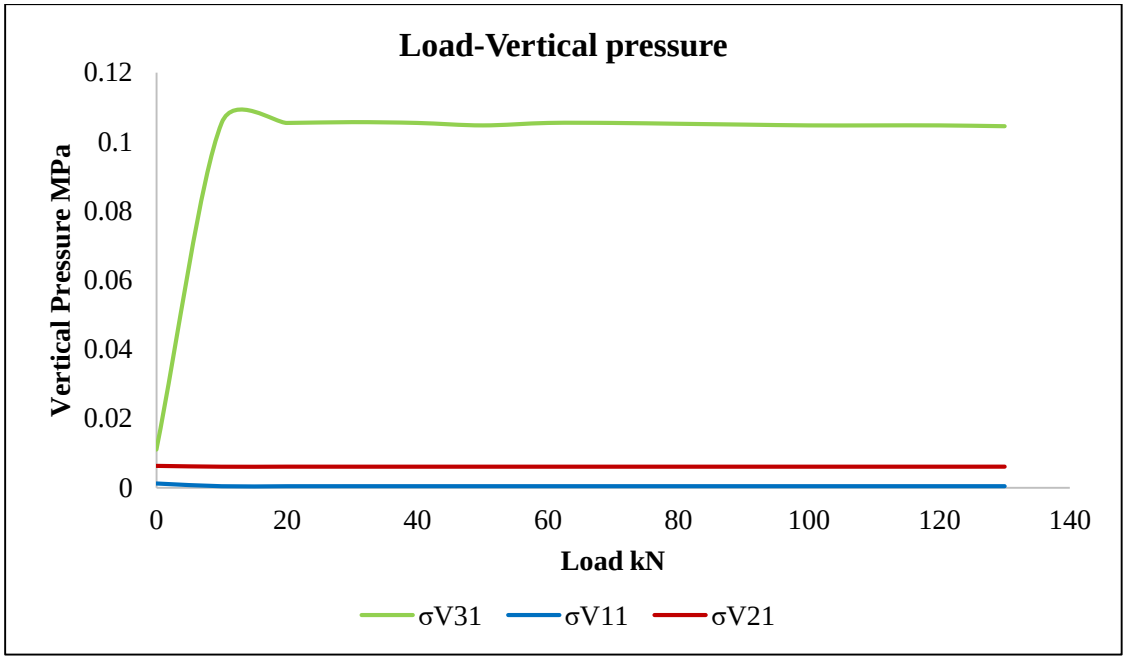

Figure 4.10. Vertical pressure of soil in three levels edge panel in straight strips strengthening.

Figure 4.10 shows the vertical pressure of soil on MSE in three soil layers, there is a significant difference between soil vertical pressure in the upper layer, and both middle and bottom layers. The upper layer carried the highest vertical pressure with about 0.11 MPa.

4.7. The linear variable differential transducer (LVDT)

This section will discuss the lateral displacement of MSE wall due to the static load. As mentioned in chapter three, the LVDT was distributed in different levels along the height of MSW wall. Data were recorded from the LVDT to

measure the lateral displacement. Building up a computer program has been developed to modify the recorded data from the LVDT (remove the noise) to return the results to their original form, as shown in figures below:

➢ Case One (Zigzag reinforcement shape)

Using Zigzag strips shape to reinforce the compacted soil in MSE wall the relationship between load and the displacement of LVDT for different soil layer depth indicated that increasing the soil depth led to decrease the lateral displacement of the wall as shown in Figure 4.11, layer three records the highest displacement ratio while layer one records the lowest value.

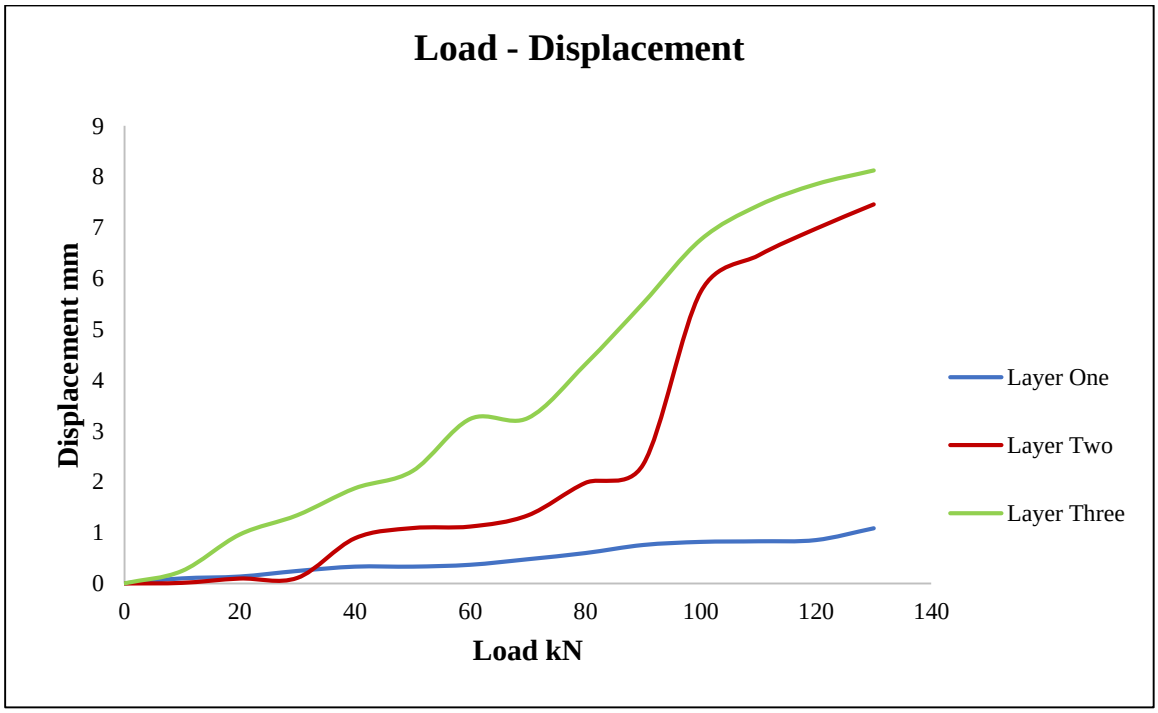

Figure 4.11. Load - Displacement for LVDT in Zigzag strips shape at the edge panel.

When using Zigzag strips shape to reinforce the compacted soil in MSE wall the relationship between load and the displacement of LVDT for different LVDT positions. Figure 4.12 shows that LVDT6 records highest displacement while LVDT1 records lowest displacement value.

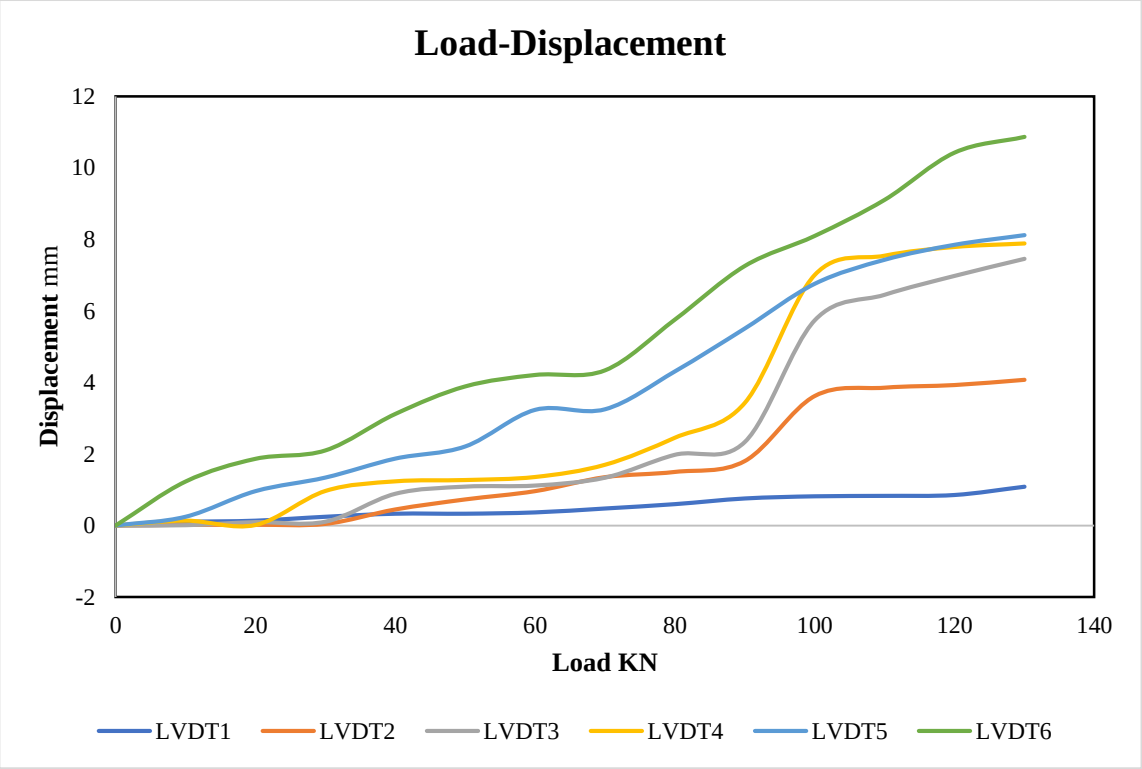

Figure 4.12. Load-lateral displacement for different LVDT locations with Zigzag strips shape.

➢ Case Two (Straight reinforcement shape)

When using straight strips shape to reinforce the compacted soil in MSE wall the relationship between load and the displacement of LVDT for different soil layer depth indicated that increasing the soil depth led to decrease the lateral displacement of the wall as shown in Figure 4.13 , layer three records the highest displacement ratio while layer one records the lowest value. In comparison with Figure 4.12for similar condition with Zigzag strips, using of straight records highest displacement value due to effect of force directly on panel, while Zigzag records lowest displacement value due to analysis the force into two components vertical and horizontal one.

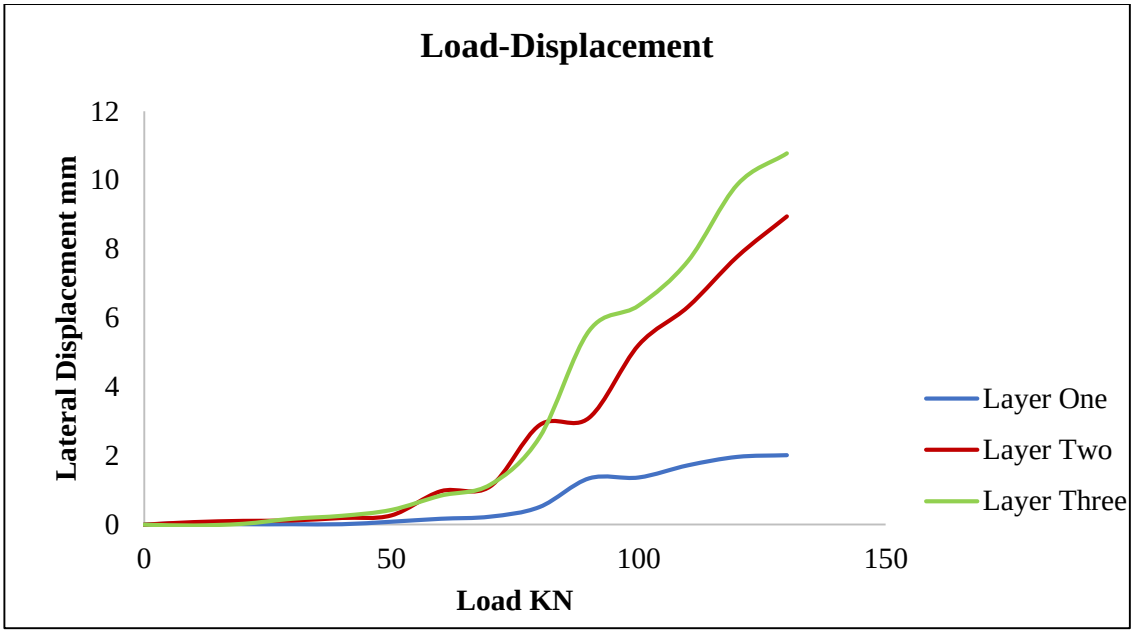

Figure 4.13: Load - Displacement LVDT for straight strips shape

When using straight strips shape to reinforce the compacted soil in MSE wall the relationship between load and the displacement of LVDT for different LVDT positions. Figure 4.14 shows that LVDT6 records highest displacement while LVDT1 records lowest displacement value.

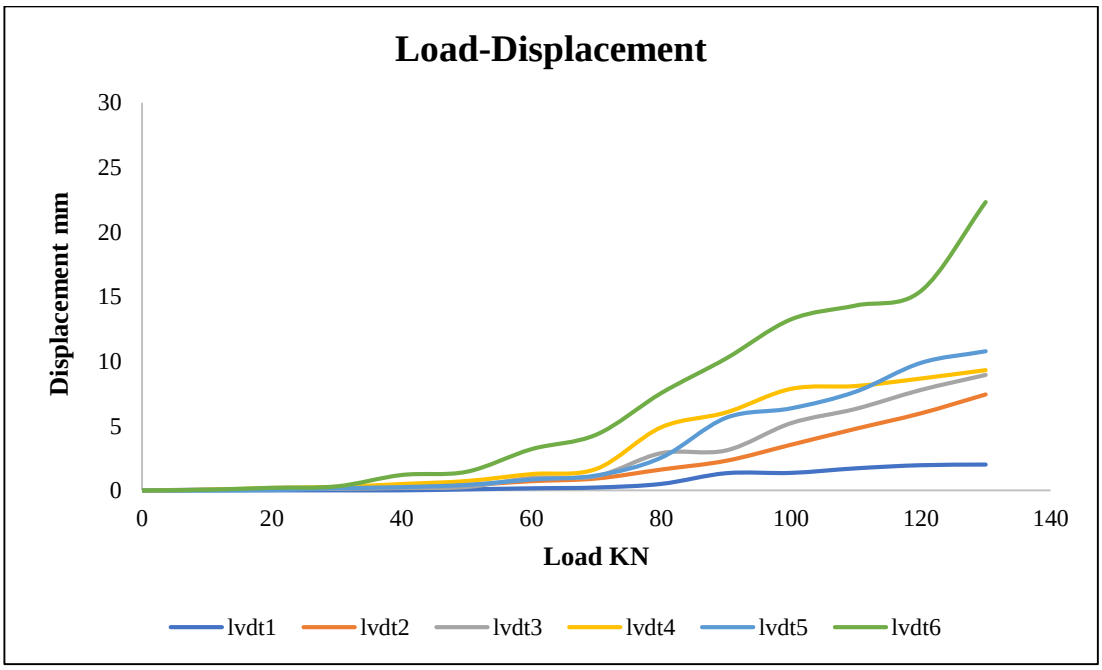

Figure 4.14: Load-lateral displacement for different LVDT locations with straight strips shape.

The experimental LVDT values range between (1-11) mm in zigzag type while the displacement values range between (2-22) mm in the straight type. In both cases we noticed that the max. value of lateral displacement appeared in the layer near the applied load. Furthermore, from the comparison between the zigzag type and straight type, it can be noticed that the MSE walls exhibit less lateral movement in case one.

4.8. Concrete strain

In this part of the experimental work, six strain gauges used to determine the concrete strain gauges. Two strain gauges in each layer. It has been installed the strain gauge in the inner face of the concrete panel in two locations, the first one in the mid-span on the panel and the second one near the hook as shown in Figure 4.15:

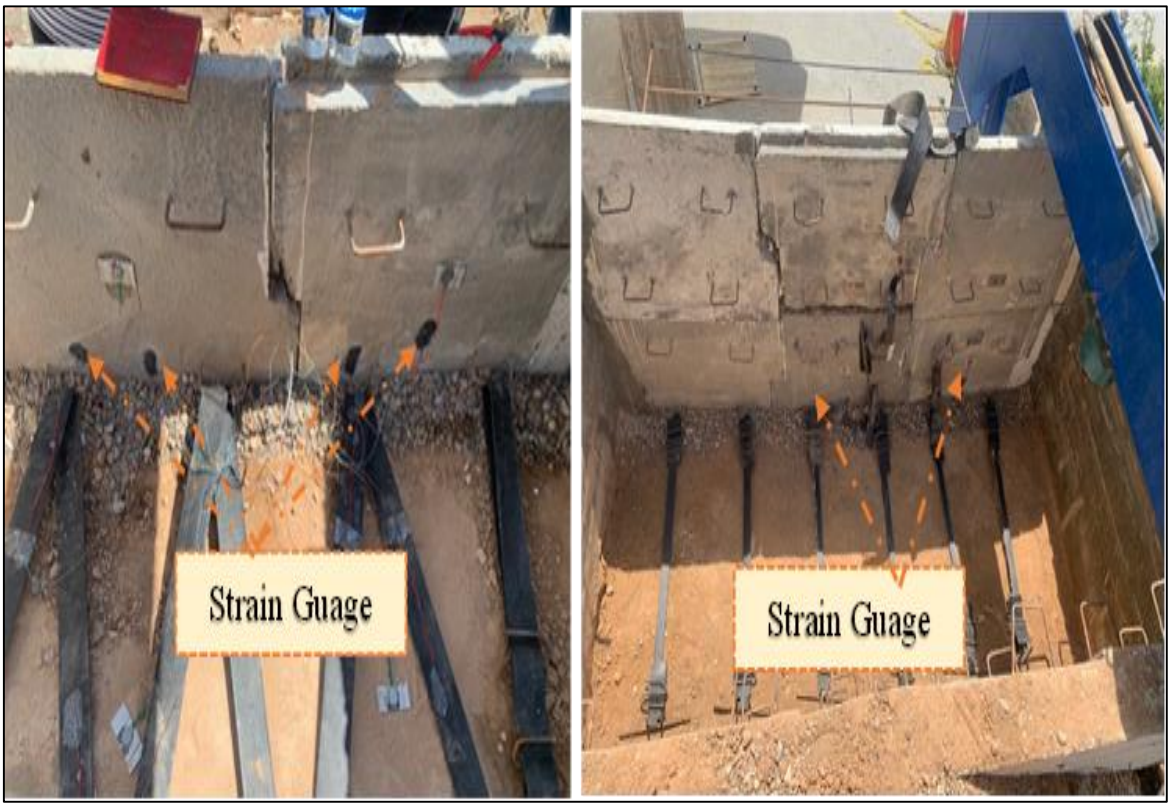

Figure 4.15: The arrangement of strain gauge for strips Zigzag and straight shapes.

➢ Case One (Zigzag reinforcement shape)

When using Zigzag strips shape to reinforce the compacted soil in MSE wall the relationship between load and the displacement to investigate concrete strain for different soil layer depth. With increasing soil depth, the concrete strength was reduced as shown in Figure 4.16 due to the high friction force in the upper layer, which reduce with increasing the soil depth because of carrying most of the load by the upper layer.

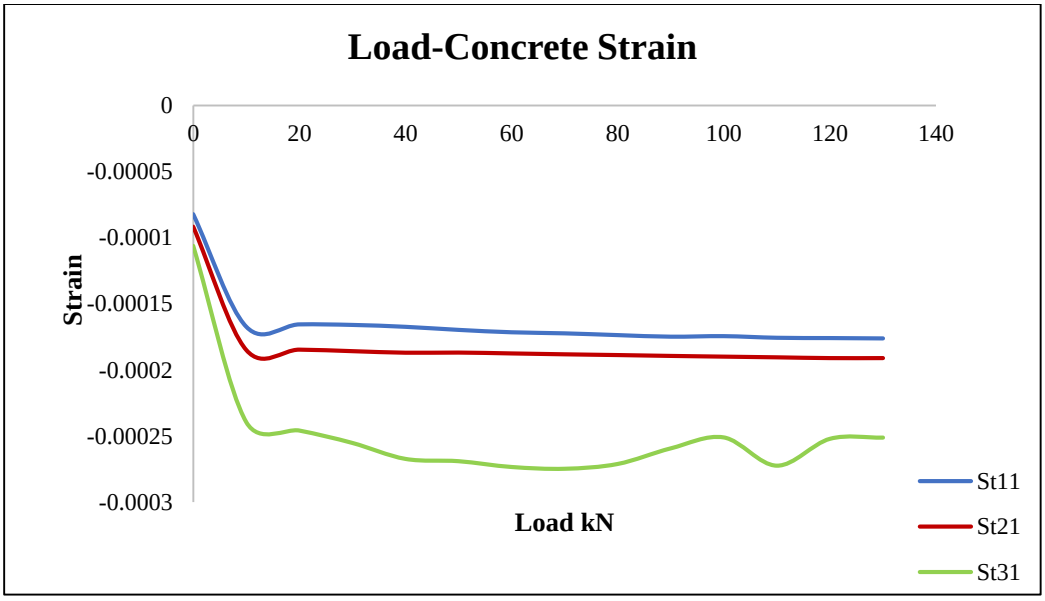

Figure 4.16: load-concrete strain for Zigzag strips shape on different soil layer.

When using zigzag strips shape to reinforce the compacted soil in MSE wall the relationship between load and the displacement of concrete strain for different soil layer depth indicated that increasing the soil depth led to increase the displacement as shown in Figure 4.17 , layer one records the highest concrete strain value while layer three records the lowest value. However, the nearest strain gauge to concrete panel edge considers the lowest value.

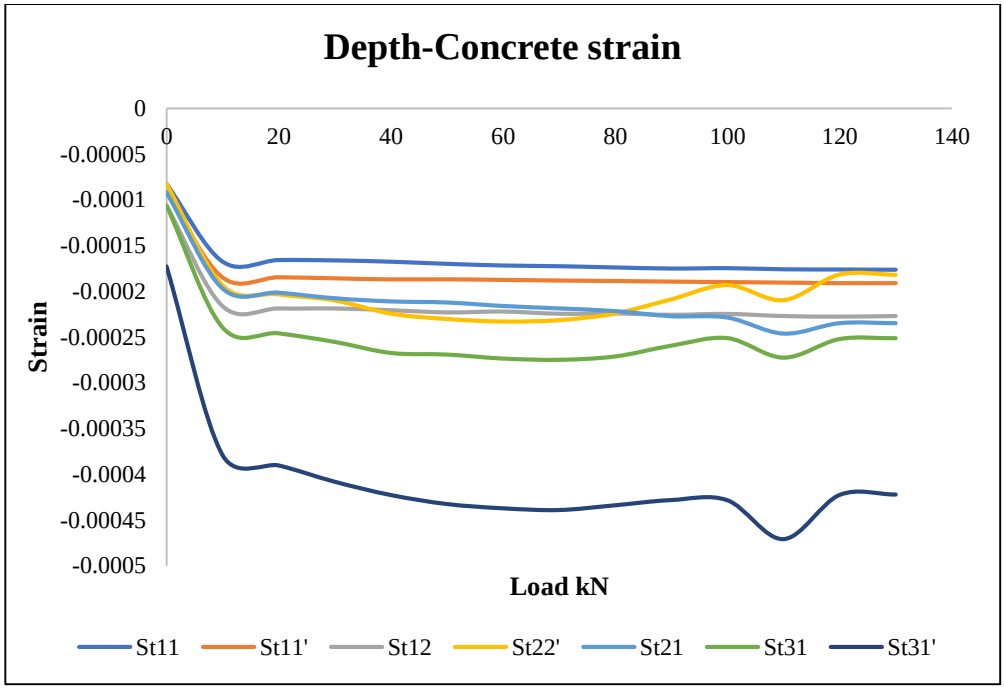

Figure 4.17. Depth- strain for different concrete strain locations with zigzag strips shape.

Figure 4.18 shows the relationship between the concrete strain value for concrete value and the depth of the soil, where the upper soil layer records the lowest value, and the bottom layer records the highest value.

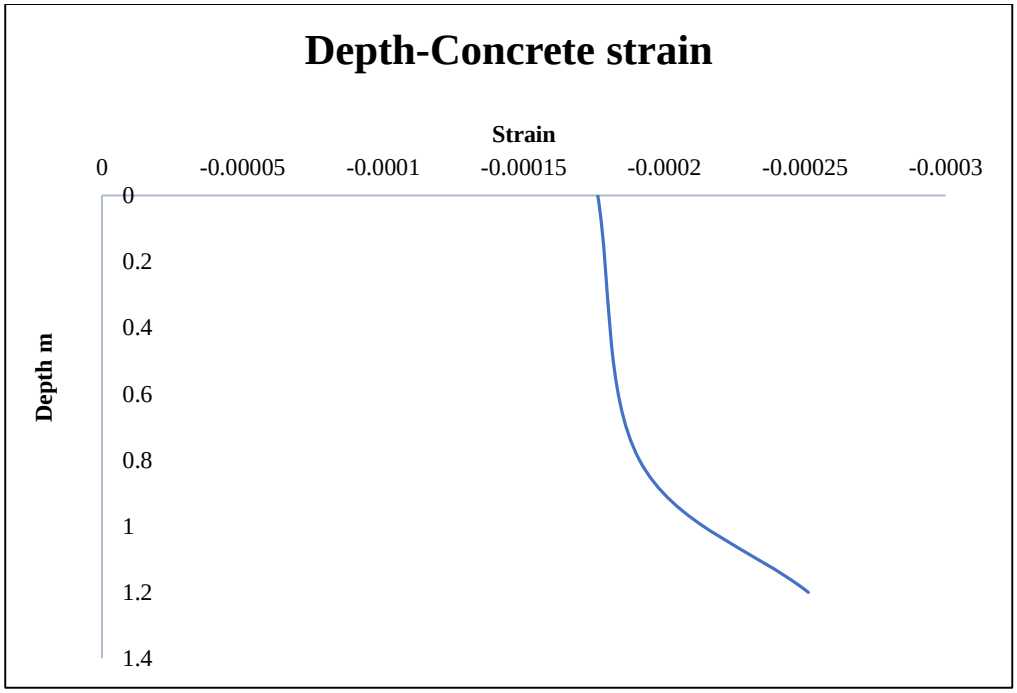

Figure 4.18: Depth vs Concrete strain for three different layers in zigzag strips shape.

➢ Case Two (Straight reinforcement shape)

When using straight strips shape to reinforce the compacted soil in MSE wall the relationship between load and the displacement to investigate concrete strain for different soil layer depth. With increasing soil depth, the concrete strength was reduced as shown in Figure 4.19 due to the high friction force in the upper layer, which reduce with increasing the soil depth because of carrying most of the load by the upper layer. In comparison with Figure 4.17 for similar condition with Zigzag strips, using of straight records highest displacement value due to effect of force directly on panel, while Zigzag records lowest displacement value due to analysis the force into two components vertical and horizontal one.

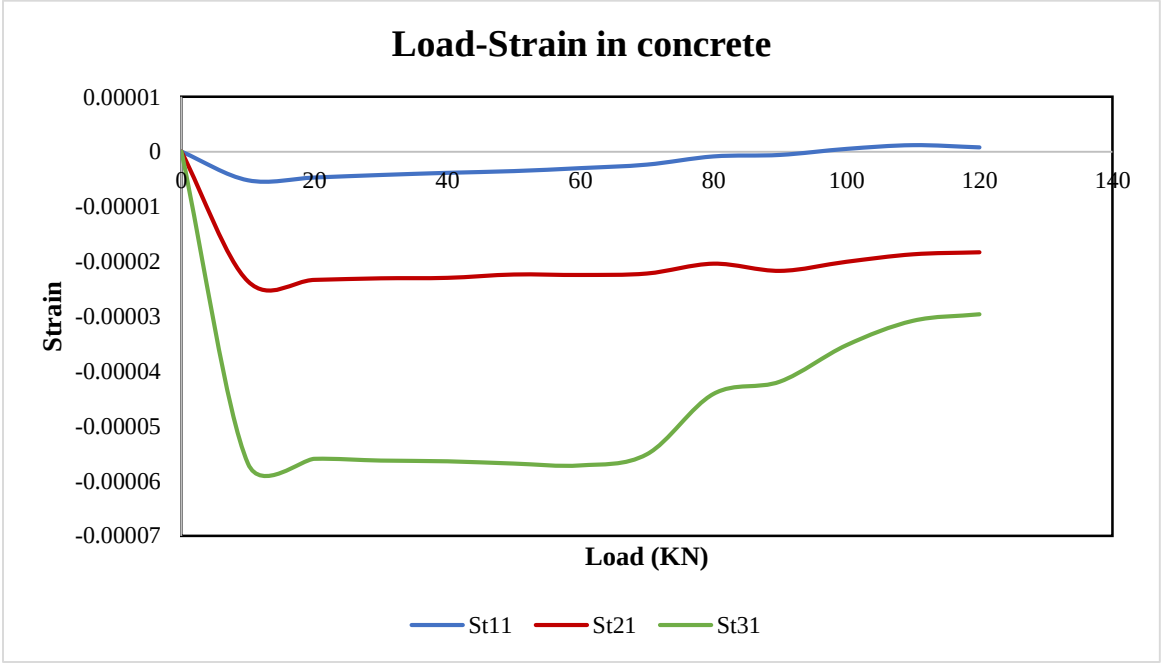

Figure 4.19: load-concrete strain for straight strips shape.

In straight strips reinforcements, Figure 4.20 shows the relationship between the concrete strain value for concrete value and the depth of the soil, where the upper soil layer records the lowest value, and the bottom layer records the highest value. The using straight strips cause approximately linear concrete strain.

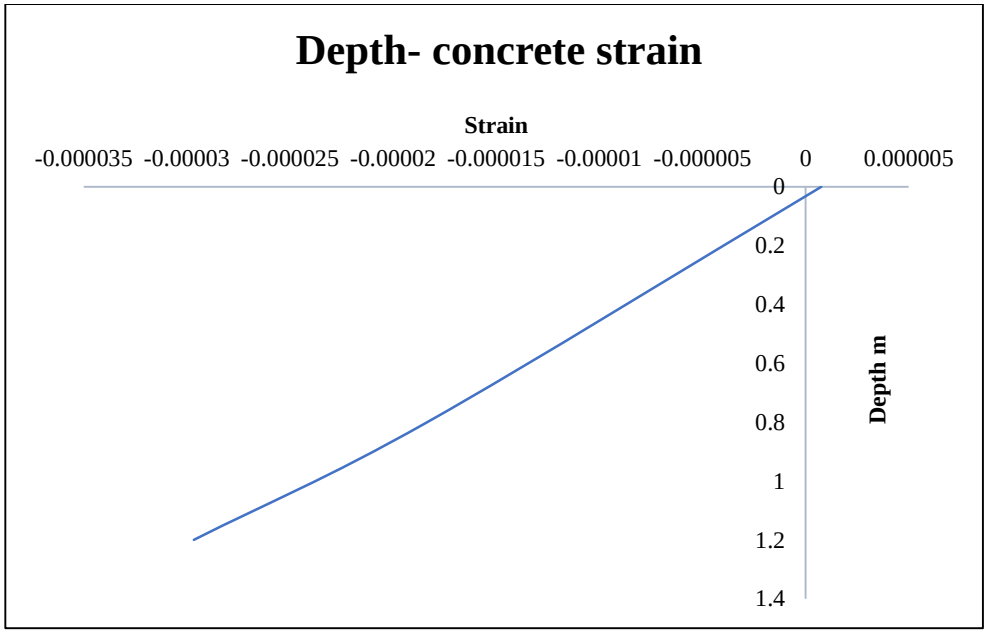

Figure 4.20: Depth vs Concrete strain for three different layers in straight strips shape.

The recorded data by strain gauges shows that the strains developed in the concrete strengthen with zigzag shape are less than the values of strain in case two. Also, we can notice that the maximum value of strain happened in layer one in both cases.

4.9. Strip Strain

In this part we installed twelve strain gauges to evaluate the strain values in the geosynthetics strips. These gauges were distributed in three layers, each layer consisting of four strain gauges. Two of them putted in the mid span of strips and the other two putted in the end of strip that connected with the MSE wall as shown in Figure 4.21 and Figure 4.22.

Figure 4.21: The arrangement of strip strain for strips Zigzag shape.

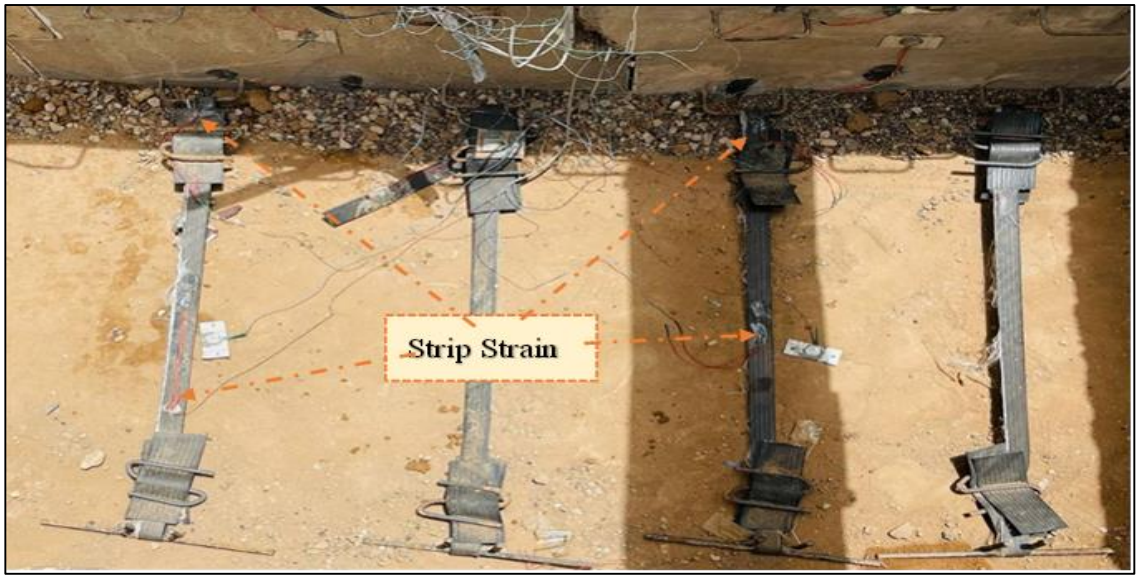

Figure 4.22: The arrangement of strip strain for strips straight shape.

➢ Case One (Zigzag reinforcement shape)

When using zigzag strips shape to reinforce the compacted soil in MSE wall the relationship between load and the displacement to investigate strips strain for different soil layer depth. With increasing soil depth, the strips stain was reduced as shown in Figure 4.23 due to the high friction force in the upper layer, which reduced with increasing the soil depth as a result of carrying most of the load by the upper layer.

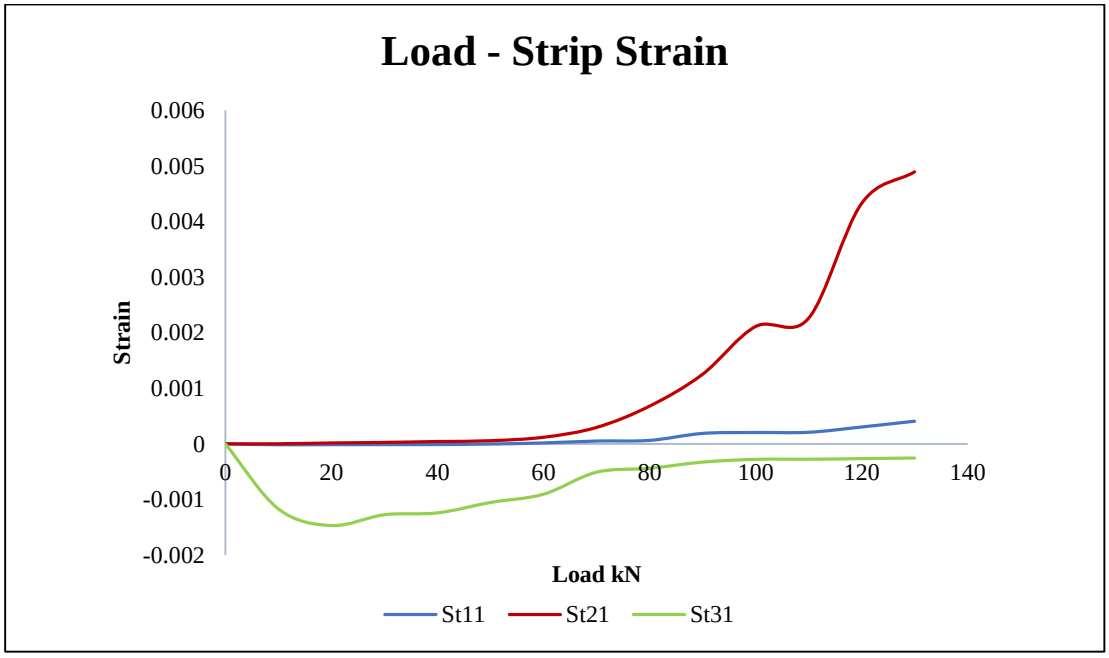

Figure 4.23: load-strip strain for Zigzag strips shape on different soil layer.

When using zigzag strips shape to reinforce the compacted soil in MSE wall the relationship between load and the displacement to investigate strips strain for different soil layer depth. With increasing soil depth, the strips stain was reduced as shown in Figure 4.24 due to the high friction force in the upper layer, which reduced with increasing the soil depth because of carrying most of the load by the upper layer.

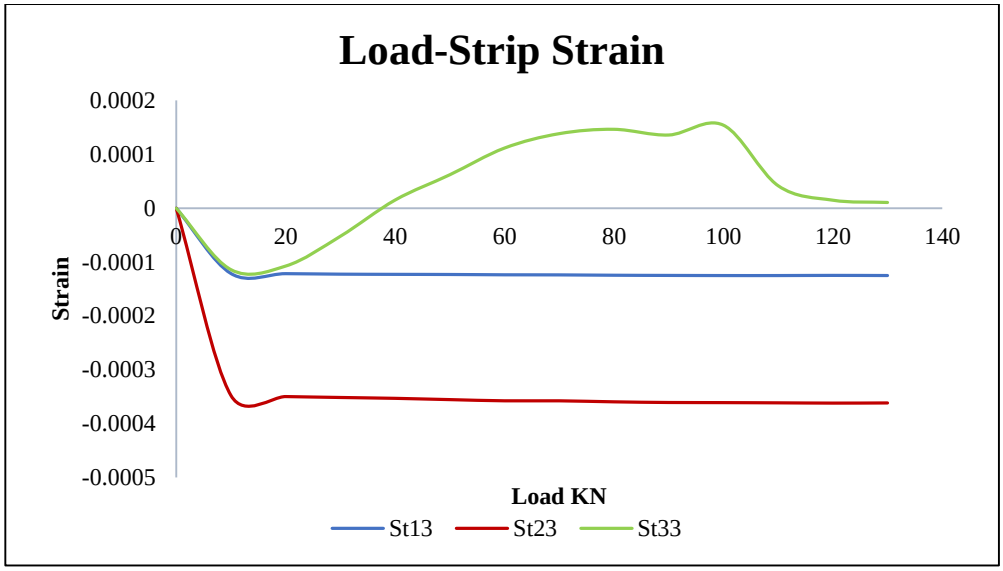

Figure 4.24: Load-Strip Strain for different strips strain locations with zigzag strips shape.

➢ Case One (straight reinforcement shape)

When using straight strips shape to reinforce the compacted soil in MSE wall the relationship between load and the displacement to investigate strips strain for different soil layer depth. With increasing soil depth, the strips stain was reduced as shown in Figure 4.25 due to the high friction force in the upper layer, which reduced with increasing the soil depth because of carrying most of the load by the upper layer.

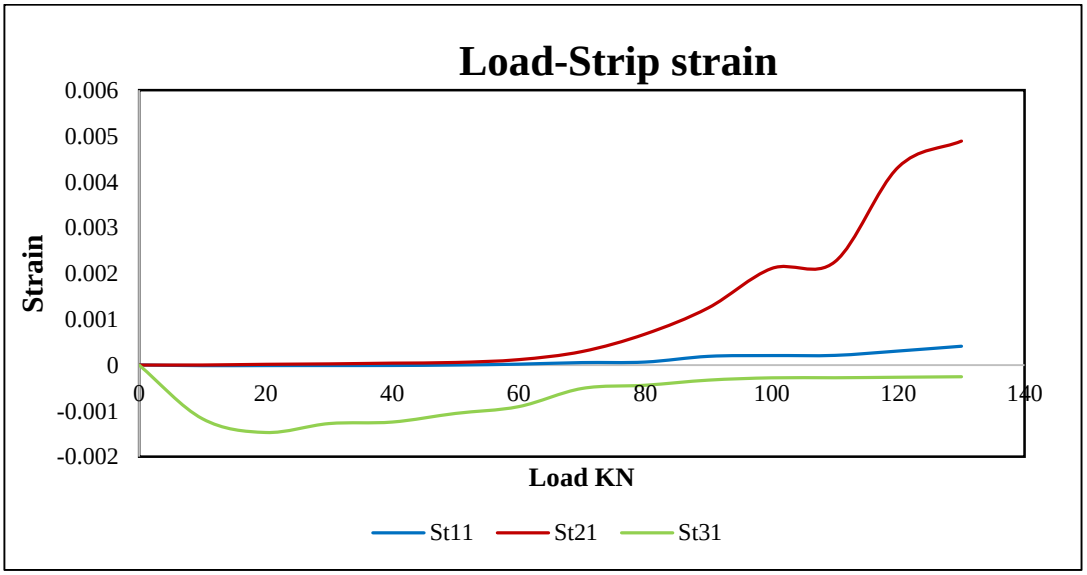

Figure 4.25. load-strip strain for straight strips shape on different soil layer.

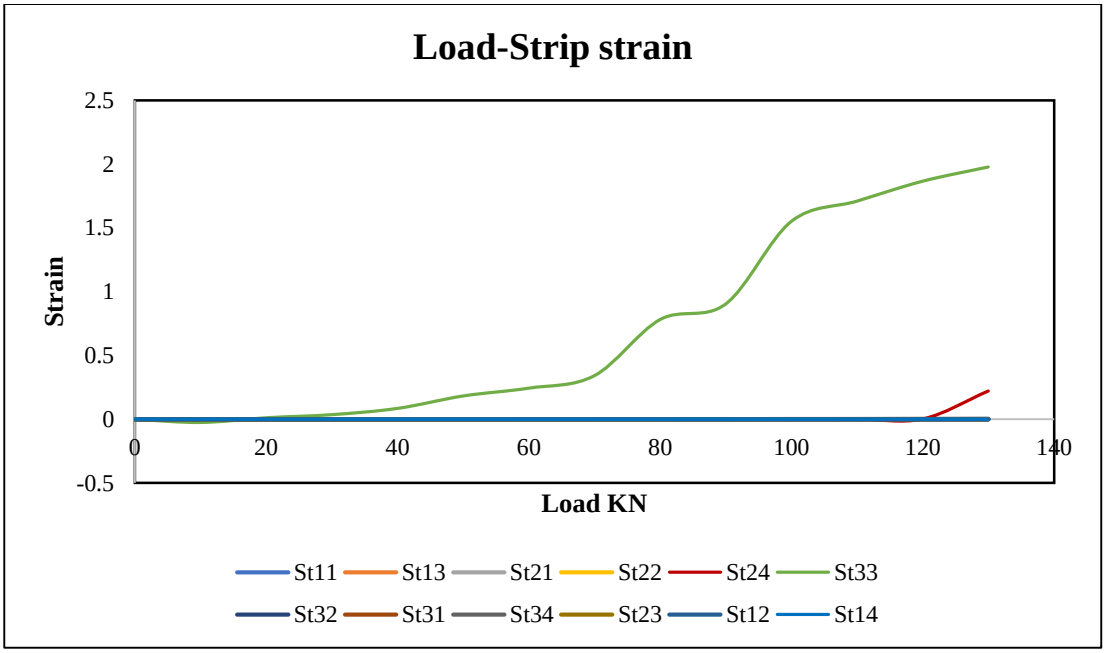

Figure 4.26. Load-Strip Strain for different strips strain locations with zigzag strips shape.

4.10. Depth displacement curve

➢ Case One (Zigzag reinforcement shape)

In Zigzag strips reinforcement the relationship between the soil depth and panel displacement is positive one due to increasing the load with increasing the depth of soil as illustrated in Figure 4.27.

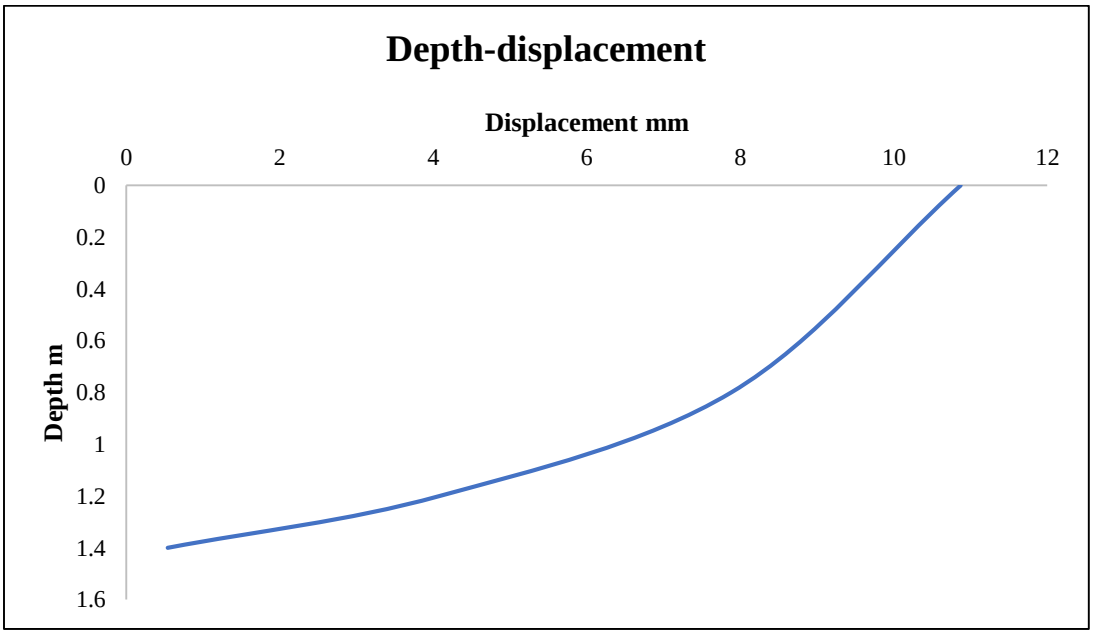

Figure 4.27. Depth-displacement for Zigzag strips shape.

➢ **Case Two (Straight reinforcement shape)**

In straight strips reinforcement the relationship between the soil depth and panel displacement is positive one due to increasing the load with increasing the depth of soil as illustrated in Figure 4.28 in comparison with Figure 4.27 zigzag strips resists soil more than straight one.

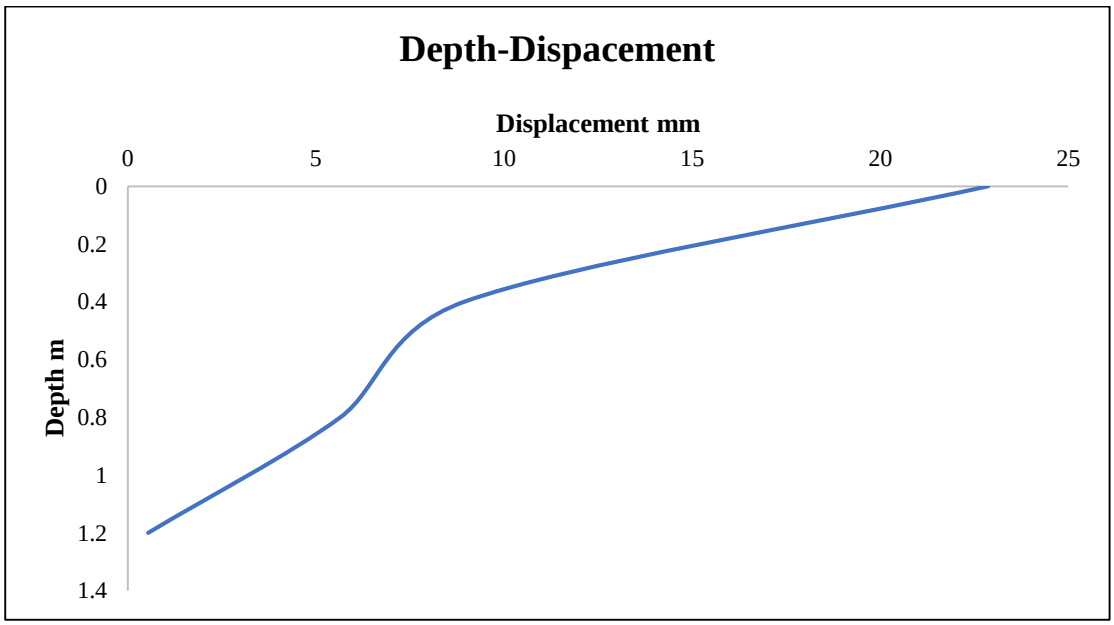

Figure 4.28: Depth-displacement for Straight strips shape.

It can notice that the change in the shape of reinforcement from the Zigzag (Z-shape) to the straight (I-shape) at the same width increased the lateral displacement in both edge and middle panel about 32% & 50% respectively.

4.11. Case Study

The Alum intersection MSE bridge in the centre of Hilla, Babylon governorate, which was referred for implementation by the municipality of Hilla in late 2012. The project is financed from the budget for the development of the regions allocated to the province of Babylon, and it consists of 3 axes of movement in addition to an intersection. and 40th Street. The bridge details and cross-sectional area are demonstrated in Figure 4.29 to Figure 4.32.

Figure 4.29: Location of Alum intersection MSE bridge in Hilla.

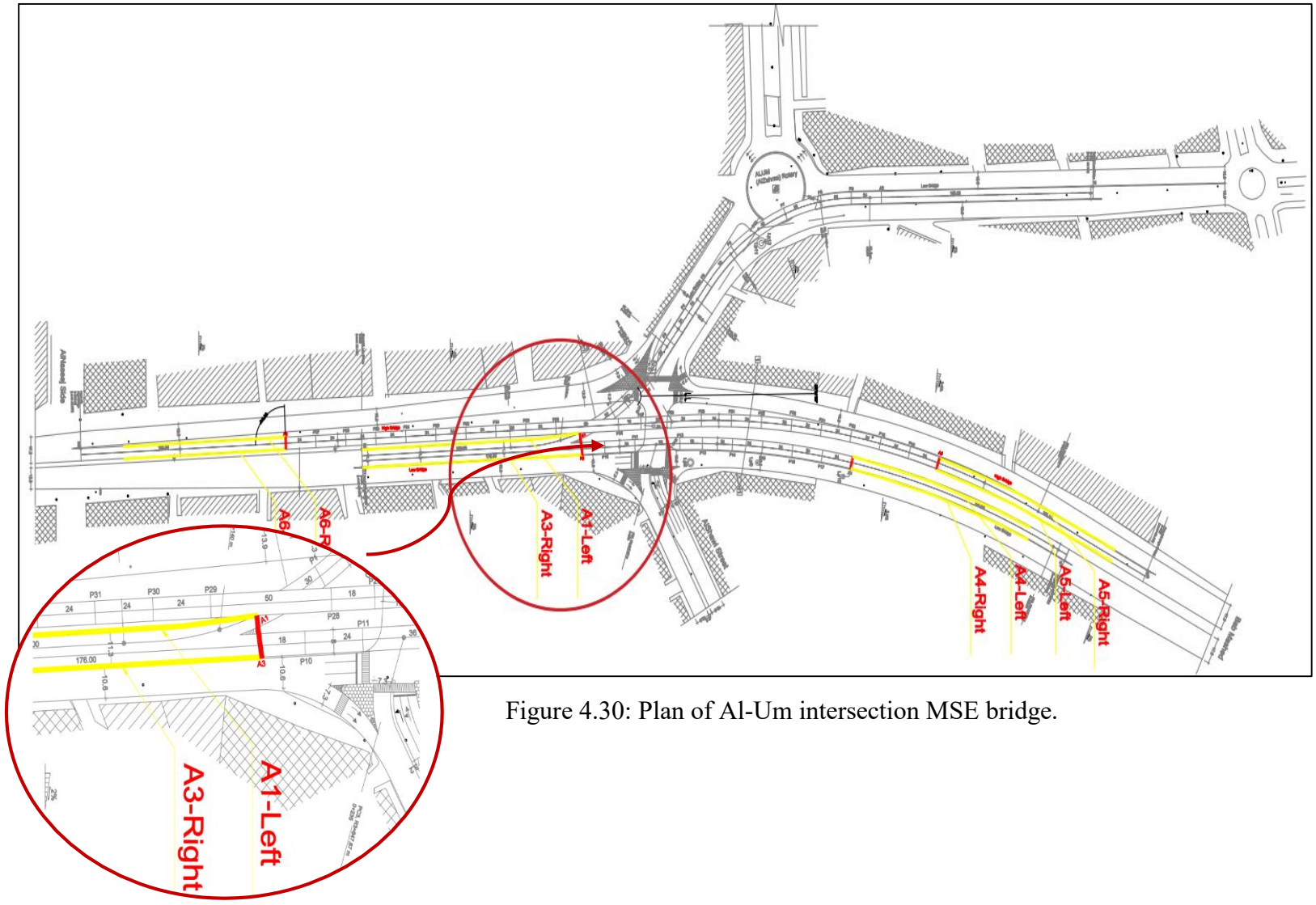

Figure 4.30: Plan of Al-Um intersection MSE bridge.

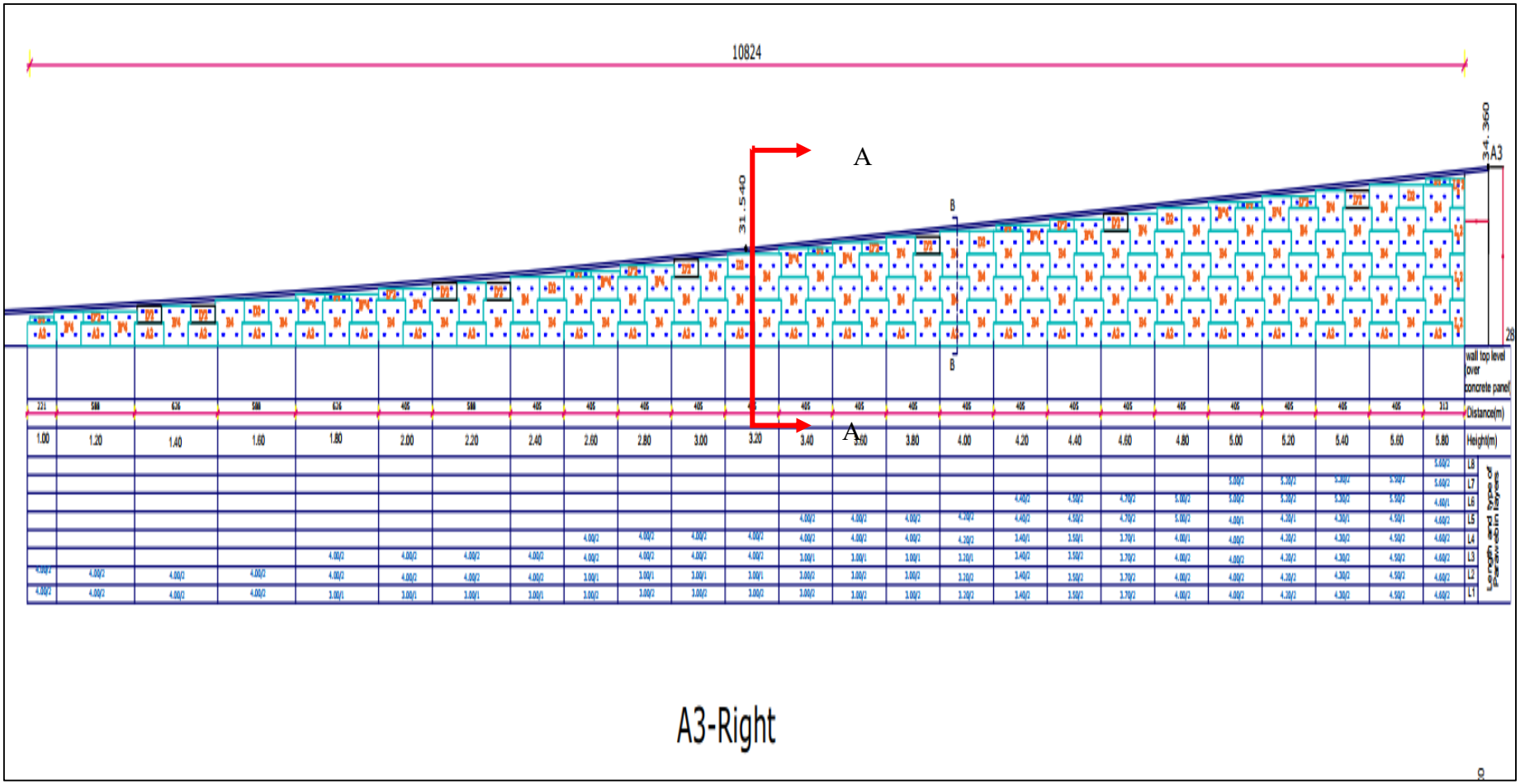

a) abutment side of bridge

Figure 4.31. Cross-sectional area of Alum intersection MSE bridge.

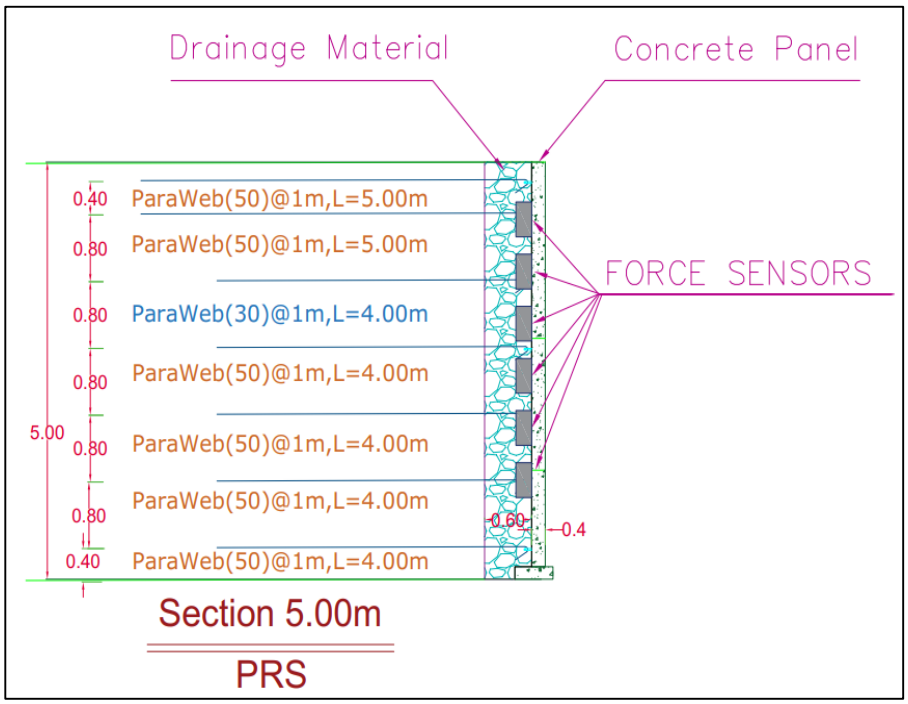

b) Section A-A in bridge abutment

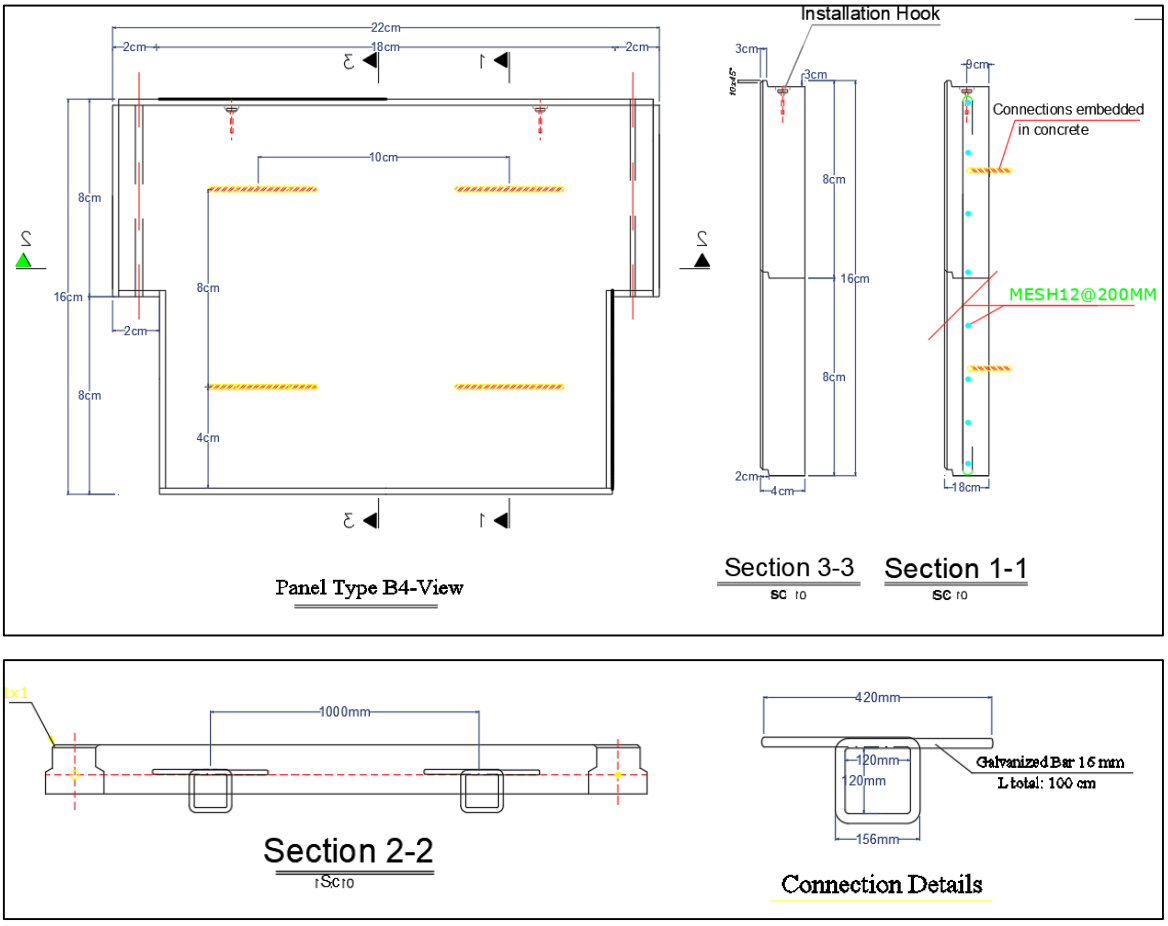

c) Details of panels in MSE wall

Figure 4.31. Cross-sectional area of Alum intersection MSE bridge (continued).

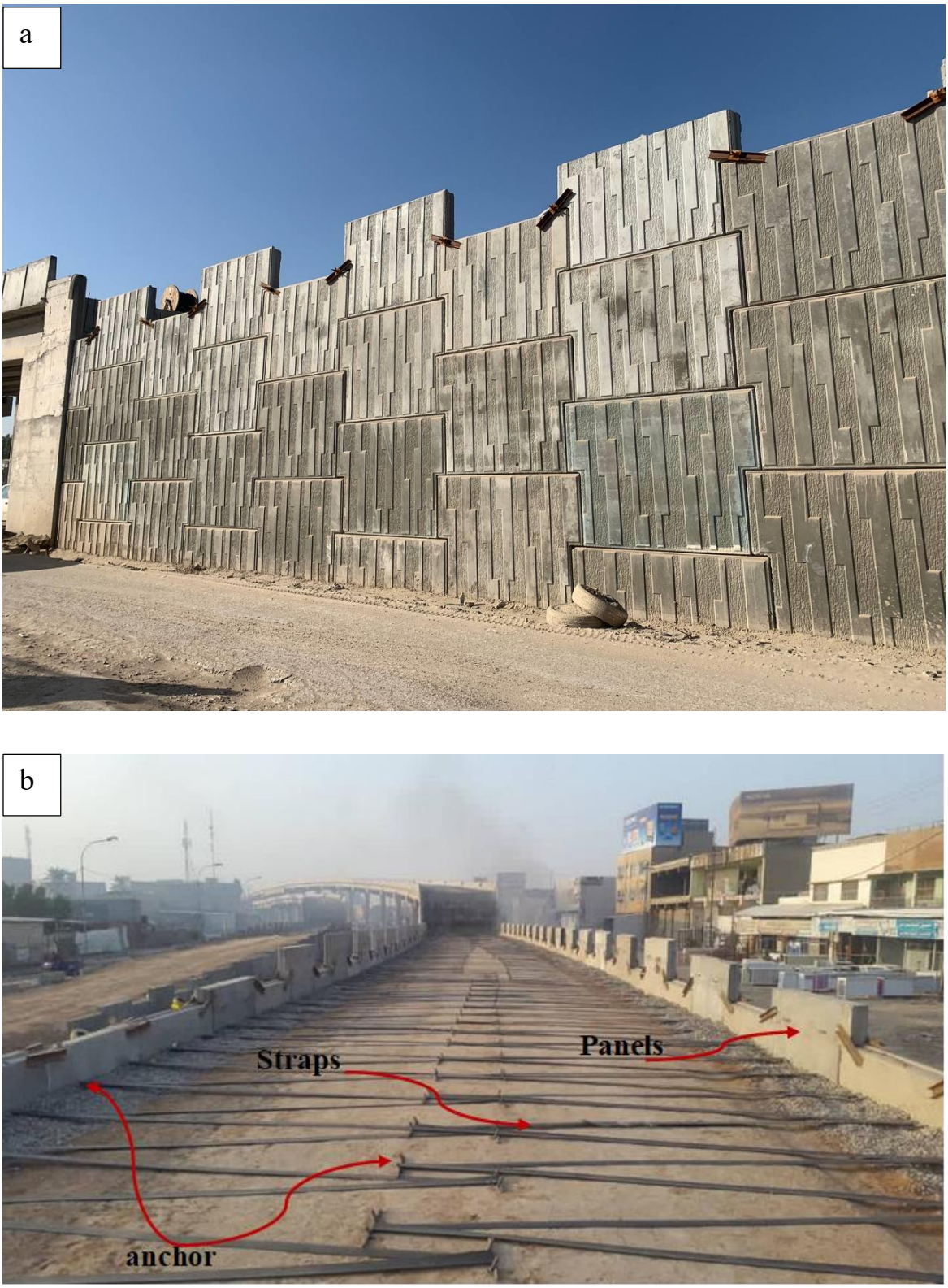

Figure 4.32. Alum bridge Overview during the construction process.

4.11.1 Execution Sequence

4.11.1.1 Foundation Preparation

Inappropriate stuff shall be removed from the surface on which the PRS walls are to be constructed. Such materials include organic soil, plants, waste stuff or any sort of irrelevant materials. After by, the soil of foundation must be compacted so that a minimum density of 90% is achieved.

4.11.1.2 Placing Levelling Pad and Erecting First Row of Concrete Panels

At this stage, a layer of lean concrete with cement content of 150 kg/m^3 shall be poured over the foundation based on the characteristics given by the supervisor It should be noted that the purpose of such surface is merely to provide a guidance level as shown in Figure 4.33 for installing the panels and it does not function as a structural foundation. At next step, first the half-size concrete panels are implemented, then the full-height ones are installed and levelled vertically afterwards.

Figure 4.33. Concrete placing and leveling

4.11.1.3 Conducting First Backfill Layer, Compaction up to the level of 1st reinforcement tier:

At this stage, the first soil layer is conducted with approximately 20 cm thickness and then compacted. The minimum density of backfill soil is 95% based on AASHTO T-99.

4.11.2 Soil analysis of the bridge

The compacted soil that is used in Alum intersection MSE bridge has been characterized as shown in Table 4.4. The particle size distribution is compatible with limits of the Iraqi requirement No.45/1984 (zone 2) as shown in Figure 4.34.

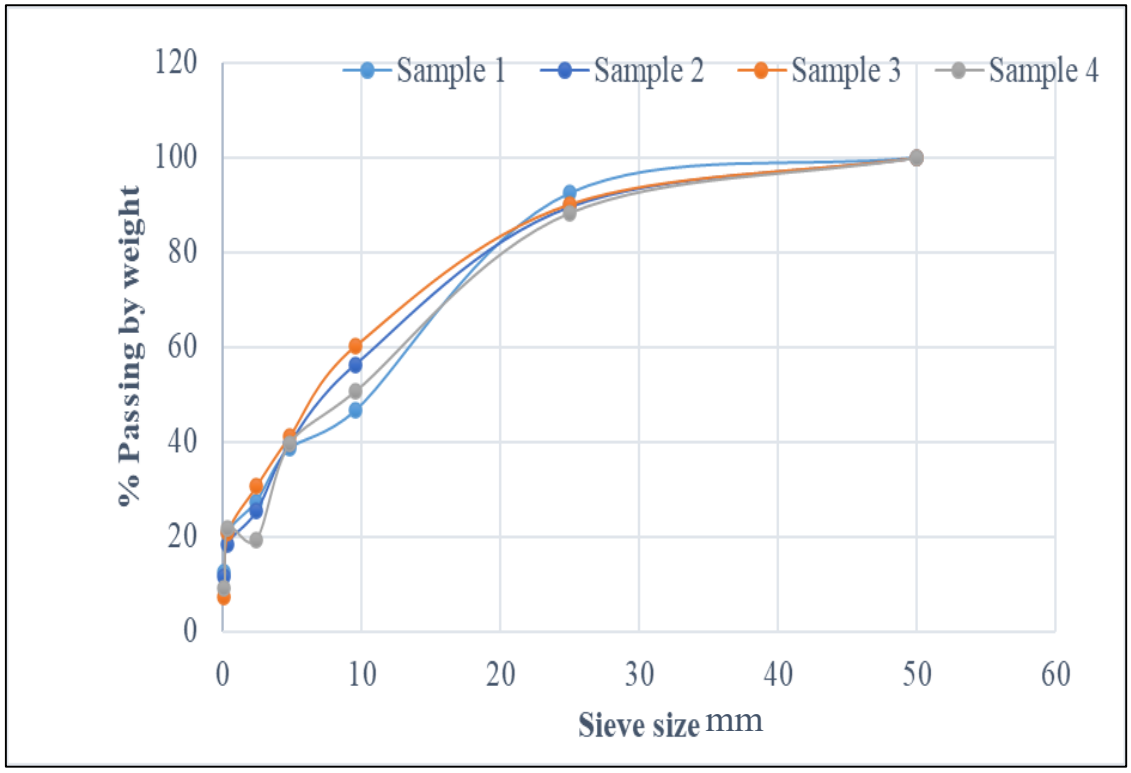

Figure 4.34. Soil sample particle size distribution.

Table 4.4. The compacted soil characteristics that are used in Alum intersection MSE.

Properties	Test results Sample				Limits of the Iraqi requirement No.45/1984 (zone 2)
	1	2	3	4	
Max. dry density (MDD) (gm/cm^3)	2.206	2.214	2.209	2.206	-
Optimum moisture content (OMC) %	9.32	10.76	10.00	10.36	-
The California loading Ratio for 95%.	40.17	38.56	41.75	38.56	≥ 35 (class B)
Liquid Limit LL %	22.46	20.36	20.89	22.89	≤ (25- 35)
Plasticity Index PI %	4.36	3.91	3.95	4.55	≤ 6 ≤ (4-9)
Sulfate content %	4.08	4.49	4.11	4.08	≤ 5
soluble salts %	6.92	7.93	7.36	6.97	≤ 10
Gypsum ratio %	8.77	9.65	8.836	8.772	≤ 10.75
Organic matter ratio %	1.85	1.66	1.16	1.5	≤2

4.11.3 Technical Requirements and Considerations for PRS System

4.11.3.1 Criteria of Material Loading, Design and Test

The principles and criteria of loading, design and testing of PRS walls are based upon the standard of AASHTO 1996.

4.11.4 Specifications of Backfill Soil

4.11.4.1 Particle Size Distribution

Gradation of the backfill soil must be conducted according to AASHTO T-27 and be compatible with the quantities below.

Table 4.5: Gradation of the Backfill soil according to AASHTO.

	U.S. Sieve Size	Percent Passing
Gradation (AASHTO T-27)	4 in. (102 mm)	100
	No. 10 (0.425 mm)	0-60
	No. 200 (0.075 mm)	0-15

4.11.4.2 Plastic Index

Plastic index (PI) for the backfill material must be smaller than 6, according to AASHTO T-90.

4.11.4.3 Integrity and Accuracy

Backfill soil must be free from organic material, loose particles, Shale, industrial remnants, and waste material. Based on AASHTO T-104.material's weight loss is not permissible to either exceed 15% following 5 cycles by Sodium Sulfate solution, or 30% following 4 cycles by Magnesium Sulfate solution.

4.11.4.4 Electrochemical Qualifications of Backfill Soil

The permissible range of PH for the backfill soil with polymeric straps is 4-10 (Y.-J. Kim et al., 2019).

4.11.4.5 Specifications and Compaction of Backfill Soil

Each fill layer must be maximum 20cm thick and compacted to achieve a minimum density of 95% according to AASHTO T-180 (Officials, 2011).

4.11.5 Polymeric Straps Qualifications

Polymeric straps must be in accordance with the specifications mentioned in the drawings. Final confirmation of the Polymeric straps will be upon the supervisor. Responsibility of the compatibility of Polymeric straps specifications with the technical characteristics mentioned in data sheet is with the contractor. Installing of Polymeric straps was: First layer of reinforcement shall be connected to the concrete panels and be laid Z-shape on the soil behind panels via a 16mm diameter steel bar. However, the Polymeric Straps that used in Alum bridge with the method of fixing is shown in Figure 4.35.

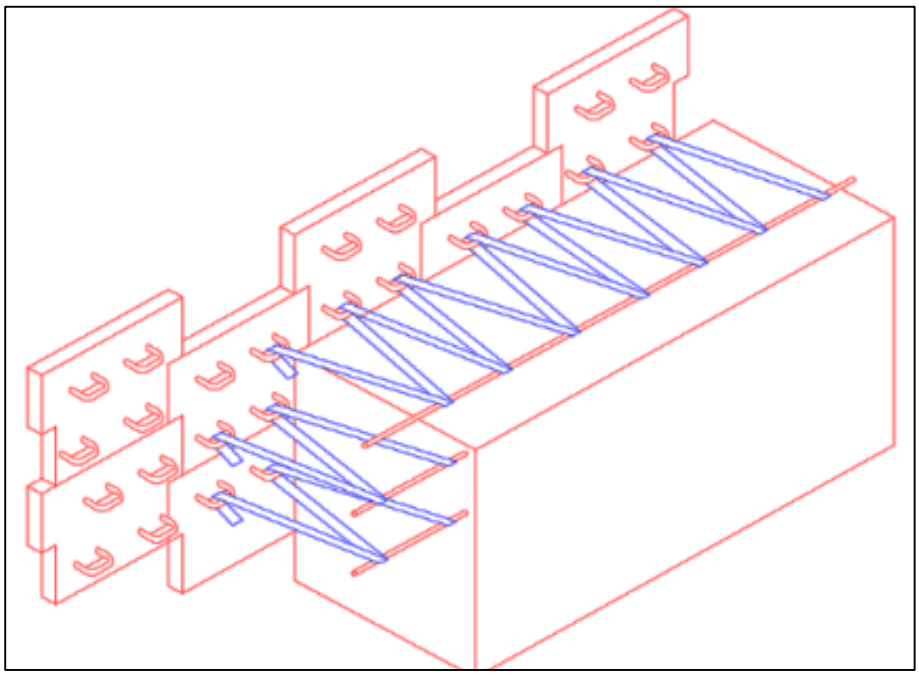

Figure 4.35. Polymeric Straps that are used in Alum bridge with fixing process.

4.11.6 Specifications for Connections of Polymeric Straps and Precast Concrete Panels

The connection between the Polymeric straps and the facing concrete panels is mechanical.

4.11.6.1 Facing Precast Concrete Panel Qualifications

The standard shape of the panels is T form and dimension is 2.21x1.6x0.18 m. They shall be reinforced by thermal mesh. The minimum cylindrical compression strength for 28-day concrete samples is 250 kg/cm^2. Due to the contact between facing panels and susceptibility to weather conditions, the cement applied in making the molds shall be of a moderately sulfate resistant cement or high levels of sulfates. Panels must be inspected meticulously to ensure they are clean of any sort of porosity, breakage, crack or other flaws. Installation of Facing Panels Conducting and Compaction of Soil for Items 6-3 and 6-4 must continue until the wall top. The fixing of panel as shown in Figure 4.36.

Figure 4.36. Facing Precast Concrete Panel Casting and fixing

4.11.7Sensors

Curiotec, SS300-2T, S-Type Load cell, 2T, has been used in Alum intersection MSE bridge as shown in Figure 4.37.

Figure 4.37. Load cell SS300-2T sensor that is used in Alum intersection.

The method of placing the sensor within the bridge structure and the preparation for installing the sensors on the inner face of the wall toward the soil is shown in the figures below. The first step was calibrating the sensors by applying standard loads, and then it has been manufactured a steel box to keep the sensor from damage. Then it has been made a hole near the panel and put it in a plastic pipe. When the sensors were calibrated, the sensors were placed inside the plastic pipe. Then, the pipe was gradually lifted, and the sensors remained inside the soil. The sensors have been distributed on the MSE wall in different depth and location to investigate lateral load on the wall near abutment as demonstrated in Figure 4.38 to Figure 4.39.

Figure 4.38. Method of preparation of the sensors to install in Alum bridge.

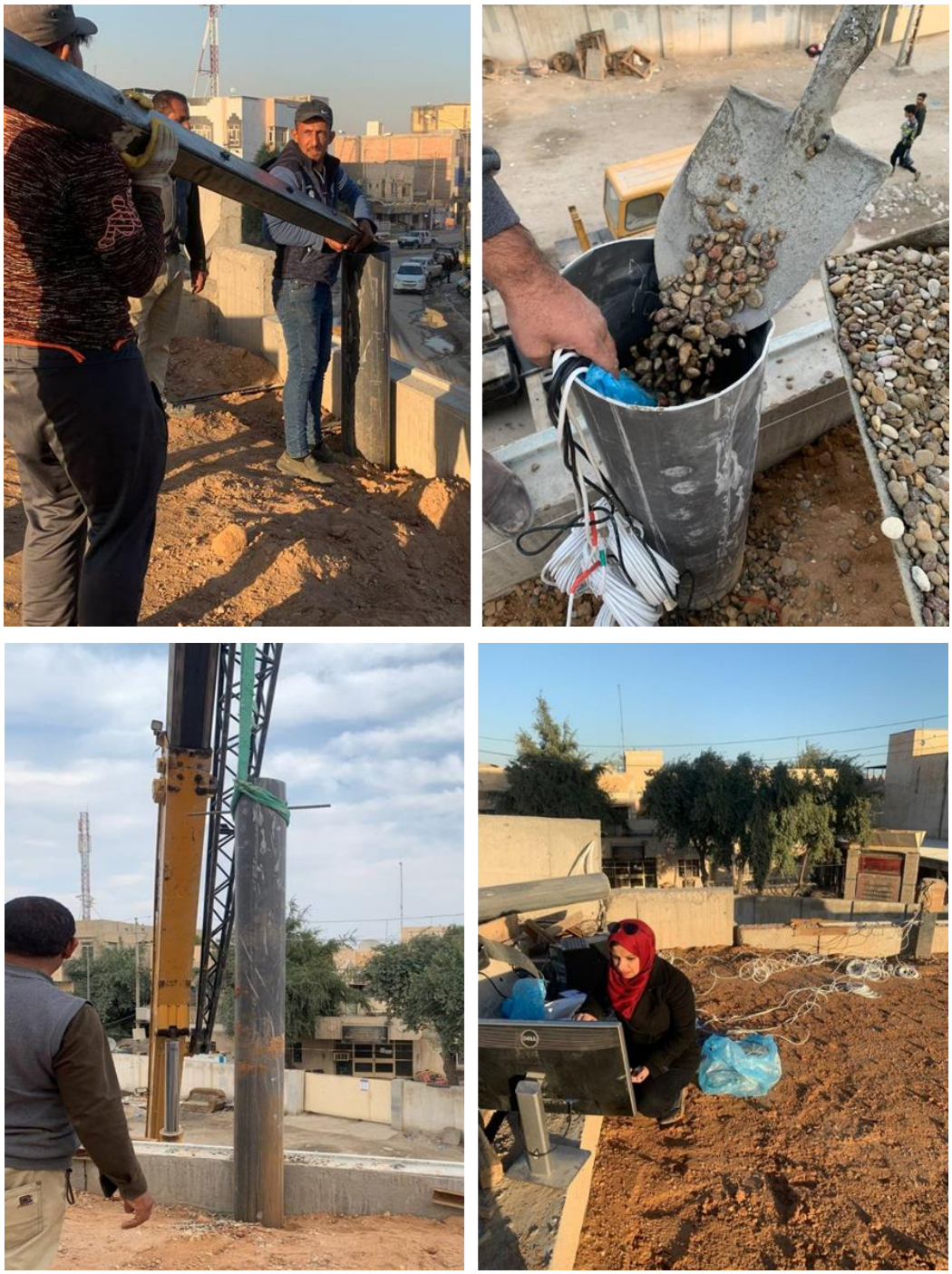

Figure 4.39. Method of placing and instilling the sensors in Alum bridge.

4.11.8 Results and discussion

Based on Figure 4.40, the sensors were computerized setting to record the loads on sensors continuously without stopping for any conditions such as working hour or load availability.

Figure 4.40. Photos taken during the load test in AL-Um intersection bridge.

4.11.8.1 Load-Depth Under static load

Figure 4.41 shows the relationship beteen load-depth under static load for different sensors at depths at the bridge, where the relationship is positive and increasing the depth led to increase lateral load, but overall, the relationship is not linear one and increasing the depth from 1.5 to 2 m has insignificant effect on the lateral load, which refer to high load on the surface and decrease the lateral pressure with increasing the depth of soil. Based on Pathak et al., (Pathak et al., 2021) the lateral load increased with increasing the depth of the soil due to increase the pressure of soil that resulting from increasing the soil weight along with increasing depth of sensor.

On the other hands, the absence of polymer strips on soil strengthening lead to increasing the static load on the foundation of bridge due to the dead load of soil and increasing the depth of soil lead to increase the load on the foundation (Madabhushi et al., 2009; Shukla, 2017), as shown in Figure 4.41.

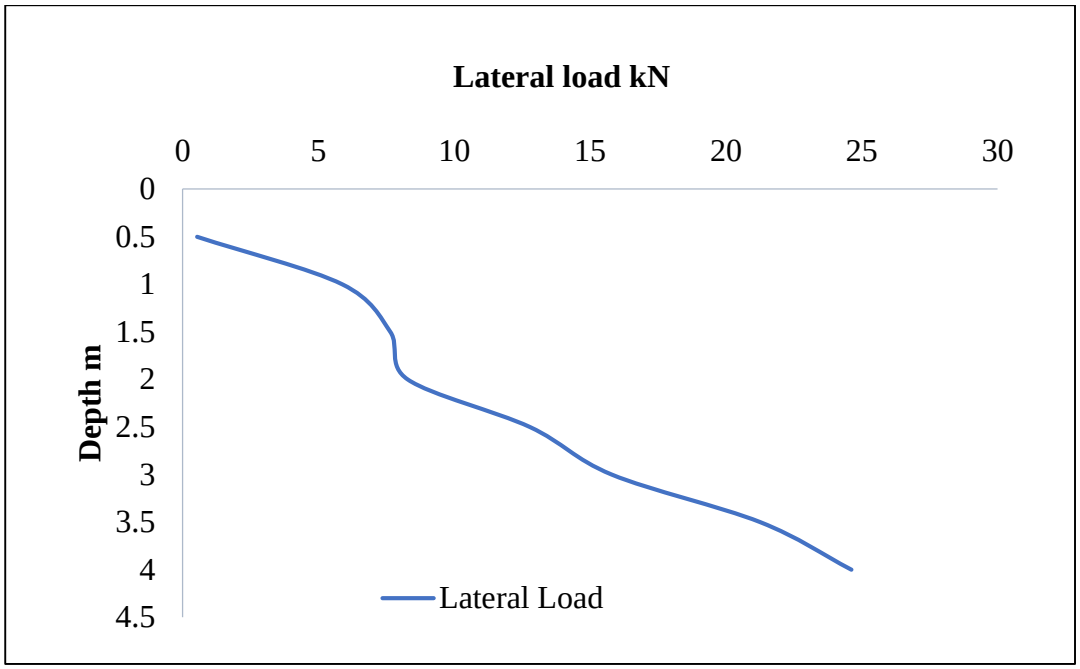

Figure 4.41. Load-depth under static load

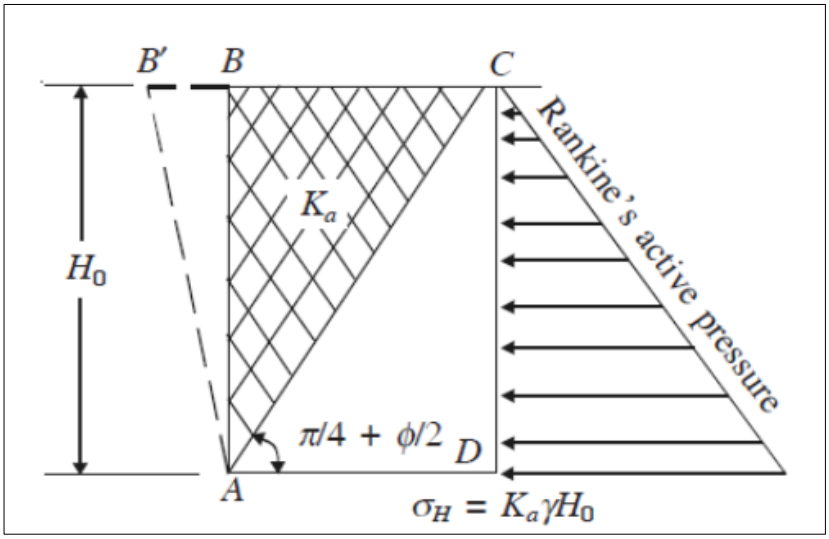

Figure 4.42. Pressure Distribution for non-strengthened soil (Varghese, 2005).

4.11.8.2 Load-Depth Under Moving Load

Figure 4.43 and Figure 4.44 show the relationship beteen load-depth under dynamic load for different sensors at depths at the bridge, where the

relationship is positive and increasing the depth lead to increase lateral load, but overall the relationship is not linear one as a load-depth under statical load and increasing the depth from 0.5 to 1.5 m has insignificant effect on the lateral load (Rameesha et al., 2019).

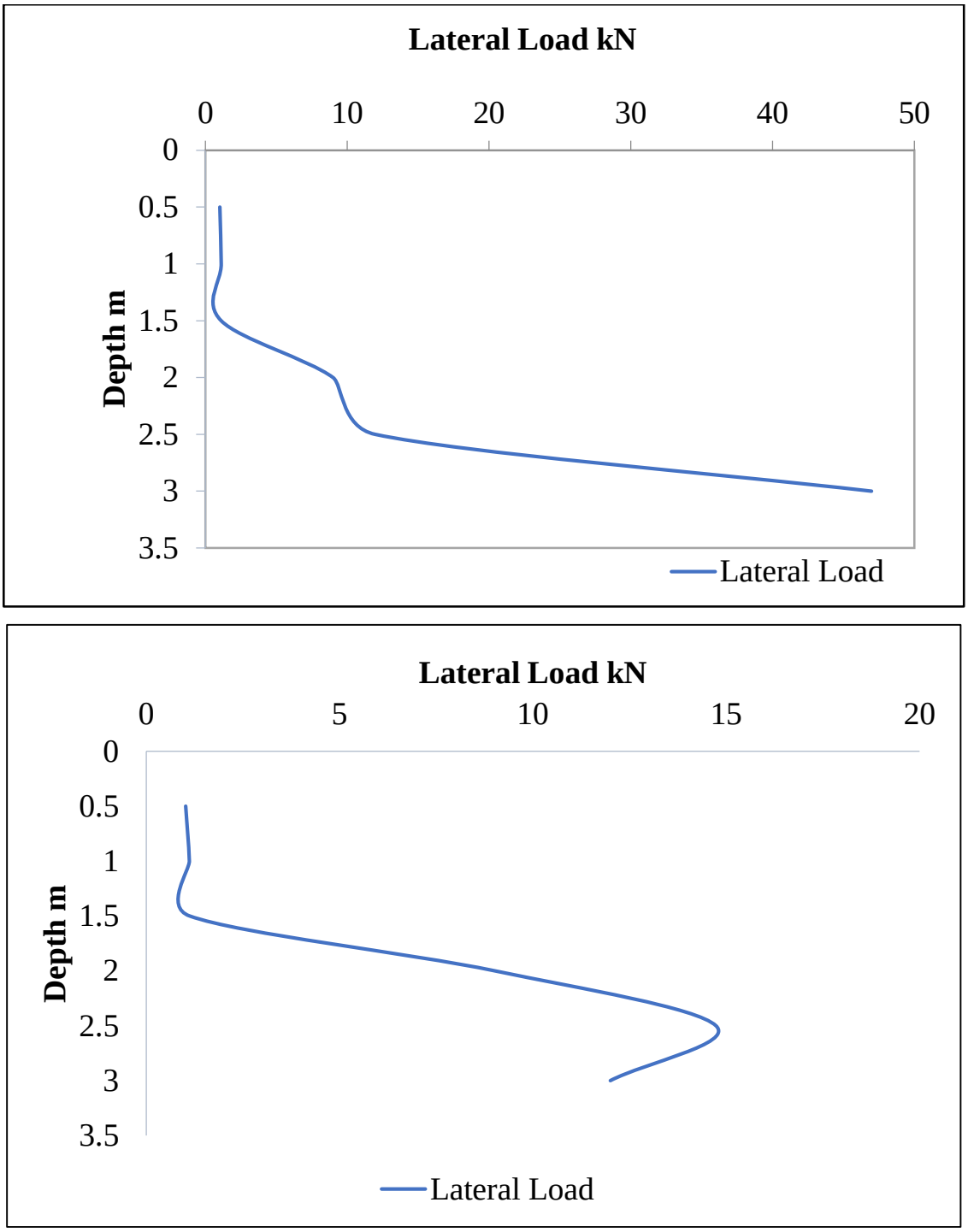

Figure 4.43. Load-Depth of wall under dynamic load with time.

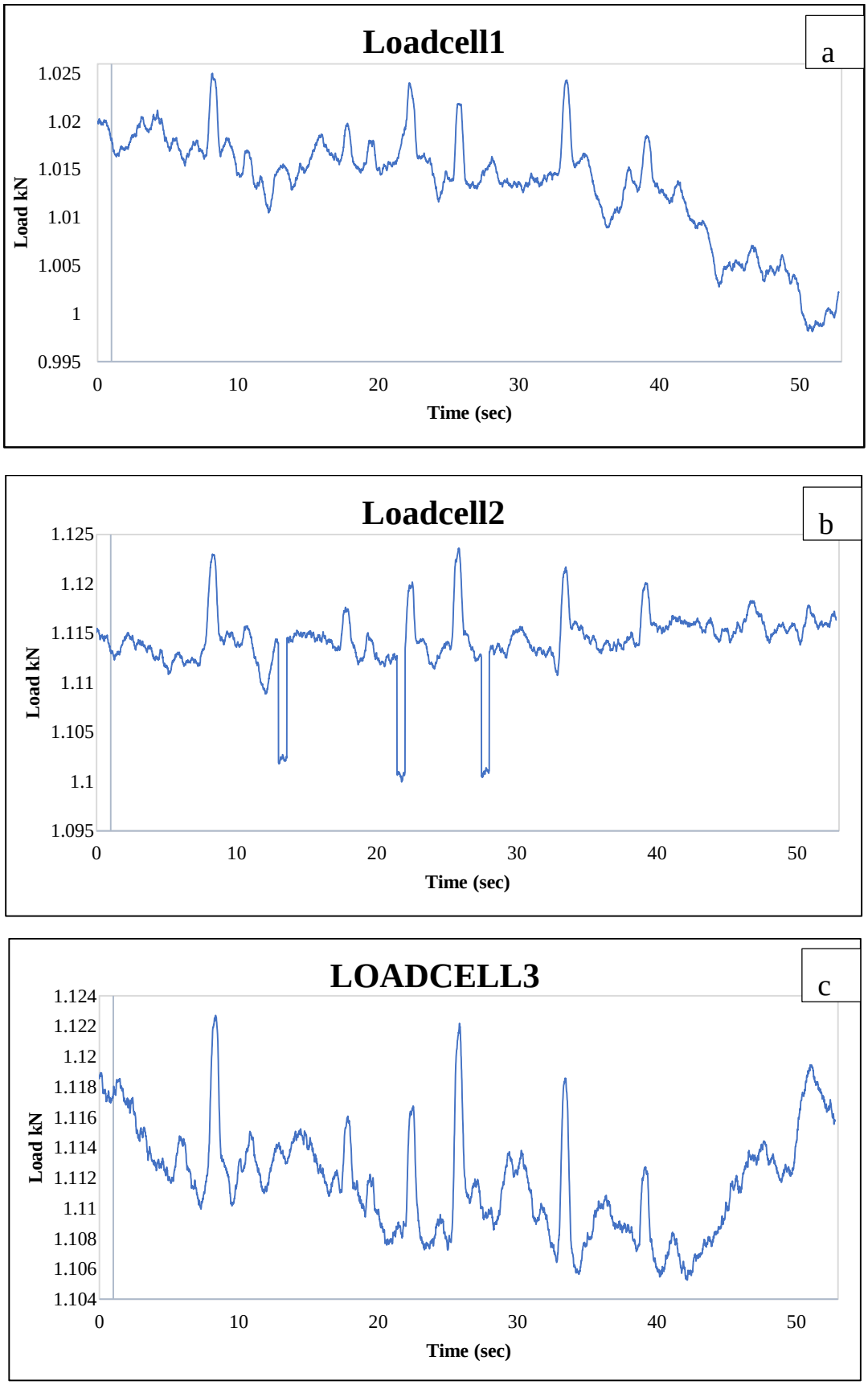

Figure 4.44. Cell 1, 2, 3, and 4 recording with time.

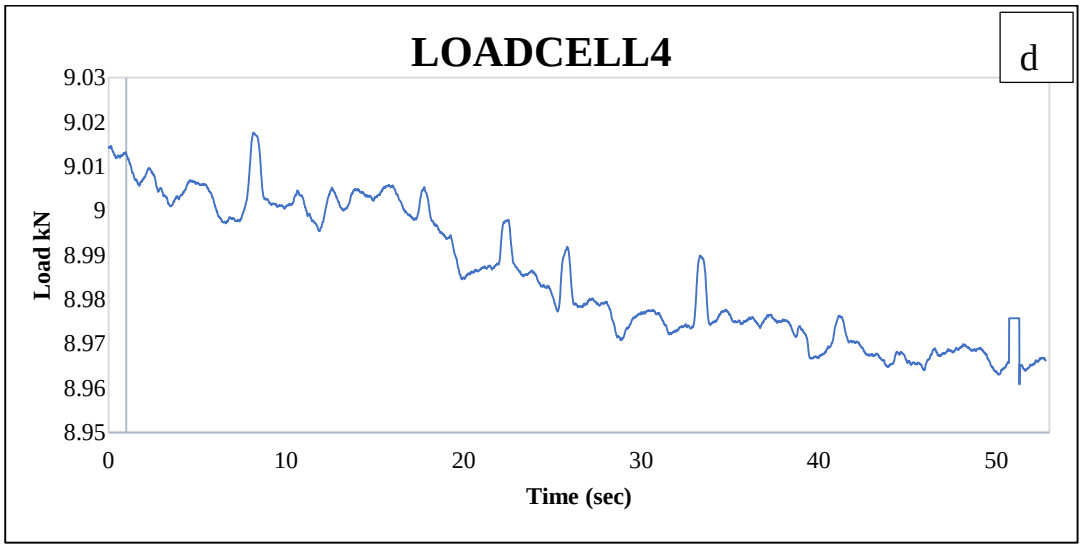

Figure 4.44. Cell 1, 2, 3, and 4 recording with time (continued).

The above relationships show us that the relationship between lateral load and time under the dynamic load (Vehicles) is nonlinear. Additionally, it is seen that the highest lateral load occurs in the load cell situated closer to the surface. Also, we can conclude that the effect of surcharge load on the lateral pressure decreases with the depth increase.

Static loads refer to forces or loads that are applied to a structure or object in a stationary or unchanging manner. These loads do not vary over time, and they can include the weight of the structure or object itself, as well as any external forces applied to it, such as gravity, wind, or other environmental forces. Static loads are typically analysed using the principles of statics, which is a branch of mechanics that deals with the analysis of forces and their effects on stationary objects. The results of a static load analysis can be used to determine the strength and stability of a structure or object under the applied loads, and to design it to meet the required performance criteria.

Dynamic loads refer to forces or loads that vary over time or that are applied to a structure or object in a changing or fluctuating manner. These loads can be caused by a variety of factors, such as the movement or vibration of a

structure or object, the impact of external forces, or the effect of changing environmental conditions. Dynamic loads can be more challenging to analyse and design for than static loads, as they often require the use of more advanced techniques and tools, such as finite element analysis or dynamic structural analysis. The results of a dynamic load analysis can be used to determine the strength and stability of a structure or object under the applied loads, and to design it to meet the required performance criteria.

However, the main difference between static and dynamic loads is explained as:

- In engineering, a load is a force that is applied to a structure or a component. Static loads are loads that are applied to a structure or a component and are not expected to change over time. Examples of static loads include the weight of a building or the weight of a car.
- Dynamic loads, on the other hand, are loads that vary with time and are often caused by the movement or vibration of a structure or component. Examples of dynamic loads include the impact of a car hitting a pothole or the vibrations caused by wind gusts.
- It is important to consider both static and dynamic loads when designing a structure or component, as different materials and designs may be better suited to handling one type of load over the other.

CHAPTER FIVE

FINITE ELEMENT MODELLING BY ABAQUS

CHAPTER FIVE

Finite Element Modeling By ABAQUS

5.1 General

This chapter discusses the outcomes of numerical work, also, presenting a comparison between the results of the investigational work and the finding from the finite element analysis (FEA) method. Three variables were considered, including the impacts of load position, the thickness of strips, width of the strips under static load. Abaqus/Standard 3D Experience R2019x, which is an advanced 3D finite element computer program was adopted to perform a nonlinear FEA to analyze the behavior of the MSE wall that was conducted experimentally in the current study.

5.2 ABAQUS

Numerical simulation can be employed to examine the interaction among various constituents of retaining structures. This may facilitate a more comprehensive understanding of the responsive characteristics of retaining walls. The primary advantage of utilizing a FEM for the analysis of soil-structure interaction is its potential to accommodate variations in the soil medium or structure, also irregularities in the materials and geometry. The FEM of the MSE wall is generated using ABAQUS/CAE19, a computer-aided engineering software. The ABAQUS/CAE19 software is a valuable tool for the modelling and analysis of mechanical components, parts, and assemblies. It is primarily utilized for preprocessing and predicting the outcomes of finite element analysis. The software provides accurate and resilient resolutions to non-linear problems, in addition to a diverse array of linear dynamic implementations and standard design simulations. This software facilitates the

generation and incorporation of geometric shapes from the beginning. The software allows users to strategically utilize a comprehensive range of analytical functions, including but not limited to failure, fracture, damage, connections, and acoustics. The principles of contents, sections, interactions, and steps are well-established in ABAQUS, contributing to a user-friendly interface. The MSE wall simulation has been conducted utilizing the finite elements ABAQUS. The 3D truss was utilized to represent the reinforcement, while the 3D deformable body was employed to depict the concrete.

5.3 Finite element approach (FEA)

The FEA is a branch of numerical analysis that adopted in a lot of engineering applications and to solve complex problems under the effects static and dynamics loadings because of it power full method to simulate the actual environments conditions of tests. The selected a suitable element and the method of solving the iterations are very important to reach to the final solution and find the unknown parameters. The selected element needs to define the geometry and material properties with the mechanical properties for each element **(Abaqus, 2011).**

The general solutions of the finite elements are to combine all variables in set of equations by applying the equilibrium and compatibility equations. The final equations are represented by matrix and then assembly for all elements that represent the known geometry and then by iterative the solution of these equations gave the approximate with acceptable round off error that relay on the assumed tolerance. Finite elements approached passing by steps starting from creating key points, lines, area and then volume with suitable meshes around unity for cubic element shape to create whole geometry of the problem.

5.3.1 Materials Properties

In three-dimensional finite element analysis, the performance of any structure under load was determined by the behavior of the material used to construct the member (modulus of elasticity, Poisson's ratio, and material stress-strain relationship).

Appendix **C** shows the behavior and properties of the materials used in this study.

5.3.2 Modeling of specimens

This section discusses the MSE wall parts and assembly, the interactions between the elements and the load and boundary conditions used in this study.

5.3.3 Parts and Assembly

The model consisted of many parts: A Blinding layer, Soil and strips, bearing plate at load, reinforcing bar, rigid wall, foundation, and concrete panel, as shown in Figure 5.1. Each component is drawn separately, assembled, and merged with the other elements to form the MSE wall. The assembly of parts used in modelling specimens is shown in Figure 5.2.

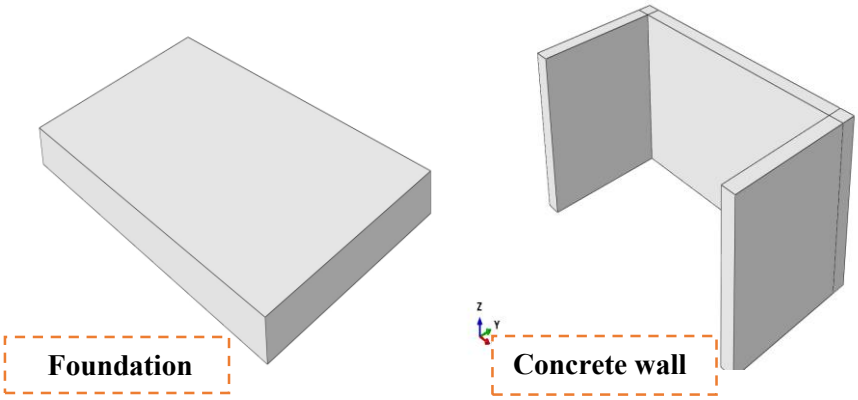

Figure 5.1. Creating parts in ABAQUS software program.

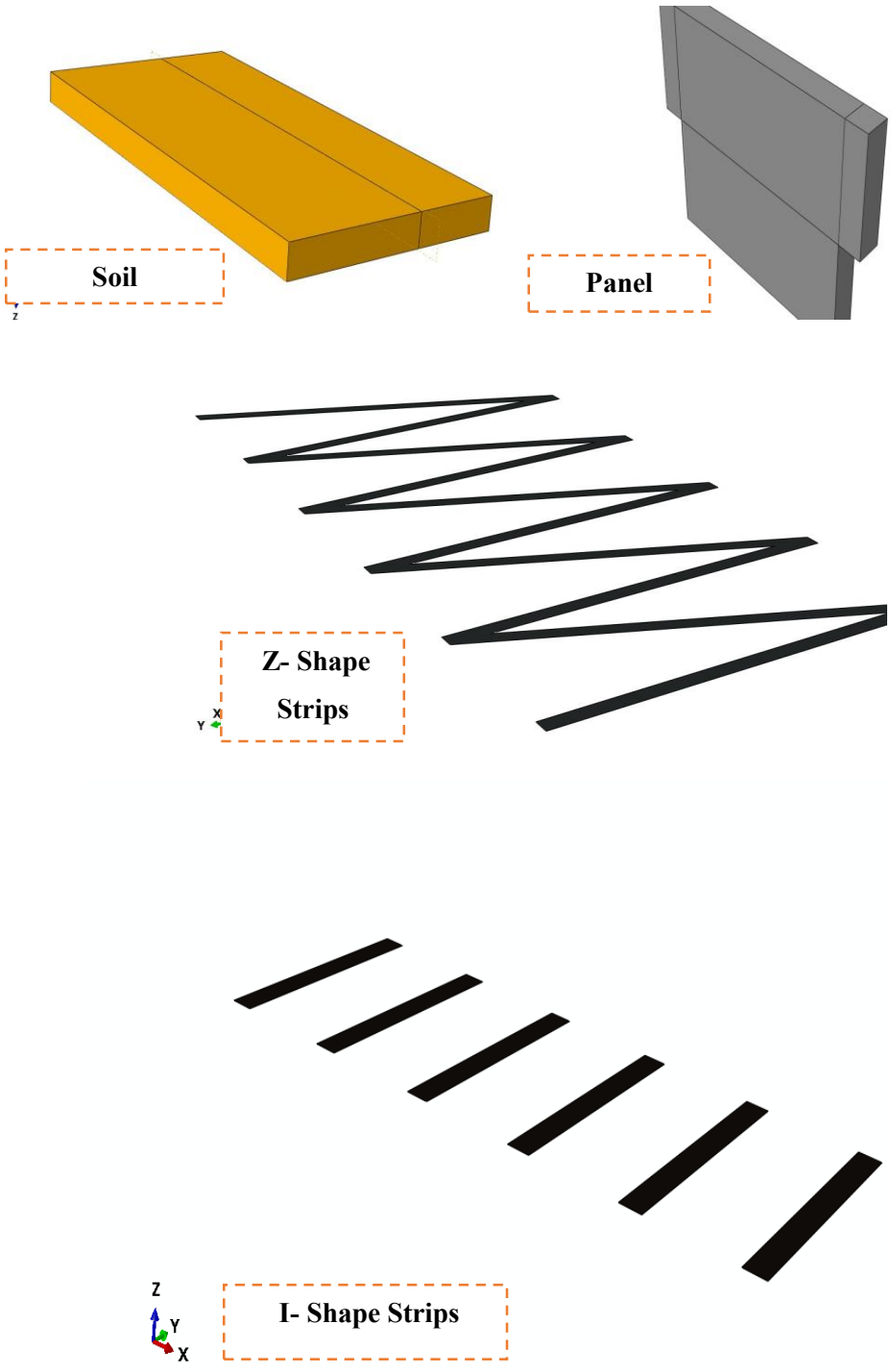

Figure 5.1. Creating parts in ABAQUS software program (continued).

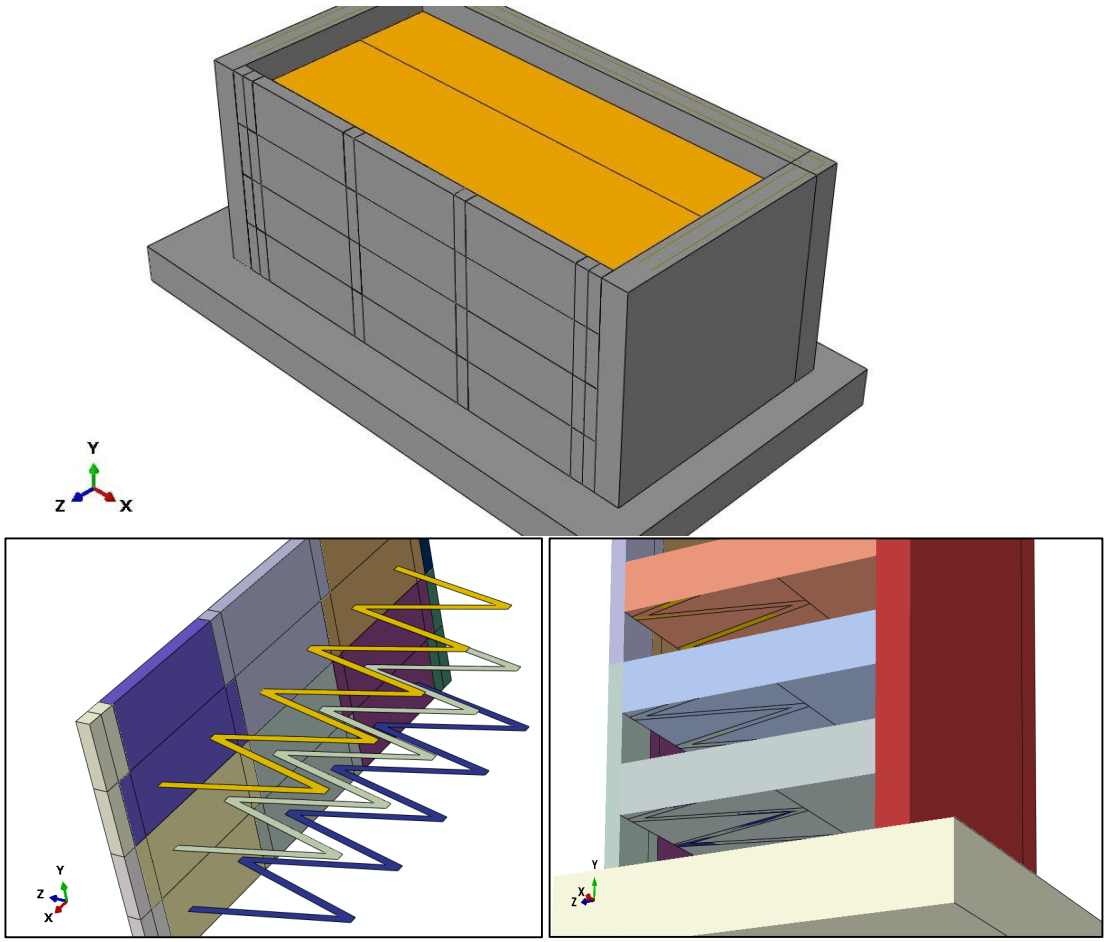

Figure 5.2. The assembly parts of MSE wall.

5.4 Finite element modeling Interaction Between parts

After assembling the parts, which must be connected to operate a composite system, Surface to surface interaction was adopted to simulate contact behavior between soil and MSE wall with normal and tangential behavior with 0.45 coefficient of friction.

Contact finite element formulation introduced in the modeling is based on the kinematic method: contact without penetration and friction conditions are described kinematically at the nodes. They are expressed in terms of displacements and forces. In accordance with Figures 5.3-5.7, the normal displacement and corresponding normal force are (Un, N) and tangent displacement with corresponding force are (Ut, T), both conditions can be written as follows (N.-H. Kim, 2015):

Contact without penetration.

$$(U_n \geq 0, N \geq 0) \Rightarrow U_n N = 0 \tag{5.1}$$

$$\left(U_t > 0 \Rightarrow -\vec{T} = \mu \vec{D}\right) \Rightarrow U_n N = 0 \text{or} \left(U_t = 0 \Longrightarrow -\vec{T} < \mu \vec{D}\right) \tag{5.2}$$

Where $\mu = \frac{T}{N}$ is the friction coefficient $\left(\frac{T}{N}\right)$ and $\vec{D} = \frac{\vec{U}_t}{|\vec{U}_t|}$

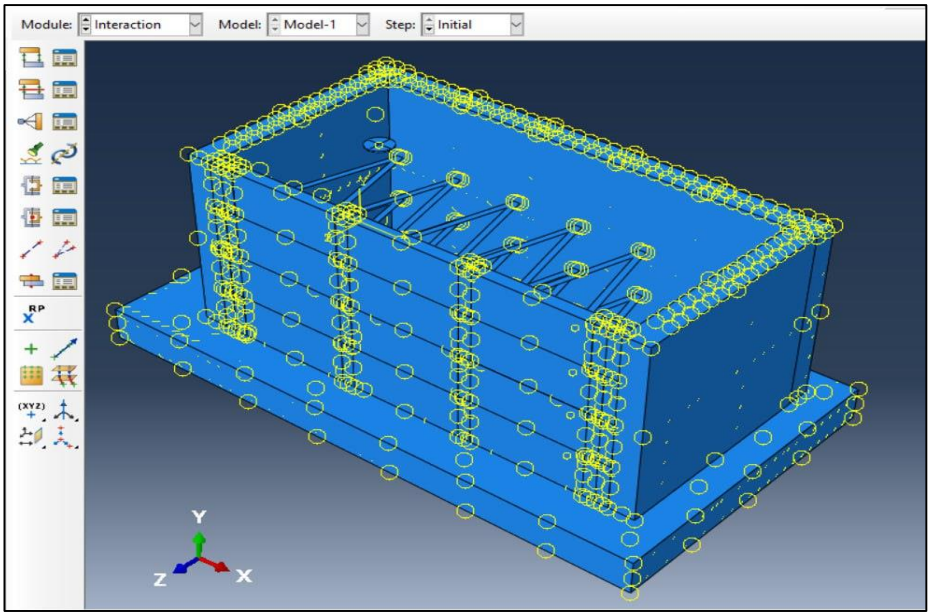

Figure 5.3: Interaction between soil and MSE wall

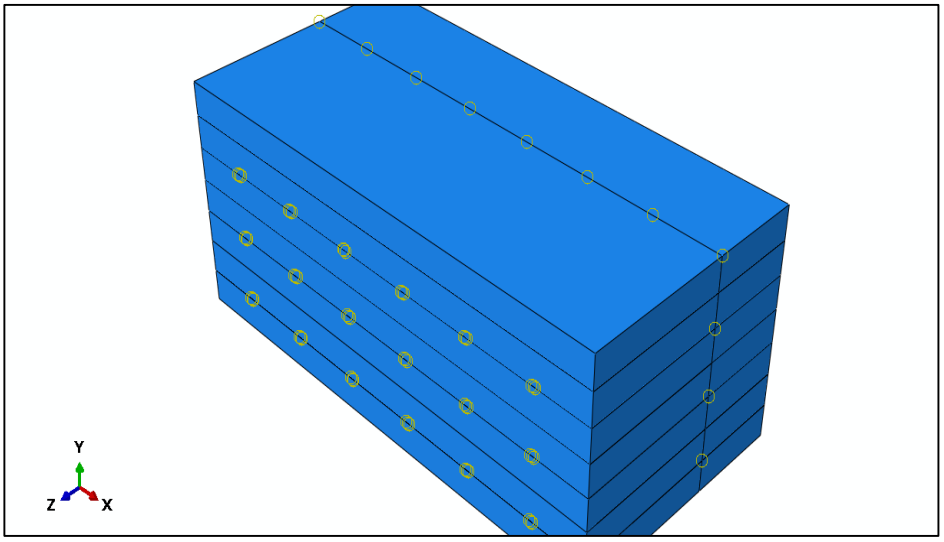

Figure 5.4: Interaction between soil and soil

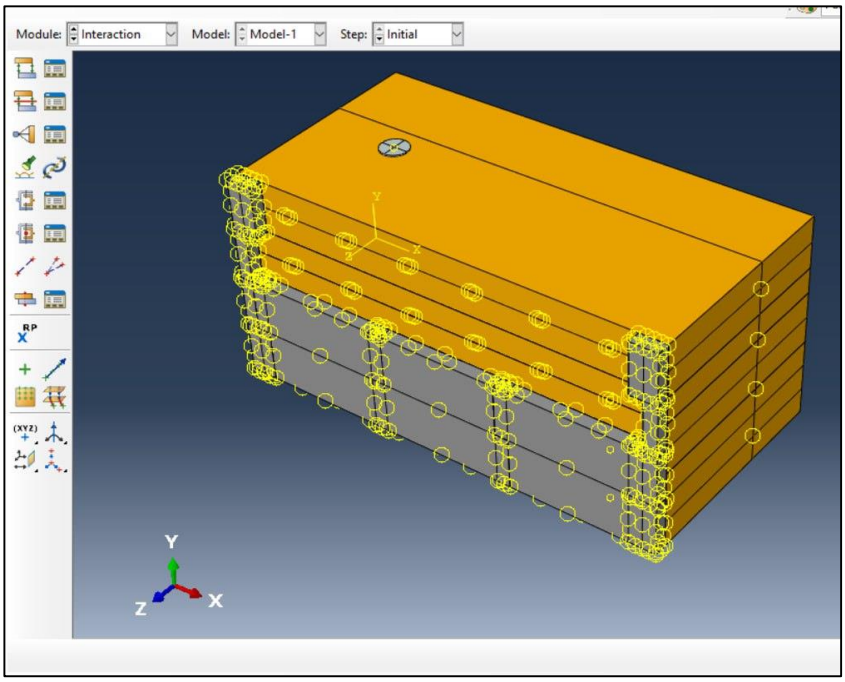

Figure 5.5: Interaction between concrete -soil

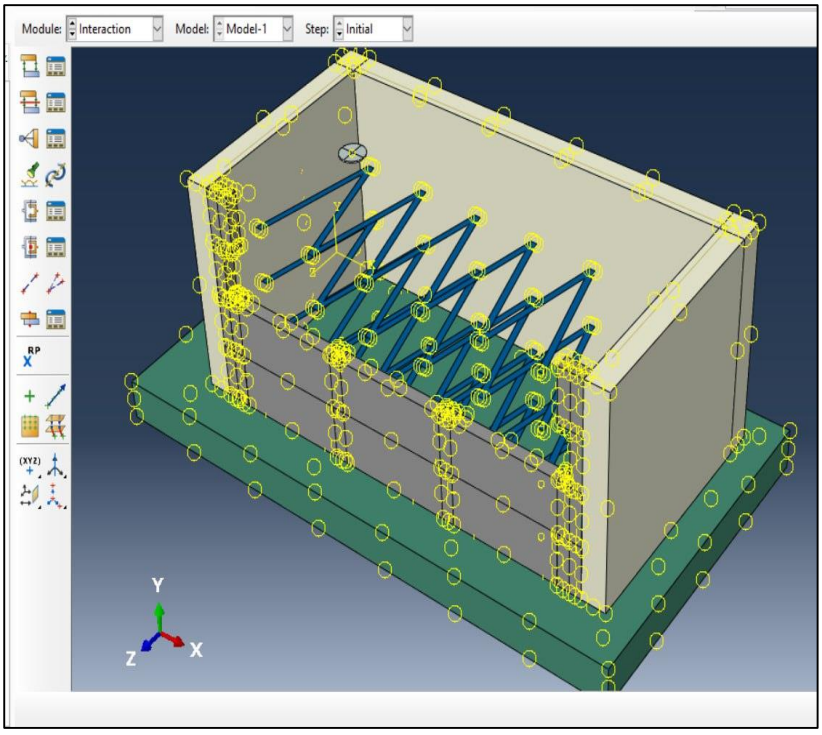

Figure 5.6: Interaction between steel -concrete.

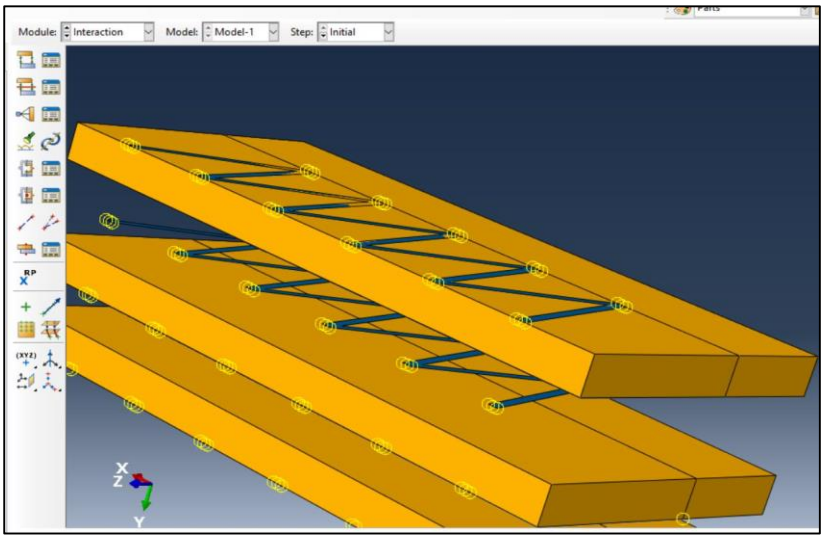

Figure 5.7: Interaction between soil-strip.

5.4.1 Assigning Boundary Condition

The boundary conditions have a significant influence in predicting the response of the model, the bottom surface of the foundation and the retained wall is assumed to be fixed, and that means that nodes at the bottom of the subgrade and sides of layer cannot move horizontally or vertically. Figure 5.8 shows the boundary conditions used in the analysis.

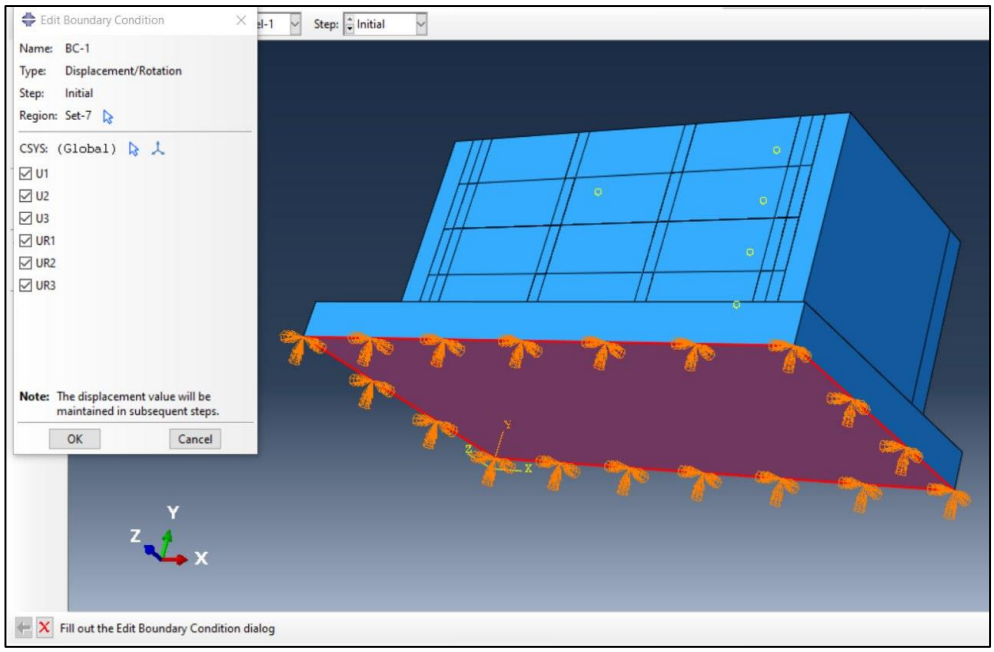

Figure 5.8: Fixed MSE walls

5.4.2 Elements mesh details

To determine the best mesh density (i.e., number of elements), selecting a suitable mesh size is a significant step in FEM. MSE wall models were subjected to a convergence analysis to obtain an appropriate mesh size by dividing MSE wall models into an appropriate number of elements. When the reduction in mesh size (increment in the elements' number) has no effect on the finding, the results have reached a suitable convergence.

The convergence study was performed for MSE wall models by evaluating the effects of increasing the number of elements from (6224 to 5495182) on the lateral displacement. As could be noticed in Figure 5.9 and Figure 5.10, an increasing number of the elements from 6224 to 5495182 led to negligible effects on the lateral displacement and lateral pressure. In addition, selecting several of an element equal to 545462 was adopted in this study because it led to more compatible lateral displacement in comparison with the experimental outcomes.

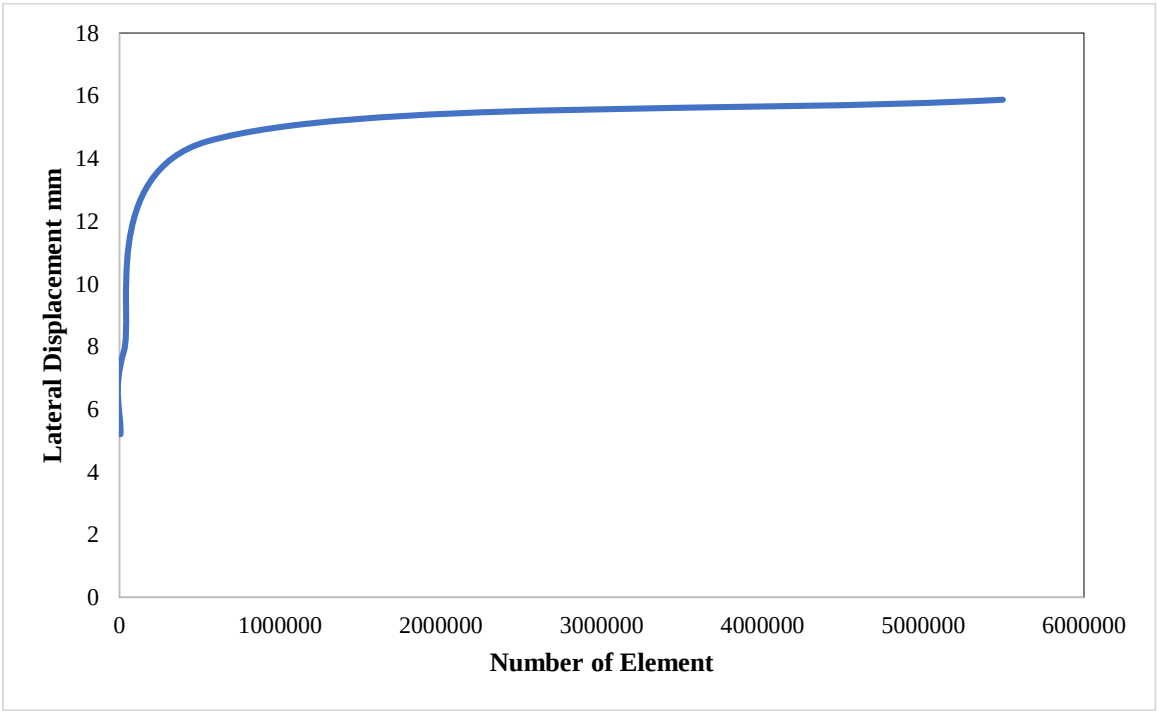

Figure 5.9:The convergence study results.

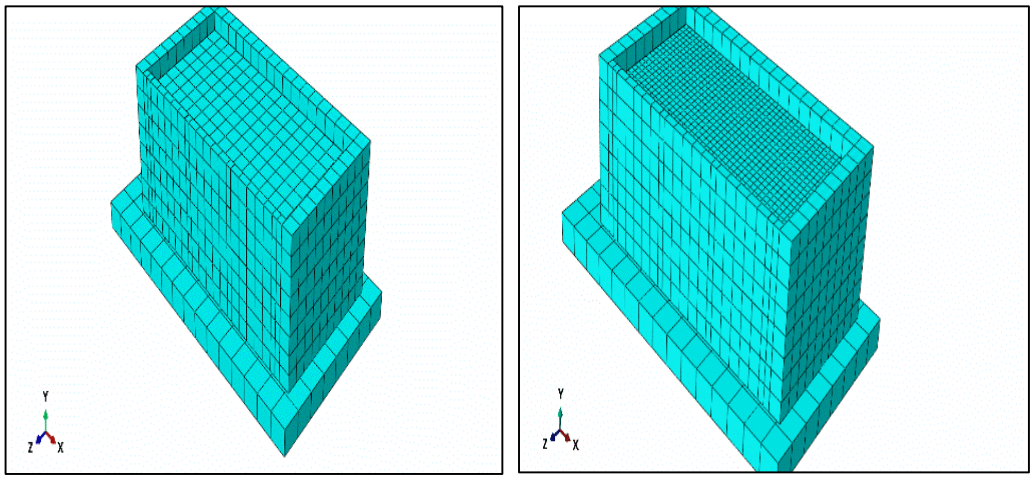

Mesh A (No. of Element= 6224) Mesh B (No. of Element= 26802)

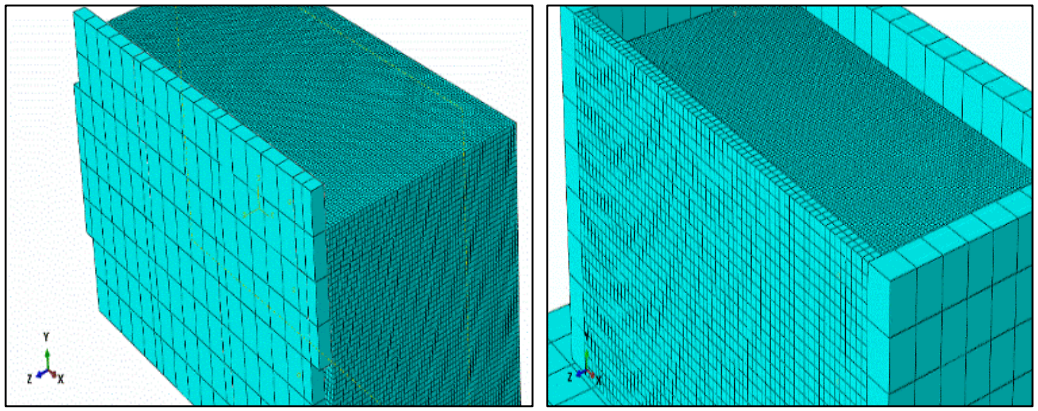

Mesh C (**No. of Element= 545462**) Mesh D (**No. of Element= 5495182**)

Figure 5.9: The convergence study results (continued).

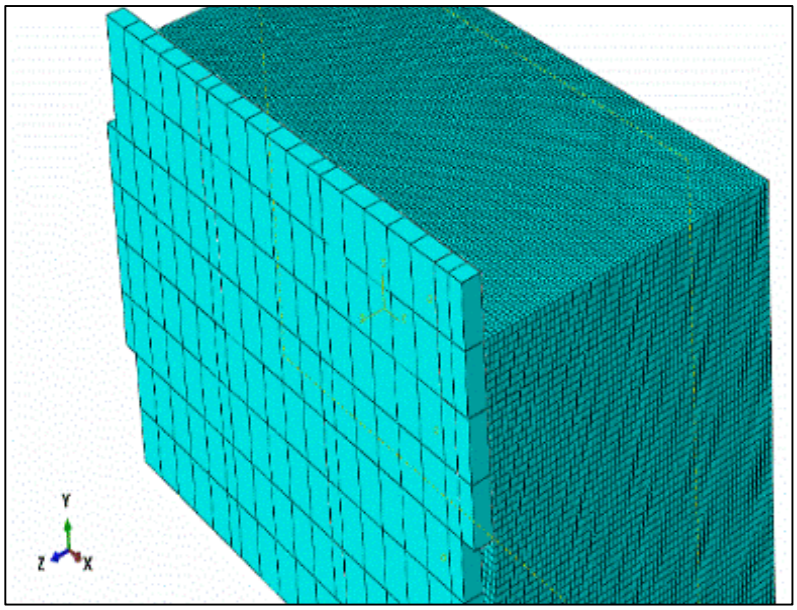

Figure 5.10: Finite element mesh density

5.5 Results of Finite Element Analysis

The experimental results for laboratory MSE wall with different shapes of soil reinforcement under static load are compared to the results of finite element analysis using the ABAQUS program, 2019. ABAQUS results, including the lateral pressure, lateral displacement of panel, strains in concrete, strain in strips and vertical pressure were compared with the experimental results and showed good convergence. As a result, and after determining the validity of these models, expanding the experimental program by studying many numerical cases that affected the MSE wall behavior.

5.5.1 Depth Lateral Displacement

❖ **MSE-Z-L1-0.5W**

One of the main goals of the test was to study the displacement of wall. In this case we used the zigzag type of shape, and we applied the load at the center of the span. We tested the lateral displacement in the laboratory and in the computer program in two regions, the first one in the edge panel and the second one in the middle panel in three layers as mentioned in chapter three. The differences between the EXP. and FEM results are shown in the figures (5.11-5.13). We notice that there is a compatibility between the theoretical results and the practical results in terms of the lateral displacement of the wall in the edge and middle panel. Maximum deformation of wall occurred in the upper layer near the applied load in both edge and middle panel. Maximum deformation of wall occurred in the upper layer near the applied load in both edges about 8.12 mm in experimental, 9 mm in FEM while the displacement in middle panel is 10.87 mm in the EXP. and 13.9 mm in the FEM. The differences between the results of EXP. and FEM in the edge and middle panel are about 10% and 27% respectively.

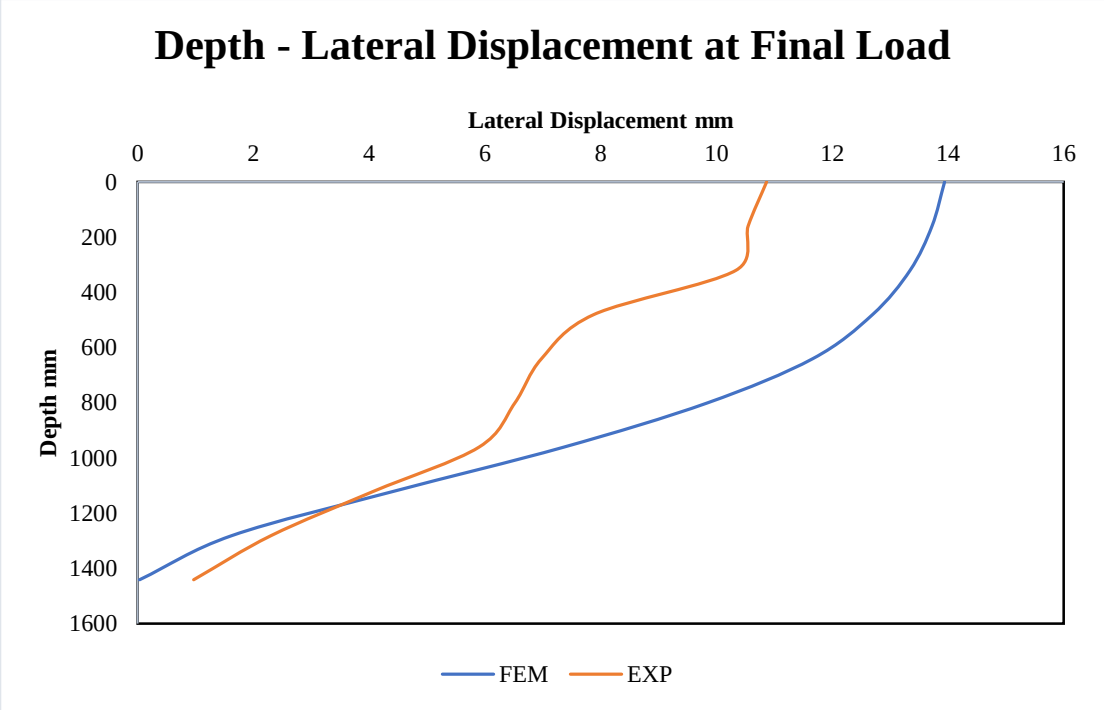

Figure 5.11. Comparison between FEM & EXP. In the Lateral Displacement in middle panel.

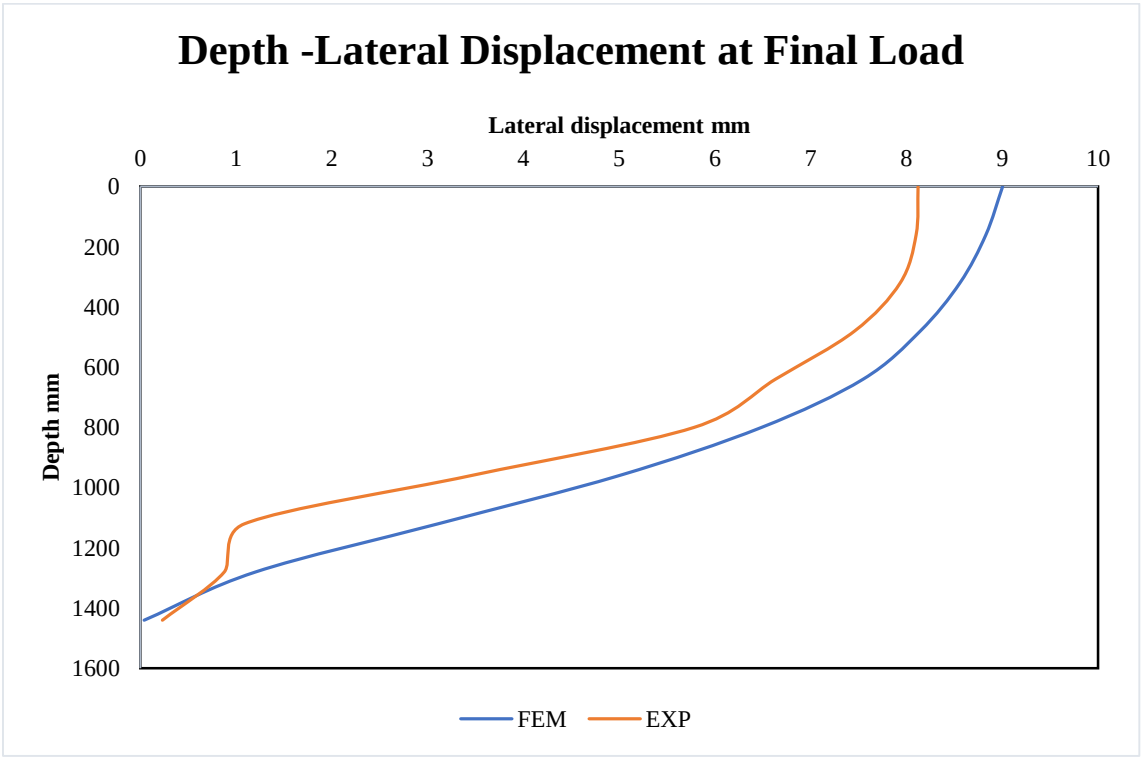

Figure 5.12. Comparison between FEM & EXP. In the Lateral Displacement in Edge panel.

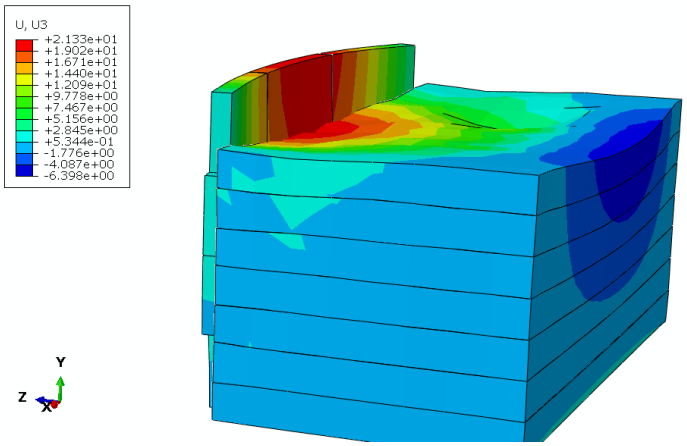

Figure 5.13: Deformation of MSE wall.

❖ **MSE-I-L1-0.5W**

In the straight shape type of reinforcement, the maximum deformation of the wall occurred at the upper surface near the applied load in both edge and middle panel. Figures (5.14-5.15) show the difference between the FEM. & EXP. in the lateral displacement in both edge panel and middle panel. The difference between the EXP. & FEM is about 32% in the edge panel and about 15% in the middle panel.

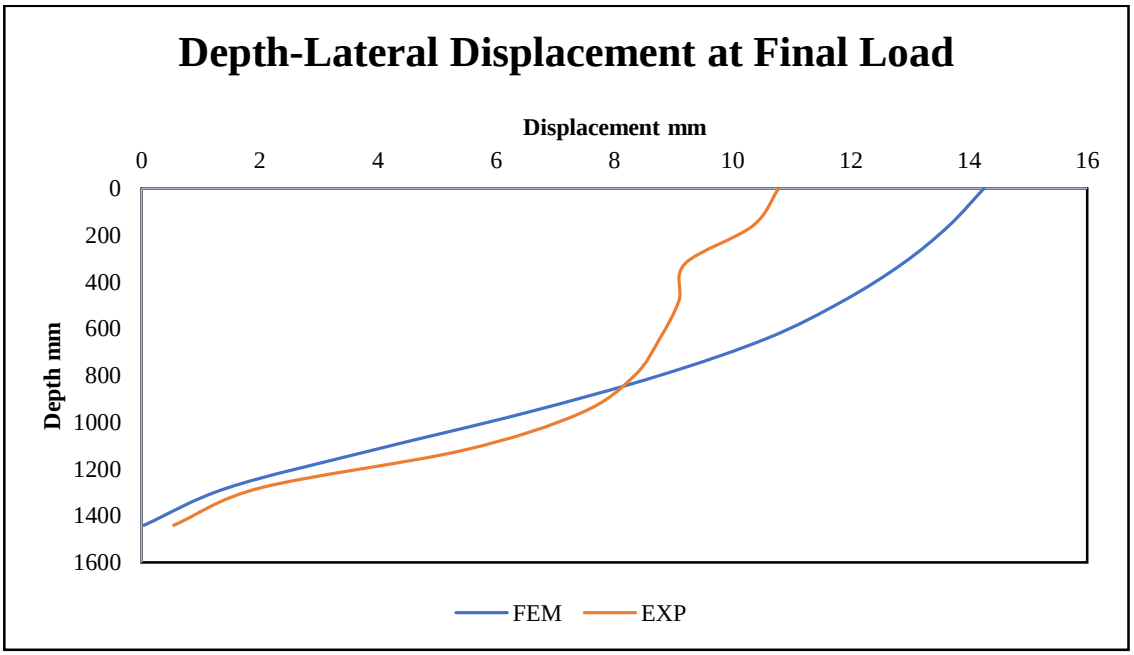

Figure 5.14. Comparison between FEM & EXP. In the Lateral Displacement in Edge panel.

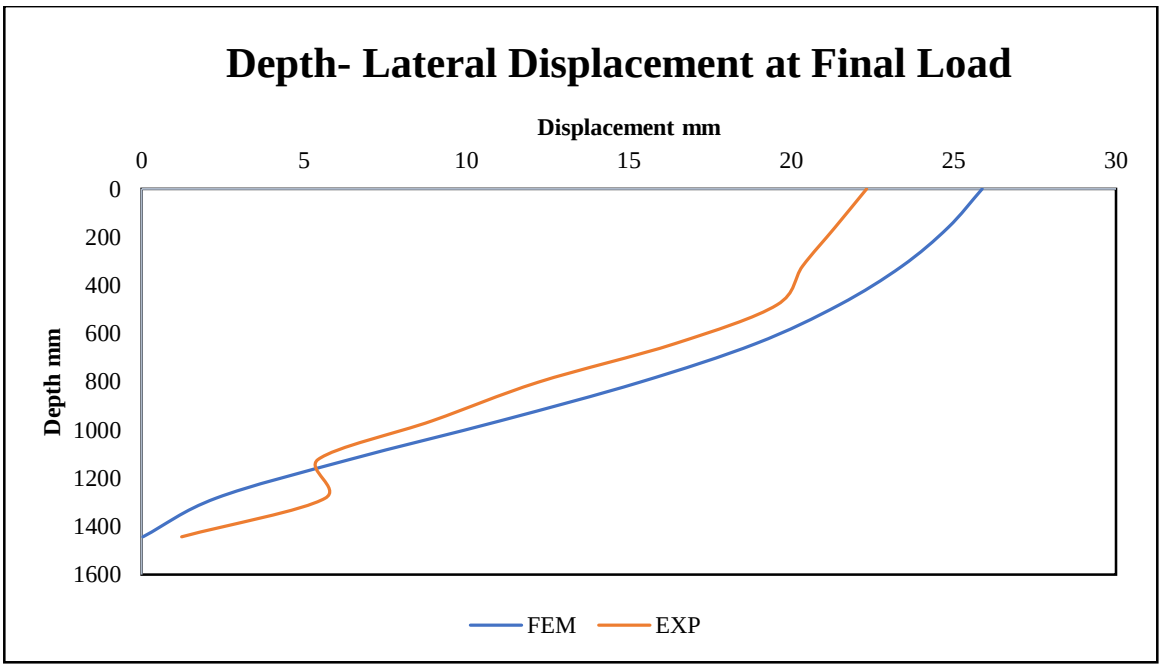

Figure 5.15. Comparison between FEM & EXP. In the Lateral Displacement in middle panel.

5.6 Parametric Study

After studying the convergence of samples with different shapes of reinforcement and obtaining a good convergence in the lateral displacement between the practical and numerical results, the experimental program was expanded by studying a set of variables and their impact on MSE wall behavior. The variables studied include:

1- Effect of the strip width.

2- Location of applied load.

Figure 5.16: Location of edge and middle panel

The details and suggested names of the specimens studied in the parametric study is shown in Table 5.1.

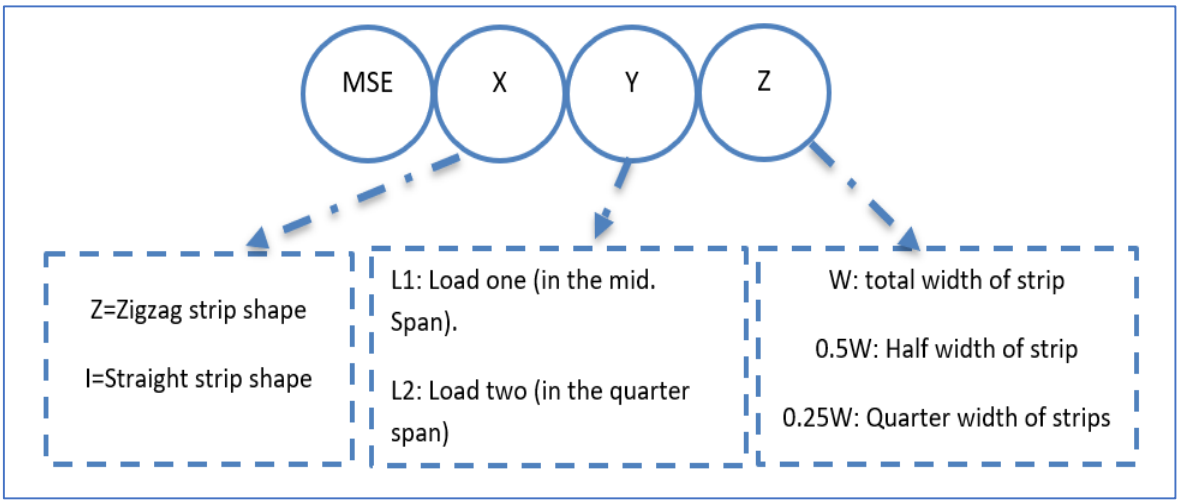

Figure 5.17: Description of the specimens in the FEM.

Table 5.1:Description of specimens

Specimens Name	Description
MSE-L1 (Without strip)	**L1:** Load location at distance x=80 cm from the panel face
MSE-L2 (Without strip)	**L2:** Load location at distance x=40 cm from the panel face.
MSE-L3 (Without strip)	**L1 and L2** applied at the same time
MSE-L4 (Without strip)	**L1 followed by L2**
MSE-Z-L1-0.25W	**Z:** Zigzag shape strips **L1:** Load location at distance x=80 cm from the panel face. **0.25W:** quarter width of strip.
MSE-Z-L2-0.25W	**Z:** Zigzag shape strips **L2:** Load location at distance x=40 cm from the panel face. **0.25W:** quarter width of strip.
MSE-Z-L1-0. 5W	**Z:** Zigzag shape strips **L1:** Load location at distance x=80 cm from the panel face. **0.5W:** Half width of strip.
MSE-Z-L2-0. 5W	**Z:** Zigzag shape strips **L2:** Load location at distance x=40 cm from the panel face. **0. 5W:** Half width of strip.
MSE-Z-L1-W	**Z:** Zigzag shape strips **L1:** Load location at distance x=80 cm from the panel face. **W:** Total width of strip.
MSE-Z-L2-W	Z: Zigzag shape strips L2: Load location at distance x=40 cm from the panel face. **W**: Total width of strip.
MSE-I-L1-0. 5W	I: Straight shape strips **L1:** Load location at distance x=80 cm from the panel face. **0.5W:** Half width of strip.
MSE-I-L2-0. 5W	**I:** Straight shape strips **L2:** Load location at distance x=40 cm from the panel face. **0.5W**: Half width of strip.
MSE-I-L1-W	**I:** Straight shape strips **L1:** Load location at distance x=80 cm from the panel face. **W:** Total width of strip.
MSE-I-L2-W	**I:** Straight shape strips **L2:** Load location at distance x=40 cm from the panel face. **W:** Total width of strip.

5.6.1 Effect of the strip width on the lateral displacement

This part studied the effect of the strip width on the behavior of MSE wall. Three widths were used in this study (W, 0.5W, 0.25W). It is noted that the increase in width of strip reduce the lateral displacement in the edge and middle panel because when the width of strip increases the contact area between the strip surface and soil increase, and this is affected on the friction resistance. The relation between all cases shown in Figure 5.18 and Figure 5.19. As a result, it can be concluded that the best one is MSE-Z-L1-W in both cases in the edge and middle panel. Also, we can notice that the zigzag shape gave less deformation in comparison with the straight shape this result because the zigzag shape the strip is inclined with respect to the wall and the forces analysis in to two component the first one applied on the panel and the second one applied on the soil, while the straight shape here the strip perpendicular on the wall and all the tensile force applied on the panel.

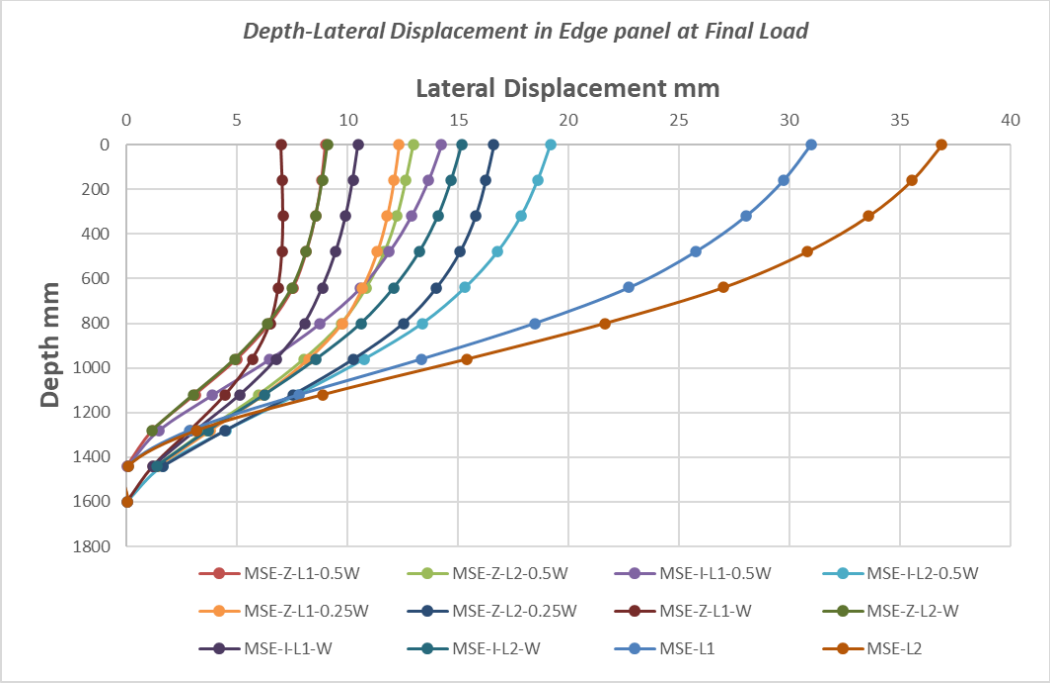

Figure 5.18. Comparison between All Cases in the Lateral Displacement in Edge panel.

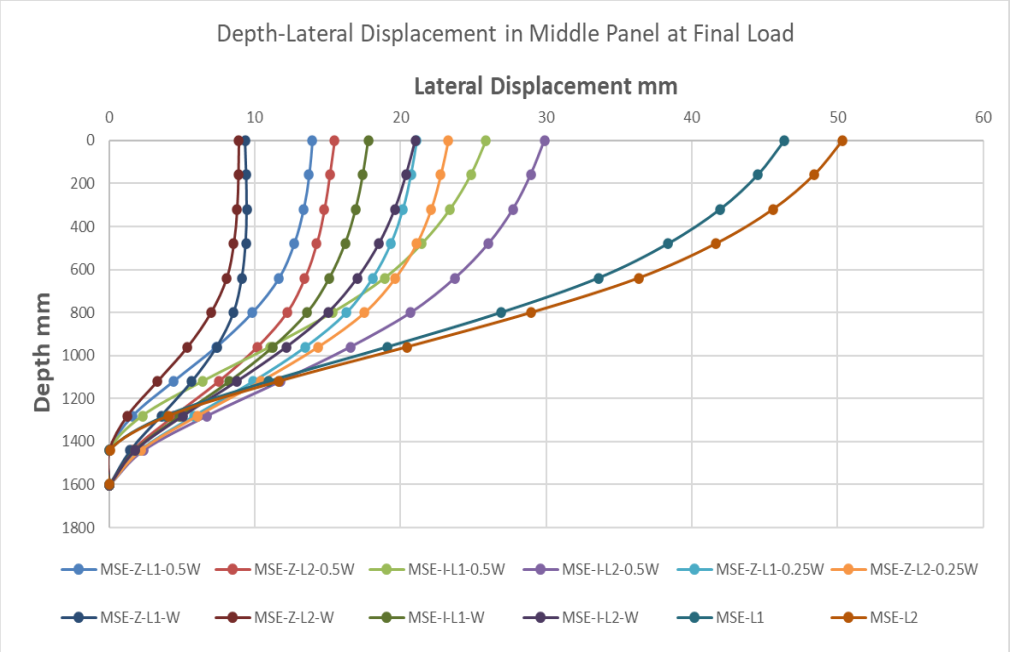

Figure 5.19. Comparison between All Cases in the Lateral Displacement in middle panel.

Table 5.2 displays the lateral displacement results for all the samples. It is evident from the data that reinforcing the soil significantly decreased the lateral displacement of the wall in both the edge and middle panels by approximately 50% when compared to the unreinforced specimen.

Table 5.2: Results of Lateral displacement in the parametric study.

Specimens name	Lateral Displacement in the edge panel (mm)	Lateral Displacement in the middle panel (mm)
MSE-L1 (Without strip)	31.89	47.76
MSE-L2 (Without strip)	37.84	51.82
MSE-Z-L1-0.25W	12.329	21.13
MSE-Z-L2-0.25W	16.626	23.28
MSE-Z-L1-0. 5W	9.000	13.94
MSE-Z-L2-0. 5W	12.971	15.47
MSE-Z-L1-W	7.000	9.36
MSE-Z-L2-W	9.100	8.92
MSE-I-L1-0. 25W	21.57	29.95
MSE-I-L2-0. 25W	27.58	33.17

Table 5.2: Results of Lateral displacement in the parametric study (continued).		
MSE-I-L1-0. 5W	14.248	25.88
MSE-I-L2-0. 5W	19.183	29.89
MSE-I-L1-W	10.491	17.80
MSE-I-L2-W	15.178	21.04
MSE-L3 (Without strip)	38.76	52.86
MSE-L4 (Without strip)	33.72	52.54
MSE-Z-L3-0.25W	22.42	23.60
MSE-Z-L4-0.25W	18.17	26.16
MSE-Z-L3-0. 5W	17.21	15.86
MSE-Z-L4-0. 5W	13.39	18.12
MSE-Z-L3-W	13.25	11.74
MSE-Z-L4-W	11.94	15.63
MSE-I-L3-0. 25W	29.69	35.38
MSE-I-L4-0. 25W	24.19	36.16
MSE-I-L3-0. 5W	25.79	29.54
MSE-I-L4-0. 5W	21.69	32.67
MSE-I-L3-W	19.85	20.56
MSE-I-L4-W	15.99	23.83

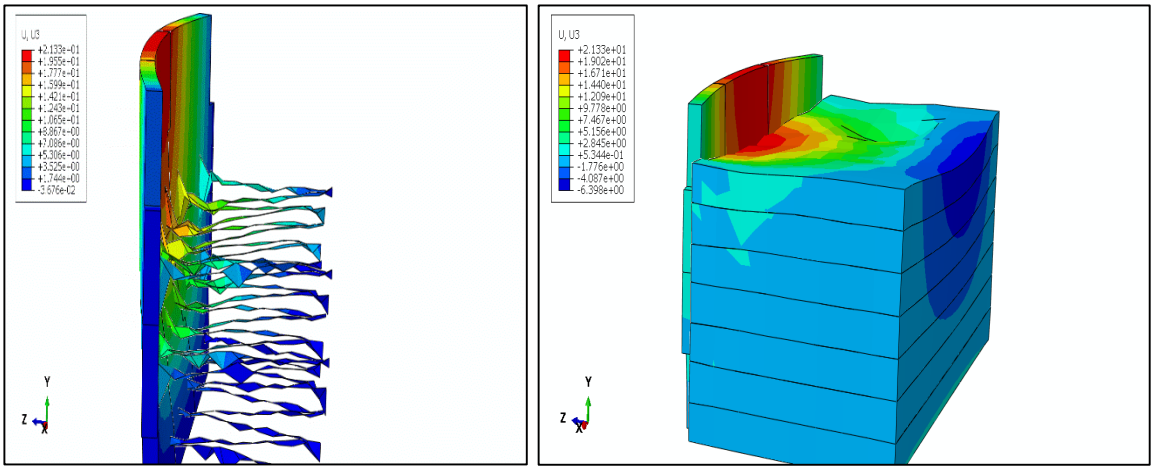

Figure 5.20: Deformation pattern for lateral displacement

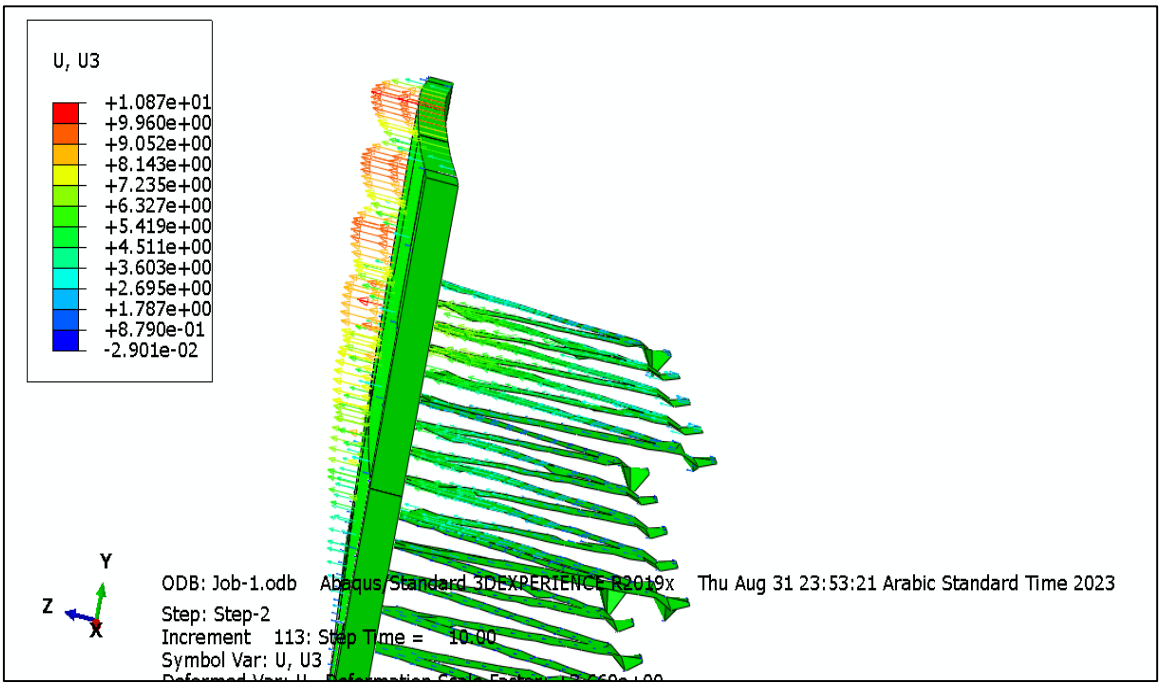

Figure 5.20: Deformation pattern for lateral displacement (continued).

5.6.2 Effect of the strip width on the strip stresses

Other very relevant results obtained from the FEM were the stresses developed in the strips during loading. The strip width effected on the stresses of strip because the width effected on the cross section of strip the result effected of the stresses the comparison between all cases (Shaw & Kyriakides, 1997) shown in figures 5.21 and 5.23. In comparison between all the specimens it can be found that the maximum stresses happened in the strip near the load in all cases. While the minimum stresses appeared in the strips that were in the first layer near the base of wall. Also, we can notice that the minimum strip stresses happened in the edge panel in MSE-Z-L2-W about 3 MPa in the layer near the base of wall and the layer near the load gave about 18 MPa. In MSE-Z-L2-0.25W gave the maximum value of stresses.

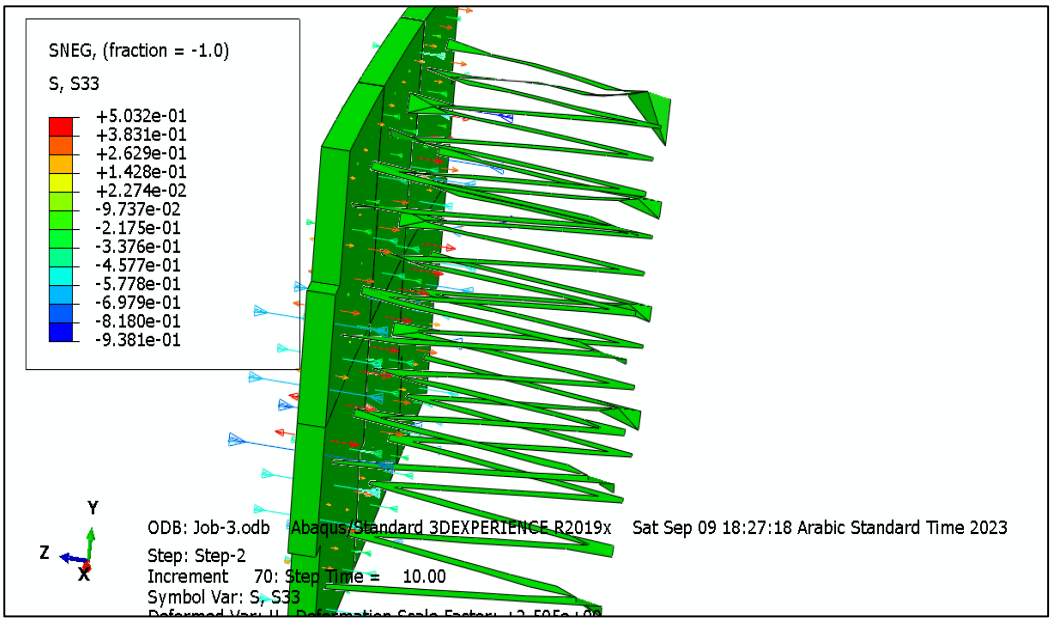

Figure 5.21: Deformation pattern for strips width effect.

Table 5.3:Results of Strips stresses in the edge strips in all parametric study.

Specimens name	Layer one (Near The base) (MPa)	Layer Three (Near the surface) (MPa)
MSE-Z-L1-0.25W	9	35
MSE-Z-L2-0.25W	11	62
MSE-Z-L1-0. 5W	3.3	23
MSE-Z-L2-0. 5W	15	39
MSE-Z-L1-W	7.22	13.20
MSE-Z-L2-W	4	20
MSE-I-L1-0. 5W	10	30
MSE-I-L2-0. 5W	13	41
MSE-I-L1-W	6	26

From the table above it has can conclude that the increases in strip width led to decrease is the tensile stresses. Also, for the specimens have the same width with different shape of reinforcement we can noticed that the Z shape decreases the stresses in strip.

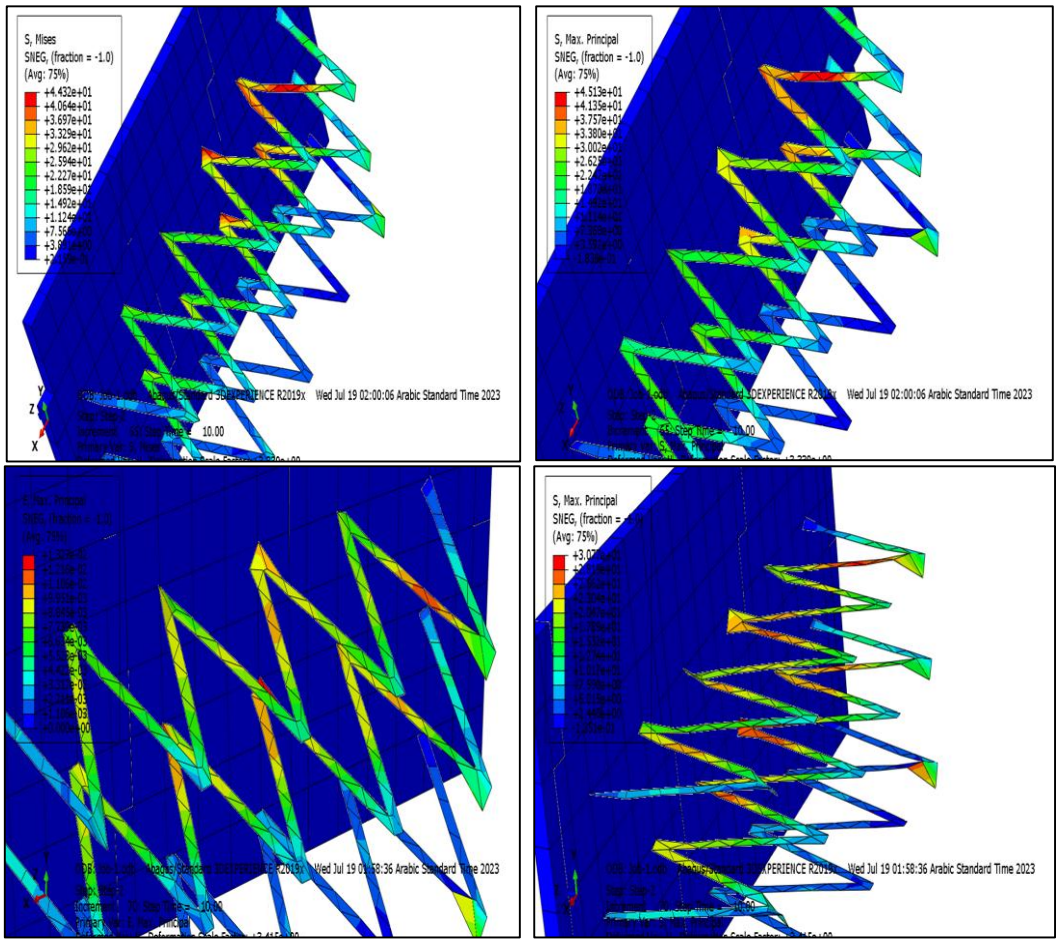

Figure 5.22: Deformation pattern for strips stresses.

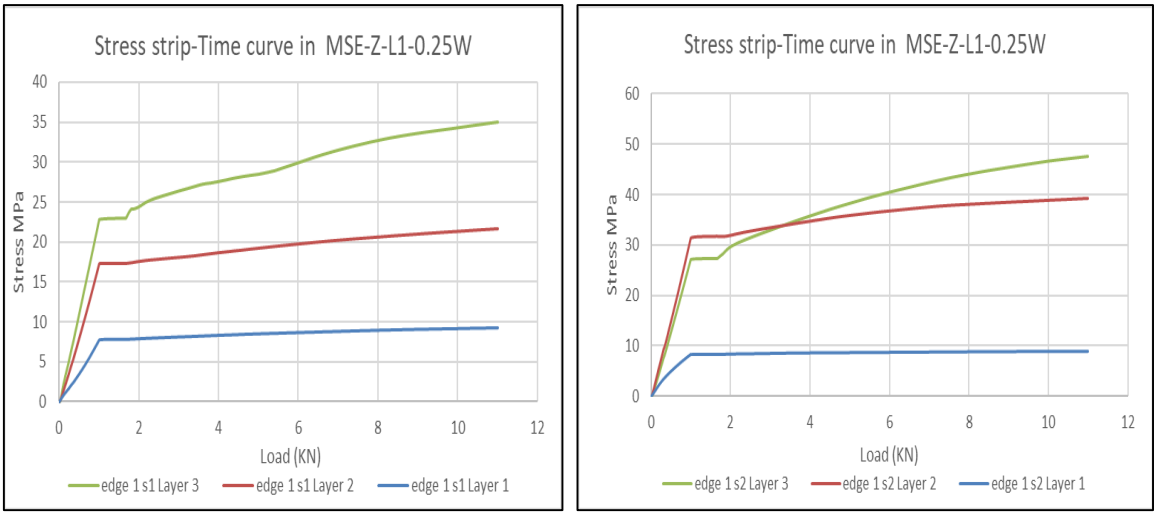

Figure 5.23. Comparison between All Cases in the strip width on the strip stresses.

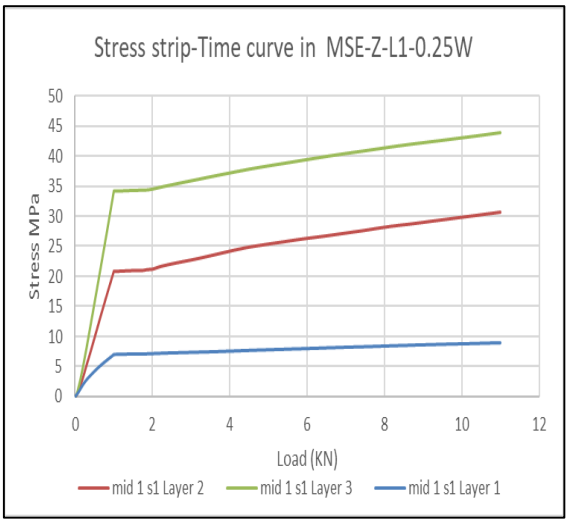

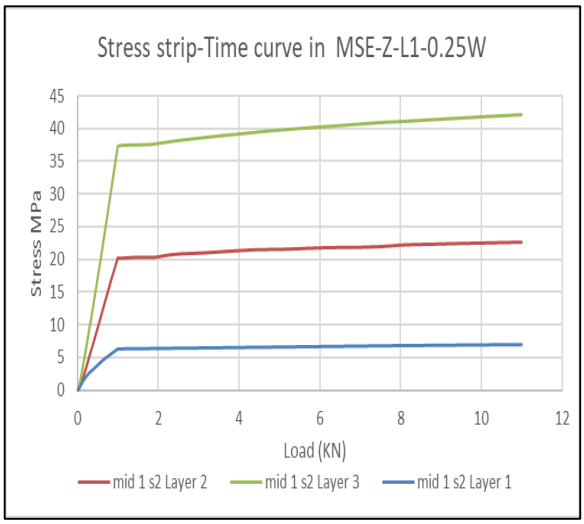

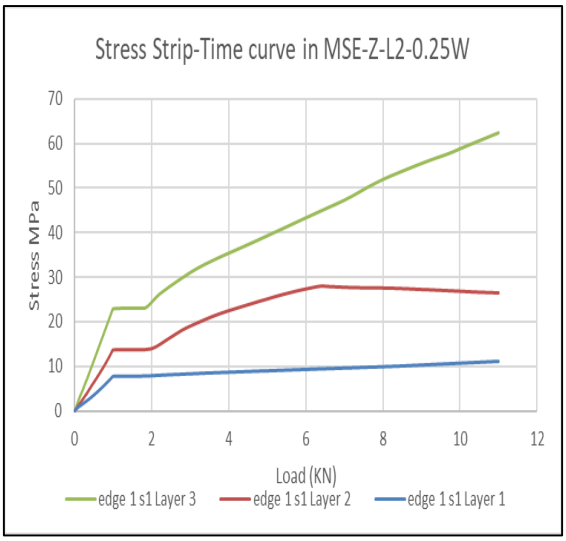

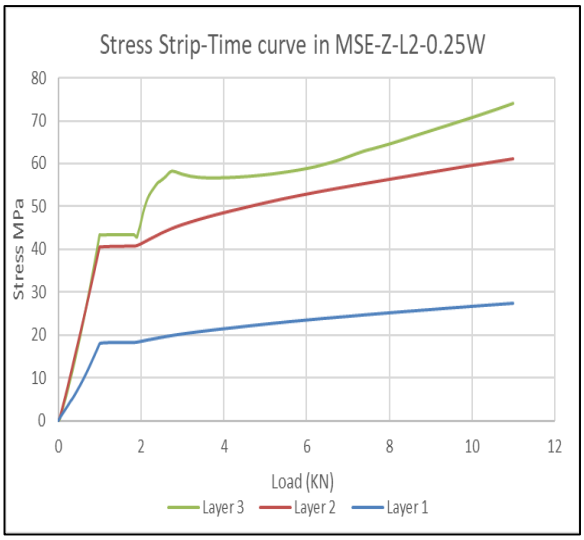

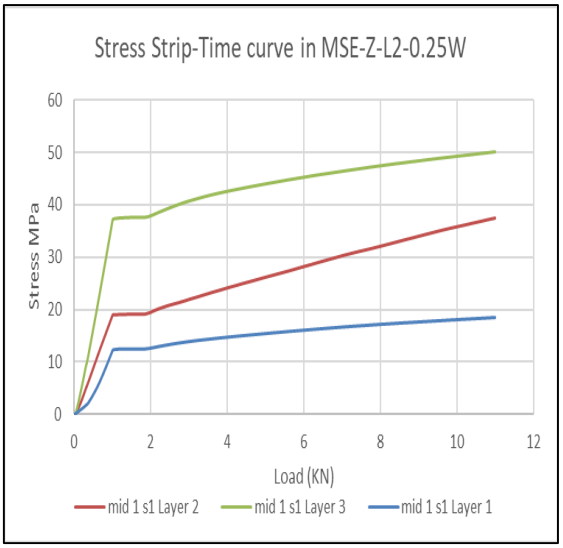

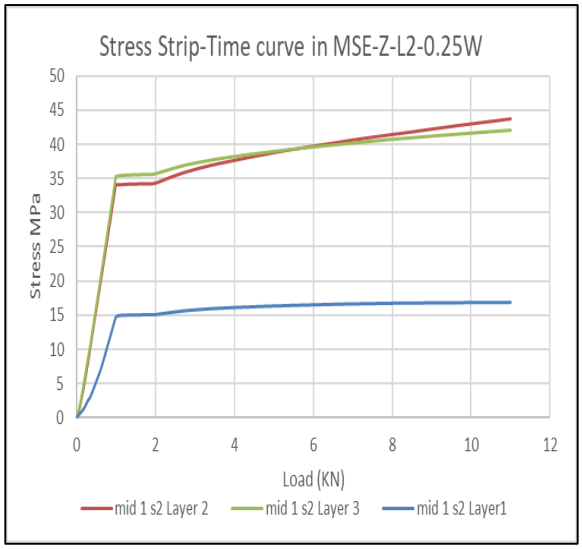

Figure 5.23. Comparison between All Cases in the strip width on the strip stresses (continued).

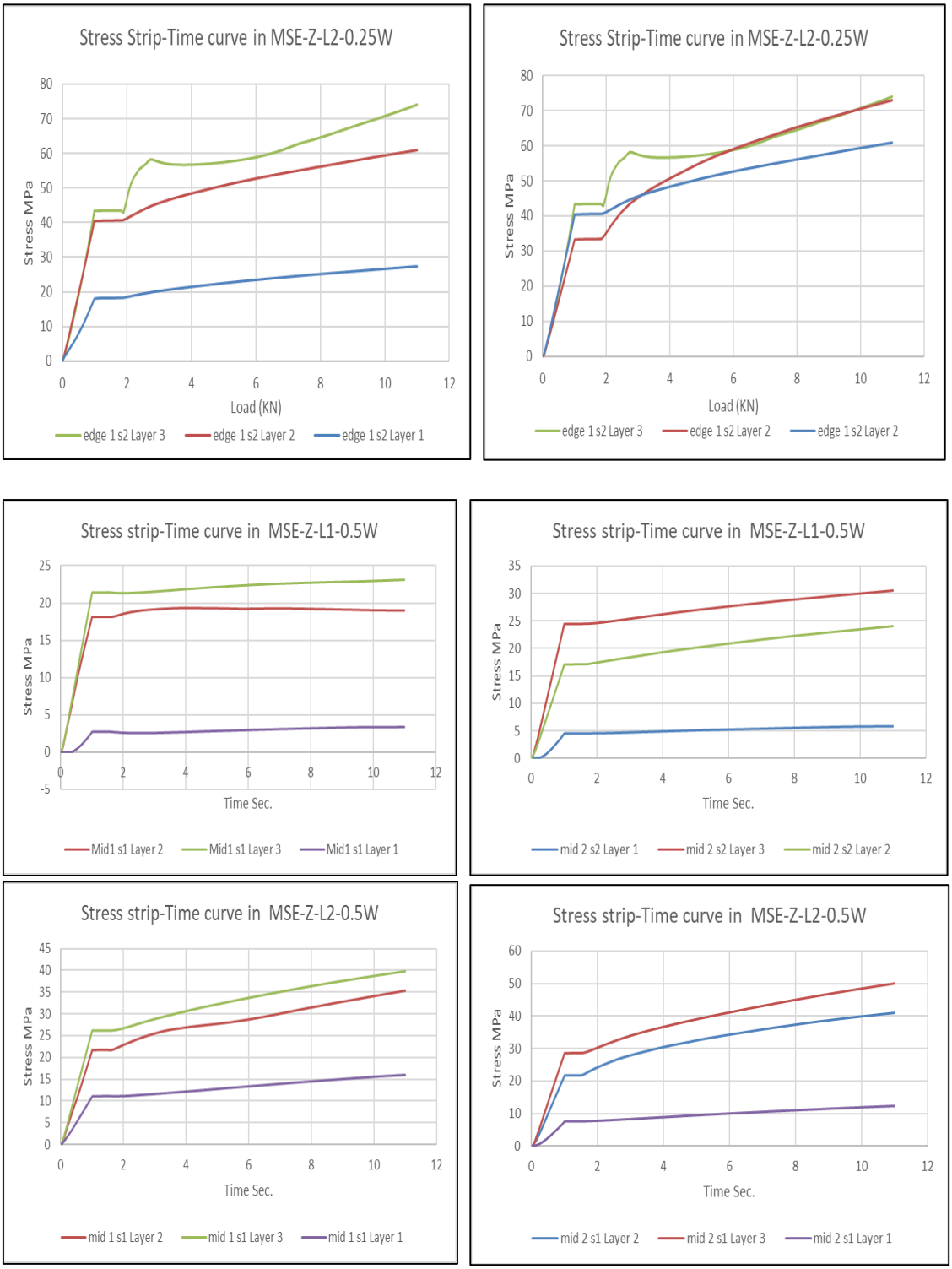

Figure 5.23. Comparison between All Cases in the strip width on the strip stresses (continued).

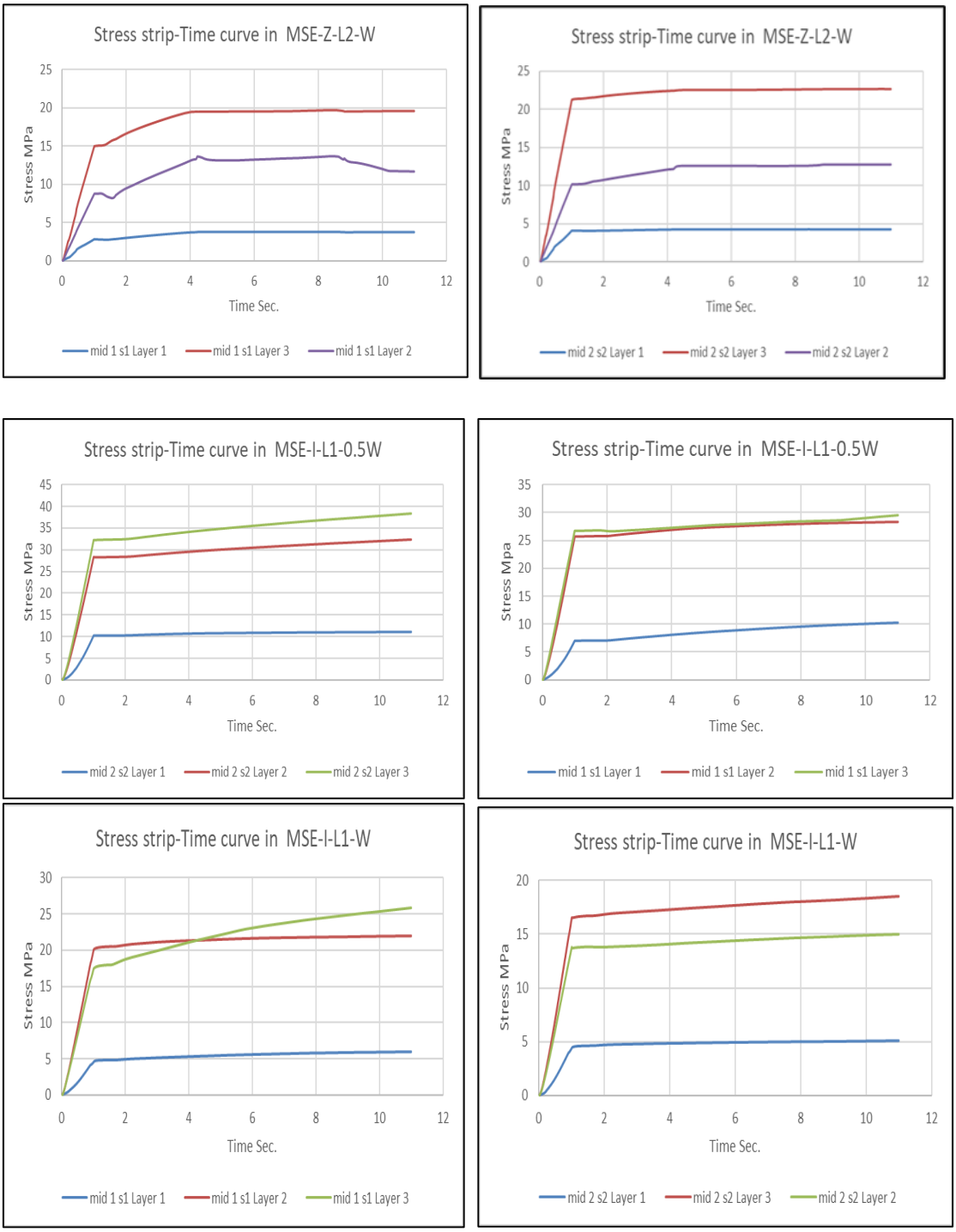

Figure 5.23. Comparison between All Cases in the strip width on the strip stresses (continued).

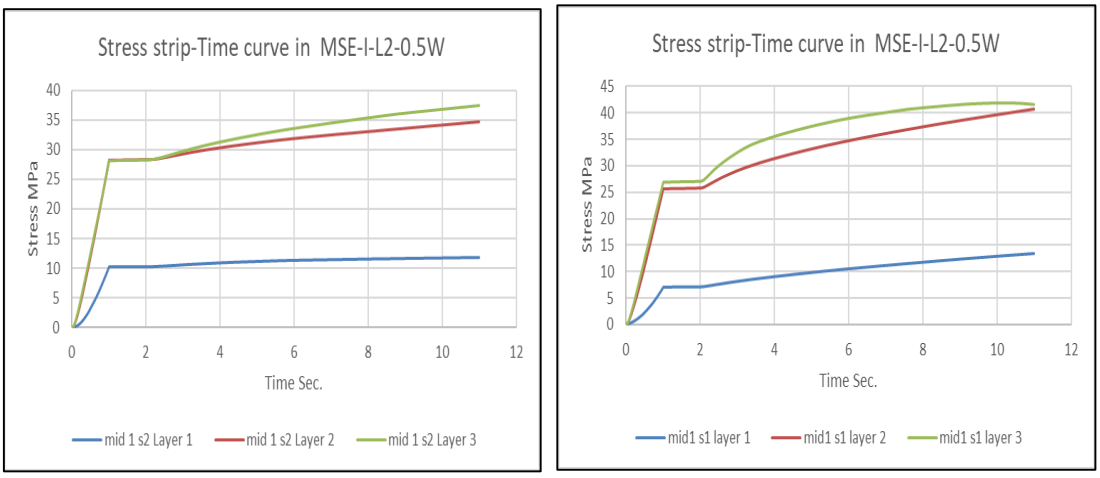

Figure 5.23. Comparison between All Cases in the strip width on the strip stresses (continued).

5.6.3 Effect of the strip width on the strip strain

The change of width effected on the strip strain the strip with 0.25W gave the maximum value of strain in comparison with the other cases. That means that the strip with smaller width reached the yield point at smaller load (Paulay & Goodsir, 1985; Tong et al., 2017). All the strains result in all cases shown in Figures 5.24 and 5.28:

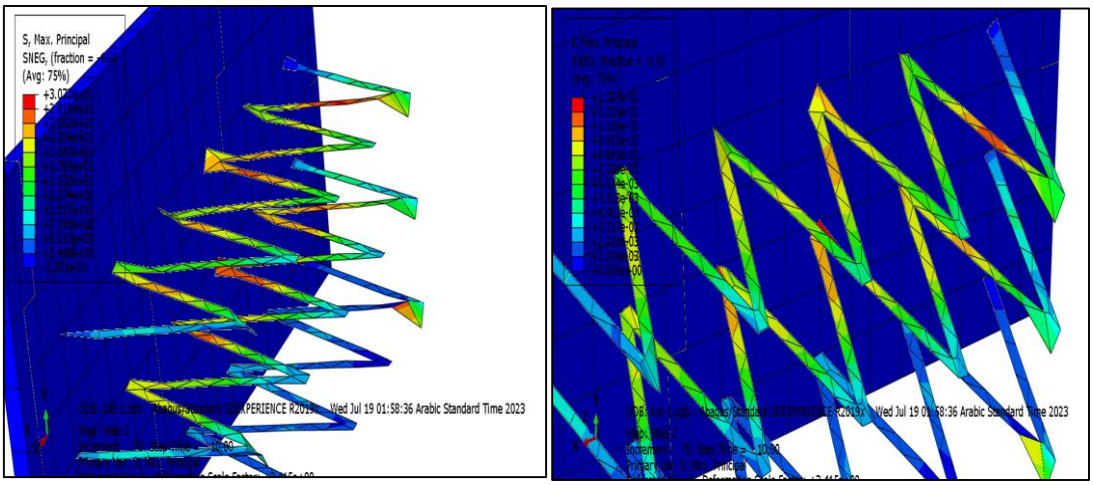

Figure 5.24: Deformation pattern for different strips width.

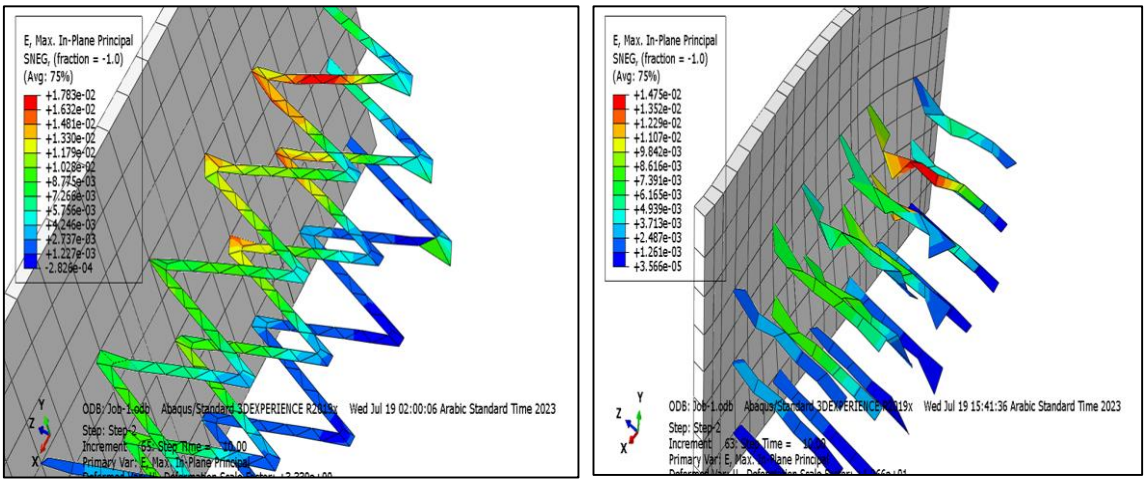

Figure 5.24: Deformation pattern for different strips width (continued).

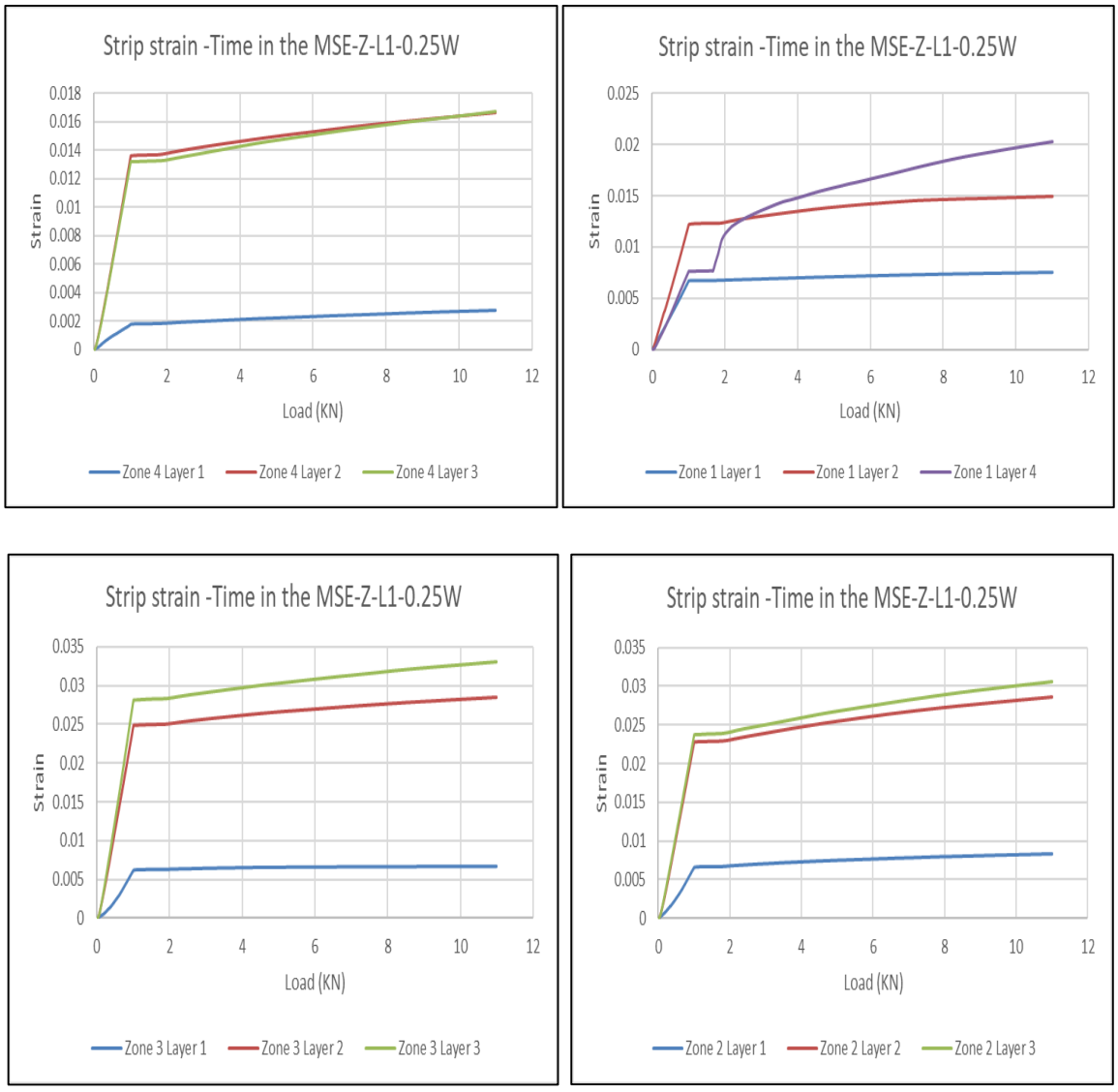

Figure 5.25. Comparison between All Cases in the strip width on the strip strain.

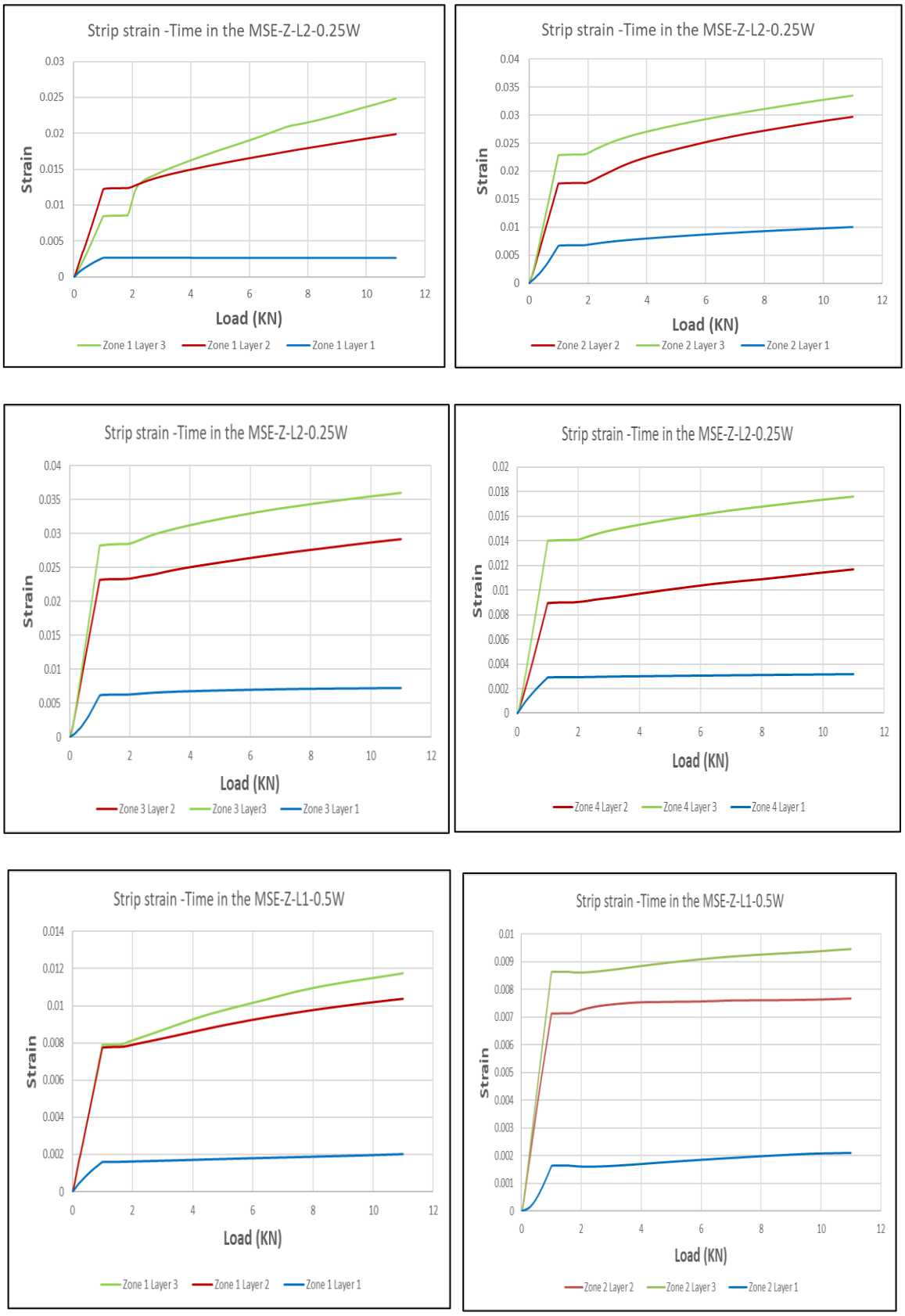

Figure 5.25. Comparison between All Cases in the strip width on the strip strain (continued).

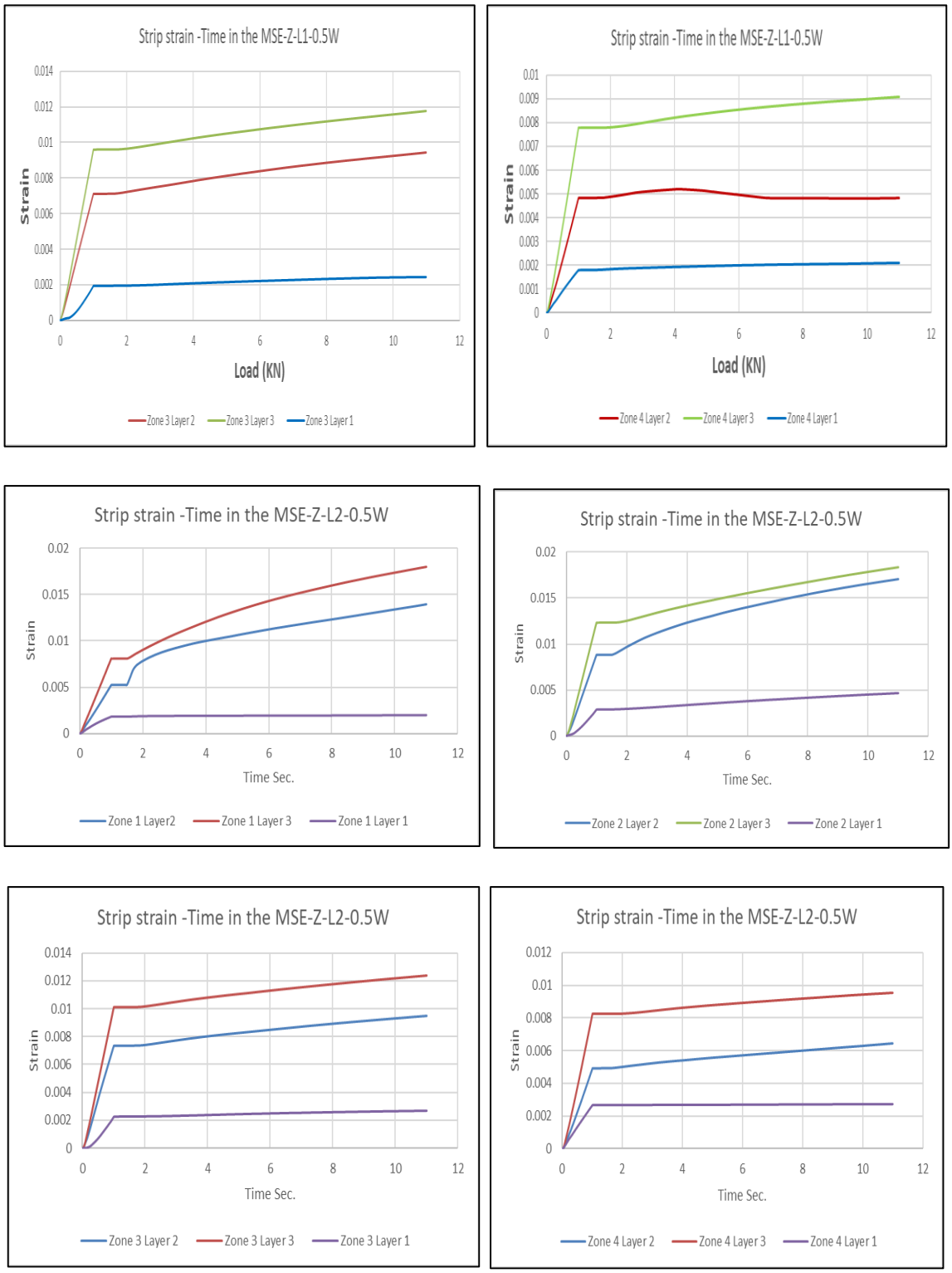

Figure 5.25. Comparison between All Cases in the strip width on the strip strain (continued).

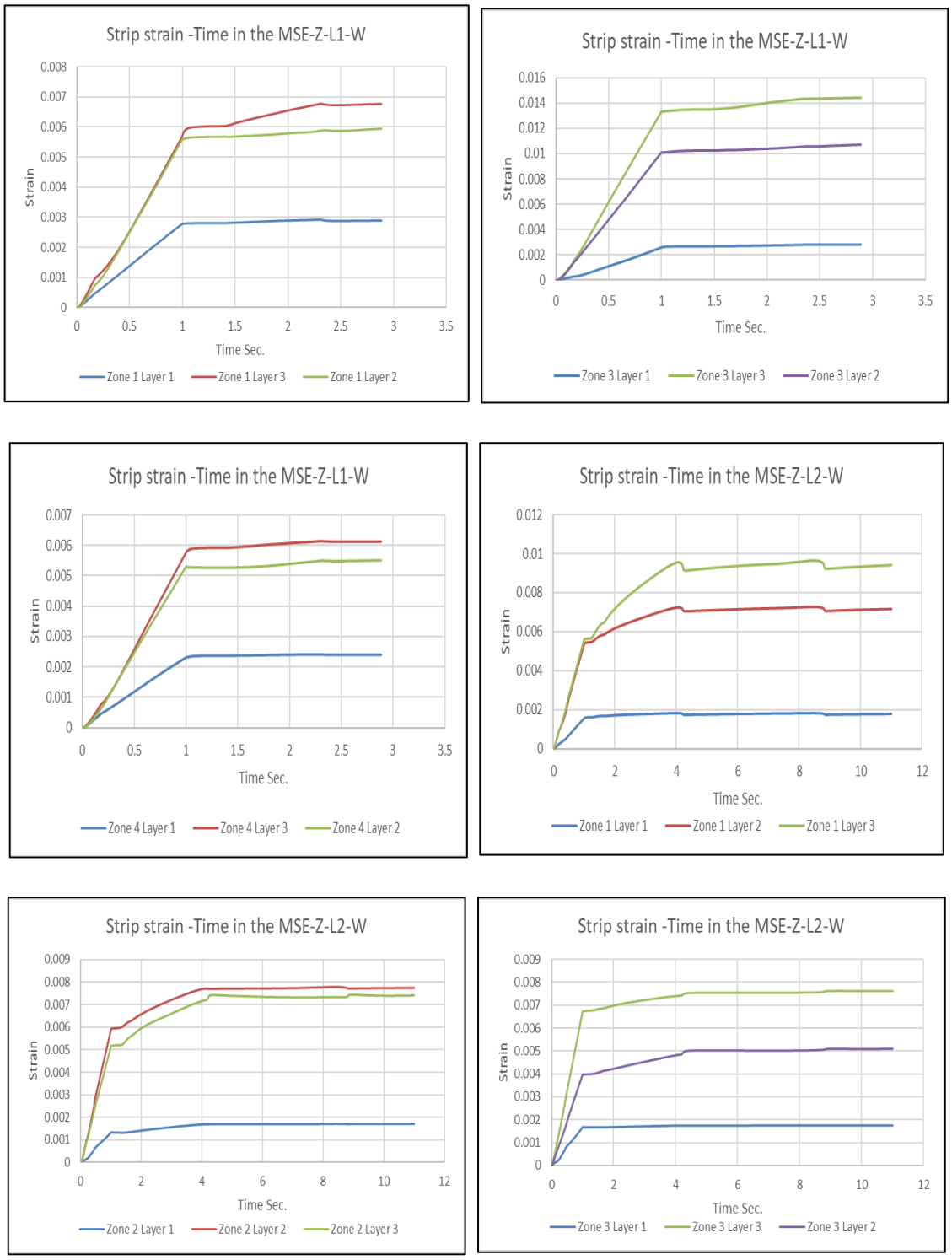

Figure 5.25. Comparison between All Cases in the strip width on the strip strain (continued).

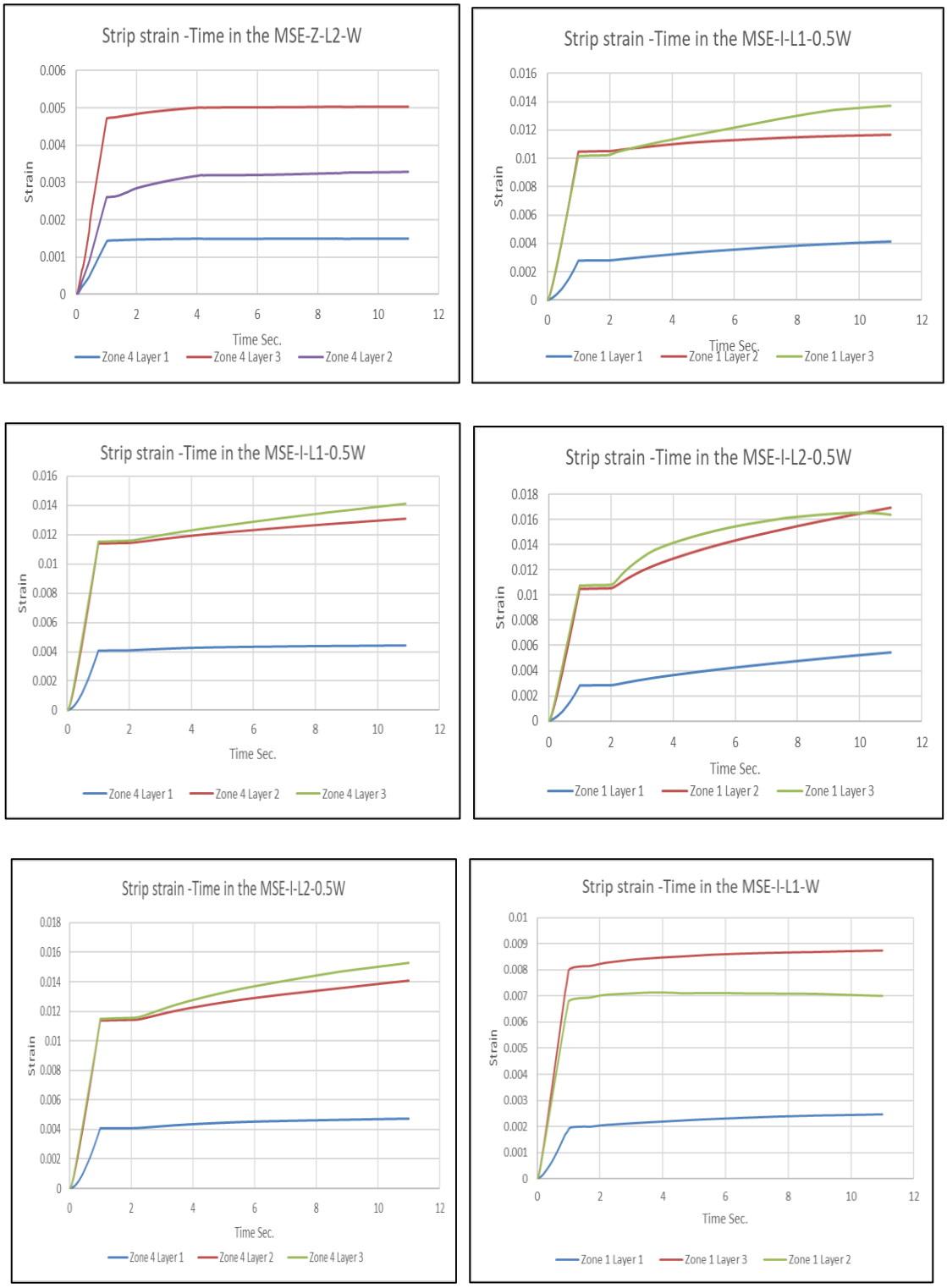

Figure 5.25. Comparison between All Cases in the strip width on the strip strain (continued).

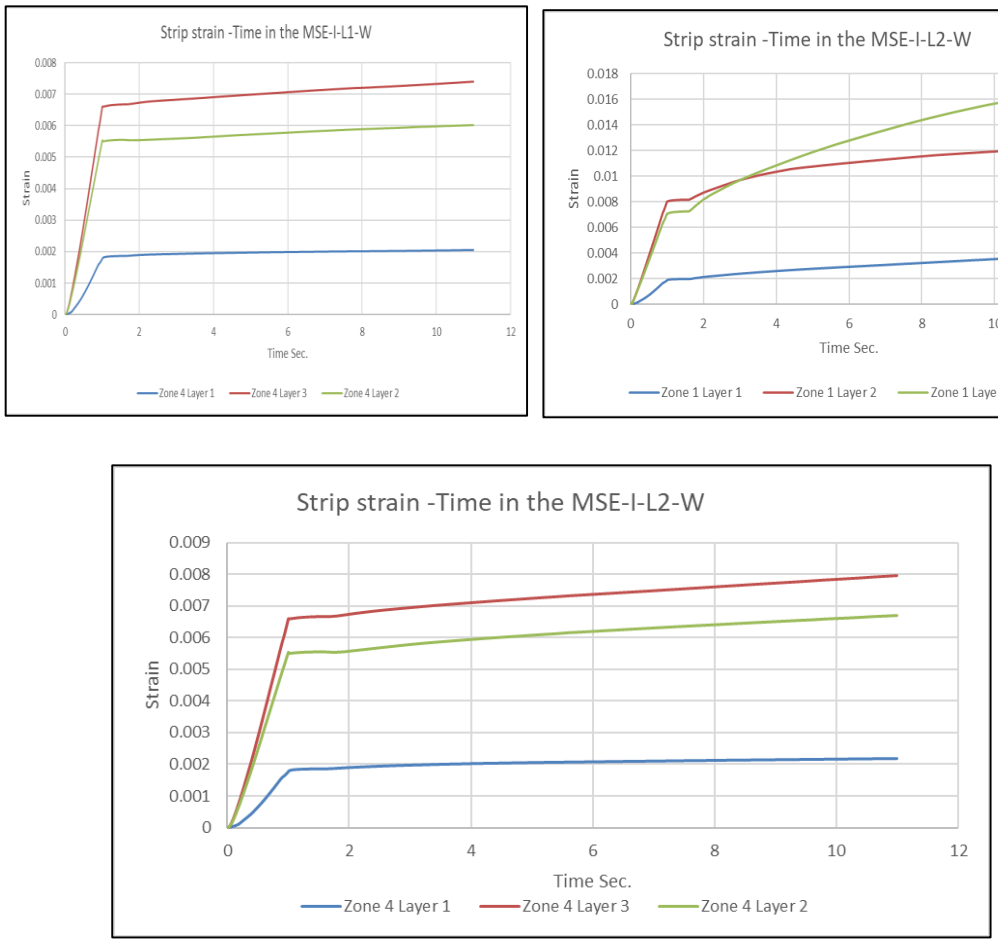

Figure 5.25. Comparison between All Cases in the strip width on the strip strain.

5.6.4 Effect of the strip width on the lateral soil pressure

The effect of strips width on the soil lateral pressure for different cases has been presented in figure 5.26-5.27. Three widths were used in this study (W, 0.5W, 0.25W). It is noted that the increase in width of strip reduce the lateral pressure of soil due to confinement the soil and increase the surface of friction when increase the strips width the opposite action occurred when reduced width of strips (Dash et al., 2004; Shivananda & Bincy, 2019).

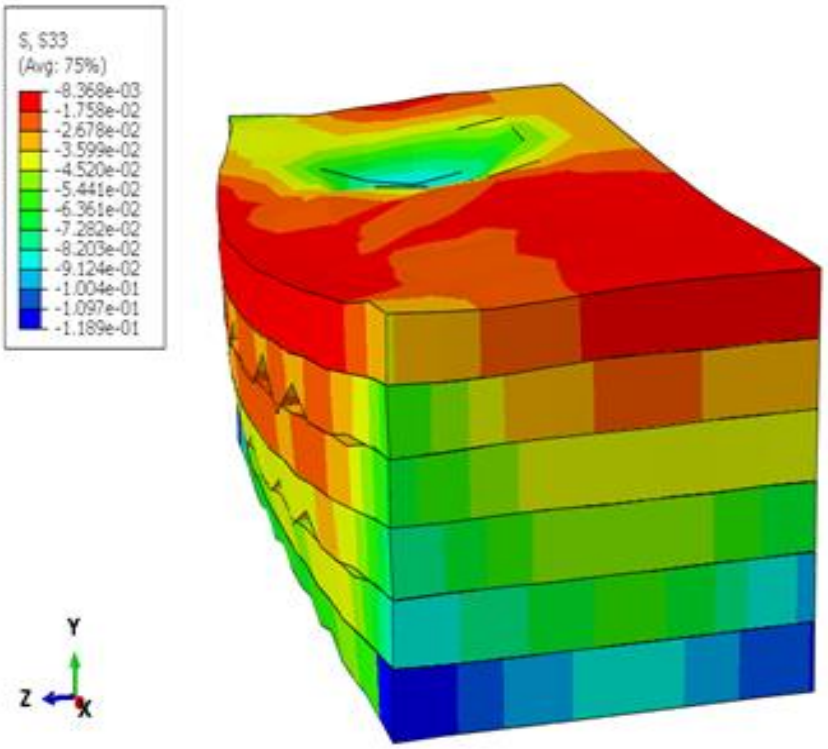

Figure 5.26. Distribution of lateral pressure.

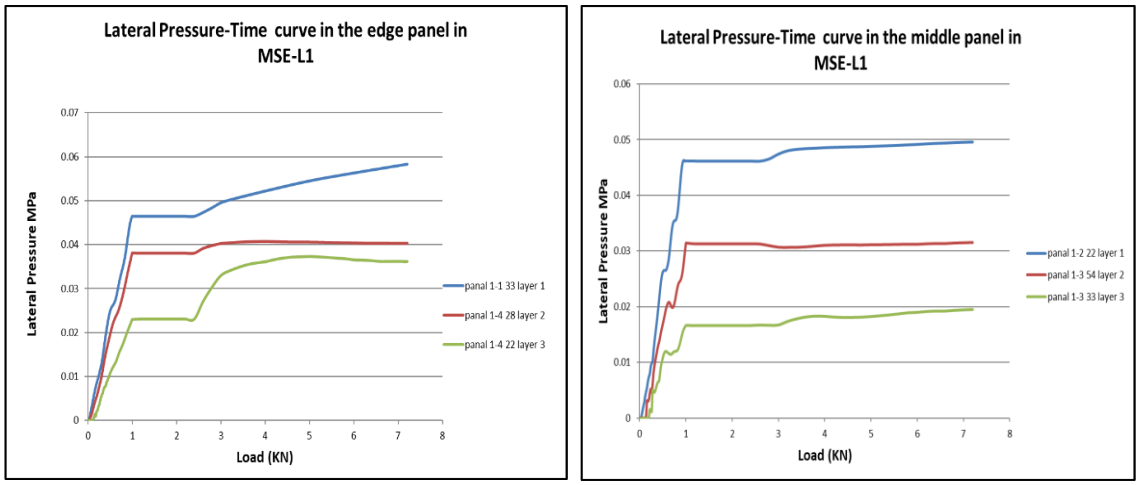

Figure 5.27. Comparison between All Cases in the strip width on the lateral pressure.

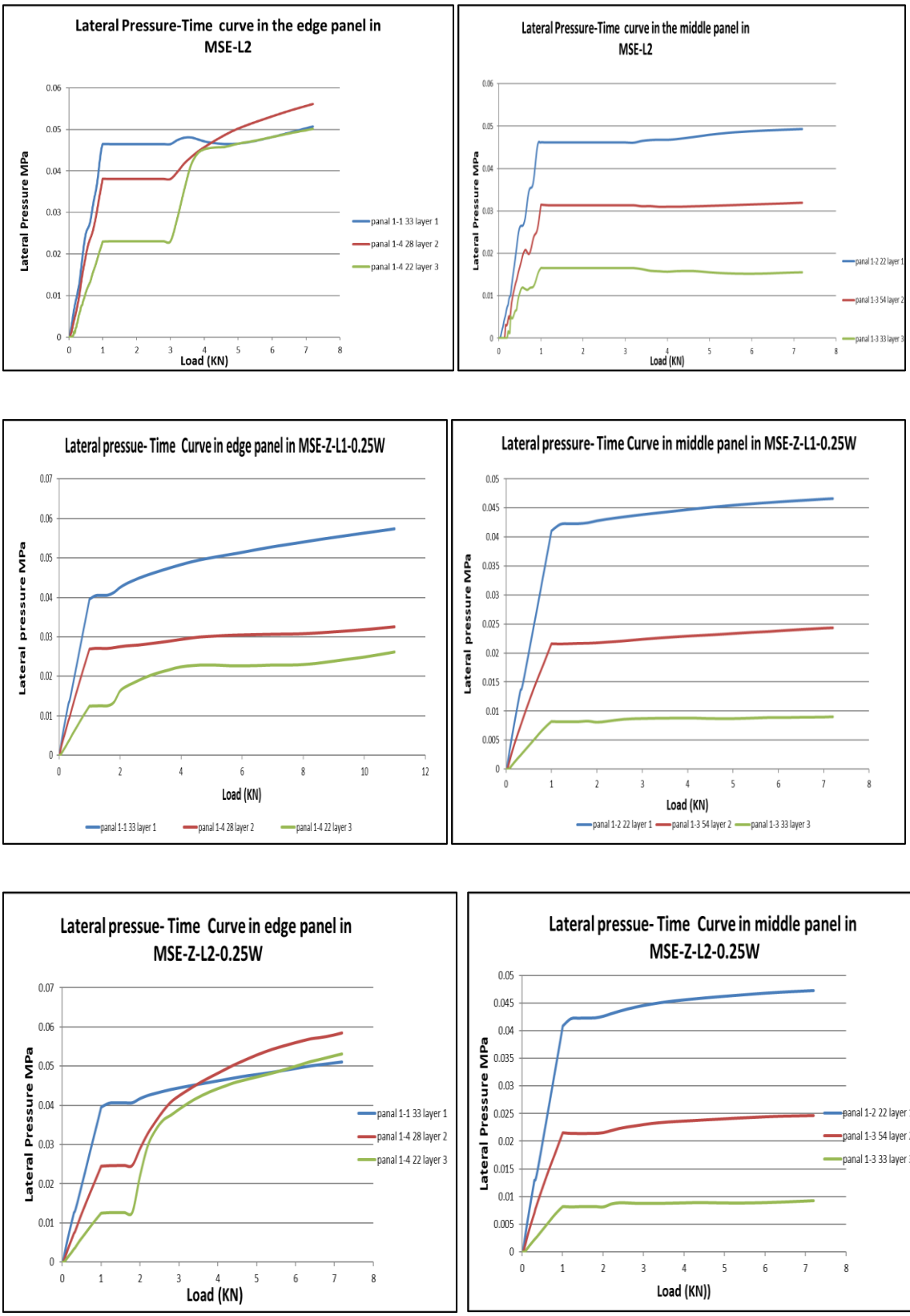

Figure 5.27. Comparison between All Cases in the strip width on the lateral pressure (continued).

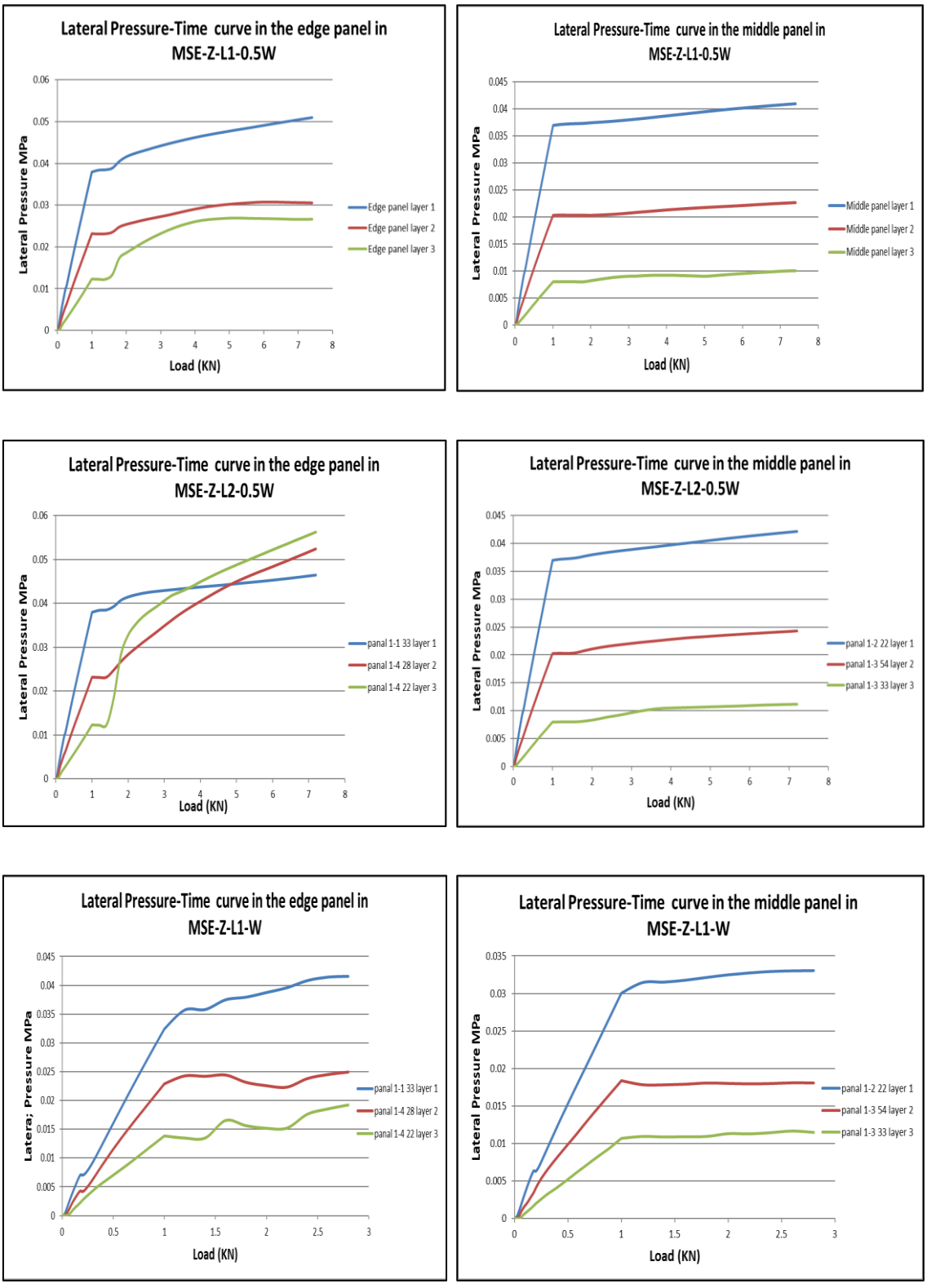

Figure 5.27. Comparison between All Cases in the strip width on the lateral pressure (continued).

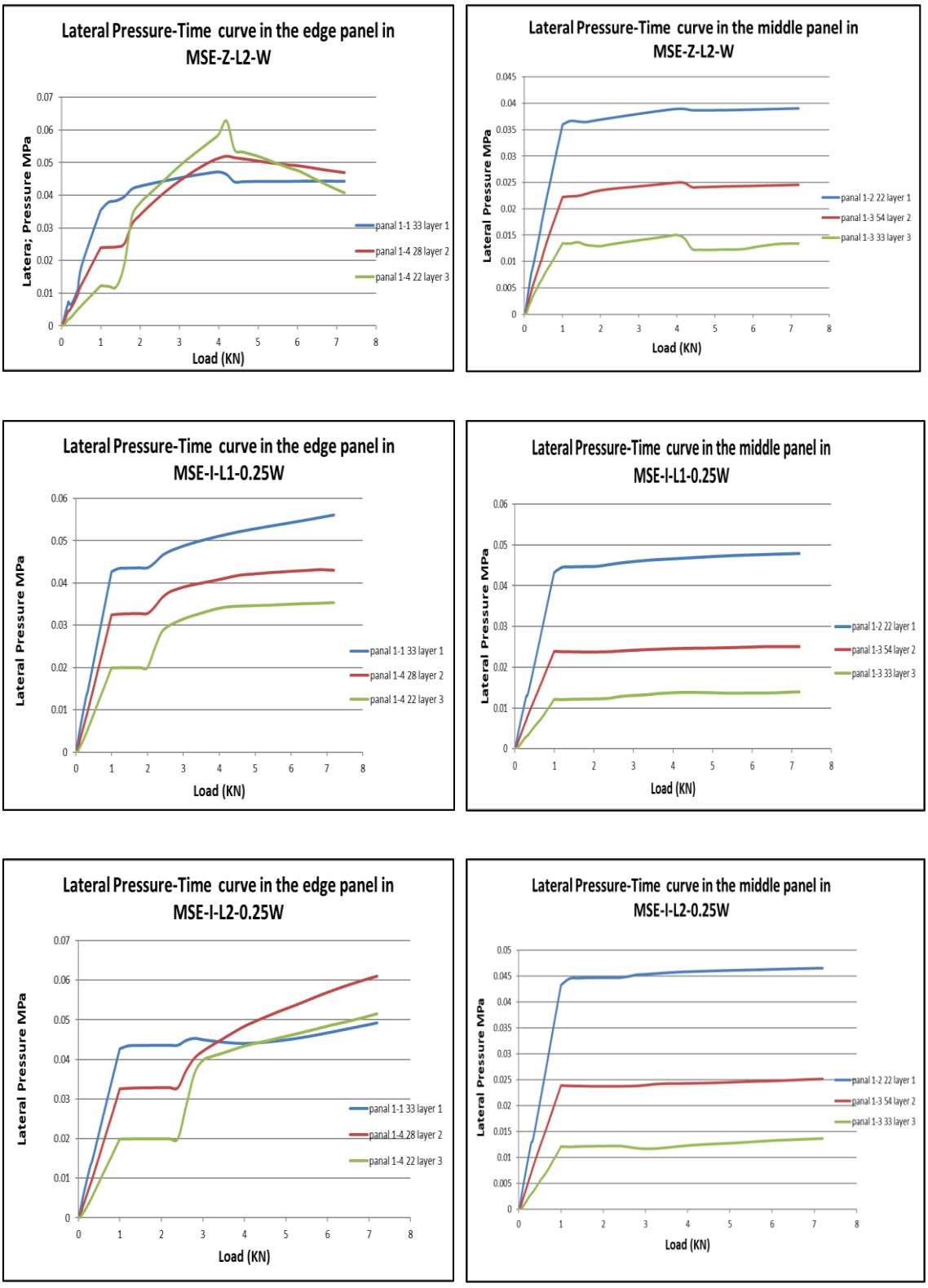

Figure 5.27. Comparison between All Cases in the strip width on the lateral pressure (continued).

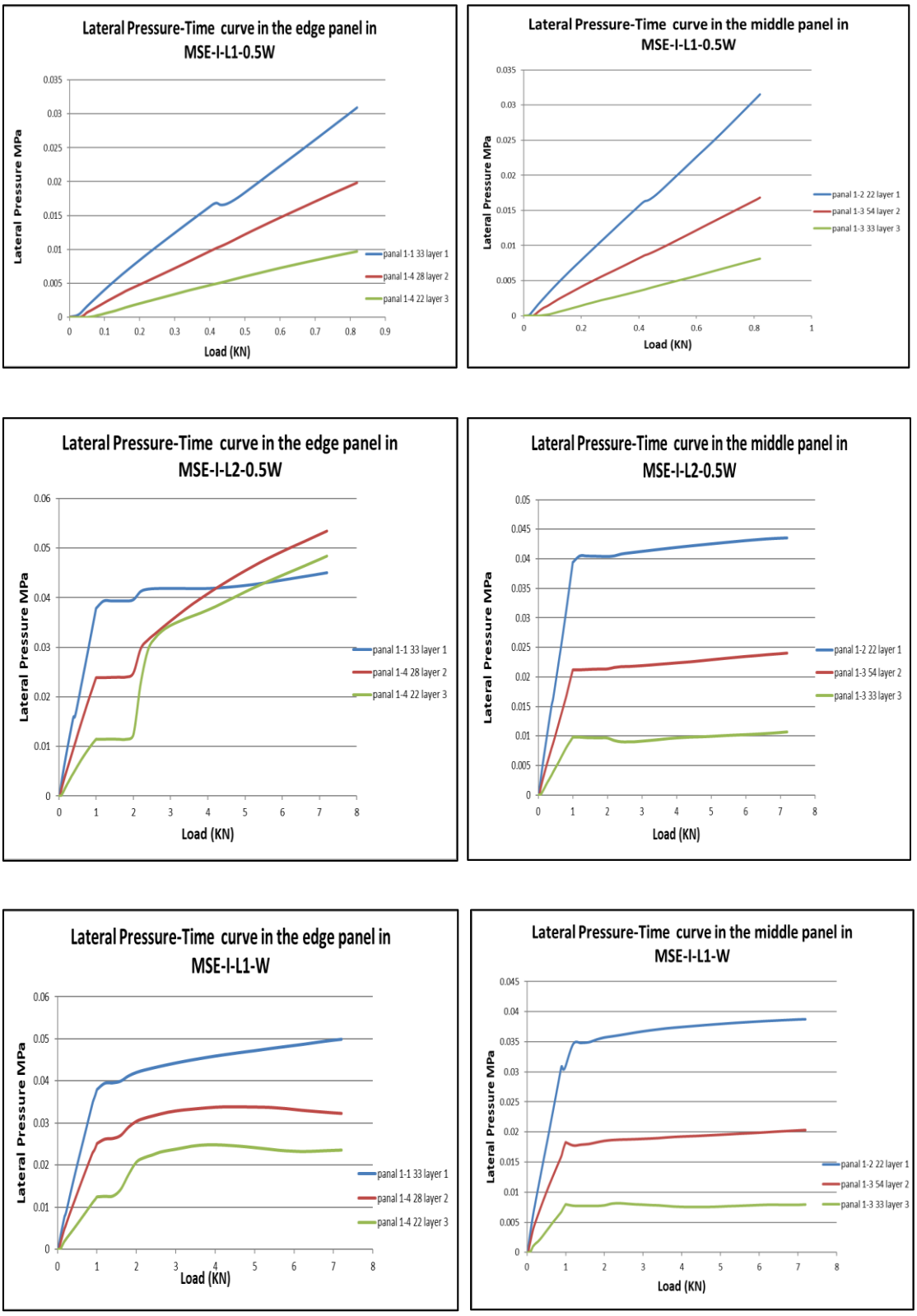

Figure 5.27. Comparison between All Cases in the strip width on the lateral pressure (continued).

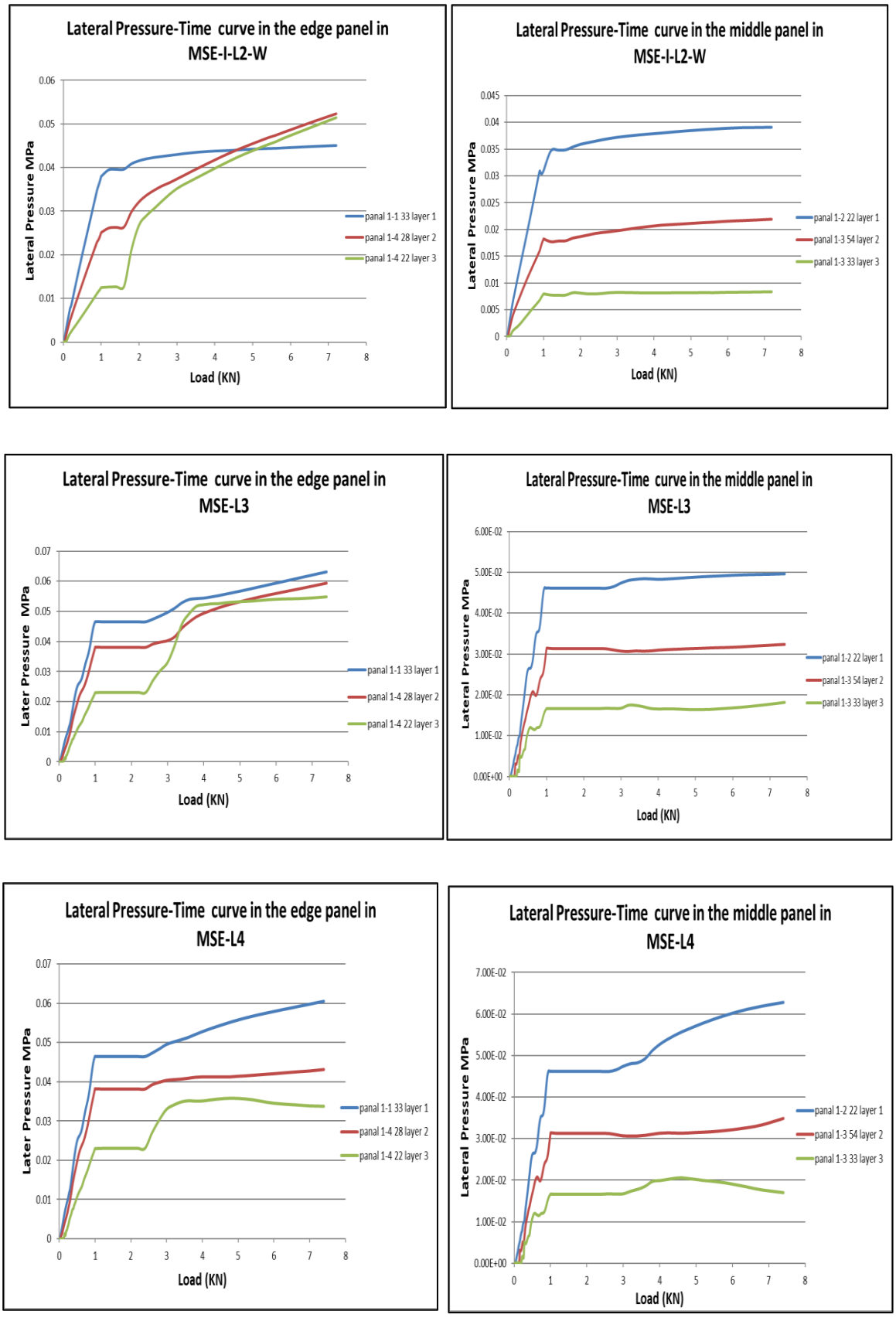

Figure 5.27. Comparison between All Cases in the strip width on the lateral pressure (continued).

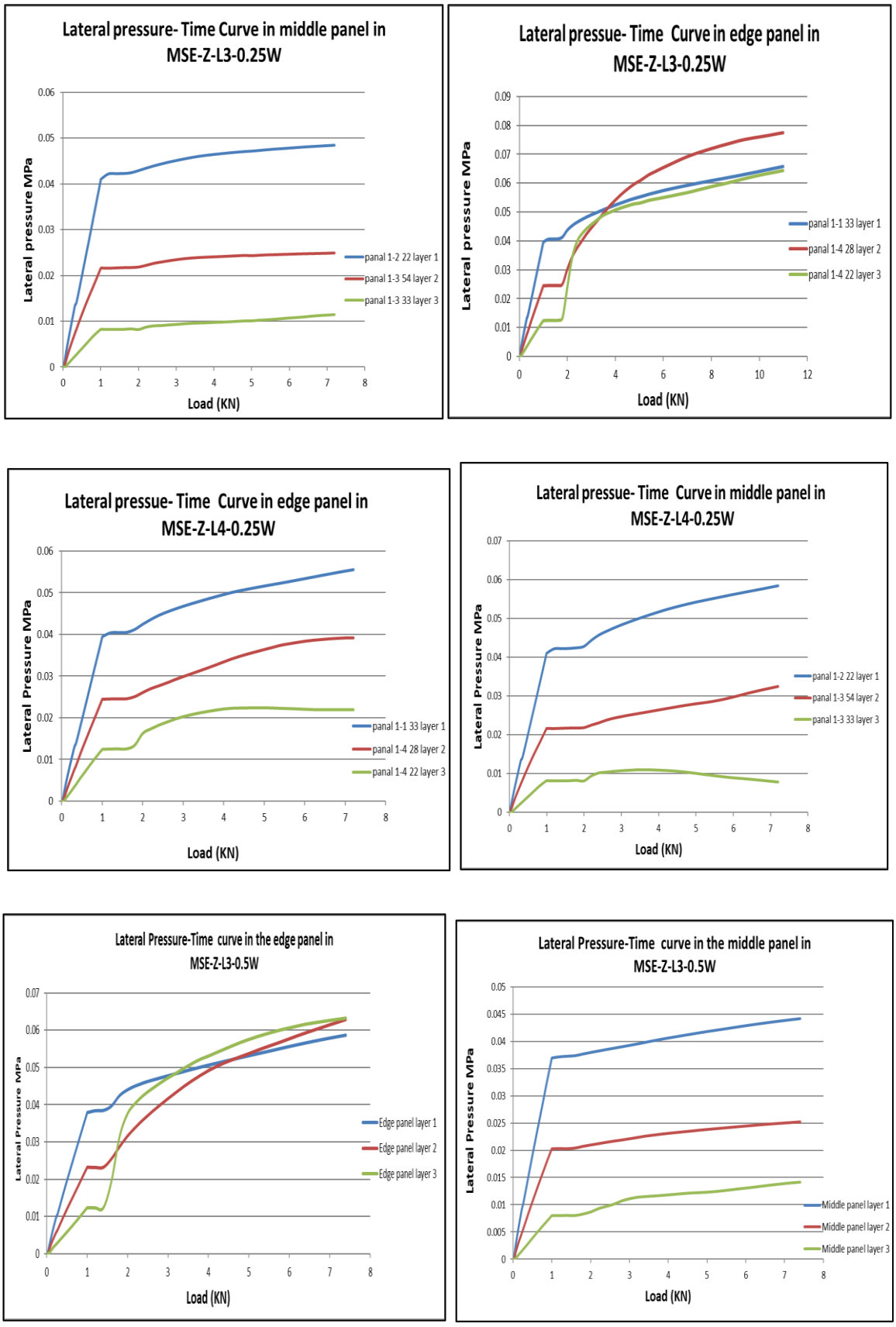

Figure 5.27. Comparison between All Cases in the strip width on the lateral pressure (continued).

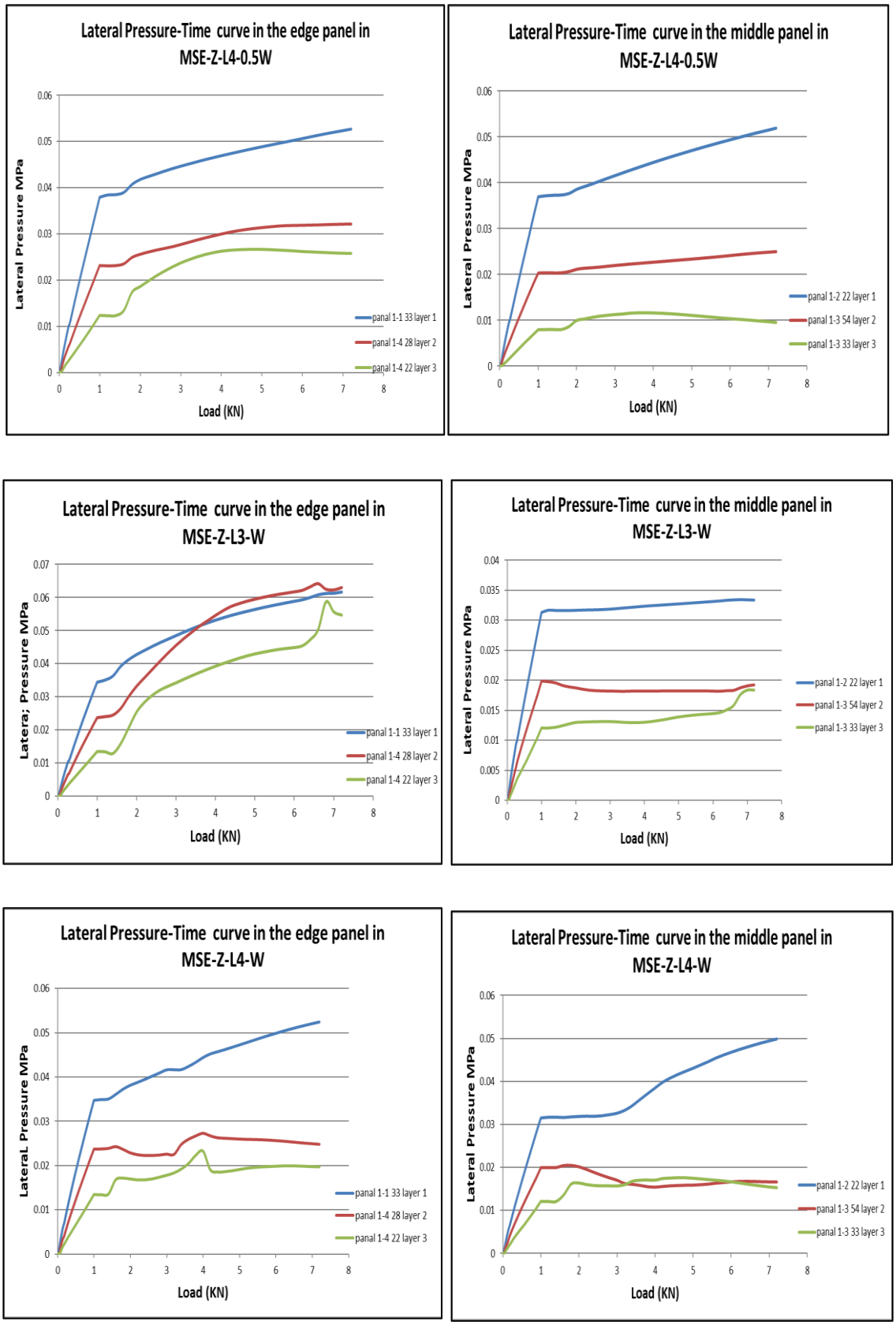

Figure 5.27. Comparison between All Cases in the strip width on the lateral pressure (continued).

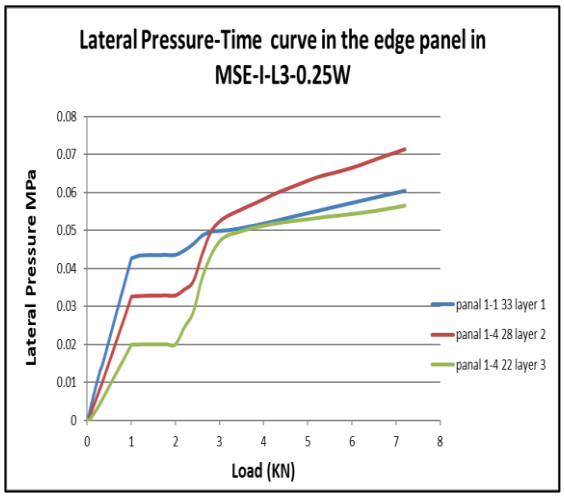

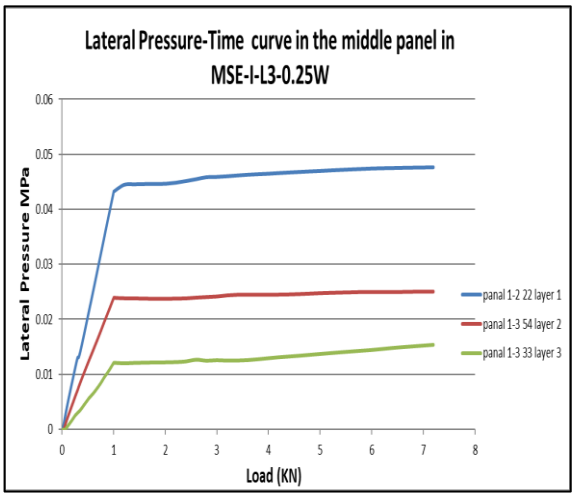

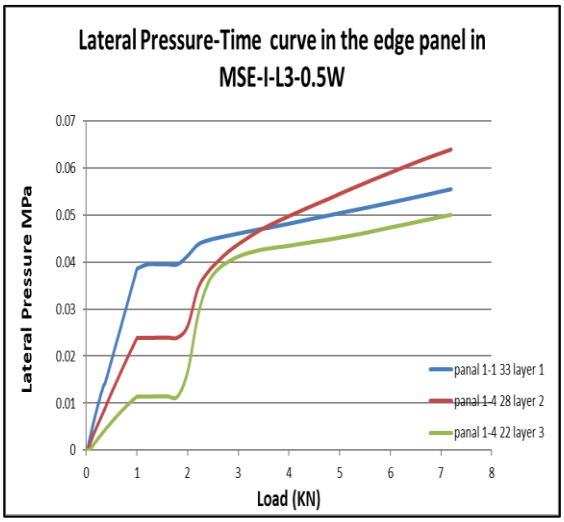

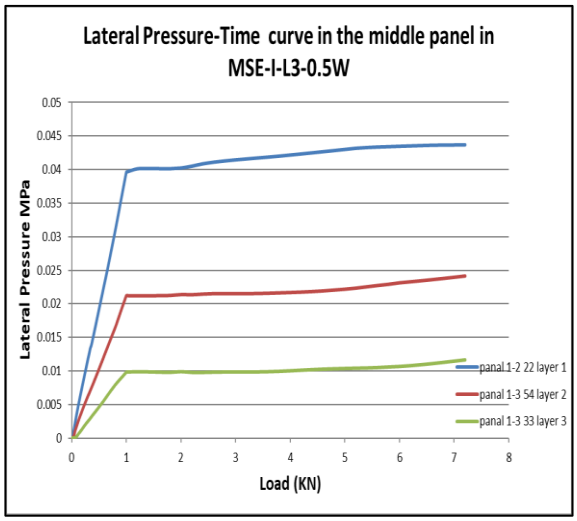

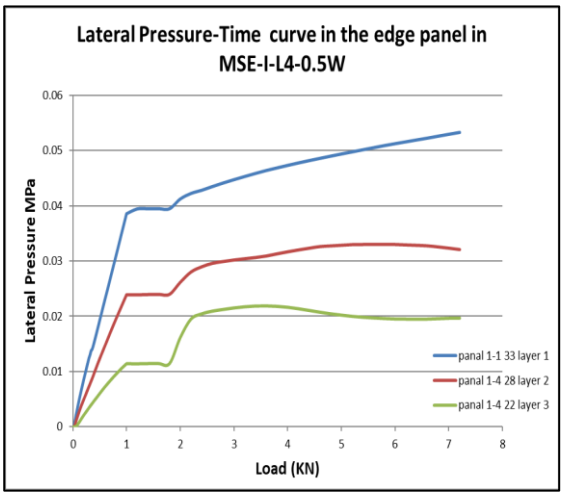

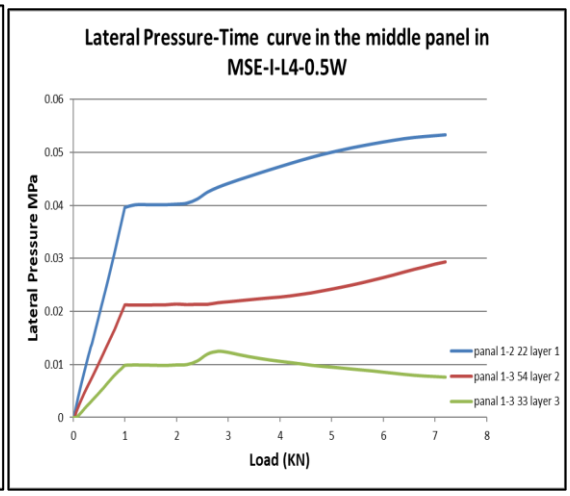

Figure 5.27. Comparison between All Cases in the strip width on the lateral pressure (continued).

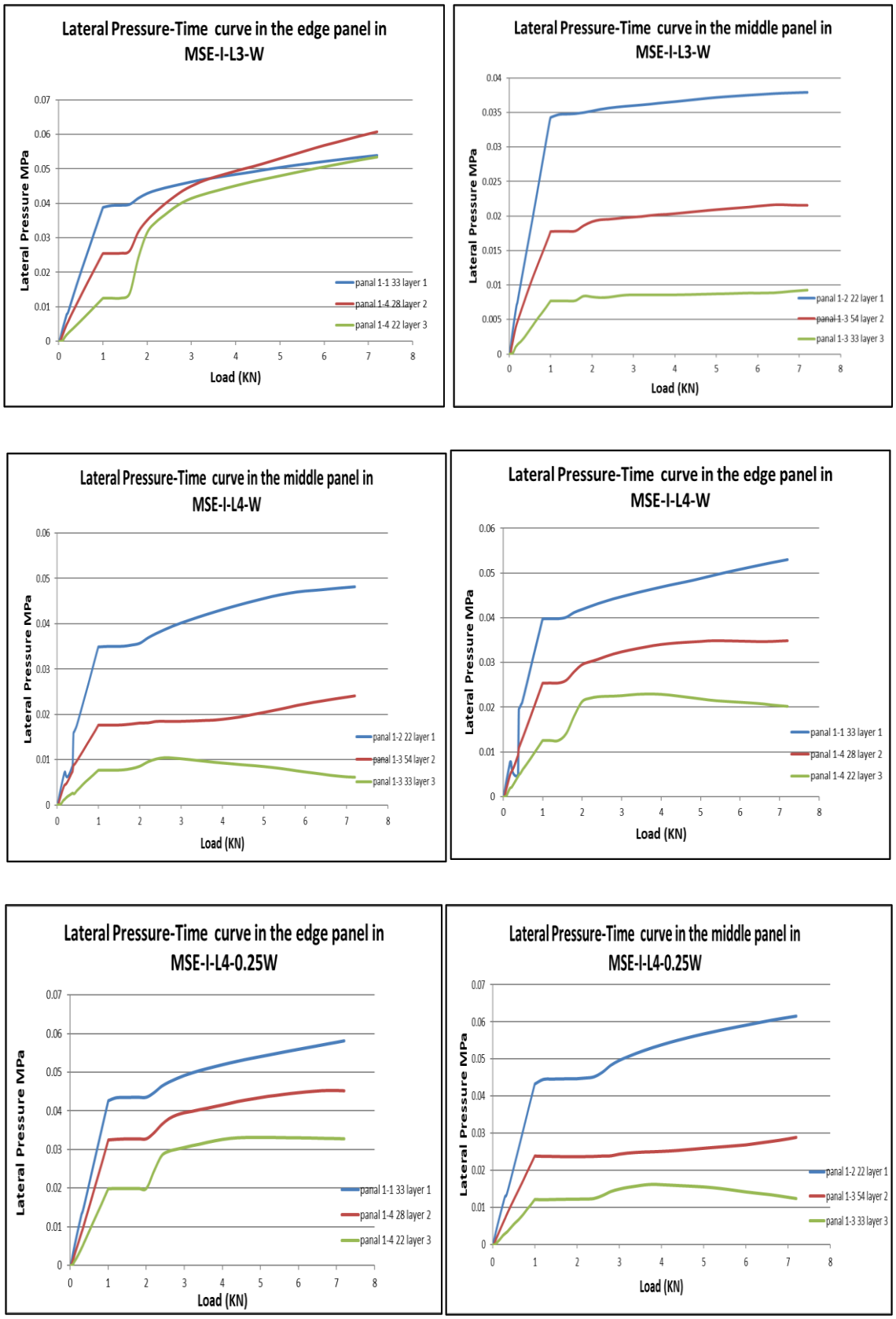

Figure 5.27. Comparison between All Cases in the strip width on the lateral pressure (continued).

5.6.5 Effect of the strip width on the vertical soil pressure

The effect of strips width on the vertical soil pressure for different cases has been presented in Figure 5.28 and Figure 5.29. Three widths were used in this study (W, 0.5W, 0.25W). It has been detected that the increase in width of strip reduce the vertical pressure of soil due to confinement the soil and increase the surface of friction when increase the strips width the opposite action occurred when reduced width of strips (Dash et al., 2004; Shivananda & Bincy, 2019).

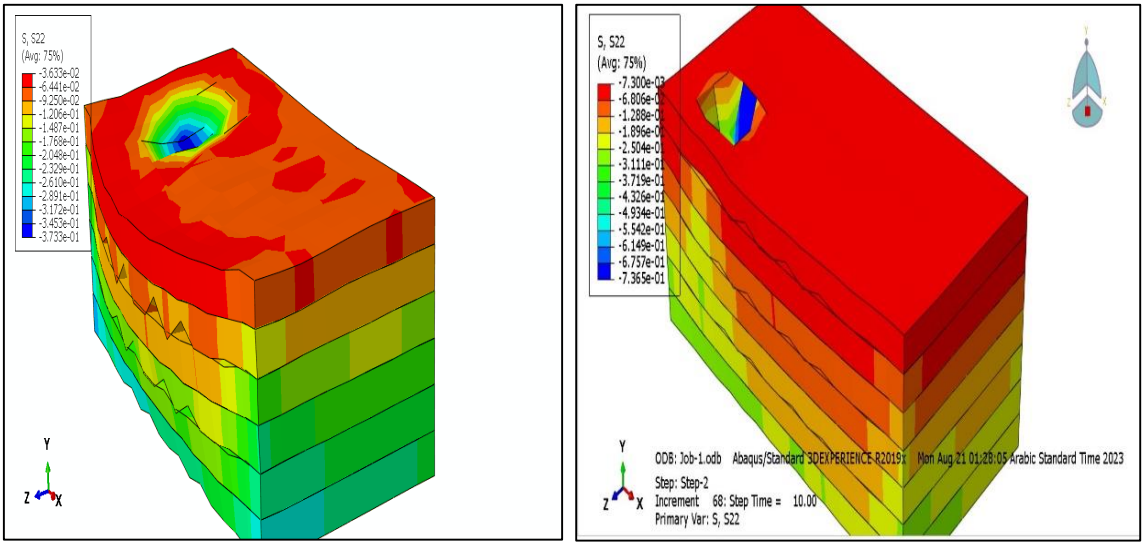

Figure 5.28. Distribution of vertical pressure.

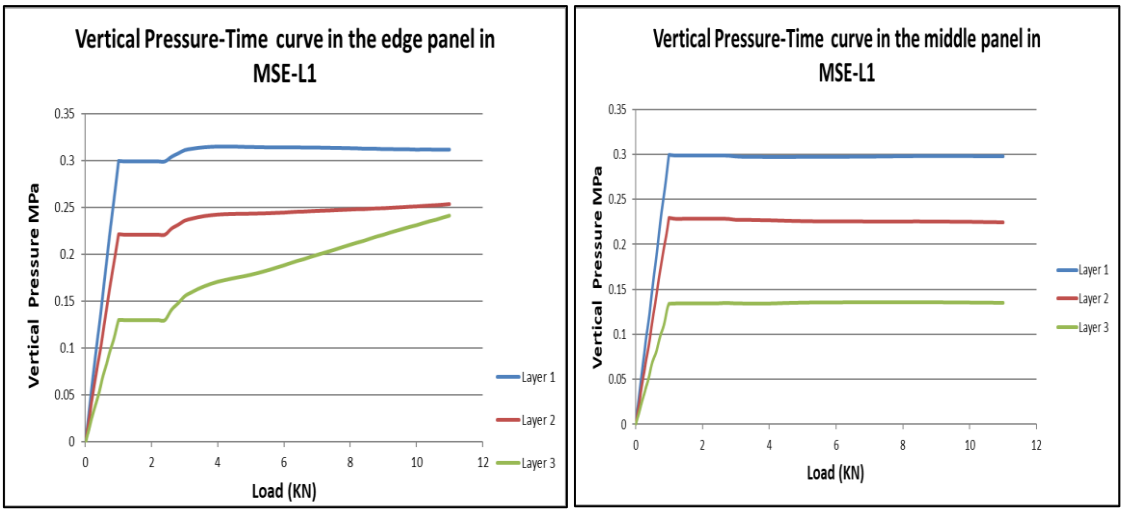

Figure 5.29. Comparison between All Cases in the strip width on the Vertical pressure.

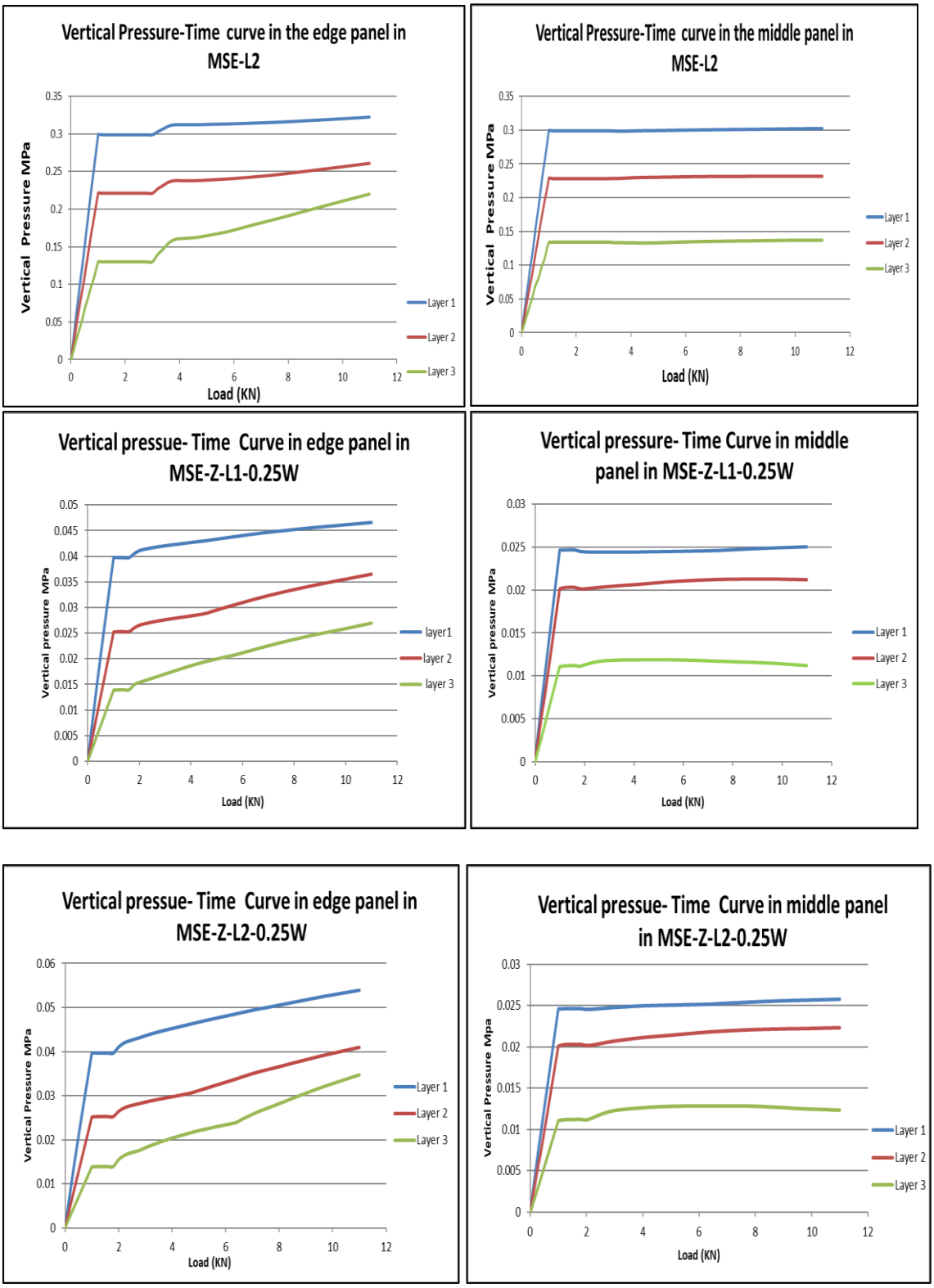

Figure 5.34. Comparison between All Cases in the strip width on the Vertical pressure (continued).

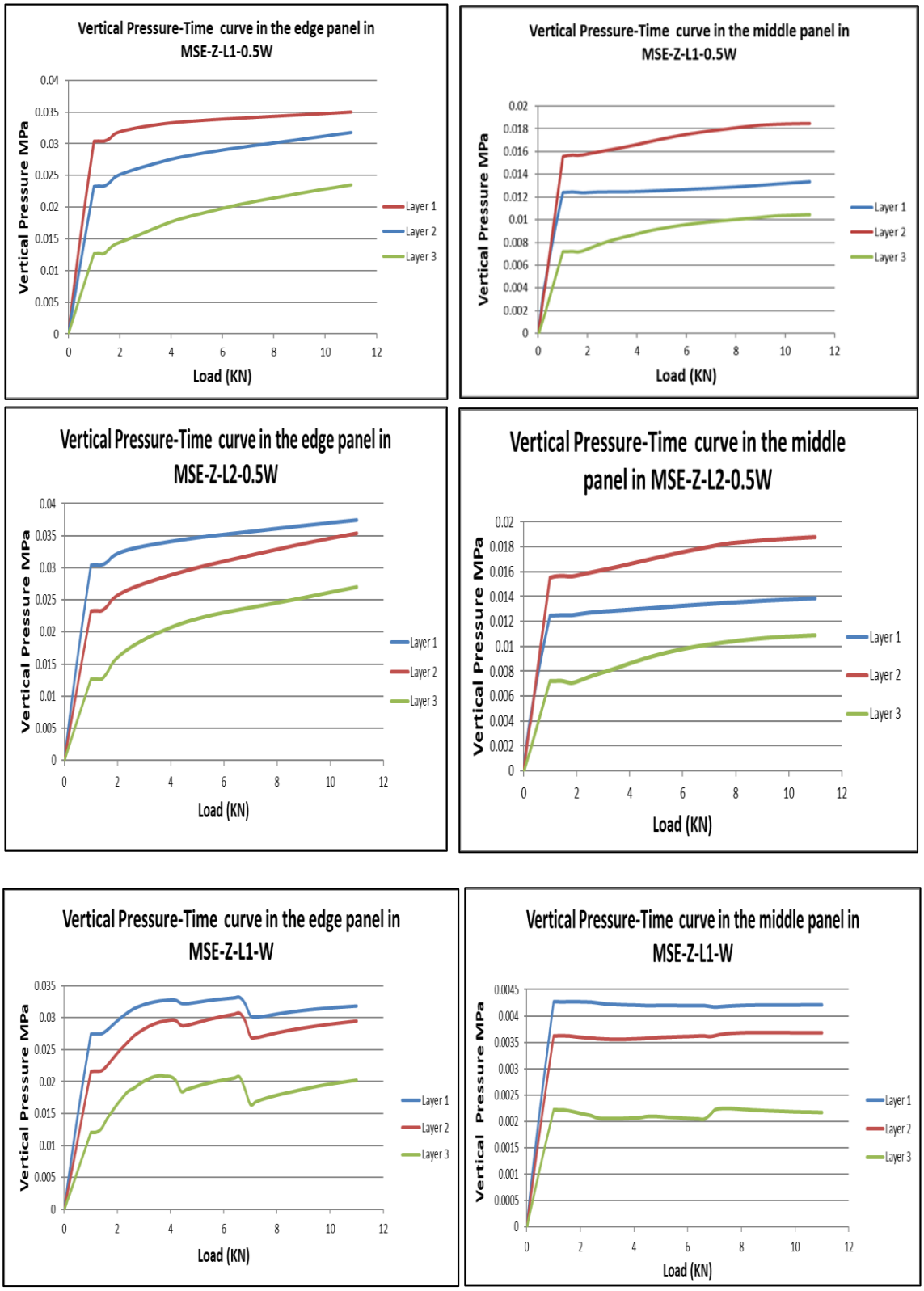

Figure 5.34. Comparison between All Cases in the strip width on the Vertical pressure (continued).

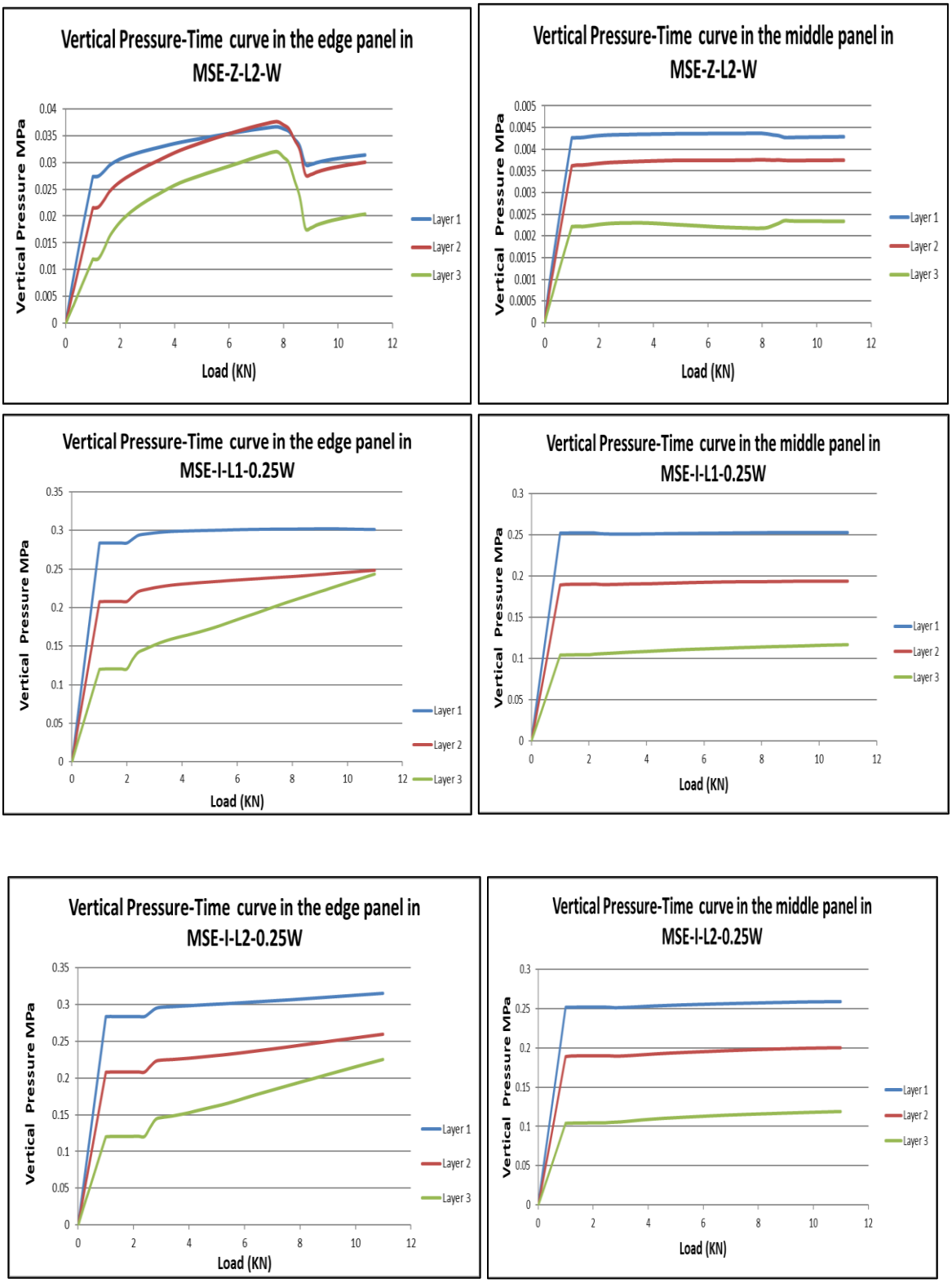

Figure 5.34. Comparison between All Cases in the strip width on the Vertical pressure (continued).

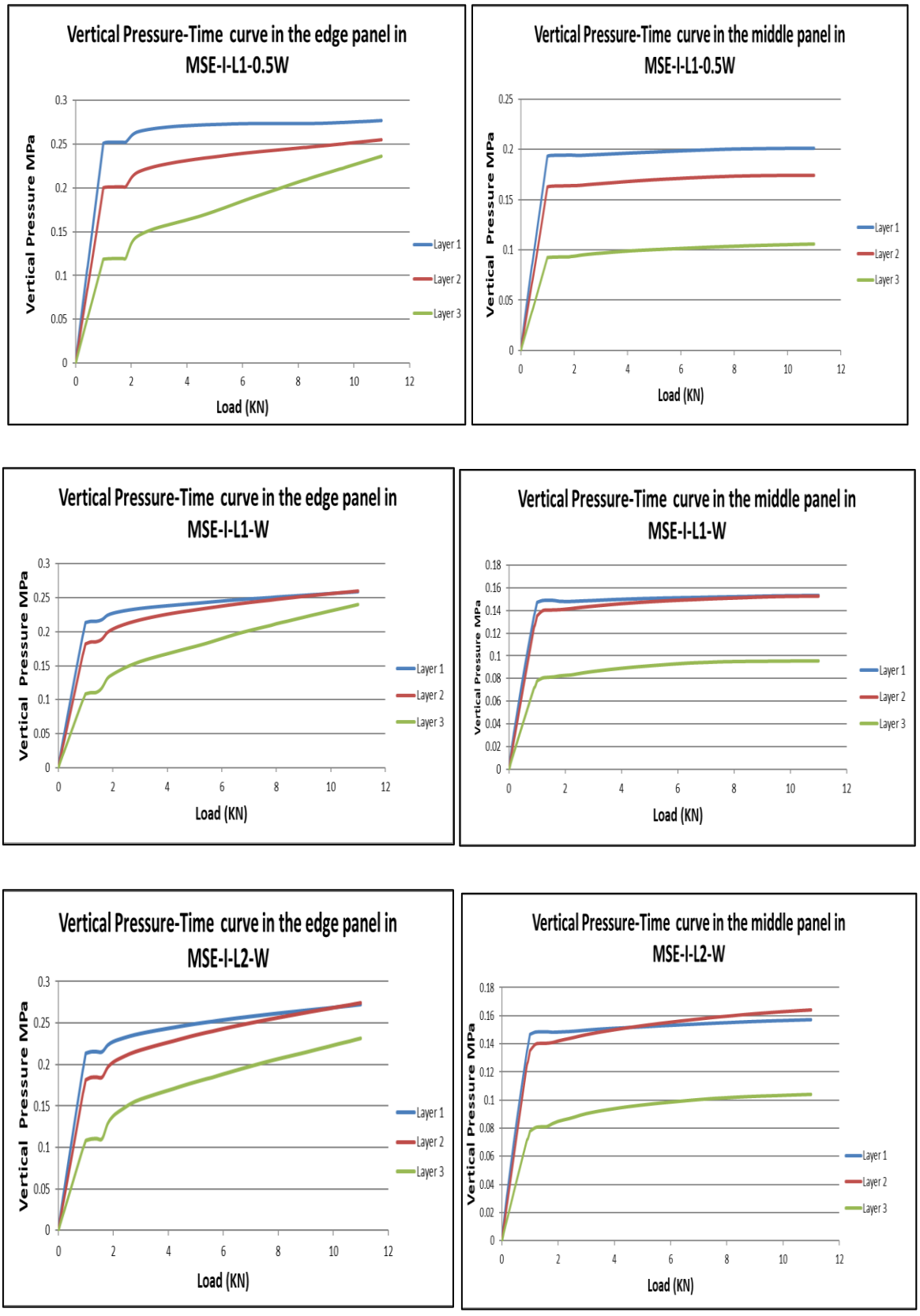

Figure 5.34. Comparison between All Cases in the strip width on the Vertical pressure (continued).

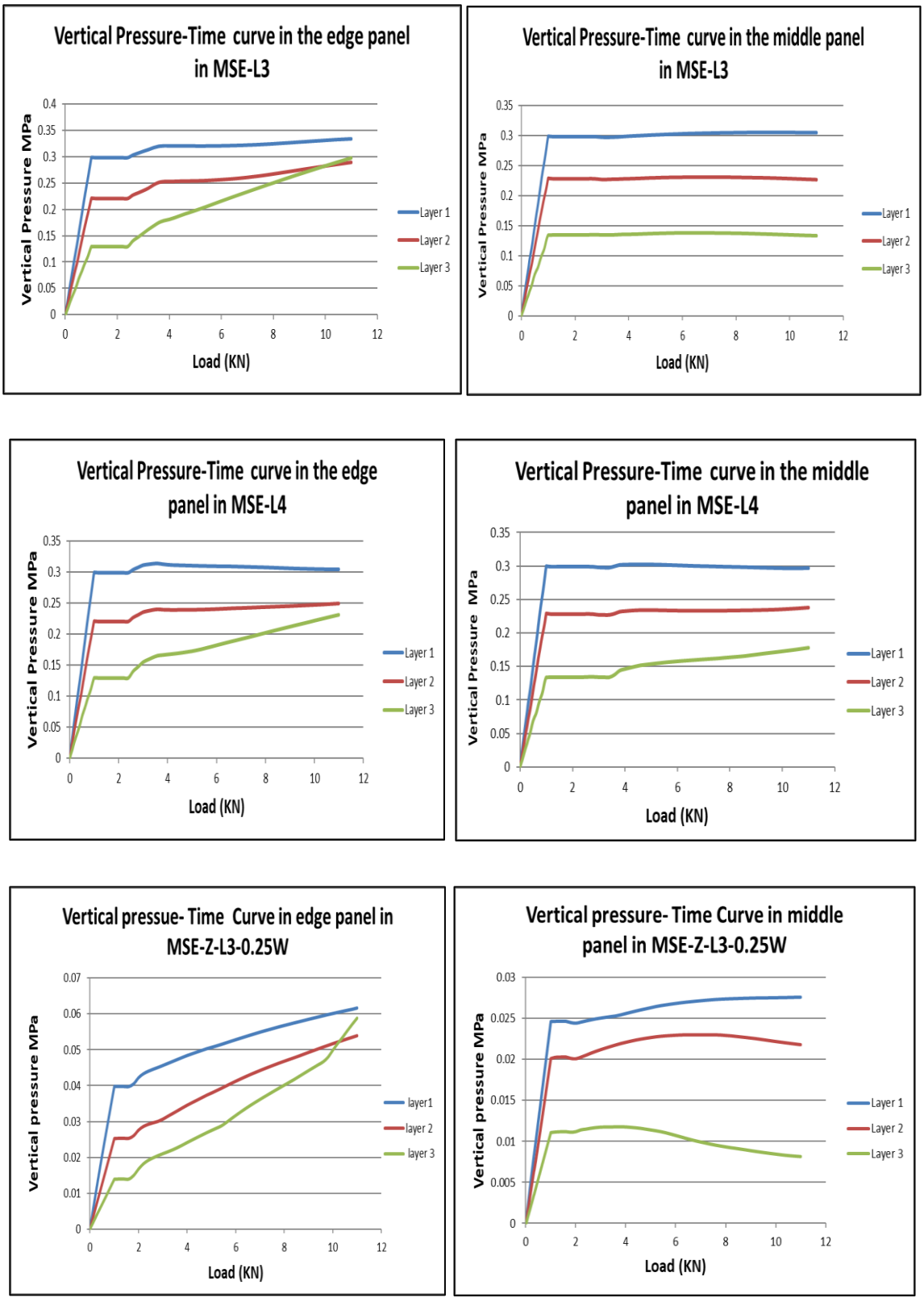

Figure 5.34. Comparison between All Cases in the strip width on the Vertical pressure (continued).

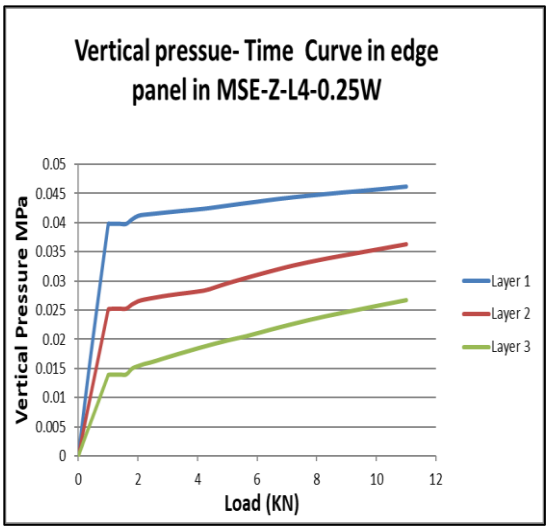

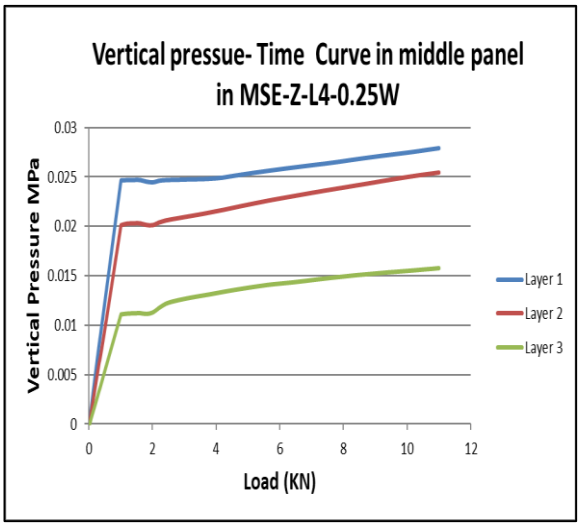

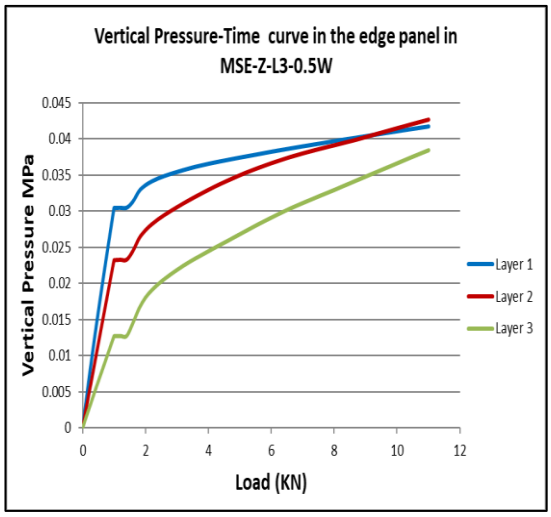

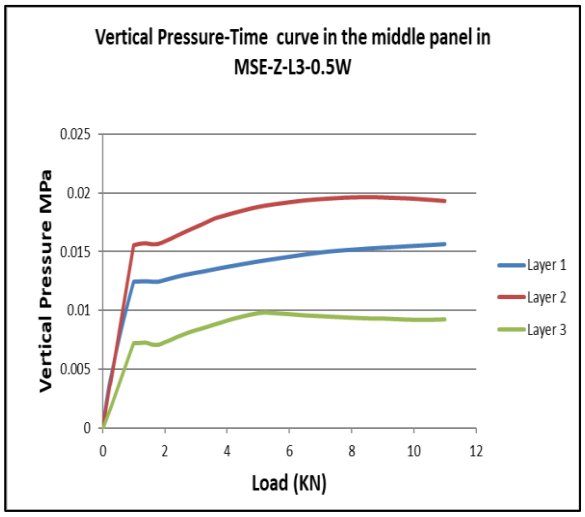

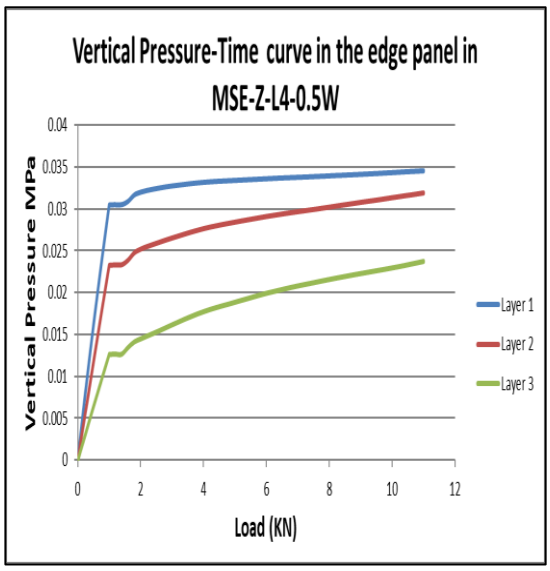

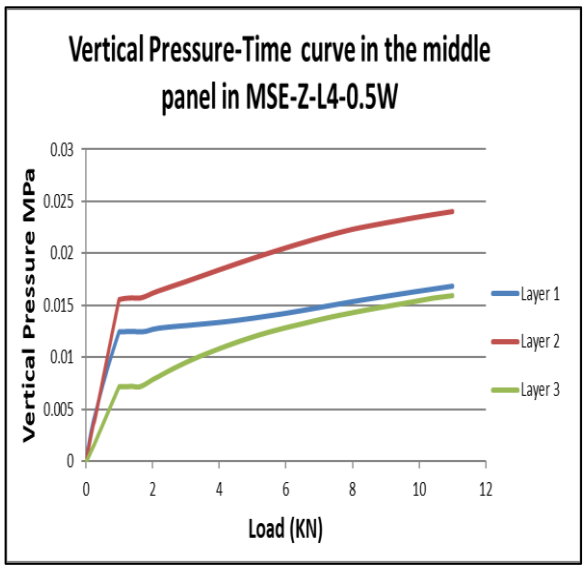

Figure 5.34. Comparison between All Cases in the strip width on the Vertical pressure (continued).

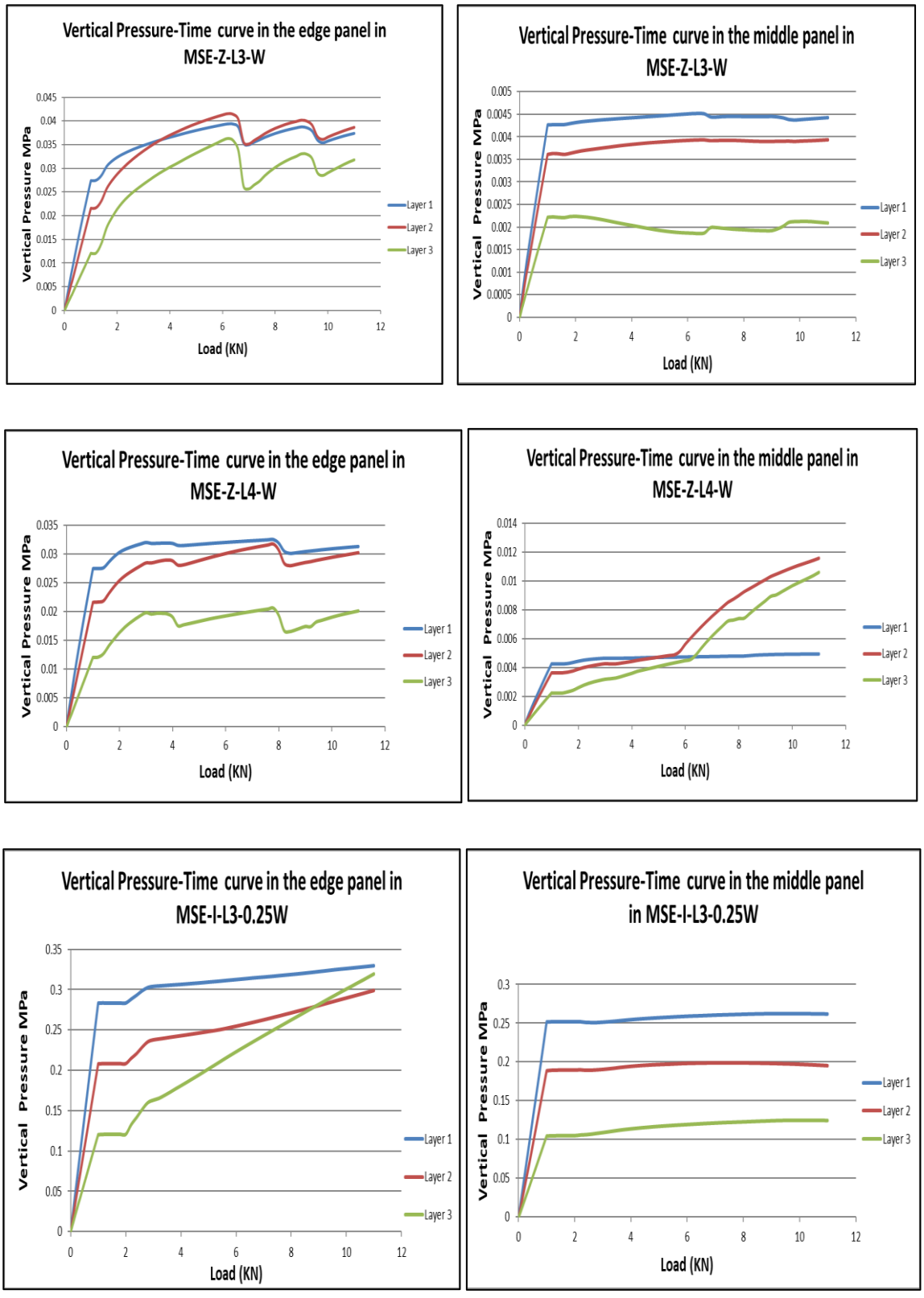

Figure 5.34. Comparison between All Cases in the strip width on the Vertical pressure (continued).

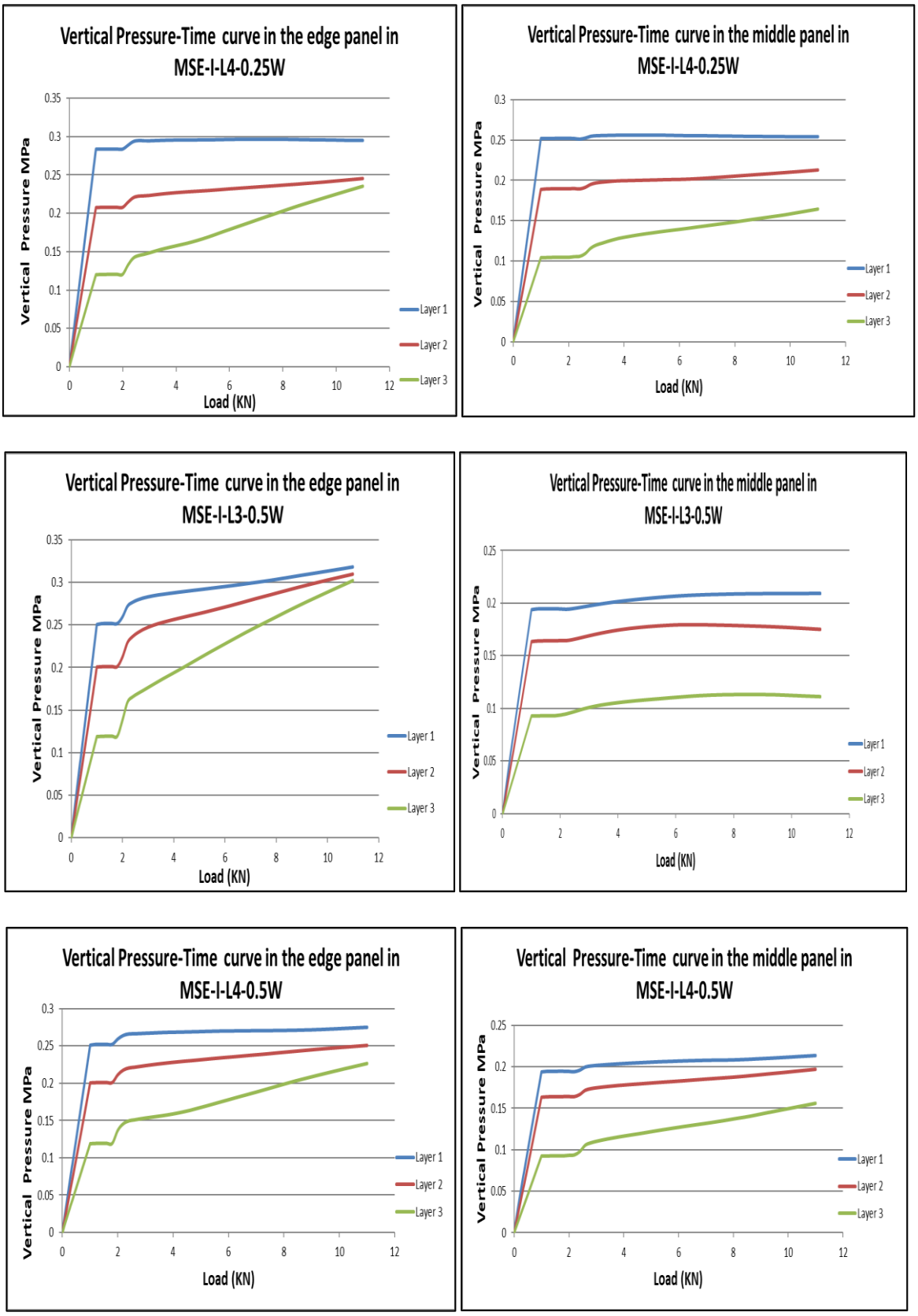

Figure 5.34. Comparison between All Cases in the strip width on the Vertical pressure (continued).

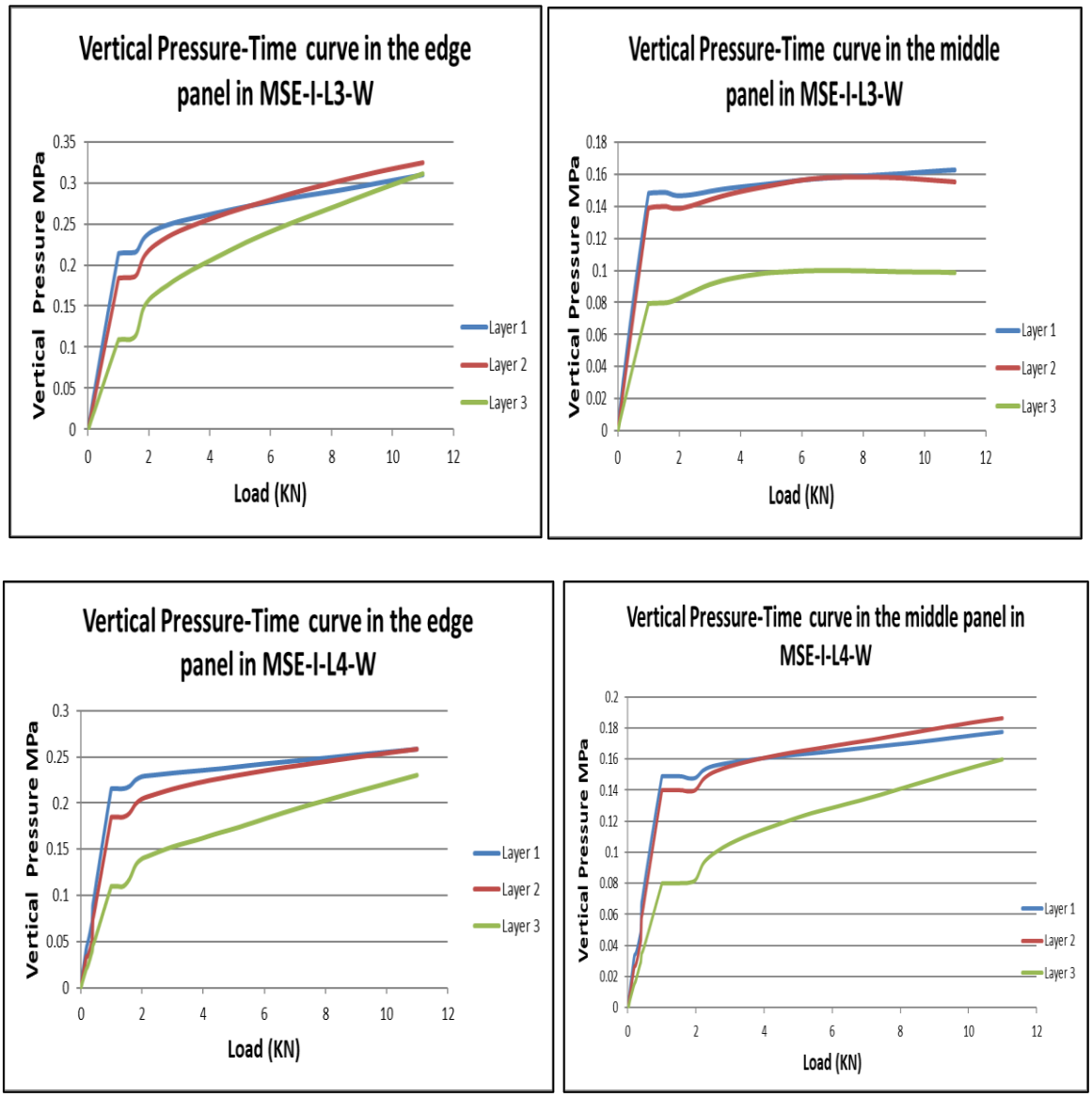

Figure 5.30. Comparison between All Cases in the strip width on the Vertical pressure.

CHAPTER SIX

CONCLUSIONS AND RECOMMENDATIONS

Chapter Six

Conclusions and Recommendations

6.1. Introduction

The primary aim of the present research is to investigate the behavior of mechanically stabilized earth (MSE) walls that have been reinforced with geosynthetic strips when subjected to static loading. The current investigation encompasses an experimental program alongside the development of a nonlinear finite element model. The primary objective of this model is to accurately forecast the vertical and lateral pressure exerted by soil on the Mechanically Stabilized Earth (MSE) wall. This chapter presents the findings derived from the analytical and experimental outcomes. Additionally, recommendations for future endeavors are also put forth.

6.2. Conclusions

Based on the results obtained from the experimental work and by finite element analysis for the zigzag and straight soil reinforcement, the following conclusions can be drawn:

- Based on the experimental findings using of zigzag strips reinforcement give better resistance for both lateral and vertical pressure than straight strips reinforcement. And the zigzag shape gives better results than straight shape by 19% in lateral pressure. While the zigzag shape gives better results than straight shape by 60% in vertical pressure.
- Using of zigzag strips reinforcement give lower displacement in MSE wall than straight strips. In addition to that using both kinds of soil strips reinforcement led to decrease later displacement with depth. And the straight shape gives better results than zigzag shape by 50% in reducing the displacement.

- Applying soil strips reinforcement for two selected shapes led to decrease the lateral and vertical pressure on the MSE wall by 47% for both.
- While in numerical findings reducing the width of strips lead to reduce the resistance of soil against the load.
- Vertical pressure reduced with depth for two selected soil strips reinforcement, and all cases zigzags give better improvement for soil support than straight one.
- Stress in strips decreased with increasing the depth of soil due to the upper strips layer carrying most of the load and distributed by friction forces with soil.
- Changing the location of the load in numerical analysis affects the concrete strain significantly with low effect on soil.
- The numerical model has been obtained when MSE-Z-L1-W (Load location at distance x=80 cm from the panel face), which lower displacement in edge and middle panel.
- Applying soil strips reinforcement for two selected shapes led to decrease the lateral displacement in edge and middle panel, for example in MSE-Z-L1-0.25W the displacement was reduced by 61% comparison with model without soil strips reinforcement.
- Increasing the soil strips width led to reduce the lateral displacement, for example the lateral displacement has been improved by 27% when increasing the strips width from 0.25W in (MSE-Z-L1-0.25W) to 0.5W in MSE-Z-L1-0.5W, which means the soil resistance against displacement improved also.
- The change in load location from L1 to L2 led to an increase in the lateral displacement in the edge panel of MSEW by 26%.
- The change in load location from L1 to L3 led to an increase in the lateral displacement in the edge panel of MSEW by 45%.

- In Al-Um intersection bridge the lateral pressure from surcharge load decreased with the depth.
- In Al-Um intersection bridge changing the type of the load from static to moving load lead to change the way of load effect on soil and panel from linear to nonlinear behaivor.

6.3. Recommendations

To improve MSE wall behavior as well as reduce the limitation of the current study, the following future aspect could be taken in the considerations:

- Improve the soil of model by chemical stabilizer to investigate the differences between the strip's mechanism in failure resistance and chemical stabilizers effect on stabilization of bridge soil.
- Change the support type in the experimental model to investigate the effect of support on the behavior of MSE wall.
- Using Plaxis software program to simulate same parametric study to identify the differences in the obtained results from ABAQUS software and Plaxis.
- Change the load type from static to dynamic one in both experimental and numerical model to investigate the effect of load type on MSE wall behavior.
- Using similar strips, but with different horizontal spacing to identify the optimum strip spacing in both experimental and numerical model.
- Using similar strips, but with different vertical spacing to identify the optimum strip spacing in both experimental and numerical model.
- Using other strips shape as X-shape to evaluate the selected shape with existence shapes straight and zigzag one.
- Study the effect of joints between the panels on the MSEW stability and behavior.

REFERENCES

References

AASHTO 2nd, L. (1998). Bridge design specifications. *American Association of State Highway and Transportation Officials, Washington, DC*.

Abaqus, G. (2011). Abaqus 6.11. *Dassault Systemes Simulia Corporation, Providence, RI, USA*.

Aggregates, A. I. C. C. on C. and C. (2017). *Standard test method for splitting tensile strength of cylindrical concrete specimens1*. ASTM international.

Alisawi, A. T., Collins, P. E. F., & Cashell, K. A. (2023). Novel Methodology for Scaling and Simulating Structural Behaviour for Soil–Structure Systems Subjected to Extreme Loading Conditions. *Applied Sciences*, *13*(15), 8626.

Allen, T., Christopher, B., Elias, V., & DiMaggio, J. (2001). *Development of the simplified method for internal stability design of mechanically stabilized earth walls*. The Department.

Allen, T. M., & Bathurst, R. J. (2001). Application of the Ko-Stiffness Method to Reinforced Soil Limit States Design. *Washington State Department of Transportation Report No. WA-RD*, *528*.

Allen, T. M., & Bathurst, R. J. (2002). Soil reinforcement loads in geosynthetic walls at working stress conditions. *Geosynthetics International*, *9*(5–6), 525–566.

Alonso, E. E., Pinyol, N. M., Puzrin, A. M., Alonso, E. E., Pinyol, N. M., & Puzrin, A. M. (2010). Earth Dam Sliding Failure: Aznalcóllar Dam, Spain. *Geomechanics of Failures. Advanced Topics*, 129–164.

Amadei, B., & Stephansson, O. (1997). *Rock stress and its measurement*. Springer Science & Business Media.

Anderson, D. G. (2008). *Seismic analysis and design of retaining walls, buried structures, slopes, and embankments* (Vol. 611). Transportation Research Board.

Anderson, P. L., Gladstone, R. A., & Withiam, J. L. (2010). Coherent gravity: The correct design method for steel-reinforced MSE walls. *Earth Retention Conference 3*, 512–521.

Armour, T. A., Bickford, J., & Pfister, T. (2004). Repair of failing MSE railroad bridge abutment. In *GeoSupport 2004: Drilled Shafts, Micropiling, Deep Mixing, Remedial Methods, and Specialty Foundation Systems* (pp. 380–394).

ASTM, A. (2005). 370-05," Standard Test Method and Definition for Mechanical Testing of Steel Products", Annual Book of ASTM Standard, Vol. 01.01. *ASTM, Philadelphia, PA*.

ASTM, A. (2017). D7928-17. *Standard Test Method for Particle-Size Distribution (Gradation) of Fine-Grained Soils Using the Sedimentation (Hydrometer) Analysis*.

ASTM, A. (2018). C78/C78M-18 Standard Test Method for Flexural Strength of Concrete Using Simple Beam with Third-Point Loading. *West Conshohocken: ASTM International*.

ASTM, C. (1986). C 33-86; Standard Specification for Concrete Aggregates, Annual Book of ASTM Standards. *ASTM: West Conshohocken, PA, USA*.

ASTM, C. (1996). 496-96. *Standard Test Method for Splitting Tensile Strength of Cylindrical Concrete Specimens*.

ASTM, D. (n.d.). 6637 (2011) Standard test method for determining the tensile properties of geogrid by the single or multi-rib tensile method. *ASTM International, West Conshohocken, PA, USA*.

Bagherpour, S. (2012). Fibre reinforced polyester composites. *Polyester*, 135–166.

Balunaini, U., Yoon, S., Prezzi, M., & Salgado, R. (2009). *Tire shred backfill in mechanically stabilized earth wall applications*.

Bangash, M. Y. H. (1989). *Concrete and concrete structures: Numerical modelling and applications*.

Bathurst, R. J. (2020). Developments in MSE wall research and design. *Innovative Infrastructure Solutions Using Geosynthetics: Proceedings of the 3rd GeoMEast International Congress and Exhibition, Egypt 2019 on Sustainable Civil Infrastructures–The Official International Congress of the Soil-Structure Interaction Group in Egypt (SSIGE)*, 22–50.

Bathurst, R. J., Walters, D., Vlachopoulos, N., Burgess, P., & Allen, T. M. (2000). Full scale testing of geosynthetic reinforced walls. In *Advances in transportation and geoenvironmental systems using geosynthetics* (pp. 201–217).

Bell, J. R., Stilley, A. N., & Vandre, B. (1975). Fabric retained earth walls. *Engineering Geology & Soils Engineering Symp Proc*, *13*.

Berg, R. R., Samtani, N. C., & Christopher, B. R. (2009). *Design of mechanically stabilized earth walls and reinforced soil slopes–Volume II*. United States. Department of Transportation. Federal Highway Administration.

Bhandari, P. (2021). *Evaluation of recycled plastic pins as shear keys in MSE wall base*. The University of Texas at Arlington.

Brabant, K. (2001). Mechanically Stabilized Earth walls for support of highway bridges. *Advanced Foundation Engineering UMASS Lowell–Course (14.533)*, *58*.

Briaud, J.-L. (1997). *Settlement of bridge approaches* (Vol. 234). Transportation Research Board.

Brooks, H., & Nielsen, J. (2010). Basics of retaining wall design. *HBA Publication*, *11*.

BROUTHEN, A. (2022). *3D Numerical Analysis of the Interaction of Back-to-Back Reinforced Soil Walls Analyse Numérique Tridimensionnelle de l'Interaction des Murs de Soutènement à Parements Opposés en sols Renforcés*. Faculté des Sciences et de la technologie.

Burke, C., Ling, H. I., & Liu, H. (2004). Seismic response analysis of a full-scale reinforced soil retaining wall. *Proc. 17th ASCE Engineering Mechanics Conf., Newark, DE*.

C78/C78M, A. (2018). Standard test method for flexural strength of concrete (using simple beam with third-point loading). In *ASTM International*. West Conshohocken PA.

Cakir, T. (2013). Evaluation of the effect of earthquake frequency content on seismic behavior of cantilever retaining wall including soil–structure interaction. *Soil Dynamics and Earthquake Engineering*, *45*, 96–111.

Chalisgaonkar, R. (2021). *Design of Breast Walls: A Practical Solution Approach*. CRC Press.

Chaudhari, S. V, & Chakrabarti, M. A. (2012). Modeling of concrete for nonlinear analysis using finite element code ABAQUS. *International Journal of Computer Applications*, *44*(7), 14–18.

Chen, W.-F. (2007). *Plasticity in reinforced concrete*. J. Ross Publishing.

Christopher, B. R., Gill, S., Giroud, J.-P., Juran, I., Mitchell, J. K., Schlosser, F., & Dunnicliff, J. (1990). *Reinforced soil structures. Volume I. Design and construction guidelines*.

Churilla, C. J., & Diviney, J. (1979). *Earth Pressures Behind a Counterfort Abutment Wall*.

Committee, C. (2021). Test Method for Compressive Strength of Cylindrical Concrete Specimens. *ASTM International: West Conshohocken, PA, USA*.

D1143, A. (2007). ASTM D 1143/D 1143M-07 Standard Test Methods for Deep Foundations Under Static Axial Tensile Load. *ASTM Int.*, *7*, 15.

Das, B. M. (2005). Developments on the bearing capacity of shallow foundations on geogrid-reinforced soil-a review. 한국지반신소재학회 학술발표회, 1–29.

Dash, S. K., Rajagopal, K., & Krishnaswamy, N. R. (2004). Performance of different geosynthetic reinforcement materials in sand foundations. *Geosynthetics International*, *11*(1), 35–42.

Datta, T. K. (2010). *Seismic analysis of structures*. John Wiley & Sons.

David, T. K., & Forth, J. P. (2011). Modelling of soil structure interaction of integral abutment bridges. *World Acad Sci Eng Technol*, *78*, 769–774.

Dobie, M. J. D. (2001). *The two-part wedge method used for seismic design of reinforced soil retaining walls, including connection strength*. IGEF, Taipei, Taiwan.

Elias, V., Christopher, B. R., Berg, R. R., & Berg, R. R. (2001). *Mechanically stabilized earth walls and reinforced soil slopes: design and construction guidelines (updated version)*. United States. Federal Highway Administration.

Ellis, E. A., & Springman, S. M. (2001). Modelling of soil–structure interaction for a piled bridge abutment in plane strain FEM analyses. *Computers and Geotechnics*, *28*(2), 79–98.

Eriksson, D., & Gasch, T. (2010). FEM-modeling of reinforced concrete and verification of the concrete material models available in ABAQUS. *Royal Institute of Technology, Department of Mechanics: Stockholm, Sweden*.

Fiorentino, G., Cengiz, C., De Luca, F., Mylonakis, G., Karamitros, D., Dietz, M., Dihoru, L., Lavorato, D., Briseghella, B., & Isakovic, T. (2021). Integral abutment bridges: Investigation of seismic soil-structure interaction effects by shaking table testing. *Earthquake Engineering & Structural Dynamics*, *50*(6), 1517–1538.

Fitzpatrick, B. J. (n.d.). *Mechanically Stabilized Earth Structures–Part 3*.

Greenway, H. R. V., Rella, A. J., & Miller, J. K. (2012). *Engineered approaches for limiting erosion along sheltered shorelines: a review of existing methods*.

Hai, L. D., Thien, D. Q., & Chinkulkijniwat, A. (2022). *COMPARE INFLUENCES OF HORIZONTAL AND VERTICAL MSE WALL DIMENSIONS WITH GEOCOMPOSITE BACK DRAINAGE SYSTEM TO MAXIMUM COMPARE INFLUENCES OF HORIZONTAL AND VERTICAL DRAINAGE SYSTEM TO MAXIMUM STEADY STATE*. *March 2023*. https://doi.org/10.26459/hueunijese.v130i4A.6478

Han, J., & Leshchinsky, D. (2010). Analysis of back-to-back mechanically stabilized earth walls. *Geotextiles and Geomembranes*, *28*(3), 262–267.

Hardianto, F. S., Lozano, R., Sankey, J. E., & Hughes, D. K. (2013). Geosynthetic-Strip Reinforced MSE Wall for Dam Expansion. *Geo-Congress 2013: Stability and Performance of Slopes and Embankments III*, 543–554.

Hatami, K., & Witthoeft, A. F. (2008). A numerical study on the use of geofoam to increase the external stability of reinforced soil walls. *Geosynthetics International*, *15*(6), 452–470.

Hattori, M., Okuno, Y., Goto, S., & Kanehisa, M. (2003). Development of a chemical structure comparison method for integrated analysis of chemical and genomic information in the metabolic pathways. *Journal of the American Chemical Society*, *125*(39), 11853–11865.

Hossain, M. S., Kibria, G., Khan, M. S., Hossain, J., & Taufiq, T. (2012). Effects of backfill soil on excessive movement of MSE wall. *Journal of Performance of Constructed Facilities*, *26*(6), 793–802.

Huber, T., Burger, J., Mata-Falcón, J., & Kaufmann, W. (2023). Structural design and testing of material optimized ribbed RC slabs with 3D printed formwork. *Structural Concrete*, *24*(2), 1932–1955.

Hulagabali, A. M., Solanki, C. H., Dodagoudar, G. R., & Shettar, M. P. (2018). Influence of supporting systems on behavior of mse wall. *International Journal of Civil Engineering and Technology*, *9*(4), 1000–1007.

Hulagabali, A., Solanki, C. H., Dodagoudar, G. R., & Shettar, M. (2018). *Effect of reinforcement , backfill and surcharge on the performance of reinforced earth retaining wall*. *May 2022*.

Huntington, W. C. (1957). *Earth pressures and retaining walls*.

IQS. (1984). No. 45, Aggregate from natural sources for concrete and construction. *Iraqi Specif*.

Iraqi Specification No.5 -1984, second modify 2010. (2010). *Portland cement*.

Jacobs, F., Ruiken, A., & Ziegler, M. (2016). Investigation of kinematic behavior and earth pressure development of geogrid reinforced soil walls. *Transportation Geotechnics*, *8*, 57–68.

Jain, M. A., & Sepate, V. (n.d.). *Review on Analysis of Multi-Storey Framed Structure Using ETABS in various zones considering Soil Structure*

Interaction.

Jones, C. J. F. P. (2013). *Earth reinforcement and soil structures*. Elsevier.

Kakrasul, J. I. (2018). *Geosynthetic reinforced retaining walls with limited fill space under static footing loading*. University of Kansas.

Keller, G. R., & Devin, S. C. (2003). Geosynthetic-reinforced soil bridge abutments. *Transportation Research Record*, *1819*(1), 362–368.

Kempton, G., Özçelik, H., Naughton, P., Mum, N., & Dundar, F. (2008). The long term performance of polymeric reinforced walls under static and Seismic conditions. *Proceedings of 4th European Conference on Geosynthetics Engineering (EuroGeo 4), Edinburgh, Paper*, *181*.

Khan, M. A. (2010). *Bridge and highway structure rehabilitation and repair*. McGraw-Hill Education.

Khan, M. A. (2014). *Accelerated bridge construction: Best practices and techniques*. Elsevier.

Khodair, Y., & Abdel-Mohti, A. (2014). Numerical analysis of pile–soil interaction under axial and lateral loads. *International Journal of Concrete Structures and Materials*, *8*, 239–249.

Kibria, G., Hossain, M. D. S., & Khan, M. S. (2014). Influence of soil reinforcement on horizontal displacement of MSE wall. *International Journal of Geomechanics*, *14*(1), 130–141.

Kibria, G., Hossain, M. S., Hossain, J., & Khan, M. S. (2012). Investigation of Moisture Variation of Backfill Soil in MSE Wall. In *GeoCongress 2012: State of the Art and Practice in Geotechnical Engineering* (pp. 2629–2638).

Kim, N.-H. (2015). Finite element analysis for contact problems. *Introduction to Nonlinear Finite Element Analysis*, 367–426.

Kim, Y.-J., Kotwal, A. R., Cho, B.-Y., Wilde, J., & You, B. H. (2019). Geosynthetic reinforced steep slopes: current technology in the United States. *Applied Sciences*, *9*(10), 2008.

Kulczykowski, M., Przewłócki, J., & Konarzewska, B. (2017). Application of soil nailing technique for protection and preservation historical buildings. *IOP Conference Series: Materials Science and Engineering*, *245*(2), 22055.

Kumar, S., & Roy, L. B. (2022). Rainfall induced geotextile reinforced model slope embankment subjected to surcharge loading: a review study. *Archives of Computational Methods in Engineering*, 1–19.

Kupfer, H., Hilsdorf, H. K., & Rusch, H. (1969). Behavior of concrete under biaxial stresses. *Journal Proceedings*, *66*(8), 656–666.

Lamis, B. (n.d.). *Behavior and design of back-to-back mechanically stabilized earth walls*.

Lan, C. (2012). *On the performance of super-long integral abutment bridges: Parametric analyses and design optimization*. University of Trento.

Lee, T.-W. (1993). *Finite element analysis of reinforced soil structures*. The University of Texas at Arlington.

Leshchinsky, D. (2005). MSE Drainage Issues and Design. In *Geosynthetics Research and Development in Progress* (pp. 1–2).

Lin, H. (2023). Coherent state excitations and string-added coherent states in gauge-gravity correspondence. *Nuclear Physics B*, *986*, 116066.

Liu, H., Han, J., Jawad, S., & Parsons, R. L. (2020). Literature review of causes and mitigation techniques for bumps at ends of bridges. *Geo-Congress 2020*, 862–871.

Madabhushi, G., Haigh, S., & Knappett, J. (2009). *Design of pile foundations*

in liquefiable soils. World Scientific.

Malm, R. (2006). *Shear cracks in concrete structures subjected to in-plane stresses*. KTH.

Maw, R. B. (2009). *Development of Mechanically Stabilized Earth (MSE) Wall Inspection Procedure for Failure Mode Analysis and Risk Assessment*.

McKittrick, D. P., & DP, M. (1979). *Reinforced earth: application of theory and research to practice*.

Melville, B., Van Ballegooy, S., Coleman, S., & Barkdoll, B. (2006). Countermeasure toe protection at spill-through abutments. *Journal of Hydraulic Engineering*, *132*(3), 235–245.

Mills, V. (2023). *Certificate of acceptance of a geosynthetic material Product : subject to the conditions of expiry of certificate below Expiry date : November 2020*, 1–5.

MIWA, S., & IKEDA, T. (2006). Shear modulus and strain of liquefied ground and their application to evaluation of the response of foundation structures. *Structural Engineering/Earthquake Engineering*, *23*(1), 167s-179s.

Molina-Moreno, F., García-Segura, T., Martí, J. V, & Yepes, V. (2017). Optimization of buttressed earth-retaining walls using hybrid harmony search algorithms. *Engineering Structures*, *134*, 205–216.

Morsy, K. M., & Thakeb, H. (2022). Comparative evaluation of the environmental impacts of geosynthetic Mechanically Stabilized Earth walls. *Journal of Cleaner Production*, *374*, 133912.

Mulligan, M., & Wainwright, J. (2013). Modelling and model building. *Environmental Modelling: Finding Simplicity in Complexity*, 7–26.

Muteb, H. H., & Falah, M. W. (2021). Mechanically Stabilized Earth MSE Walls Applications. *IOP Conference Series: Earth and Environmental Science*, *856*(1), 12031.

Naji, M., Firoozi, A. A., & Firoozi, A. A. (2020). A review: Study of integral abutment bridge with consideration of soil-structure interaction. *Latin American Journal of Solids and Structures*, *17*, e252.

Nejad, M. M. (2017). *Design optimization of geosynthetic reinforced earth walls using harmony search algorithm*. University of Delaware.

Neville, A. M., & Brooks, J. J. (1987). Concrete Technology. 2010. *Essex, England: Pearson Education Limited*.

Ng, C., Springman, S., & Norrish, A. (1998). Soil-structure interaction of spread-base integral bridge abutments. *Soils and Foundations*, *38*(1), 145–162.

Norhasri, M. S. M., Hamidah, M. S., & Fadzil, A. M. (2017). Applications of using nano material in concrete: A review. *Construction and Building Materials*, *133*, 91–97.

Norris, P., & Norris, P. (1992). *The behaviour of jacked concrete pipes during site installation*. University of Oxford.

Nowak, A. S., & Iatsko, O. (2017). Revised load and resistance factors for the AASHTO LRFD Bridge Design Specifications. *PCI Journal*, *62*(3), 46–58.

Nyamabo, A. K., Yu, H., & Shi, J.-Y. (2021). SSI–DDI: substructure–substructure interactions for drug–drug interaction prediction. *Briefings in Bioinformatics*, *22*(6), bbab133.

O'Shaughnessy, V. (1999). *Reinforcement of earth structures using scrap tires.* University of Ottawa.

Officials, T. (2009). *AASHTO LRFD Bridge Design Guide Specifications for GFRP-Reinforced Concrete Bridge Decks and Traffic Railings*. AASHTO.

Officials, T. (2011). *Standard specifications for transportation materials and methods of sampling and testing*. AASHTO.

Olkowski, D. E. (2021). *Deleuze, Bergson, Merleau-Ponty: The logic and pragmatics of creation, affective life, and perception*. Indiana University Press.

Olson, S. M., Holloway, K. P., Buenker, J. M., Long, J. H., & LaFave, J. M. (2013). Thermal behavior of IDOT integral abutment bridges and proposed design modifications. *FHWA-ICT-12-022*.

Palmeira, E. M., Tatsuoka, F., Bathurst, R. J., Stevenson, P. E., & Zornberg, J. G. (2008). Advances in geosynthetics materials and applications for soil reinforcement and environmental protection works. *Electronic Journal of Geotechnical Engineering*, *13*, 1–38.

Patel, A. (2019). *Geotechnical investigations and improvement of ground conditions*. Woodhead Publishing.

Pathak, M., Pathak, R., & Vyas, J. N. (2021). Simulating the model for consolidation of short bored pile in pure friction soil media. *GSC Advanced Research and Reviews*, *8*(1), 66–81.

Paulay, T., & Goodsir, W. J. (1985). The ductility of structural walls. *Bulletin of the New Zealand Society for Earthquake Engineering*, *18*(3), 250–269.

Pawtucket, R. I. (2001). ABAQUS user's manual version 6.2. *Hibbitt, Karlsson and Sorensen Inc*.

Qin, L., & Liu, G. (2009). Mechanical Characteristics of Reinforced Gravity Oblique High U-Shaped Abutment. In *ICCTP 2009: Critical Issues In*

Transportation Systems Planning, Development, and Management (pp. 1–7).

Rafalko, S. D., Sankey, J. E., & Freitag, N. (2010). Sustainability measures for MSE walls and baseline environmental impact evaluations. *Earth Retention Conference 3*, 486–493.

Raghu Kanth, S. T. G., & Dash, S. K. (2010). Evaluation of seismic soil-liquefaction at Guwahati city. *Environmental Earth Sciences*, *61*, 355–368.

Rameesha, K., Kannanayakkal, A., Chithira, P. U., Shamsudheen, N., & Vibitha, P. K. (2019). Stability Analysis of Retaining Wall using GEO5 in Kuranchery. *Int. J. Innov. Sci. Res. Technol*, *4*, 529–621.

Ramli, M., Karasu, Tj., & Dawood, E. T. (2013). The stability of gabion walls for earth retaining structures. *Alexandria Engineering Journal*, *52*(4), 705–710.

RANJAN, S. (2020). *ANALYSIS OF RETAINING WALL FOR STATIC AND DYNAMIC CONDITION BY USING GEO-5 SOFTWARE*.

Sankey, J. E., & Anderson, P. L. (1999). Effects of stray currents on performance of metallic reinforcements in reinforced earth structures. *Transportation Research Record*, *1675*(1), 61–66.

Sankey, J. E., & Soliman, A. (2004). Tall wall mechanically stabilized earth applications. In *Geotechnical engineering for transportation projects* (pp. 2149–2158).

Sayeed, S. M., & Reddy, S. (2014). *Seismic Analysis And Design of Cantilever Retaining Walls*.

Scholzen, A., Chudoba, R., & Hegger, J. (2015). Thin-walled shell structures made of textile-reinforced concrete: Part II: Experimental

characterization, ultimate limit state assessment and numerical simulation. *Structural Concrete*, *16*(1), 115–124.

Sextos, A. G., Pitilakis, K. D., & Kappos, A. J. (2003). Inelastic dynamic analysis of RC bridges accounting for spatial variability of ground motion, site effects and soil–structure interaction phenomena. Part 1: Methodology and analytical tools. *Earthquake Engineering & Structural Dynamics*, *32*(4), 607–627.

Sharbatdar, M.-K. (2003). *Concrete columns and beams reinforced with FRP bars and grids under monotonic and reversed cyclic loading*. University of Ottawa (Canada).

Shaw, J. A., & Kyriakides, S. (1997). Initiation and propagation of localized deformation in elasto-plastic strips under uniaxial tension. *International Journal of Plasticity*, *13*(10), 837–871.

Shivananda, P., & Bincy, V. K. (2019). *Experimental Behavior of Model Mse Wall*. *8*(2), 4101–4106.

Shrestha, S. (2013). *Reanalysis of Full Scale Test Embankment with Polymer and Metallic Reinforcement on Hard Ground Using FEM-PLAXIS 2D*. Asian Institute of Technology.

Shukla, S. K. (2017). *Fundamentals of fibre-reinforced soil engineering*. Springer.

Sieira, A. C. C. F., Gerscovich, D. M. S., & Sayao, A. S. F. J. (2009). Displacement and load transfer mechanisms of geogrids under pullout condition. *Geotextiles and Geomembranes*, *27*(4), 241–253.

Silva, P. H. S., Costa, Y. D. J., Walter, J. R., Kouchaki, B. M., Zornberg, J. G., & Costa, C. M. L. (2023). Numerical Evaluation of a Semi-Integral Bridge Abutment under Cyclic Thermal Movements. *Transportation*

Geotechnics, *39*, 100938.

Sivan, B. S., & Mathew, B. S. (2010). *Effect of Gradation of Aggregates on the Properties of Stone Matrix Asphalt*.

Sommers, A. N., & Viswanadham, B. V. S. (2009). Centrifuge model tests on the behavior of strip footing on geotextile-reinforced slopes. *Geotextiles and Geomembranes*, *27*(6), 497–505.

Specification, I. S. (1984). No. 5/1984, Portland Cement. *Central Organization for Standardization & Quality Control (COSQC), Baghdad, Iraq*.

Sravanam, S. M., Balunaini, U., & Madhav, M. R. (2019). Behavior and design of back-to-back walls considering compaction and surcharge loads. *International Journal of Geosynthetics and Ground Engineering*, *5*(4), 1–17.

Standard, A. C. I. (2008). Building Code Requirements for Structural Concrete (ACI 318M-08) and Commentary. *Reported by ACI Committee*, *318*.

Standard, B. (2009). Testing hardened concrete. *Compressive Strength of Test Specimens, BS EN*, 12390–12393.

Stengel, R. F. (1994). *Optimal control and estimation*. Courier Corporation.

Stulgis, R. P. (2005). Selecting reinforced fill materials for mse retaining walls. In *Geosynthetics Research and Development in Progress* (pp. 1–6).

Suidan, M., & Schnobrich, W. C. (1973). Finite Element Analysis of Reinforced Concrete. In *ASCE J Struct Div* (Vol. 99, Issue ST10, pp. 2109–2122). https://doi.org/10.1061/jsdeag.0003623

System, I. B., & Won, M. (2021). *Numerical Analyses on the Behavior of Geosynthetic-Reinforced Soil : Integral applied sciences Numerical Analyses on the Behavior of Geosynthetic-Reinforced Soil : Integral*

Bridge and Integrated Bridge System. *September*. https://doi.org/10.3390/app11178144

Tadesse, Z. L., Padavala, H. K., & Koteswara, V. R. P. (2022). Seismic response assessment of building structures with underground stories: a state-of-the-art review. *Innovative Infrastructure Solutions*, *7*(6), 1–18.

Tan, S. H., Seah, L. K., & Fok, S. C. (1996). Connections in cold-formed thin-walled structures. *Computers & Structures*, *60*(1), 169–172.

Tarawneh, B., Al Bodour, W., & Masada, T. (2018). Inspection and risk assessment of mechanically stabilized earth walls supporting bridge abutments. *Journal of Performance of Constructed Facilities*, *32*(1), 4017131.

Tatsuoka, F., Tateyama, M., Aoki, H., & Watanabe, K. (2005). Bridge abutment made of cement-mixed gravel back-fill. In *Elsevier Geo-Engineering Book Series* (Vol. 3, pp. 829–873). Elsevier.

Tatsuoka, F., Tateyama, M., Mohri, Y., & Matsushima, K. (2007). Remedial treatment of soil structures using geosynthetic-reinforcing technology. *Geotextiles and Geomembranes*, *25*(4–5), 204–220.

Tavakolian, R., & Sankey, J. (2009). Sandwich Connection design for Shored Reinforced Earth Walls. *Proceedings of the 17th International Conference on Soil Mechanics and Geotechnical Engineering: The Academia and Practice of Geotechnical Engineering*, *2*, 1441–1444. https://doi.org/10.3233/978-1-60750-031-5-1441

Thakkar, K., Rana, A., & Goyal, H. (2023). Fragility analysis of bridge structures: a global perspective & critical review of past & present trends. *Advances in Bridge Engineering*, *4*(1), 1–28.

Thorenfeldt, E. (1987). Mechanical properties of high-strength concrete and

applications in design. *Symposium Proceedings, Utilization of High-Strength Concrete, Norway, 1987*.

Tong, L. W., Xu, G. W., Yang, D. L., Mashiri, F. R., & Zhao, X. L. (2017). Stress concentration factors in CHS-CFSHS T-joints: Experiments, FE analysis and formulae. *Engineering Structures*, *151*, 406–421.

Toufigh, V. (2012). *Experimental and analytical studies of Geo-Composite applications in soil Reinforcement*.

Tourse, R. W., Hamilton-Mason, J., & Wewiorski, N. J. (2018). Systemic racism in the United States. *Cham, Switzerland: Springer International*.

Tsinker, G. P. (1997). Gravity-Type Quay Walls. In *Handbook of Port and Harbor Engineering* (pp. 397–547). Springer.

Usami, T., Lu, Z., & Ge, H. (2005). A seismic upgrading method for steel arch bridges using buckling-restrained braces. *Earthquake Engineering & Structural Dynamics*, *34*(4-5), 471–496.

Van Der Steen, R. (2007). *Tyre/road friction modeling: literature survey*.

Van Nguyen, T., Seo, J., Ahn, J.-H., Haldar, A., & Huh, J. (2021). Finite element analysis-aided seismic behavior examination of modular underground arch bridge. *Tunnelling and Underground Space Technology*, *118*, 104166.

Varghese, P. C. (2005). *Foundation engineering*. PHI Learning Pvt. Ltd.

Voight, B., & Elsworth, D. (1997). Failure of volcano slopes. *Geotechnique*, *47*(1), 1–31.

Walls, A. B. R. (n.d.). AB Engineering Manual. *Obtenido de Https://Www. Allanblock. Com/Literature/PDF/EngManual. Pdf*.

Warren, B. (2015). *Field application of expanding rigid polyurethane*

stabilization of railway track substructure.

Weerasekara, L. (n.d.). *Improvements to Pullout Failure Estimation in MSE Walls*.

Wei, M. (1990). *Frictional Behaviour of Reinforcement in Reinforced Earth Fill Materials*. University of Glasgow (United Kingdom).

Weldu, M. T., Han, J., Rahmaninezhad, S. M., Parsons, R. L., & Kakrasul, J. I. (2015). *Pullout resistance of mechanically stabilized earth wall steel strip reinforcement in uniform aggregate.* University of Kansas. Dept. of Civil, Environmental, and Architectural ….

Wilhelmi, A. J. (n.d.). *CITIZENS TO BE HEARD*.

Won, M.-S., & Langcuyan, C. P. (2020). A 3D numerical analysis of the compaction effects on the behavior of panel-type MSE walls. *Open Geosciences*, *12*(1), 1704–1724.

Xie, Y., & Leshchinsky, B. (2015). MSE walls as bridge abutments: Optimal reinforcement density. *Geotextiles and Geomembranes*, *43*(2), 128–138.

Yoo, C., & Jung, H.-Y. (2006). Case history of geosynthetic reinforced segmental retaining wall failure. *Journal of Geotechnical and Geoenvironmental Engineering*, *132*(12), 1538–1548.

Yoon, W. S., Jeong, U. J., & Kim, J. H. (2002). Kinematic analysis for sliding failure of multi-faced rock slopes. *Engineering Geology*, *67*(1–2), 51–61.

Younas, M. J. (2017). *Advanced Soil Mechanics Labortary Manual (Ge-501)*.

Yu, X., Zhou, Y. F., & Peng, S. Z. (2005). Stability analyses of dam abutments by 3D elasto-plastic finite-element method: a case study of Houhe gravity-arch dam in China. *International Journal of Rock Mechanics and Mining Sciences*, *42*(3), 415–430.

Yu, Y., Bathurst, R. J., & Allen, T. M. (2017). Geotextiles and Geomembranes Numerical modelling of two full-scale reinforced soil wrapped-face walls. *Geotextiles and Geomembranes*, *45*(4), 237–249. https://doi.org/10.1016/j.geotexmem.2017.02.004

Zevgolis, I. E., & Bourdeau, P. L. (2008). Stochastic modeling of redundancy in Mechanically Stabilized Earth (MSE) walls. In *GeoCongress 2008: Geosustainability and Geohazard Mitigation* (pp. 1179–1186).

Zhang, Y., Liu, J. P., Chen, S. Y., Xie, X., Liaw, P. K., Dahmen, K. A., Qiao, J. W., & Wang, Y. L. (2017). Serration and noise behaviors in materials. *Progress in Materials Science*, *90*, 358–460.

Zheng, Y., Fox, P. J., & Shing, P. B. (2014). Numerical simulations for response of MSE wall-supported bridge abutments to vertical load. In *Ground improvement and geosynthetics* (pp. 493–502).

Zhou, G. D., Yi, T. H., & Chen, B. (2017). Innovative design of a health monitoring system and its implementation in a complicated long-span arch bridge. *Journal of Aerospace Engineering*, *30*(2), B4016006.

Zhu, D., Li, Y., Dong, Y., & Yuan, P. (2021). Long-term loss assessment of coastal bridges from hurricanes incorporating overturning failure mode. *Advances in Bridge Engineering*, *2*, 1–15.

APPENDIX A

MATERIAL PROPERTIES OF STRIPS

Appendix A

Material Properties

MACCAFERRI

TECHNICAL DATA SHEET

Rev: 03, Issue Date 11.12.2015

PARAWEB ™2

GEOSYNTHETICS REINFORCEMENT STRIP

ParaWeb™ 2 range is manufactured from high tenacity, mutifilament polyester yarns aligned and co-extruded with polyethylene (LLDPE) to form polymeric strips. ParaWeb™ strips are planar structures consisting of a core of high tenacity polyester yarn tendons encased in a polyethylene (LLDPE) sheath; it enables **ParaWeb™ 2** range to be used as reinforcement of contaminated or high aggressive materials for use in environmental applications. The strips are suitable for reinforcement applications in combination with concrete wall facing panels. The **ParaWeb™ 2** range has been tested internally and independently (NTPEP) in accordance to published standards and will conform to the property values listed below.

PARAWEB 2E		30	40	50	75	100	
MECHANICAL PROPERTIES							
Ultimate Tensile Strength (ASTM 6637)	lb	6744	8992	11240	16861	22481	1
Creep Reduced Strength @100y, 20°C	lb	4958	6611	8264	12397	16530	1
Long term Design Strength (AASHTO LRFD)	lb	4087	5449	6812	10218	13624	1, 2
PHYSICAL PROPERTIES (nominal values)							
Strip width & thickness	in	3.27 / 0.06	3.27 / 0.07	3.43 / 0.08	3.54 / 0.10	3.54 / 0.12	4
Strip weight	lb/328ft	19.18	24.03	27.34	39.46	53.13	4
PARAWEB 2D		**30**	**40**	**50**	**75**	**100**	
MECHANICAL PROPERTIES							
Ultimate Tensile Strength (ASTM 6637)	lb	6744	8992	11240	16861	22481	1
Creep Reduced Strength @100y, 20°C	lb	4958	6611	8264	12397	16530	1
Long term Design Strength (AASHTO LRFD)	lb	4087	5449	6812	10218	13624	1, 2
PHYSICAL PROPERTIES (nominal values)							
Strip width & thickness	in	3.27 / 0.07	3.31 / 0.09	3.54 / 0.10	3.54 / 0.12	3.54 / 0.15	4
Strip weight	lb/328ft	28.00	36.82	42.99	56.44	68.56	4
PARAWEB 2S		**30**	**40**	**50**	**75**	**100**	
MECHANICAL PROPERTIES							
Ultimate Tensile Strength (ASTM 6637)	lb	7550	10067	13584	18876	25168	1
Creep Reduced Strength @100y, 20°C	lb	5551	7402	9988	13879	18505	1
Long term Design Strength (AASHTO LRFD)	lb	4575	6101	8232	11440	15253	1, 3
PHYSICAL PROPERTIES (nominal values)							
Strip width & thickness	in	3.35 / 0.09	3.35 / 0.10	3.54 / 0.14	3.54 / 0.16	3.54 / 0.24	4
Strip weight	lb/328ft	32.63	40.79	50.71	66.14	83.11	4

1. Minimum average roll values (MARV) are calculated as typical minus two standard deviations. Statistically, it yields a 97.7% degree of confidence that any samples taken from quality assurance testing will exceed the value reported;
2. LTDS calculated for a standard temperature of 20°C, 4≤ph≤9 in coarse gravel soil; on request more data available;
3. As above but for 9<ph≤11; product for lime-soil mix applications and aggressive environments.
4. Width, thickness and weight values per roll are nominal a tolerance of 5% on the reported value is admitted.

Maccaferri can engineer specific solutions in any of our products; please contact us for specific solution targeted to your project.

NTPEP CERTIFIED MATERIAL

AASHTO NATIONAL TRANSPORTATION PRODUCT EVALUATION PROGRAM

Disclaimer: The short term and long term mechanical properties listed in this TDS are in compliance with the Paraweb™ NTPEP certifications and AASHTO LRFD regulation; it means that different values can be reported in other TDS not because not accurate but simply because listed following different testing method or different standards.

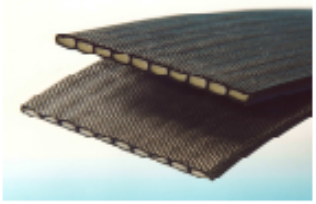

Maccaferri reserves the right to amend product specifications without notice and specifiers are requested to check as to the validity of the pecifications they are using.

Maccaferri, Inc.
10303 Governor Lane Blvd., Williamsport, MD 21795
Tel. (800) 638-7744 - Fax (301) 223-4590
E-mail: info@maccaferri-usa.com - Web site: www.maccaferri-usa.com

Area Offices:
Phoenix, Arizona
Sacramento, California
Miami, Florida
St. Louis, Missouri
Trenton, New Jersey
Albuquerque, New Mexico
Caguas, Puerto Rico
Dallas/Ft. Worth, Texas

APPENDIX B

STEPS DESIGN OF MSE WALL

Appendix B

Design of MSE Wall

Step 1.	Establish Project Requirements – including all geometry, loading conditions (permanent, transient, seismic, etc.), performance criteria, and construction constraints.	
Step 2.	Establish Project Parameters – evaluate existing topography, site subsurface conditions, reinforced wall fill properties, and retained backfill properties.	
Step 3.	Estimate Wall Embedment Depth, Design Height(s), and Reinforcement Length	
Step 4	Define nominal loads	
Step 5	Summarize Load Combinations, Load Factors, and Resistance Factors	
Step 6.	Evaluate External Stability	
	a.	Evaluate sliding
	b.	Evaluate eccentricity
	c.	Evaluate bearing on foundation soil
	d.	Settlement analysis (at service limit state)
Step 7.	Evaluate Internal Stability	
	a.	Select type of soil reinforcement
	b.	Define critical failure surface (for selected soil reinforcement type)
	c.	Define unfactored loads
	d.	Establish vertical layout of soil reinforcements
	e.	Calculate factored horizontal stress and maximum tension at each reinforcement level.
	f.	Calculate nominal and factored long-term tensile resistance of soil reinforcements
	g.	Select grade (strength) of soil reinforcement and/or number of soil reinforcement elements at each level.
	h.	Calculate nominal and factored pullout resistance of soil reinforcements, and check established layout
	i.	Check connection resistance requirements at facing
	j.	Estimate lateral wall movements (at service limit state)
	k.	Check vertical movement and compression pads
Step 8.	Design of Facing Elements	
Step 9.	Assess Overall Global Stability	
Step 10.	Assess Compound Stability	
Step 11.	Design Wall Drainage Systems.	
	a.	Subsurface drainage
	b.	Surface drainage

Reinforcement Type and Loading Condition			Resistance Factor
Metallic reinforcement and connectors	Strip reinforcements [A]		
		Static loading	0.75
		Combined static/earthquake loading	1.00
		Combined static/traffic barrier impact [B]	1.00
	Grid reinforcements [A, C]		
		Static loading	0.65
		Combined static/earthquake loading	0.85
		Combined static/traffic barrier impact [B]	0.85
Geosynthetic reinforcement and connectors		Static loading	0.90
		Combined static/earthquake loading	1.20
		Combined static/traffic barrier impact [B]	1.20
Pullout resistance of tensile reinforcement (metallic and geosynthetic)		Static loading	0.90
		Combined static/earthquake loading	1.20
		Combined static/traffic barrier impact [B]	1.00

Notes:

A. Apply to gross cross-section less sacrificial area. For sections with holes, reduce gross area in accordance with AASHTO (2007) Article 6.8.3 and apply to net section less sacrificial area.

B. Combined static/traffic barrier impact resistance factors are not presented in AASHTO.

C. Applies to grid reinforcements connected to rigid facing element, e.g., a concrete panel or block. For grid reinforcements connected to a flexible facing mat or which are continuous with the facing mat, use the resistance factor for strip reinforcements.

APPENDIX C

MODELLING OF MATERIAL PROPERTIES

Appendix C: Modelling of Material Properties

C.1. INTRODUCTION

The behavior of any structure under loading depends upon the stress-strain relationship of the material from which it is made. MSE wall consist of different materials (concrete, strips, soil, and reinforcing steel) which are connected in a certain form to work as a composite system. This system is designed to exploit the material relationship for each one according to its designated position to form a composite relationship describing the behavior of the whole configuration under a loading condition.

When considering the performance or behavior of the MSE wall materials independently, it will be clear that each of the concrete panel, soil and steel reinforcement has different properties. Where steel can be considered as a homogeneous material that exhibits a similar stress-strain relationship in tension and compression. However, concrete is a heterogeneous nonlinear material, dependent upon the properties of its components, cement mortar, aggregates, additives, and air voids.

C.2 MECHANICAL BEHAVIOR OF CONCRETE

Concrete is a heterogeneous nonlinear material. The hardened concrete contains a large number of micro-cracks at interface between aggregate and mortar, even before any loads have been applied (Chen, 2007). The gradual growth of these micro-cracks under additional load contributes to the nonlinear

behavior of concrete. Since the aggregate-mortar interface has a significantly lower tensile strength than the mortar (because of the presence of these micro-cracks). This interface forms the weakest link in the structure of concrete (Neville & Brooks, 1987). Many experimental studies of the concrete behavior under uniaxial and multi-axial loading conditions have been performed. The

behavior of concrete under these states of stress is described in the following sections.

C.2.1 Uniaxial Stress Behavior of Concrete

C.2.1.1 Compression behaviour

Figure C.1 shows a typical stress-strain relationship curve for normal weight concrete in compression and tension. The main characteristics in this curve can be summarized, as follows (Chen, 2007; A. C. I. Standard, 2008):

1. The axial stress-strain curve, Figure C.1, has a nearly linear elastic behavior up to about 30 % of its maximum compressive strength (f_c'). Above this point 0.30 f_c', concrete begins to soften and the curve shows a gradual increase in curvature up to about (0.75f_c'– 0.90 f_c'), after which the curve bends more sharply until it approaches the peak point at f_c', after it reaches the maximum compressive strength f_c' (σ_{cu}), the curve descends into a softening region, and eventually crushing failure occurs at an ultimate strain εu (ε_{cu}).
2. The modulus of elasticity of conventional-strength concrete generally increases proportionally to the square root of the compressive strength.

$$Ec = 4700 * \sqrt{f'c} \qquad \text{(C-1)}$$

3. Poisson's ratio (v) of concrete has been approximately observed constant and ranged from about 0.15 to 0.22 up to a stress level equal to 0.8 fc'. Beyond this level, Poisson's ratio increases rapidly and becomes equal to1.0 at plastic stage. In the present study was taken equal to 0.18.

C.2.1.2 Tensile behavior

The stress-strain curve for concrete under uniaxial tension is shown in Figure C.1. It is nearly linear up to about 0.6 f_t (0.6 σ_{cu}). This is because the creation of new micro cracks is negligible. Hence, this stress level corresponds to a limit of elasticity. Then, the bond micro cracks start to grow and nonlinearity of the curve increases as the stress level increases until peak stress is reached.

The ratio between uniaxial tensile strength (f_t) and compressive strength (fc') may vary considerably but usually ranges between 0.05 and 0.1 (Chen, 2007). The modulus of elasticity under uniaxial tension is somewhat higher and Poisson ratio somewhat lower than in compression (Norhasri et al., 2017). The direct tensile strength of concrete is difficult to measure and is normally taken as approximately (Chen, 2007).

$$f_t = 0.33\sqrt{fc'} \quad \text{MPa} \qquad \text{(C-2)}$$

The split-cylinder tensile strength is usually lower, and it is approximately:

$$f_t = 0.45\sqrt{fc'} \quad \text{MPa} \qquad \text{(C-3)}$$

The modulus of rupture fr is often used to approximate the tensile strength of concrete. The value of the modulus of rupture varies widely but is normally taken as (Norhasri et al., 2017).

$$f_t = 0.62\sqrt{fc'} \quad \text{MPa} \qquad \text{(C-4)}$$

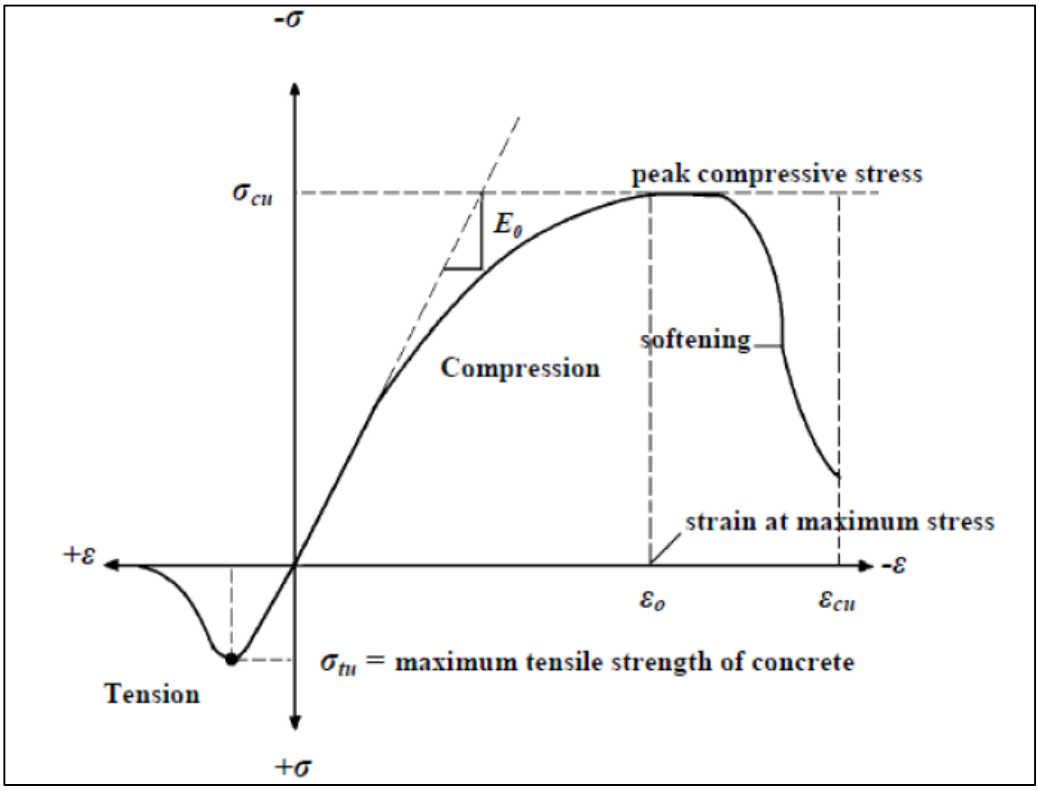

Figure C.1. Typical Uniaxial Compressive and Tensile Stress-Strain Curve for Concrete (Bangash, 1989).

C.2.2 Biaxial Stress Behavior of Concrete

Knowledge of the concrete behavior subjected to multi-axial states of stress is essential to a better understanding of the failure mechanism of concrete. The test results of Kupfer (Kupfer et al., 1969) show that the ultimate strength of concrete in biaxial compression is greater than in uniaxial compression, and it is dependent on the principal stress ratio. Figure C.2 shows a typical biaxial strength envelope. The maximum compressive strength increased for a biaxial compression state at about 25% at a stress ratio equal to (σ_2/σ_1= 0.5) but, when the stress ratio is equal to (σ_2/σ_1= 1), the maximum compressive strength increased at about 16%. Under biaxial compression-tension state, the compressive strength decreases almost linearly as the applied tensile stress is increased (Chen, 2007). While under biaxial tension, the strength is almost the same as that of the uniaxial tensile strength.

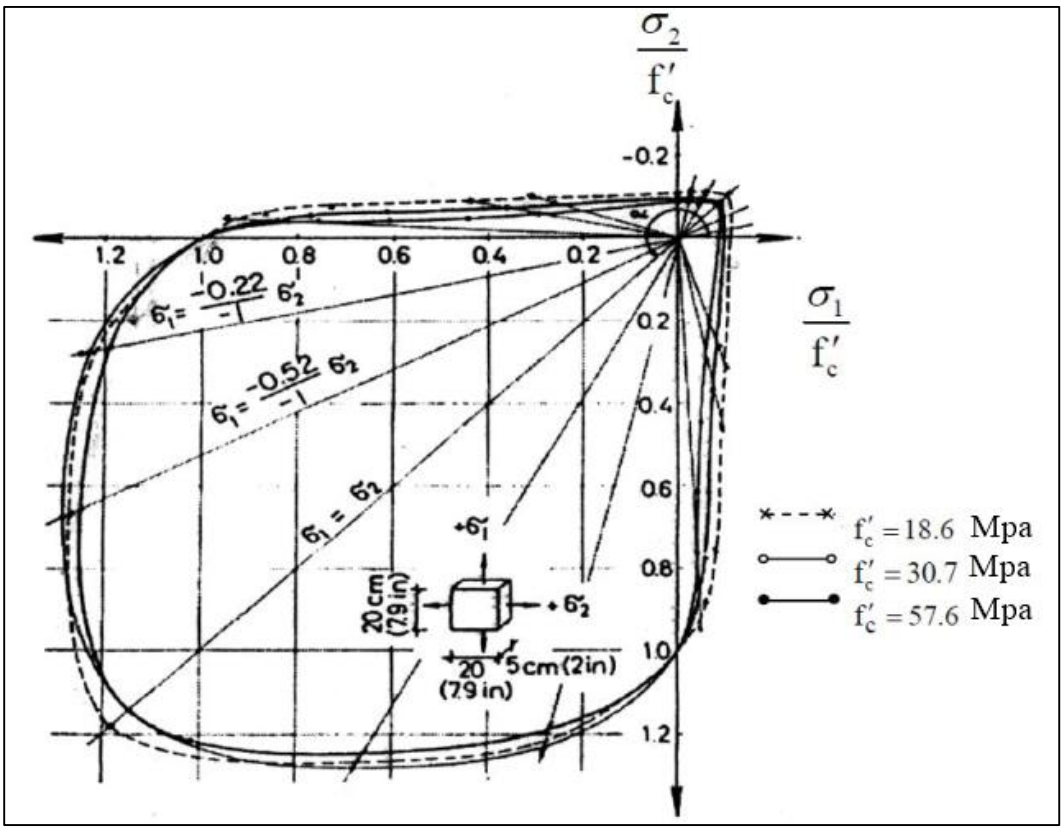

Figure C.2: Biaxial Strength of Concrete (Kupfer et al., 1969).

C.2.3 Tri-axial Stress Behavior of Concrete

Experimental studies indicate that the three-dimensional failure envelope is a function of the three principal stresses. Figure C.3 shows a diagram failure surface of concrete in three-dimensional stress space. The failure envelope is smooth, convex and its deviatoric sections (planes perpendicular to the hydrostatic axis, line of $\sigma_1 = \sigma_2 = \sigma_3$) become more circular in shape for increasing hydrostatic pressures. For smaller hydrostatics pressures, these cross sections are convex and non-circular. The limiting tensile stress required to define the onset of cracking can be calculated for states of tri-axial tensile stress and for combinations of tension and compression principal stresses. Both the function of stress and the failure surface are expressed in terms of principal stresses denoted asσ_1, σ_2 and σ_3 where, σ_1= max (σ_x; σ_y; σ_z) and σ3 = min (σ_x; σ_y; σ_z) and if $\sigma_1 \geq \sigma_2 \geq \sigma_3$, the failure of concrete is categorized into four domains:

- $0 \geq \sigma1 \geq \sigma2 \geq \sigma3$ (compression- compression- compression).
- $\sigma1 \geq 0 \geq \sigma2 \geq \sigma3$ (tension- compression- compression).
- $\sigma1 \geq \sigma2 \geq 0 \geq \sigma3$ (tension- tension- compression).
- $\sigma1 \geq \sigma2 \geq \sigma3 \geq 0$ (tension- tension- tension).

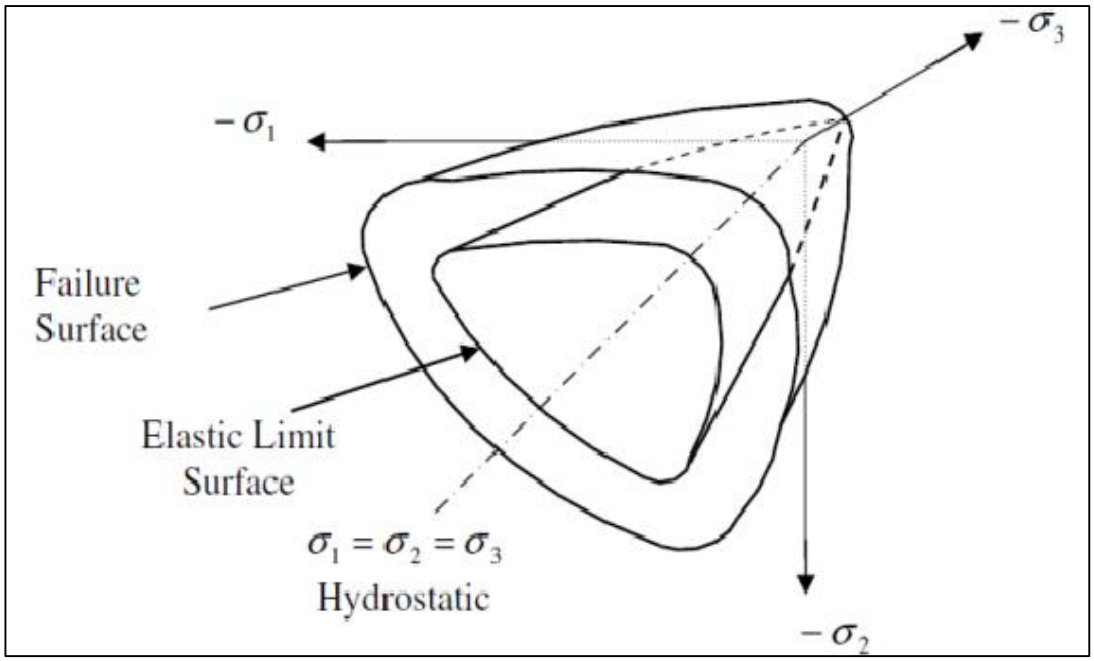

Figure C.3: Tri-axial Strength Envelope of Concrete (Chen, 2007).

C.3 ABAQUS

C.3.1 Introduction to ABAQUS

The most reliable method to evaluate accurate behavior of concrete structural elements is to experimentally study actual structures, but because of being expensive and time consuming, usually experiments are not always possible to perform. Therefore, other methods, which consider the anisotropic behavior of concrete including the effect from tensile cracks, are required. One method is Finite Element Modeling (FEM), which needs less cost and time to be implemented. Different commercial FEM software has been developed over the years and one of them is ABAQUS**,** which was used in this study (Eriksson & Gasch, 2010).

ABAQUS is a finite element program to evaluate the behavior of structures and solids under external loads. This program can analyze both static and dynamic problems and it can model a wide range of 2D and 3D shapes and contacts between solids. It has an advanced and extensive library for elements and materials.

C.3.2 Constitutive Concrete Material Model

There are three material models for analyzing concrete at low confining pressures in ABAQUS: Concrete smeared cracking model in ABAQUS/Standard, Brittle cracking model in ABAQUS/Explicit and Concrete damaged plasticity model in both ABAQUS/Standard and ABAQUS/Explicit. Each model is designed to provide a general capability for modeling plain and reinforced concrete (as well as other similar quasi-brittle materials) in all types of structures: beams, trusses, shells, and solids.

The smeared crack concrete is intended for applications in which the concrete is subjected to essentially monotonic straining and a material point exhibits either tensile cracking or compressive crushing. Plastic straining in compression is controlled by a "compression" yield surface. Cracking is assumed to be the most important aspect of the behavior and the representation of cracking and post cracking anisotropic behavior dominates the modeling.

Brittle cracking is intended for applications in which the concrete behavior is dominated by tensile cracking and compressive failure is not important. The model includes consideration of the anisotropy induced by cracking. In compression, the model assumes elastic behavior. A simple brittle failure criterion is available to allow the removal of elements from a mesh.

The concrete damaged plasticity assumes of scalar (isotropic) damage and is designed for applications in which the concrete is subjected to arbitrary loading conditions, including cyclic loading. The model takes into consideration the degradation of the elastic stiffness induced by plastic straining both in tension and compression. It also accounts for stiffness recovery effects under cyclic loading (Eriksson & Gasch, 2010).

The concrete damage plasticity (CDP) model was selected in this study due to the following reasons (C. ASTM, 1996; Chaudhari & Chakrabarti, 2012; Pawtucket, 2001):

- It has higher potential for convergence compared to the smeared crack model;
- It can consider different yield strength in tension and compression.
- It counts true post yield (plastic) response like softening behavior in tension as opposed to initial hardening followed by softening in compression.
- Different degradation of the elastic stiffness in tension and compression can be considered in this model.

C.3.3 Concrete Damage Plasticity

Concrete damaged plasticity can model all structural types of reinforced or unreinforced concrete or other quasi-brittle materials subjected to monotonic, cyclic, or dynamic loads. This model is based on a coupled damage plasticity theory and the multi-axial behavior of concrete in damaged plasticity model governs by a yield surface which proposed by
Lubliner et al. and was modified later by Lee and Fenves (Malm, 2006). Tensile cracking and compressive crushing of concrete are two assumed main failure mechanisms in this model. Furthermore, the degradation of material for both tension and compression behavior have been considered in this model.

C.3.4 Uniaxial and Multi-axial Behavior

Under uniaxial tension, as can be seen in Figure C.4, the stress increases with a linear elastic relationship with strain up to the ultimate tensile strength, f_t and then micro-cracks form microscopically with a tension softening response. There are three different methods to define tension softening

response in ABAQUS: stress-strain, stress-displacement or by use of fracture energy (Eriksson & Gasch, 2010).

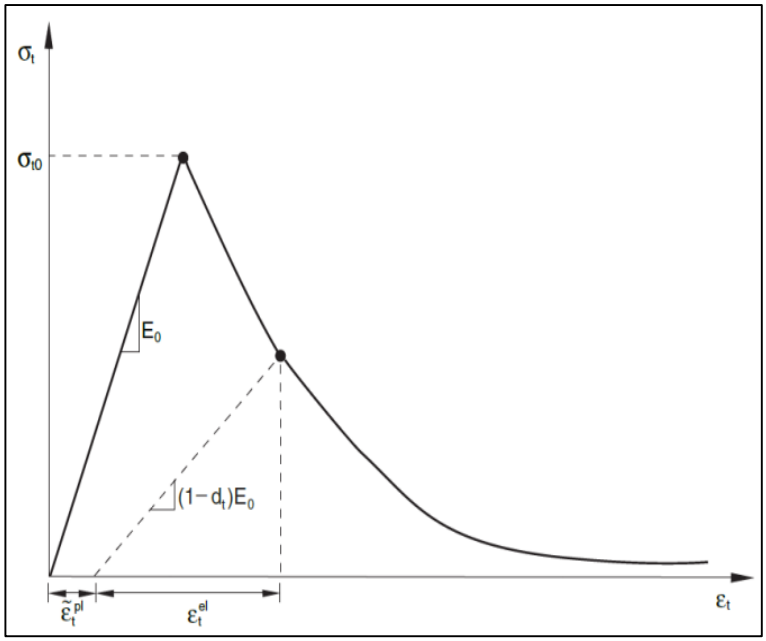

Figure C.4: Uniaxial Tensile Behavior of Concrete (Eriksson & Gasch, 2010).

In addition, under uniaxial compression, there is a linear elastic relationship between stress-strain until initial yield, f_{co}. After losing stiffness due to bond failure between the aggregates and the cement paste, the behavior becomes nonlinear. In stresses greater than ultimate strength, plastic response is defined by stress hardening and strain softening. In other words, compressive stress decreases while the corresponding strain increases (Tan et al., 1996). The uniaxial compressive behavior of concrete is depicted in Figure C.5.

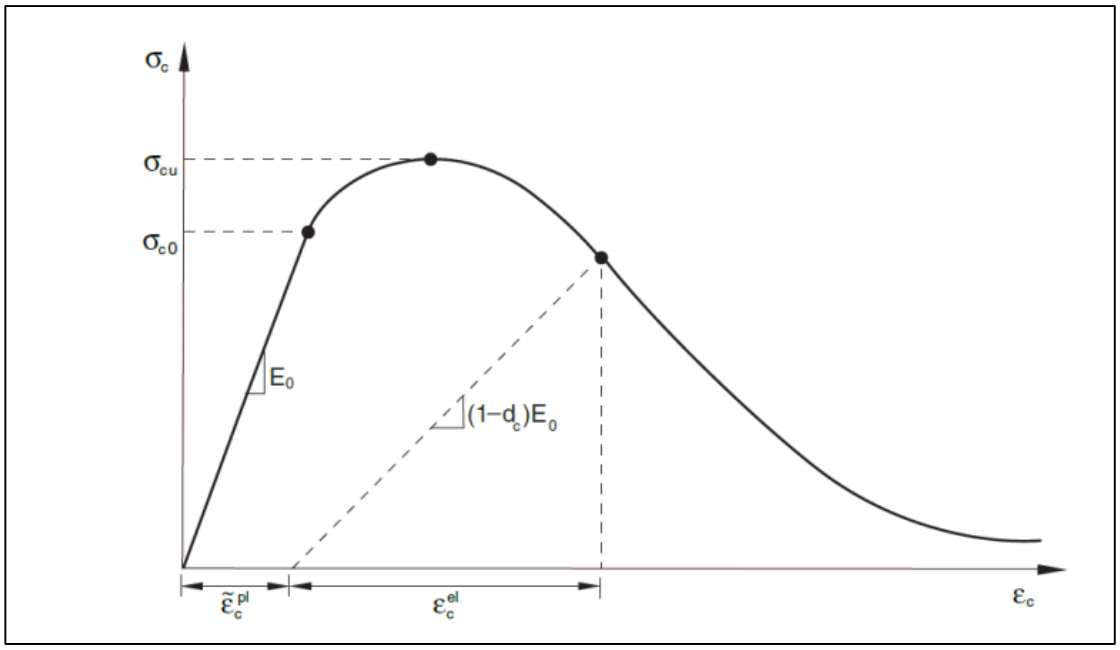

Figure C.5: Uniaxial Compressive Behavior of Concrete (Eriksson & Gasch, 2010).

C.3.5 Concrete Damaged Plasticity Definition

Different input data, which should be defined in concrete damaged plasticity, are:

1- **ψ** is the dilation angle, measured in p -q plane and should be defined to calculate the inclination of the plastic flow potential in high confining pressures, Figure C.6. The dilation angle is equal to the friction angle in low stresses. In higher levels of confinement stress and plastic strain, dilation angle is decreased. Maximum value of is $\psi_{max} = 56.3^{o}$ and minimum value is close to 0^{o}. Upper values represent a more ductile behavior and lower values show a more brittle behavior. According to Malm the effect of the dilation angle in values between $30^{o} \leq \psi \leq 40^{o}$ in some cases can be neglected and for normal concrete $\psi = 30^{o}$is acceptable.

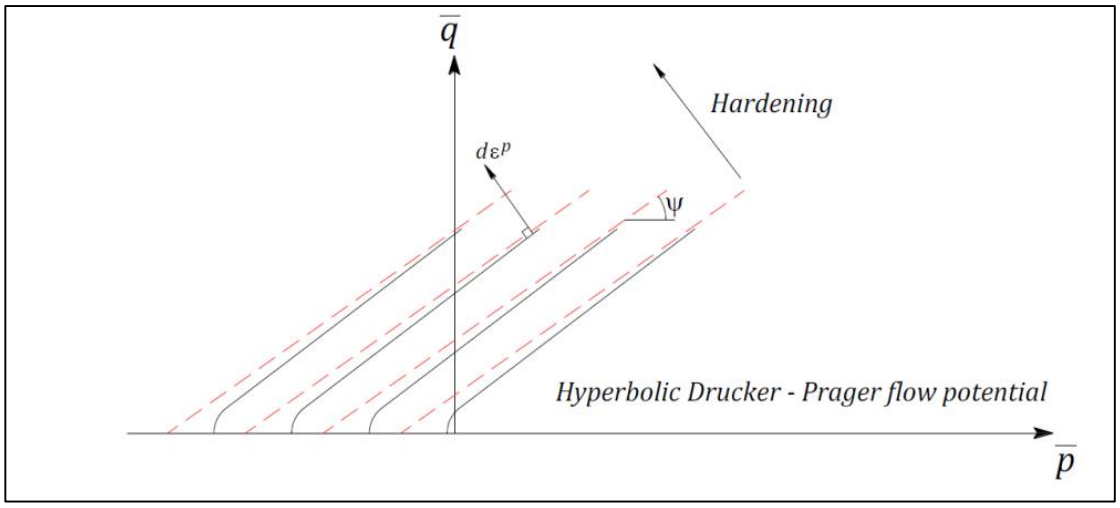

Figure C.6: Hyperbolic Plastic Flow Rule (Eriksson & Gasch, 2010).

2- ϵ : is the flow potential eccentricity. It is a small positive number, which defines the range that the plastic potential function closes to the asymptote as shown in Figure C.6. The default value in ABAQUS is 0.1 and indicates that the dilation angle is almost constant in a wide range of confining pressure. In higher value of ϵ, with reduction of confining pressure, the dilation angle increases more rapidly. Very small values of ϵ in comparison with the default value cause convergence problems in cases with low confining pressure, due to very tight flow-potential curvature at the point of intersection with the p-axis.

3- f_{b0}/f_{c0}: is the ratio of initial equiaxial compressive yield stress to initial uniaxial compressive yield stress. The default value is 1.16.

4- K_c: is the ratio of the second stress invariant on the tensile meridian to that on the compressive meridian at initial yield for any given value of the pressure invariant, such that the maximum principal stress is negative it must satisfy the condition $0.5 < Kc \leq 1$. The default value is 2/3.

5- Viscosity parameter (μ): used for the visco-plastic regularization of the concrete constitutive equations in ABAQUS/Standard analyses. This parameter is ignored in ABAQUS/Explicit. The default value is 0.0. According to Malm $\mu = 10^{-7}$is recommended because in comparison with characteristic time increment it should be small (Malm, 2006).

6- The compressive behavior of concrete can be simulated accurately using an elasto-plastic and strain-hardening model. Compressive stress data can be provided as a function of plastic strain. The stress–strain curve can be defined beyond the ultimate stress, into the strain-softening regime. In order to simulate concrete with high compressive strength, the stress –strain relationship as proposed by Thorenfeldt et al. (Thorenfeldt, 1987), Figure C.7, combined with the Hognestad's assumption on the elastic modulus of concrete was adopted. This applied a factor to increase the post-peak decay, which closely related to the real behavior of high strength concrete. This relationship was based on the concrete cylinder strength, as described in Equation (C-5).

$$\frac{fc}{fc'} = \frac{n\,(\frac{\varepsilon_c}{\varepsilon_o})}{n-1+(\frac{\varepsilon_c}{\varepsilon_o})^{nk}} \qquad \text{(C-5)}$$

$$n = 0.8 + \frac{fc'}{17}$$

$$k = 0.67 + \frac{fc'}{62}$$

$$\varepsilon_o = \frac{fc'}{E_c(\frac{n}{n-1})}$$

Where:

fc'= peak stress obtained from a cylinder test (MPa).

ε_o= strain when fc reaches fc'.

n = a curve-fitting factor.

Ec= modulus of elasticity (MPa).

k = factor to control the slopes of the ascending and descending branches of the stress–strain curve, taken equal to 1.0 for $\frac{\varepsilon_c}{\varepsilon_o}$ less than 1.0 and taken greater than 1.0 for $\frac{\varepsilon_c}{\varepsilon_o}$ greater than 1.0.

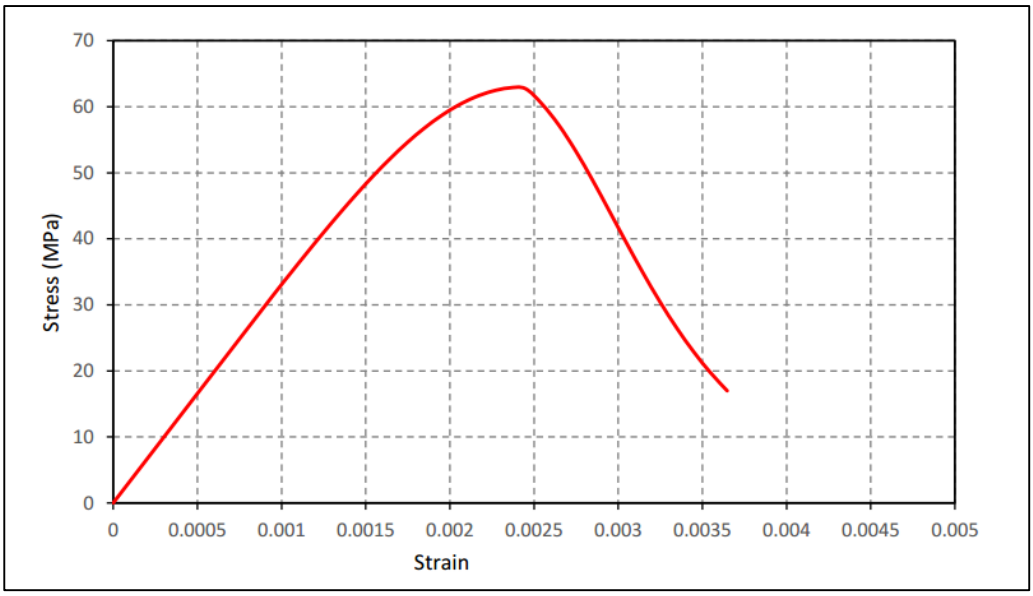

Figure C.7: Stress–strain Relationship for Concrete under Uniaxial Compression (Eriksson & Gasch, 2010).

C.3.6 Reinforcement

In ABAQUS reinforcement can be modeled with different methods including smeared reinforcement in the concrete, cohesive element method, discrete truss or beam elements with the embedded region constraint or built-in rebar layers (Pawtucket, 2001). Rebar defines the uniaxial reinforcement levels in membrane, shell, and surface elements. One or multiple layers of reinforcements can be defined and for each layer the rebar layer name, the cross-sectional area of each reinforcement layer and the rebar spacing in the plane of definition should be determined (Pawtucket, 2001). In this part, just truss element with embedded region modeling, which is used for reinforcement modeling in this study, will be explained. Truss element is a common way of reinforcement modeling of which the only required input is the cross-sectional area of bars. Beam element modeling is another common way, which takes into account the dowel effect and increases slightly the load bearing capacity of structures, but its use is not recommended because it require a large number of input parameters to be defined and consequently a

high computational effort (Eriksson & Gasch, 2010; Malm, 2006; Pawtucket, 2001). According to Hibbit et al. the effect of bond slip is not considered in the embedded region modeling method, but this effect is considered somewhat by definition of the tension stiffening behavior of concrete (Malm, 2006).

C.3.7 SOIL

The soil part is massive in an MSE structure. It commonly behaves as an elastic– plastic material. There are a large number of available soil constitutive models that can be used to predict the soil behavior, including Winkler Model, Mohr–Coulomb Model, (Modified) Cam–Clay model, Duncan–Chang Model, and Elastic Continuum Model (Khodair & Abdel-Mohti, 2014). In this research, the soil material was modeled using the Mohr–Coulomb method. This method is elastic–perfectly plastic and considers the effect of stress on soil strength. The failure criteria are defined by the friction angles and soil cohesion. It assumes that the failure is controlled by the maximum shear stress, which also depends on the normal stress as per the following formula:

$$\tau = c - \sigma . \tan\phi \qquad \text{(C-6)}$$

where τ is the shear stress, σ is the normal stress, c is the cohesion of the material, and ϕ is the material angle of friction. This can be represented by plotting Mohr's circle for states of stress at failure in terms of the maximum and minimum principal stresses (Figure C.9). The backfill soil was modeled with a cohesion (c) and friction angle (ϕ) values of 0 and 34^{o}, respectively.

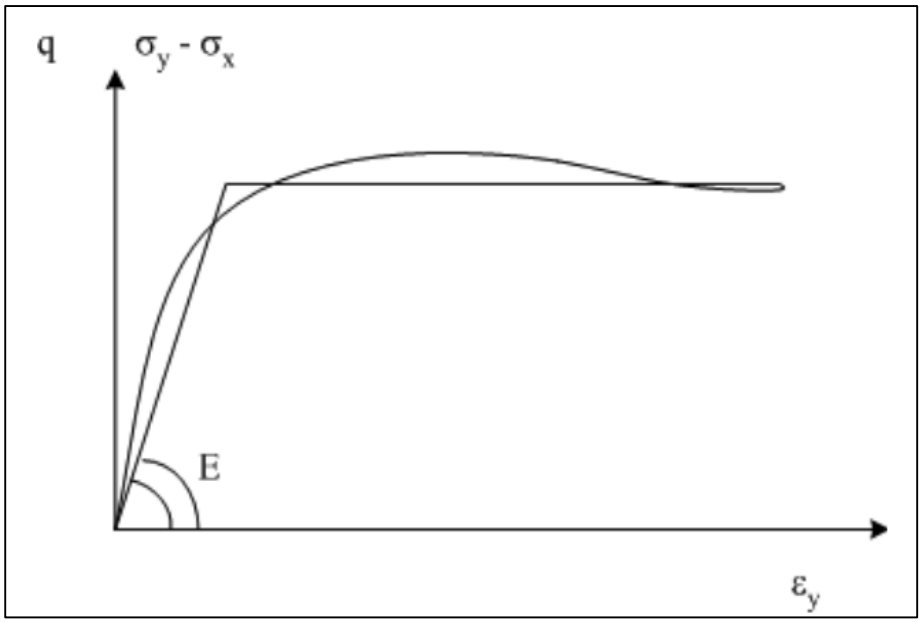

Figure C.8: Mohr-Coulomb method

C.4 MATERIAL PROPERTIES INPUT IN THIS STUDY

C.4.1 Concrete Material

The properties of concrete with compressive strength 36 MPa used in this study are listed in Tables C.1 to C.2.

Table C.1: Elastic Properties of Concrete.

	Young's Modulus (Mpa)	Poisson's Ratio
Elastic	28200	0.18

Table C.2: Plastic Properties of Concrete.

Dilation angle	Eccentricity	Fb0/fc0	k	Viscosity parameter
36	0.1	1.16	0.667	0.001

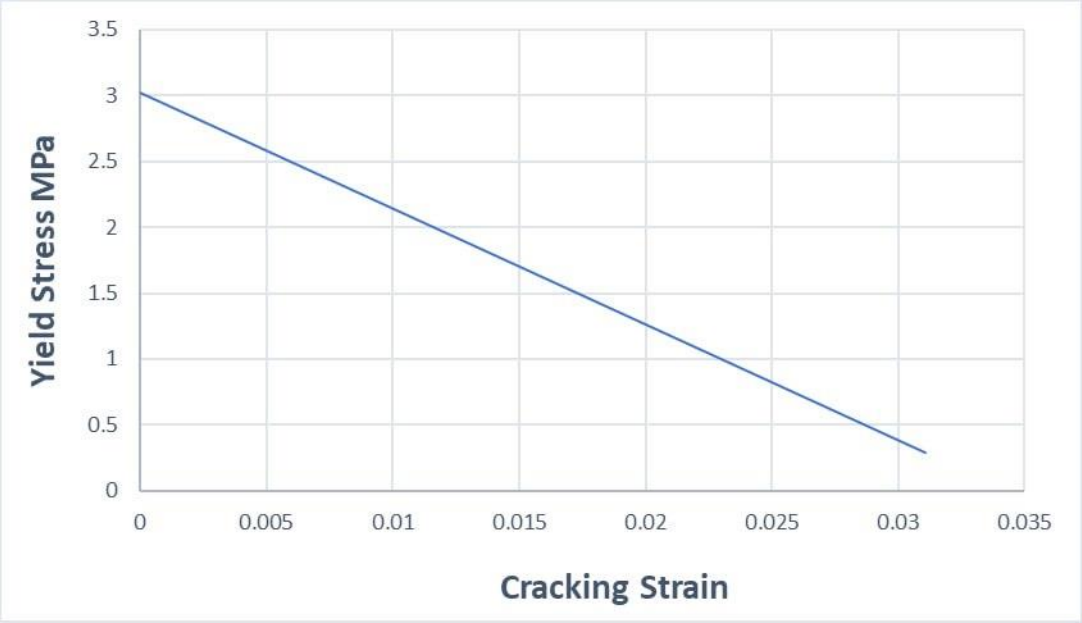

Figure C.9: yield stress- cracking Strain Relationship (Tensile behavior).

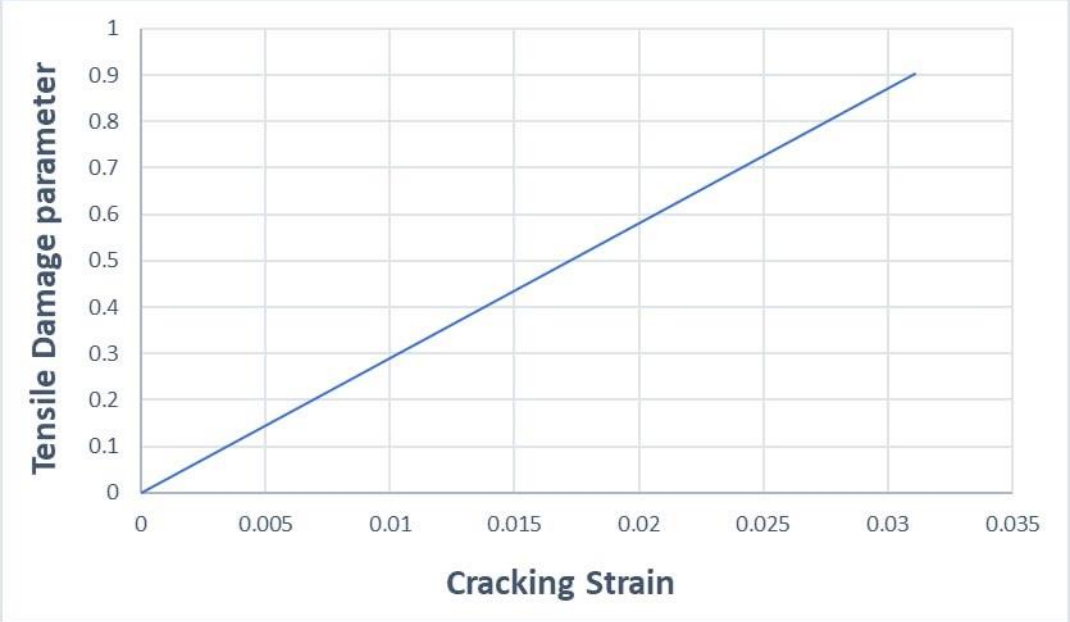

Figure C.10: Tensile Damage parameter – Cracking Strain Relationship (Concrete tensile damage).

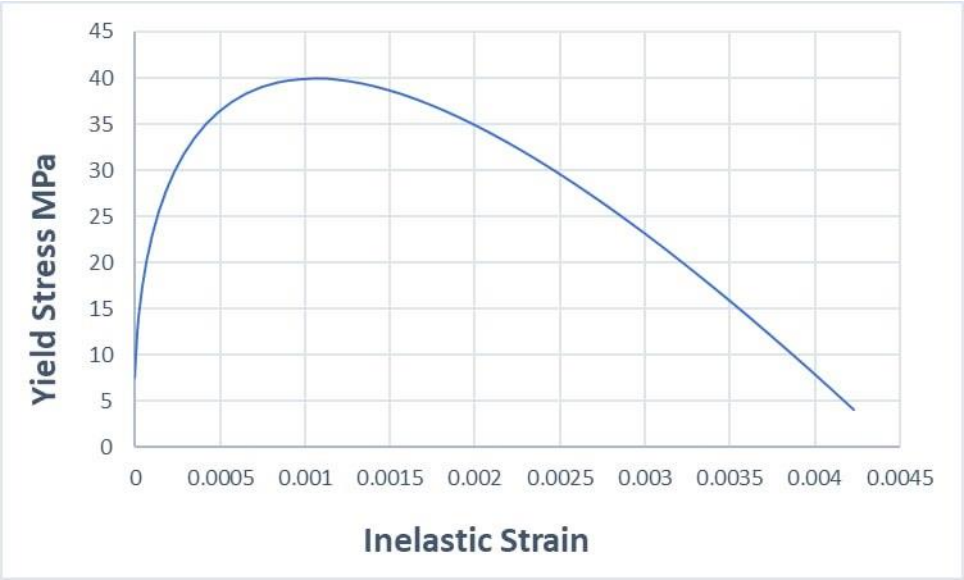

Figure C.11: Yield Stress- Inelastic Strain Relationship (Compressive Behavior).

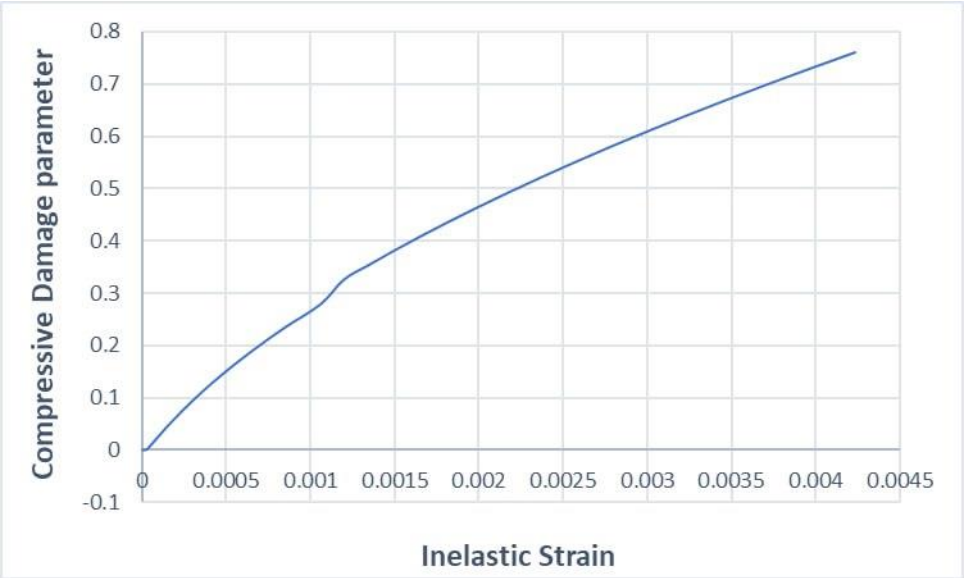

Figure C.12: Compressive Damage parameter - Inelastic Strain Relationship (Compressive Behavior).

C.4.3 Properties of Reinforcement Bar.

The elastic properties for steel reinforcement and stiffeners are shown in Tables C.3.

Table C.3. Properties of Steel Reinforcement bars.

	Young's modulus (MPa)	Passion's ratio
Elastic properties	200000	0.3

C.4.4 Element Type

Numerous elements for simulating the behavior of MSEW, concrete members, Soil, strips reinforcement and steel rebar reinforcement were applied. These components are commonly utilized in ABAQUS. The details of the elements and their descriptions has been shown in the table below.

No.	Name of materials	Type of Element	Symbol	Descriptions
1	Concrete	Solid	C3D8R	An-8 node linear brick, reduced integration, Hourglass control
2	Soil	Solid	C3D8R	An-8 node linear brick, reduced integration, Hourglass control
3	Strip	Shell	T3D2	A 2-node linear 3-D truss
4	Steel	Truss	S4R	A 4 node double curved thin of thick shell, reduced integration, hourglass control, finite membrane strains

APPENDIX D

RETURN WALL DESIGN BASED ON ACI CODE

Appendix D: Return WALL DESIGN BASED ON ACI CODE

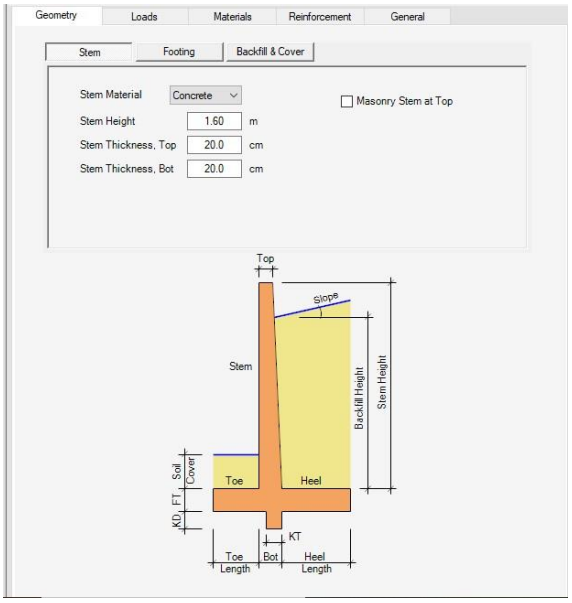

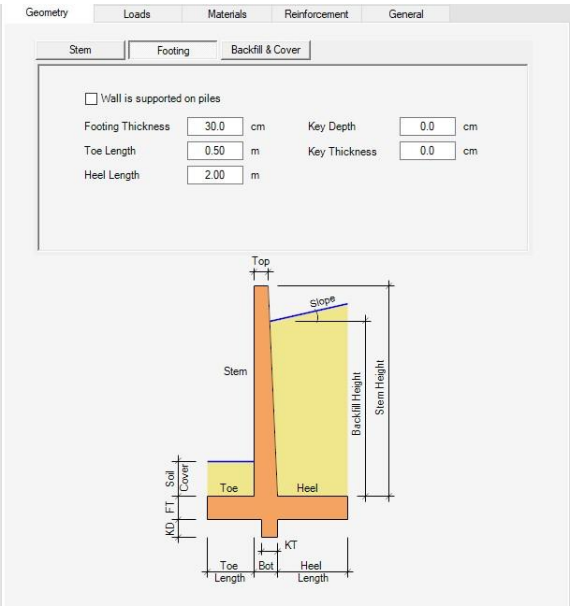

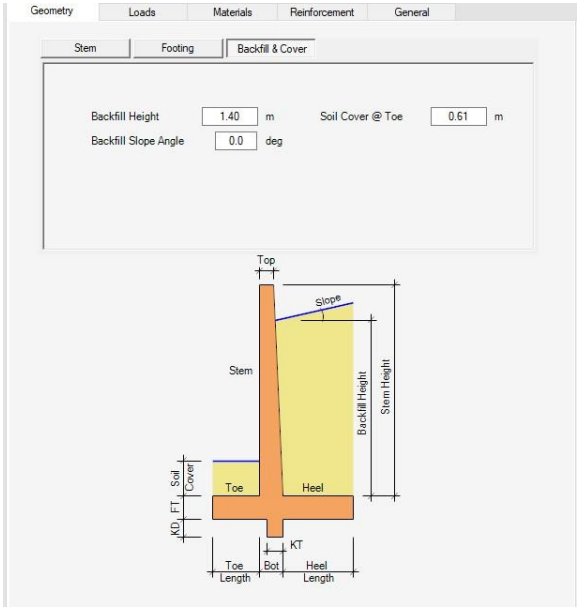

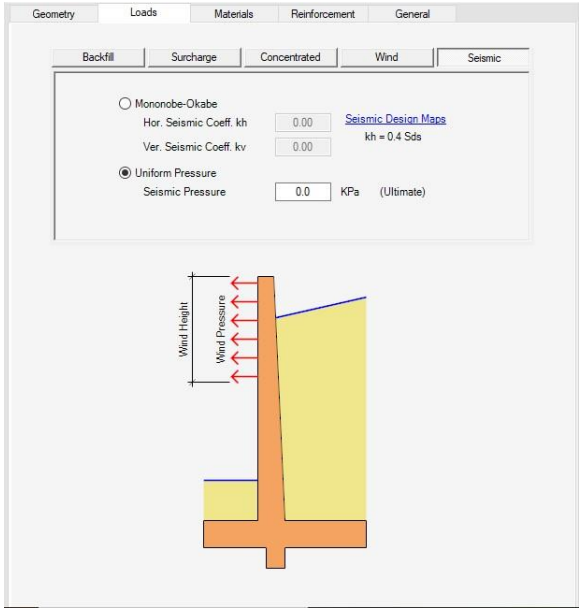

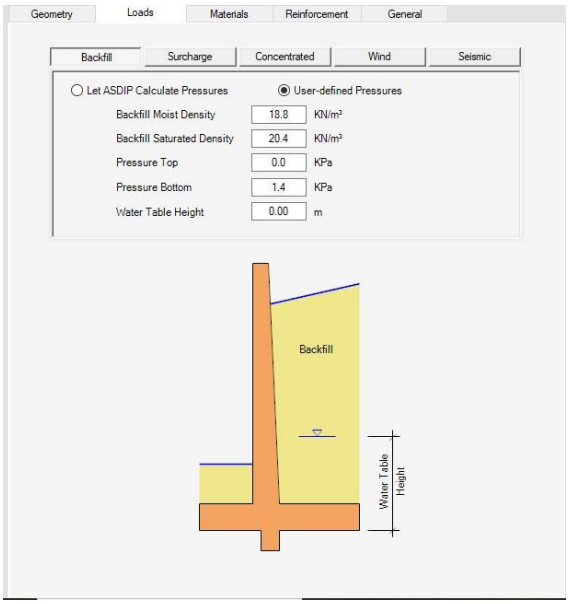
Geometry
Loads
Materials
Reinforcement
General
Backfill
Surcharge
Concentrated
Wind
Seismic
Let ASDIP Calculate Pressures
User-defined Pressures
Backfill Moist Density
18.8
KN/m³
Backfill Saturated Density
20.4
KN/m³
Pressure Top
0.0
KPa
Pressure Bottom
1.4
KPa
Water Table Height
0.00
m
Backfill
Water Table Height

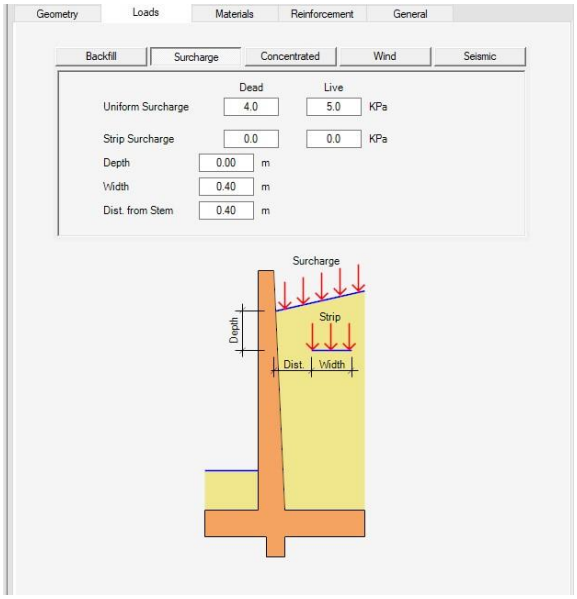
Geometry
Loads
Materials
Reinforcement
General
Backfill
Surcharge
Concentrated
Wind
Seismic
Dead
Live
Uniform Surcharge
4.0
5.0
KPa
Strip Surcharge
0.0
0.0
KPa
Depth
0.00
m
Width
0.40
m
Dist. from Stem
0.40
m
Surcharge
Strip
Depth
Dist.
Width

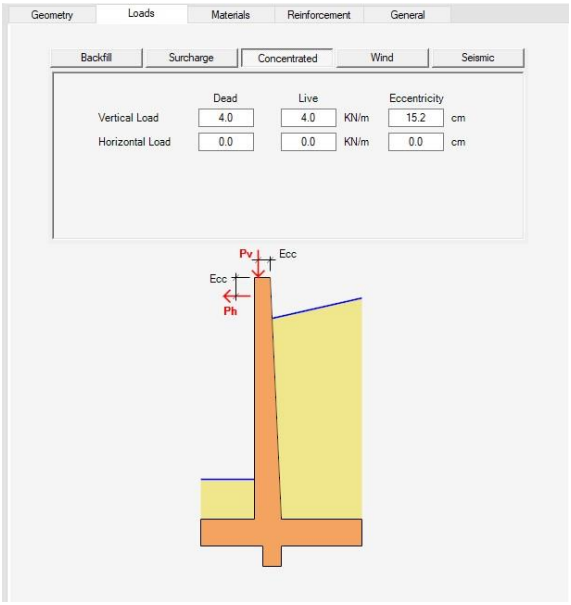
Geometry
Loads
Materials
Reinforcement
General
Backfill
Surcharge
Concentrated
Wind
Seismic
Dead
Live
Eccentricity
Vertical Load
4.0
4.0
KN/m
15.2
cm
Horizontal Load
0.0
0.0
KN/m
0.0
cm
Pv
Ecc
Ecc
Ph

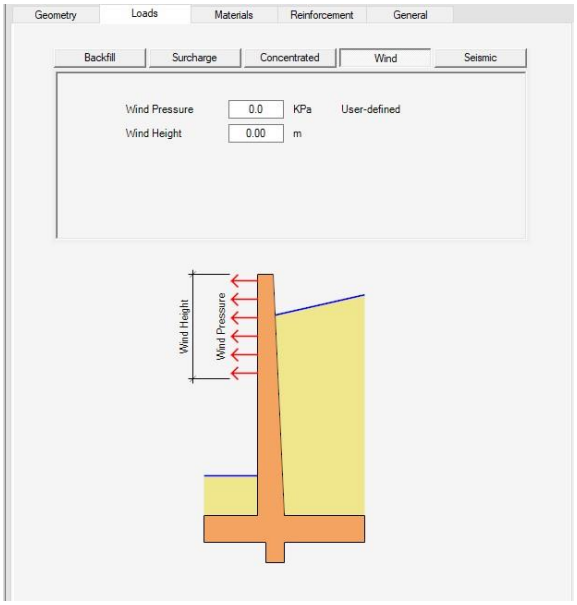
Geometry
Loads
Materials
Reinforcement
General
Backfill
Surcharge
Concentrated
Wind
Seismic
Wind Pressure
0.0
KPa
User-defined
Wind Height
0.00
m
Wind Height
Wind Pressure

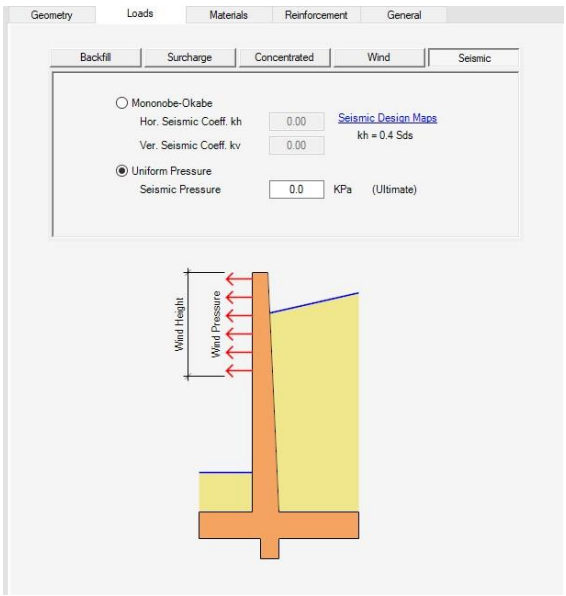
Geometry
Loads
Materials
Reinforcement
General
Backfill
Surcharge
Concentrated
Wind
Seismic
Mononobe-Okabe
Hor. Seismic Coeff. kh
0.00
Seismic Design Maps
kh = 0.4 Sds
Ver. Seismic Coeff. kv
0.00
Uniform Pressure
Seismic Pressure
0.0
KPa
(Ultimate)
Wind Height
Wind Pressure

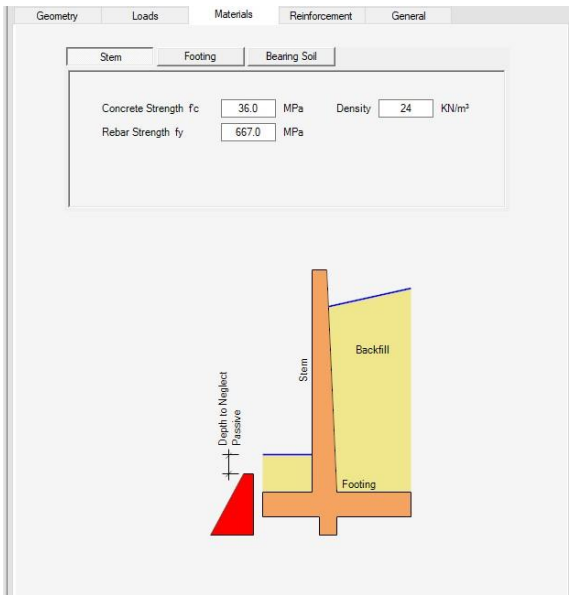
Geometry
Loads
Materials
Reinforcement
General
Stem
Footing
Bearing Soil
Concrete Strength f'c
36.0
MPa
Density
24
KN/m³
Rebar Strength fy
667.0
MPa
Backfill
Stem
Depth to Neglect Passive
Footing

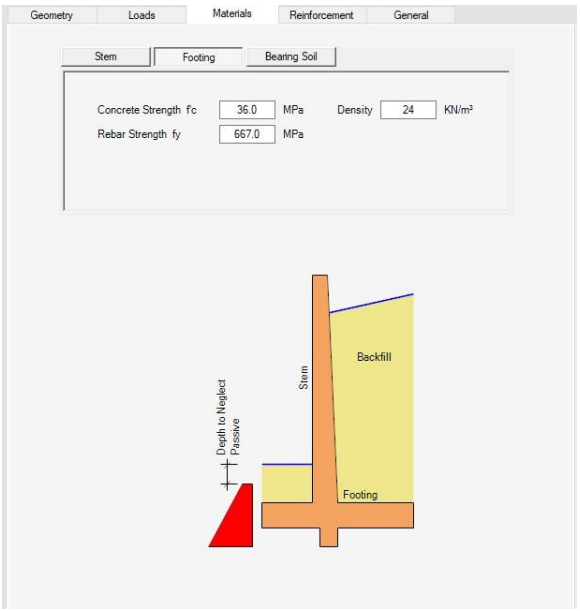
Geometry
Loads
Materials
Reinforcement
General
Stem
Footing
Bearing Soil
Concrete Strength f'c
36.0
MPa
Density
24
KN/m³
Rebar Strength fy
667.0
MPa
Backfill
Stem
Depth to Neglect Passive
Footing

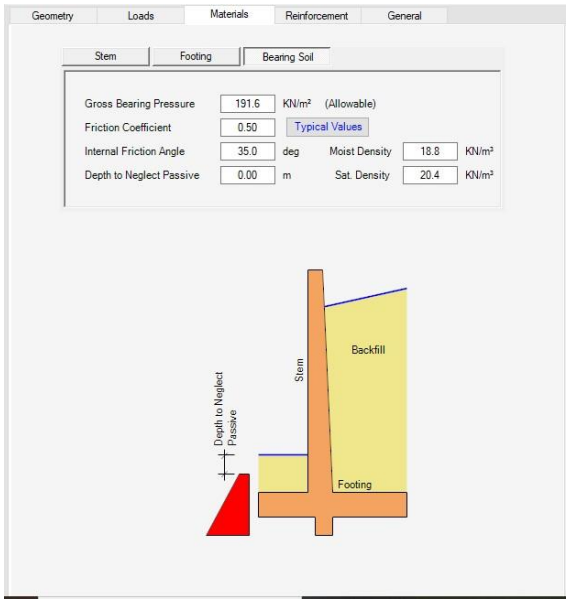
Geometry
Loads
Materials
Reinforcement
General
Stem
Footing
Bearing Soil
Gross Bearing Pressure
191.6
KN/m²
(Allowable)
Friction Coefficient
0.50
Typical Values
Internal Friction Angle
35.0
deg
Moist Density
18.8
KN/m³
Depth to Neglect Passive
0.00
m
Sat. Density
20.4
KN/m³
Backfill
Stem
Depth to Neglect Passive
Footing

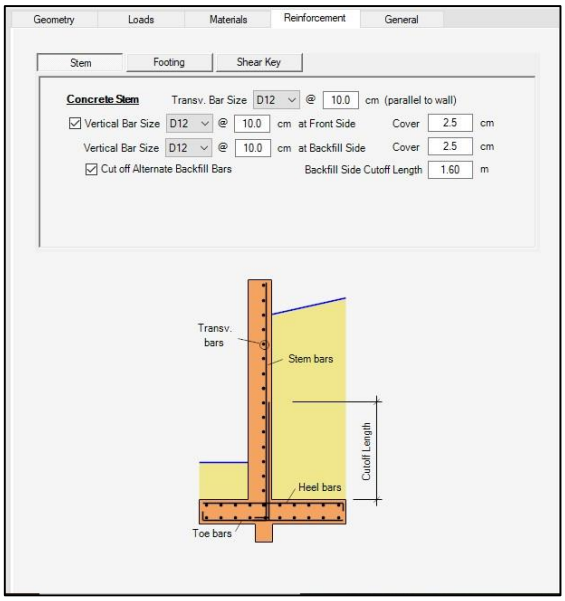
Geometry
Loads
Materials
Reinforcement
General
Stem
Footing
Shear Key
Concrete Stem
Transv. Bar Size
D12
@
10.0
cm (parallel to wall)
Vertical Bar Size
D12
@
10.0
cm at Front Side
Cover
2.5
cm
Vertical Bar Size
D12
@
10.0
cm at Backfill Side
Cover
2.5
cm
Cut off Alternate Backfill Bars
Backfill Side Cutoff Length
1.60
m
Transv. bars
Stem bars
Cutoff Length
Heel bars
Toe bars

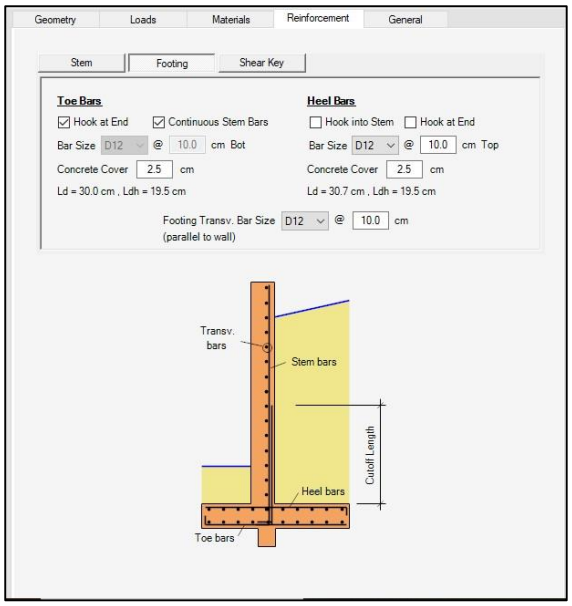
Geometry
Loads
Materials
Reinforcement
General
Stem
Footing
Shear Key
Toe Bars
Hook at End
Continuous Stem Bars
Bar Size
D12
@
10.0
cm Bot
Concrete Cover
2.5
cm
Ld = 30.0 cm , Ldh = 19.5 cm
Heel Bars
Hook into Stem
Hook at End
Bar Size
D12
@
10.0
cm Top
Concrete Cover
2.5
cm
Ld = 30.7 cm , Ldh = 19.5 cm
Footing Transv. Bar Size
D12
@
10.0
cm
(parallel to wall)
Transv. bars
Stem bars
Cutoff Length
Heel bars
Toe bars

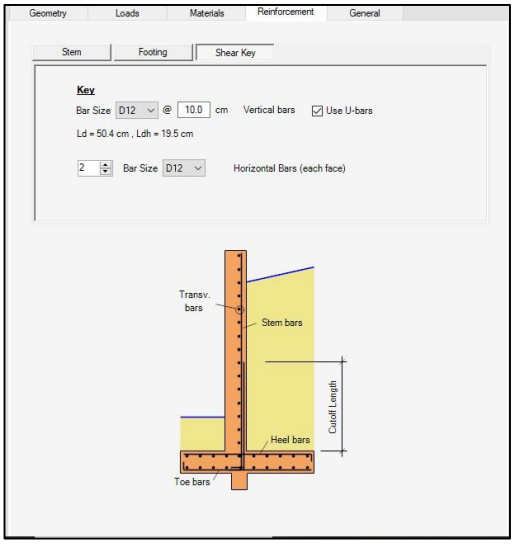
Geometry
Loads
Materials
Reinforcement
General
Stem
Footing
Shear Key
Key
Bar Size
D12
@
10.0
cm
Vertical bars
Use U-bars
Ld = 50.4 cm , Ldh = 19.5 cm
2
Bar Size
D12
Horizontal Bars (each face)
Transv. bars
Stem bars
Cutoff Length
Heel bars
Toe bars

At a Glance | Condensed | Detailed | Graph

SECTION GEOMETRY

Stem Height	1.60	m
Stem Thickness Top	20.0	cm
Stem Thickness Bot	20.0	cm
Footing Thickness	30.0	cm
Toe Length	0.50	m
Heel Length	2.00	m
Soil Cover at Toe	0.61	m
Backfill Height	1.40	m
Backfill Slope Angle	0.0	deg
Shear Key Depth	0.0	cm

DIMENSIONS ARE OK

STABILITY CHECK

Overturning Safety Factor	110.58	> 1.50 ✓
Sliding Safety Factor	56.97	> 1.50 ✓

STABILITY CHECK IS OK

SOIL BEARING PRESSURES

Allow. Bearing Capacity	191.6	KN/m²
Max. Bearing at Heel	45.8	KN/m² ✓

BEARING PRESSURES ARE OK

Footing Length	2.70	m
Resultant Eccentricity	-0.05	m

RESULTANT WITHIN MIDDLE THIRD

SHEAR FORCES (KN/m)

	Vu	ϕVn	Ratio	
Stem	2.2	96.1	0.02	✓
Toe	5.9	131.2	0.04	✓
Heel	106.0	131.2	0.81	✓

SHEAR FORCES ARE OK

REINFORCEMENT DESIGN

-Stem (Comb. 1.2D+1.6L+1.6H)		
Moment Capacity Ratio	0.03	✓
Development Length Ratio	0.71	✓
Minimum Steel Area Ratio	0.32	✓
Maximum Steel Area Ratio	0.48	✓
Vert. Bars Max. Spacing Ratio	0.22	✓
-Toe (Comb. 1.2D+1.6L+1.6H)		
Moment Capacity Ratio	0.02	✓
Development Length Ratio	0.41	✓
Minimum Steel Area Ratio	0.48	✓
Maximum Bar Spacing Ratio	0.22	✓
-Heel (Comb. 1.2D+1.6L+1.6H)		
Moment Capacity Ratio	0.61	✓
Development Length Ratio	0.46	✓
Minimum Steel Area Ratio	0.48	✓
Maximum Bar Spacing Ratio	0.36	✓

REINFORCEMENT IS OK

At a Glance | Condensed | Detailed | Graph

SECTION GEOMETRY

Conc. Stem Height	1.60	m
Stem Thickness Top	20.0	cm
Stem Thickness Bot	20.0	cm
Footing Thickness	30.0	cm
Toe Length	0.50	m
Heel Length	2.00	m
Soil Cover @ Toe	0.61	m
Backfill Height	1.40	m
Backfill Slope Angle	0.0	deg

SEISMIC EARTH FORCES

Uniform Seismic Pressure	0.0	KPa
Seismic Force (Stability)	0.0	KN/m
Seismic Force (Stem)	0.0	KN/m

SOIL PRESSURES (Comb. D+L+0.6H)

Allow. Bearing Pressure	191.6	KN/m² OK
Max. Pressure @ Toe	36.8	KN/m²
Min. Pressure @ Heel	45.8	KN/m²
Total Footing Length	2.70	m
Footing Length / 6	0.45	m
Resultant Eccentricity e	-0.05	m

Resultant is Within the Middle Third

APPLIED LOADS

Surcharge	D = 4.0	L = 5.0	KPa	
Strip Pressure	D = 0.0	L = 0.0	KPa	
Strip 0.0 m deep, 0.4 m wide @ 0.4 m from Stem				
Stem Vertical	D = 4.0	L = 4.0	KN/m	
Stem Horizontal	D = 0.0	L = 0.0	KN/m	
Eccentricity	ev = 15.2	eh = 0.0	cm	
Wind Load =	0.0 KPa	Height = 0.00	m	

BACKFILL PROPERTIES

Moist Density =	19	Saturated = 20	KN/m³
Earth Pressure Theory	User-defined		
Backfill Pressure Top	0.0	KPa	
Backfill Pressure Bottom	1.4	KPa	
Lateral Force at Wall Pa	1.2	KN/m	
Water Table Height	0.00	m	

SHEAR KEY (Comb. 1.4D+0.9H)

Shear Key Depth	0.0	cm
Shear Key Thickness	0.0	cm
No shear key has been specified		
Shear Capacity Ratio	0.00	OK
Moment Capacity Ratio	0.00	OK
Minimum Steel Area Ratio	0.00	OK

OVERTURNING CALCULATIONS (Comb. D+H+0.6W)

OVERTURNING	Force KN/m	Arm m	Moment KN-m/m
Backfill Pa	1.2	0.57	0.7
Water Table	0.0	0.00	0.0
Surcharge Dead	0.3	0.85	0.3
Surcharge Live	0.4	0.85	0.3
Strip Load Hor	0.0	0.00	0.0
Horizontal Dead	0.0	0.85	0.0
Horizontal Live	0.0	0.85	0.0
Wind Load	0.0	1.90	0.0
Seismic Backfill	0.0	0.85	0.0
Seismic Water	0.0	0.00	0.0
Seismic Selfweight	0.0	0.00	0.0
Passive Pressure	0.0	0.30	0.0
Rh =	1.9	OTM =	1.2

RESISTING	Force KN/m	Arm m	Moment KN-m/m
Stem Prism	7.7	0.60	4.6
Stem Taper	0.0	0.70	0.0
CMU Stem at Top	0.0	0.60	0.0
Footing Weight	19.4	1.35	26.2
Shear Key	0.0	0.70	0.0
Soil Cover @ Toe	5.7	0.25	1.4
Stem Wedge	0.0	0.70	0.0
Backfill Weight	52.6	1.70	89.5
Backfill Slope	0.0	2.03	0.0
Water Weight	0.0	1.70	0.0
Seismic Backfill	0.0	2.70	0.0
Pa Vert @ Heel	0.0	2.70	0.0
Vertical Dead	4.0	0.55	2.2
Vertical Live	0.0	0.55	0.0
Surcharge Dead	8.0	1.70	13.6
Surcharge Live	0.0	1.70	0.0
Strip Load Ver	0.0	1.30	0.0
Water Buoyancy	0.0	1.35	0.0
Rv =	97.5	RM =	137.6

Arm of Horizontal Resultant = $\frac{1.2}{1.9}$ = 0.67 m

Arm of Vertical Resultant = $\frac{137.6}{97.5}$ = 1.41 m

Overturning Safety Factor = $\frac{137.6}{1.2}$ = 10.58 > 1.50 OK

At a Glance | Condensed | Detailed | Graph

STEM DESIGN (Comb. 1.2D+1.6L+1.6H)

Height m	d cm	Mu KN-m/m	ϕMn KN-m/m	Ratio	
1.60	16.9	0.0	0.0	0.00	
1.44	16.9	0.6	17.5	0.03	
1.28	16.9	0.6	35.0	0.02	
1.12	16.9	0.6	52.6	0.01	
0.96	16.9	0.7	68.9	0.01	
0.80	16.9	0.8	85.1	0.01	
0.64	16.9	0.9	101.3	0.01	
0.48	16.9	1.1	106.2	0.01	
0.32	16.9	1.3	106.2	0.01	
0.16	16.9	1.6	106.2	0.01	
0.00	16.9	1.9	106.2	0.02	OK

Shear Force @ Crit. Height .... 2.2 KN/m OK

Resisting Shear ϕVn ..... 96.1 KN/m

Use vertical bars D12 @ 10 cm at backfill side

Cut off alternate bars. Cut off length = 1.60 m

Vert. Bars Embed. Ldh Reqd .... 19.5 cm OK

Vert. Bars Splice Length Ld ..... 30.0 cm

Vert. Bars Max. Spacing Ratio . 0.22 OK

Minimum Steel Area Ratio ..... 0.32 OK

Maximum Steel Area Ratio ..... 0.48 OK

SLIDING CALCS (Comb. D+H+0.6W)

Footing-Soil Friction Coeff.	0.50	
Friction Force at Base	48.7	KN/m
Passive Pressure Coeff. Kp	7.36	
Depth to Neglect Passive	0.00	m
Passive Pressure @ Wall	125.9	KPa
Passive Force @ Wall Pp	57.3	KN/m
Horiz. Resisting Force	106.0	KN/m
Horiz. Sliding Force	1.9	KN/m

Sliding Safety Factor = $\frac{106.0}{1.9}$ = 56.97 > 1.50 OK

TOE DESIGN (Comb. 1.2D+1.6L+1.6H)

	Force KN/m	Arm m	Moment KN-m/m
Upward Presssure	23.9	0.25	5.9
Water Buoyancy	0.0	0.25	0.0
Concrete Weight	-4.3	0.25	-1.1
Soil Cover	-6.9	0.25	-1.7
	12.7	Mu =	3.1

Shear Force @ Crit. Sect. .... 5.9 KN/m OK

Resisting Shear ϕVc ..... 131.2 KN/m

Use bott. bars D12 @ 10 cm , Transv. D12 @ 10 cm

Resisting Moment ϕMn ..... 174.0 KN-m/m OK

HEEL DESIGN (Comb. 1.2D+1.6L+1.6H)

	Force KN/m	Arm m	Moment KN-m/m
Upward Pressure .	0.0	0.00	0.0
Concrete Weight ..	17.3	1.00	17.3
Backfill Weight	63.2	1.00	63.2
Backfill Slope	0.0	1.33	0.0
Water Weight	0.0	1.00	0.0
Surcharge Ver.	9.6	1.00	9.6
Strip Load Ver.	0.0	0.60	0.0
	106.0	Mu =	106.0

Shear Force @ Crit. Sect.	106.0	KN/m	OK
Resisting Shear ϕVc	131.2	KN/m	
Use top bars D12 @ 10 cm , Transv. D12 @ 10 cm			
Resisting Moment ϕMn	174.0	KN-m/m	OK
Development Length Ratio at End ...	0.16		OK
Development Length Ratio at Toe ...	0.46		OK
Minimum Steel Area Ratio	0.48		OK
Maximum Bar Spacing Ratio	0.36		OK

Development Length Ratio at Toe	0.41	OK
Development Length Ratio at Stem ..	N.A.	OK
Minimum Steel Area Ratio	0.48	OK
Maximum Bar Spacing Ratio	0.22	OK

MATERIALS

	Stem	Footing	
Concrete f'c	36.0	36.0	MPa
Rebars fy	667.0	667.0	MPa
Masonry f'm	10.3		MPa

DESIGN CODES

General Analysis	IBC 2018
Concrete Design	ACI 318-19
Masonry Design	TMS 402-16
Load Combinations	ASCE 7-10/16

At a Glance | Condensed | Detailed | Graph

SECTION GEOMETRY

Conc. Stem Height	1.60	m
Stem Thickness Top	20.0	cm
Stem Thickness Bot	20.0	cm
Footing Thickness	30.0	cm
Toe Length	0.50	m
Heel Length	2.00	m
Soil Cover @ Toe	0.61	m
Backfill Height	1.40	m
Backfill Slope Angle	0.0	deg

APPLIED LOADS

Surcharge	D = 4.0	L = 5.0	KPa	
Strip Pressure	D = 0.0	L = 0.0	KPa	
Strip 0.0 m deep, 0.4 m wide @ 0.4 m from Stem				
Stem Vertical	D = 4.0	L = 4.0	KN/m	
Stem Horizontal	D = 0.0	L = 0.0	KN/m	
Eccentricity	ev = 15.2	eh = 0.0	cm	
Wind Load = 0.0 KPa	Height = 0.00	m		
Uniform Seismic Pressure ...	0.0	KPa		

BACKFILL PROPERTIES

Wall taper $\alpha = aTan(taper / H)$ = aTan ((20.0 - 20.0) / 100 / 1.60) = 0.000 rad

Backfill slope $\beta = slope * \pi / 180$ = 0.0 * 3.14 / 180 = 0.000 rad

Internal friction $\phi = Int.\ friction * \pi / 180$ = 34.0 * 3.14 / 180 = 0.593 rad

Wall-soil friction $\delta = \phi / 2$ = 0.593 / 2 = 0.297 rad

Footing length $ftg = toe + stem + heel$ = 0.50 + 20.0 / 100 + 2.00 = 2.70 m

Height for Stability $Hs = wedge + backfill + footing$ = 0.00 + 1.40 + 30.0 / 100 = 1.70 m

Earth pressure theory = User-defined Moist density = 19 KN/m³ Saturated density = 20 KN/m³

Backfill pressures: Top = 0.0 KPa Bottom = 1.4 KPa

- For stability analysis (non-seismic)

Lateral force $Pa = (pTop + pBott) * Hs / 2$ = (0.0 * 1.4) * 1.70 / 2 = 1.2 KN/m

$Pah = Pa * Cos\ \beta$ = 1.2 * Cos (0.000) = 1.2 KN/m , $Pav = Pa * Sin\ \beta$ = 1.2 * Sin (0.000) = 0.0 KN/m

Water force $Pw = \gamma w * water\ table^2 / 2$ = 9.8 * 0.00² / 2 = 0.0 KN/m

- For stem design (non-seismic)

Lateral force $Pa = (pTop + pBott) * H / 2$ = (0.0 * 1.4) * 1.40 / 2 = 1.0 KN/m

$Pah = Pa * Cos\ \beta$ = 1.0 * Cos (0.000) = 1.0 KN/m , $Pav = Pa * Sin\ \beta$ = 1.0 * Sin (0.000) = 0.0 KN/m

Water force $Pw = \gamma w * (water\ table - Ftg)^2 / 2$ = 9.8 * (0.00 - 30.0 / 100)² / 2 = 0.0 KN/m

At a Glance | Condensed | Detailed | Graph

- For stability analysis (seismic)
Seismic force = *Pressure * Hs* = 0.0 * 1.70 = 0.0 KN/m
- For stem design (seismic)
Seismic force = *Pressure * H* = 0.0 * 1.40 = 0.0 KN/m

OVERTURNING CALCULATIONS (Comb. D+H+0.6W)

- Overturning Forces

Backfill = *Lat factor * Pah* = 1.00 * 1.2 = 1.2 KN/m
Arm = *Hs / 3* = 1.70 / 3 = 0.57 m Moment = 1.2 * 0.57 = 0.7 KN-m/m
Water table = *Lat factor * Pw* = 1.00 * 0.0 = 0.0 KN/m
Arm = *Water table / 3* = 0.00 / 3 = 0.00 m Moment = 0.0 * 0.00 = 0.0 KN-m/m
Surcharge = *Factor * ka * Surcharge * Hs * Cos β* = 1.00 * 0.04 * 9.0 * 1.70 * 1.00 = 0.7 KN/m
Arm = *Hs / 2* = 1.70 / 2 = 0.85 m Moment = 0.7 * 0.85 = 0.6 KN-m/m
Strip load = *Σ Lat factor * 2 * Q / π * [β - Sin β * Cos (2α)]* = 0.00 KN/m
Arm = 0.00 m Moment = 0.0 * 0.00 = 0.0 KN-m/m
Concentrated Hor. = *Factor * Ph* = 1.00 * 0.00 + 0.00 * 0.00 = 0.0 KN/m
Arm = *Stem + (Ftg - Ecc) / 100* =1.60 + (30.0 - 0.0) / 100 = 1.90 m Moment = 0.0 * 1.90 = 0.0 KN-m/m
Wind load = *WL factor * Pressure * Wind height* = 0.60 * 0.0 * 0.00 = 0.0 KN/m
Arm = *Ftg + Stem - Wind height / 2* = 30.0 / 100 + 1.60 - 0.00 / 2 = 1.90 m
Moment = 0.0 * 1.90 = 0.0 KN-m/m
Backfill seismic = *EQ factor * (Paeh - Pah Coulomb)* = 0.00 * (6.7 - 0.0) = 0.0 KN/m
Arm = *0.6 * Hs* = 0.6 * 1.70 = 0.85 m Moment = 0.0 * 0.85 = 0.0 KN-m/m
Water seismic = *EQ factor * Pwe* = 0.00 * 0.0 = 0.0 KN/m
Arm = *Water table / 3* = 0.00 / 3 = 0.00 m Moment = 0.0 * 0.00 = 0.0 KN-m/m
Wall selfweight seismic effect not considered in calculations
Wall seismic = 0.0 KN
Moment = 0.0 KN-m/m
Passive force = 0.0 KN/m *(Ignore passive pressure in overturning)*
Arm = 0.30 m Moment = 0.0 * 0.30 = 0.0 KN-m/m
Overturning force Rh = 1.2 + 0.0 + 0.7 + 0.0 + 0.0 + 0.0 + 0.0 + 0.0 + 0.0 + 0.0 - 0.0 = 1.9 KN/m

At a Glance | Condensed | Detailed | Graph

Overturning moment OTM = 0.7 + 0.0 + 0.6 + 0.0 + 0.0 + 0.0 + 0.0 + 0.0 + 0.0 - 0.0 = 1.2 KN-m/m
Arm of hor. resultant = *OTM / Rh* = 1.2 / 1.9 = 0.67 m

- Resisting Forces

Stem weight *WStem = DL factor * Thickness * Height * yc* = 1.00 * 20.0 / 100 * 1.60 * 24.00 = 7.7 KN/m
Arm = *Toe + Thickness / 2* = 0.50 + 20.0 / 100 / 2 = 0.60 m Moment = 7.7 * 0.60 = 4.6 KN-m/m
Stem taper *WTaper = DL factor * ΔThick * Height / 2 * yc* = 1.00 * (20.0 - 20.0) / 100 * 1.60 / 2 * 24.00 = 0.0 KN/m
Arm = *Toe + Thick + ΔThick / 3* = 0.50 + 20.0 / 100 + (20.0 - 20.0) / 100 / 3 = 0.70 m
Moment = 0.0 * 0.70 = 0.0 KN-m/m
CMU stem at top = 1.00 * 1.40 = 0.0 KN/m
Arm = 0.00
Moment = 0.0 * 0.60 = 0.0 KN-m/m
Ftg. weight *WFtg = DL factor * Length * Thickness * yc* = 1.00 * 2.70 * 30.0 / 100 * 24.00 = 19.4 KN/m
Arm = *Length / 2* = 2.70 / 2 = 1.35 m Moment = 19.4 * 1.35 = 26.2 KN-m/m
Key weight *WKey = DL factor * Depth * Thickness * yc* = 1.00 * 0.00 / 100 * 0.0 / 100 * 24.00 = 0.0 KN/m
Arm = *Toe + Stem - Thickness / 2* = 0.50 + (20.0 - 0.0 / 2) / 100 = 0.70 m Moment = 0.0 * 0.70 = 0.0 KN-m/m
Soil cover = *DL factor * Toe * Soil cover * γ* = 1.00 * 0.50 * 0.61 * 18.8 = 5.7 KN/m
Arm = *Toe / 2* = 0.50 / 2 = 0.25 m Moment = 5.7 * 0.25 = 1.4 KN-m/m
Stem wedge = *DL factor * ΔThick * Height / 2 * γ* = 1.00 * 0.00 * 1.40 / 2 * 18.8 = 0.0 KN/m
Arm = *Toe + Thick - ΔThick * 2 / 3* = 0.50 + 20.0 / 100 - (20.0 - 20.0) / 100 * 2 / 3 = 0.70 m
Moment = 0.0 * 0.70 = 0.0 KN-m/m
Backfill weight = *DL factor * Heel * Height * γ* = 1.00 * 2.00 * 1.40 * 18.8 = 52.6 KN/m
Arm = *Ftg - Heel / 2* = 2.70 - 2.00 / 2 = 1.70 m Moment = 52.6 * 1.70 = 89.5 KN-m/m
Backfill slope = *DL factor * (Heel + ΔThick) * Wedge / 2 * γ* =
= 1.00 * (2.0 + (20.0 - 20.0) / 100) * 0.00 / 2 * 18.8 = 0.0 KN/m
Arm = *ftg - (Heel + ΔThick) / 3* = 2.70 - (2.00 + (20.0 - 20.0) / 100) / 3 = 2.03 m
Moment = 0.0 * 2.03 = 0.0 KN-m/m
Water = *Factor * Heel * (Water - Ftg) * (γs - γ)* = 1.00 * 2.00 * (0.00 - 30.0 / 100) * (20.4 - 18.8) = 0.0 KN/m
Arm = *Ftg - Heel / 2* = 2.70 - 2.00 / 2 = 1.70 m Moment = 0.0 * 1.70 = 0.0 KN-m/m
Seismic backfill = *EQ factor * (Paev - Pav)* = 0.00 * (2.0 - 0.0) = 0.0 KN/m
Arm = *Footing length* = 2.70 m Moment = 0.0 * 2.70 = 0.0 KN-m/m

At a Glance | Condensed | Detailed | Graph

Arm = *Ftg - Heel / 2* = 2.70 - 2.00 / 2 = 1.70 m Moment = 0.0 * 1.70 = 0.0 KN-m/m

Seismic backfill = *EQ factor * (Paev - Pav)* = 0.00 * (2.0 - 0.0) = 0.0 KN/m

Arm = *Footing length* = 2.70 m Moment = 0.0 * 2.70 = 0.0 KN-m/m

Backfill Pav = *Lat factor * Pav* = 1.00 * 0.0 = 0.0 KN/m

Arm = *Footing length* = 2.70 m Moment = 0.0 * 2.70 = 0.0 KN-m/m

Concentrated = *DL factor * Ver load* = 1.00 * 4.0 = 4.0 KN/m

Arm = *Toe + (Stem - Ecc) / 100* = 0.50 + (20.0 - 15.2) / 100 = 0.55 m Moment = 4.0 * 0.55 = 2.2 KN-m/m

Surcharge = *Srch factor * (Heel + ΔThick) * Surcharge* = 1.00 * 4.0 * (2.0 + (20.0 - 20.0) / 100) = 8.0 KN/m

Arm = *ftg - (Heel + ΔThick) / 2* = 2.70 - (2.00 + (20.0 - 20.0) / 100) / 2 = 1.70 m

Moment = 8.0 * 1.70 = 13.6 KN-m/m

Strip = *Strip factor * Surcharge * Width* = 1.00 * 0.0 * 0.40 = 0.0 KN/m

Arm = *Toe - Stem + Dist + Width / 2* = 0.50 + 20.0 / 100 + 0.40 + 0.40 / 2 = 1.30 m

Moment = 0.0 * 1.30 = 0.0 KN-m/m

Buoyancy = *DL factor * yw * Water table * Ftg* = 1.00 * 9.8 * 0.00 * 2.70 = 0.0 KN/m

Arm = *Footing / 2* = 2.70 / 2 = 1.35 m Moment = 0.0 * 1.35 = 0.0 KN-m/m

Ver. resultant Rv = *Σ Vertical forces* = 97.5 KN/m

Resisting moment RM = *Σ Moments* = 137.6 KN-m/m

Arm of ver. resultant = *RM / Rv* = 137.6 / 97.5 = 1.41 m

Overturning S.F. = *RM / OTM* = 137.6 / 1.2 = 110.58 > 1.50 OK

SOIL BEARING PRESSURES (Comb. D+L+0.6H)

Eccentricity = $\frac{Ftg}{2} - \frac{RM - OTM}{Rv} = \frac{2.70}{2} - \frac{156.8 - 0.7}{111.5} = -0.05$ m

Bearing length = *Min (Ftg , 3 * (Ftg / 2 - Ecc))* = Min (2.70, 3 * (2.70 / 2 - -0.05)) = 2.70 m

Toe bearing = $\frac{Rv}{Ftg} - \frac{6 * Rv * Ecc}{Ftg^2} = \frac{111.5}{2.70} - \frac{6 * 111.5 * -0.05}{2.70^2} = 36.8$ KN/m²

Heel bearing = $\frac{Rv}{Ftg} + \frac{6 * Rv * Ecc}{Ftg^2} = \frac{111.5}{2.70} + \frac{6 * 111.5 * -0.05}{2.70^2} = 45.8$ KN/m² < 191.6 KN/m² OK

At a Glance | Condensed | Detailed | Graph

SLIDING CALCULATIONS (Comb. D+H+0.6W)

Sliding force Rh = 1.2 + 0.0 + 0.7 + 0.0 + 0.0 + 0.0 + 0.0 + 0.0 = 1.9 KN/m

Passive coefficient *kp (Coulomb)* = 7.36

Passive depth *Dp = Soil cover + Ftg + Key - Neglect depth* = 0.61 + (30.0 + 0.0) / 100 - 0.00 = 0.91 m

Passive pressure top = *kp * γ * Neglect depth + Water* = 7.36 * 18.8 * 0.00 + 0.00 = 0.00 KN/m²

Passive pressure bot = *kp * γ * (Dp + Neglect depth) + Water* = 7.36 * 18.8 * (0.91 + 0.00) + 0.00 = 125.86 KN/m²

Passive force = *(Pressure top + Pressure bot) / 2 * Dp* = (0.00 + 125.86) / 2 * 0.91 = 57.3 KN/m

Friction force = *Max (0, Rv * Friction coeff.)* = Max (0, 97.5 * 0.50) = 48.7 KN/m

Sliding S.F. = *(Passive + Friction) / Rh* = (57.3 + 48.7) / 1.9 = 56.97 > 1.50 OK

STEM DESIGN (Comb. 1.2D+1.6L+1.6H)

Backfill = *Lat factor * Pah* = 1.6 * 1.0 = 1.6 KN/m

Arm = *Hb / 3* = 1.40 / 3 = 0.47 m Moment = 1.6 * 0.47 = 0.7 KN-m/m

Water table = *Factor * Pw* = 1.6 * 0.0 = 0.0 KN/m

Arm = *(Water table - Ftg) / 3* = (0.00 - 30.0 / 100) / 3 = 0.00 m Moment = 0.0 * 0.00 = 0.0 KN-m/m

Surcharge = *Factor * ka * Surcharge * Hs * Cos β* = 1.6 * 0.04 * 9.0 * 1.40 * 1.00 = 0.9 KN/m

Arm = *Hb / 2* = 1.40 / 2 = 0.70 m Moment = 0.9 * 0.70 = 0.6 KN-m/m

Vert. Concentrated = Factor * Shear = 1.2 * 0.00 + 1.6 * 0.00 = 0.0 KN/m

Factor * Moment = 1.2 * 0.2 + 1.6 * 0.2 = 0.6 KN-m/m

Hor. Concentrated = Factor * Load = 1.2 * 0.0 + 1.60 * 0.0 = 0.0 KN/m

Arm = Stem - Ecc = 1.60 - 0.0 / 100 = 1.60 m Moment = 0.0 * 1.60 = 0.0 KN-m/m

Strip load = *Σ Lat factor * 2 * Q / π * [β - Sin β * Cos (2α)]* = 1.60 * 0.0 = 0.0 KN/m

Arm = 0.00 m Moment = 0.0 * 0.00 = 0.0 KN-m/m

Wind load = *WL factor * Pressure * Wind height* = 0.0 * NaN * 0.00 = 0.0 KN/m

Arm = *Stem - Wind height / 2* = 1.60 - 0.00 / 2 = 1.60 m Moment = 0.0 * 1.60 = 0.0 KN-m/m

Backfill seismic = *EQ factor * (Paeh - Pah)* = 0.0 * (4.5 - 0.0) = 0.0 KN/m

Arm = *0.6 * Hb* = 0.6 * 1.40 = 0.84 m Moment = 0.0 * 0.84 = 0.0 KN-m/m

Water seismic = *EQ factor * Pwe* = 0.0 * 0.0 = 0.0 KN/m

Arm = *(Water table - Ftg) / 3* = (0.00 - 30.0 / 100) / 3 = 0.00 m Moment = 0.0 * 0.00 = 0.0 KN-m/m

At a Glance | Condensed | Detailed | Graph

Wall seismic = 0.0 KN
Moment = 0.0 KN-m/m
Max. shear = 1.6 + 0.0 + 0.9 + 0.0 + 0.0 + 0.0 + 0.0 + 0.0 + 0.0 + 0.0 + 0.0 = 2.5 KN/m
Shear at critical section = *Max shear - Max shear / Hb * d* = 2.5 - 2.5 / 1.40 * 16.9 / 100 = 2.2 KN/m
Max. Moment = 0.7 + 0.0 + 0.6 + 0.6 + 0.0 + 0.0 + 0.0 + 0.0 + 0.0 + 0.0 + 0.0 = 1.9 KN-m/m
Size factor λs = √(2 / (1 + 0.04 * d)) = √(2 / (1 + 0.04 * 16.9)) = 1.00 ACI Eq. (22.5.5.1.3)
Shear strength *φ Vc = φ * 0.66 * λs * ρ⅓ * (f'c)½ * b * d / 10* ACI Table 22.5.5.1
φ Vc = 0.75 * 0.66 * 1.00 * (0.0067)⅓ * (36)½ * 100 * 16.9 / 10 = 96.1 KN/m > 2.2 KN/m OK
Shear friction *φ Vn = φ * μ * Avf * fy / 10* ACI 22.9.4.2
φ Vn = 0.75 * 0.6 * 11.29 * 667.0 / 10 = 338.9 KN/m > 2.5 KN/m OK
Use D12 @ 10.0 cm As = 11.29 cm²/m *ρ = As / b d* = 11.29 / (100 * 16.9) = 0.0067
Bending strength *φ Mn = φ * d² * f'c * q * (1 - 0.59 * q)* q = ρ * fy / f'c = 0.124 ACI 22.2
φ Mn = 0.90 * 16.9² * 36.0 * 0.124 * (1 - 0.59 * 0.124) = 106.2 KN-m/m > 1.9 KN-m/m OK
Hooked *Ldh = Max (8 * db, 15 cm, fy / 7.2 / (f'c)½ * (db)^1.5 * ψr * ψc)* =
Max (8 * 1.20, 15 cm, 667.0 / 7.2 / (36.0)½ * (1.20)^1.5 * 1.0 * 0.96) = 19.5 cm ACI 25.4.3
Dev. length at footing = *Ftg - Cover* = 30.0 - 2.5 = 27.5 cm > 19.5 cm OK
*As min = 0.0018 * b * t* = 0.0018 * 100.0 * 20.0 = 3.60 cm²/m ACI 7.6.1.1
Min. steel area ratio = *As min / As* = 3.60 / 11.29 = 0.32 < 1.0 OK
*As S&T vert = 0.0018 * b * t* = 0.0018 * 100.0 * 20.0 = 3.60 cm²/m ACI 24.4.3.2
*As S&T hor = 0.0018 * b * t* = 0.0018 * 100.0 * 20.0 = 3.60 cm²/m ACI 24.4.3.2
Min. steel S&T ratio = *As S&T / As* = Max(3.60 / 22.58, 3.60 / 22.58) = 0.16 < 1.0 OK
Max. steel area for fy/Es + 0.003 tension strain = 23.60 cm²/m > 11.29 cm²/m OK ACI 21.2.2
*fs = Min (Msvc / (As * j * d) * 10, 0.66 Fy)* = Min (1.3 * 100 / (11.29 * 0.9 * 16.9) * 10, 0.66 * 667.0) = 7.2 MPa
*Smax cracking = Min (38 * 280 / fs - 2.5 Cc, 30 * 280 / fs)* = ACI Table 24.3.2
Min (38 * 280 / 7.2 - 2.5 * 2.5, 30 * 280 / 7.2)) = 1160.3 cm
*Smax = Min (Smax cr, 3 * t, 45.7)* = Min (1160.3, 3 * 20.0, 45.7) = 45.7 cm > 10.0 cm OK ACI 7.7.2.3

At a Glance | Condensed | Detailed | Graph

HEEL DESIGN (Comb. 1.2D+1.6L+1.6H)

Bearing force = 0.0 KN/m (Neglect bearing pressure for heel design)
Arm = N.A. Moment = 0.0 KN-m/m
Concrete weight = *DL factor * Thick * Heel * γc* = 1.20 * 30.0 / 100 * 2.00 * 24.00 = 17.3 KN/m
Arm = *Heel / 2* = 2.00 / 2 = 1.00 m Moment = 17.3 * 1.00 = 17.3 KN-m/m
Backfill weight = *DL factor * Heel * Height * γ* = 1.20 * 2.00 * 1.40 * 18.8 = 63.2 KN/m
Arm = *Heel / 2* = 2.00 / 2 = 1.00 m Moment = 63.2 * 1.00 = 63.2 KN-m/m
Backfill slope = *DL factor * (Heel + ΔThick) * Wedge / 2 * γ* =
= 1.20 * (2.0 + (20.0 - 20.0) / 100) * 0.00 / 2 * 18.8 = 0.0 KN/m
Arm = *Heel * 2 / 3* = 2.00 * 2 / 3 = 1.33 m Moment = 0.0 * 1.33 = 0.0 KN-m/m
Water = *Factor * Heel * (Water table - Ftg) * (γs - γ)* = 1.20 * 2.00 * (0.00 - 30.0 / 100) * (20.4 - 18.8) = 0.0 KN/m
Arm = *Heel / 2* = 2.00 / 2 = 1.00 m Moment = 0.0 * 1.00 = 0.0 KN-m/m
Surcharge = *Srch factor * (Heel + ΔThick) * Surcharge* = (1.20 * 4.0 + 1.60 * 5.0) * (2.0 + (20.0 - 20.0) / 100) = 25.6 KN/m
Arm = *Heel / 2* = 2.00 / 2 = 1.00 m Moment = 25.6 * 1.00 = 25.6 KN-m/m
Strip = *Strip factor * Surcharge * Width* = (1.20 * 0.0 + 1.6 * 0.0) * 0.40 = 0.0 KN/m
Arm = *Dist + Width / 2 - ΔThick / 100* = 0.40 + 0.40 / 2 - 0.0 / 100 = 0.60 m Moment = 0.0 * 0.60 = 0.0 KN-m/m
Max. Shear Vu = -0.0 + 17.3 + 63.2 + 0.0 + 0.0 + 25.6 + 0.0 = 106.0 KN/m
Max. Moment Mu = -0.0 + 17.3 + 63.2 + 0.0 + 0.0 + 25.6 + 0.0 = 106.0 KN-m/m
Size factor λs = 1.0 for footings ACI 13.2.6.2
Shear strength *φ Vc = φ * 0.66 * λs * ρ⅓ * (f'c)½ * b * d / 10* ACI Table 22.5.5.1
φ Vc = 0.75 * 0.66 * 1.0 * (0.0042)⅓ * (36)½ * 100 * 26.9 / 10 = 131.2 KN/m > 106.0 KN/m OK
Use D12 @ 10.0 cm As = 11.29 cm²/m *ρ = As / b d* = 11.29 / (100 * 26.9) = 0.0042
Bending strength *φ Mn = φ * d² * f'c * q * (1 - 0.59 * q)* q = ρ * fy / f'c = 0.078 ACI 22.2
φ Mn = 0.90 * 26.9² * 36.0 * 0.078 * (1 - 0.59 * 0.078) = 174.0 KN-m/m > Mu = 106.0 KN-m/m OK
Cover factor = *Min (2.5, (Cover + db /2, Spacing / 2) / db)* = Min (2.5, (2.5 + 1.20 / 2, 10.0 / 2) / 1.20) = 2.5
Straight *Ld = Max (30.0, fy / 1.1 / (f'c)½ * Size * Casting / Cover * Grade * db * ratio)* ACI 25.4.2.3
= Max (30.0, 667.0 / 1.1 / (36)½ * 0.8 * 1.0 / 2.5 * 1.3 * 1.20 * 0.61) = 30.7 cm
Hooked *Ldh = Max (8 * db, 15 cm, fy / 7.2 / (f'c)½ * (db)^1.5 * ψr * ψc)* = ACI 25.4.3
Max (8 * 1.20, 15 cm, 667.0 / 7.2 / (36.0)½ * (1.20)^1.5 * 1.0 * 0.96) = 19.5 cm

At a Glance | Condensed | Detailed | Graph

Max (8 * 1.20, 15 cm, 667.0 / 7.2 / (36.0)½ * (1.20)^1.5 * 1.0 * 0.96) = 19.5 cm

Dev. length at toe side = *Ftg - Heel - Cover* = (2.70 - 2.00) * 100 - 2.5 = 67.5 cm > 30.7 cm OK

Dev. length at heel side = *Heel - Cover* = 2.00 * 100 - 2.5 = 197.5 cm > 30.7 cm OK

*As min = 0.0018 * b * t* = 0.0018 * 100.0 * 30.0 = 5.40 cm²/m ACI 7.6.1.1

Min. steel area ratio = *As min / As* = 5.40 / 11.29 = 0.48 < 1.0 OK

*As S&T min = 0.0018 * b * t* = 0.0018 * 100.0 * 30.0 = 5.40 cm²/m ACI 24.4.3.2

Min. steel S&T ratio = *As S&T min / As* = Max(5.40 / 11.29, 5.40 / 11.29) = 0.48 < 1.0 OK

Max. steel area for fy/Es + 0.003 tension strain = 31.44 cm²/m > 11.29 cm²/m OK ACI 21.2.2

*fs = Min (Msvc / (As * j * d) * 10, 0.66 Fy)* = Min (85.0 * 100 / (11.29 * 0.9 * 26.9) * 10, 0.66 * 667.0) = 301.7 MPa

*Smax cracking = Min (38 * 280 / fs - 2.5 Cc, 30 * 280 / fs)* = ACI Table 24.3.2

Min (38 * 280 / 301.7 - 2.5 * 2.5, 30 * 280 / 301.7)) = 27.8 cm

*Smax = Min (Smax cr, 3 * t, 45.7)* = Min (27.8, 3 * 30.0, 45.7) = 27.8 cm >= 10.0 cm OK ACI 7.7.2.3

TOE DESIGN (Comb. 1.2D+1.6L+1.6H)

Bearing force = *(Bearing1 + Bearing2) / 2 * Toe* = (47.0 + 48.7) / 2 * 0.50 = 23.9 KN/m

Arm = *(Bearing1 * Toe² / 2 + (Bearing2 - Bearing1) * Toe² / 3) / Force*

= (48.7 * 0.50² / 2 + (47.0 - 48.7) * 0.50² / 3) / 23.9 = 0.25 m

Moment = 23.9 * 0.25 = 5.9 KN-m/m

Water Buoyancy = *Factor * yw * Water table * Toe* = 1.2 * 9.8 * 0.00 * 0.50 = 0.0 KN/m

Arm = *Toe / 2* = 0.50 / 2 = 0.25 m Moment = 0.0 * 0.25 = 0.0 KN-m/m

Concrete weight = *DL factor * Thick * Toe * yc* = 1.2 * 30.0 / 100 * 0.50 * 24.00 = 4.3 KN/m

Arm = *Toe / 2* = 0.50 / 2 = 0.25 m Moment = 4.3 * 0.25 = 1.1 KN-m/m

Soil cover = *DL factor * Toe * Height * y* = 1.2 * 0.50 * 5.73 * 18.8 = 6.9 KN/m

Arm = *Toe / 2* = 0.50 / 2 = 0.25 m Moment = 6.9 * 0.25 = 1.7 KN-m/m

Max. Shear Vu = 23.9 + 0.0 - 4.3 - 6.9 = 12.7 KN/m

Shear at crit. section Vu = *Max shear * (Toe - d) / Toe* = 12.7 * (0.50 - 26.9 / 100) / 0.50 = 5.9 KN/m

Max. Moment Mu = 5.9 + 0.0 - 1.1 - 1.7 = 3.1 KN-m/m

Size factor λs = 1.0 for footings ACI 13.2.6.2

Shear strength *φ Vc = φ * 0.66 * λs * ρ⅓ * (f'c)½ * b * d / 10* ACI Table 22.5.5.1

φ Vc = 0.75 * 0.66 * 1.0 * (0.0042)⅓ * (36)½ * 100 * 26.9 / 10 = 131.2 KN/m > 5.9 KN/m OK

At a Glance | Condensed | Detailed | Graph

Use D12 @ 10.0 cm As = 11.29 cm²/m *ρ = As / b d* = 11.29 / (100 * 26.9) = 0.0042

Bending strength *φ Mn = φ * d² * f'c * q * (1 - 0.59 * q)* q = ρ * fy / f'c = 0.078 ACI 22.2

φ Mn = 0.90 * 26.9² * 36.0 * 0.078 * (1 - 0.59 * 0.078) = 174.0 KN-m/m > Mu = 3.1 KN-m/m OK

Cover factor = *Min (2.5, (Cover + db /2, Spacing / 2) / db)* = Min (2.5, (2.5 + 1.20 / 2, 10.0 / 2) / 1.20) = 2.5

Straight *Ld = Max (30.0, fy / 1.1 / (f'c)½ * Size * Casting / Cover * Grade * db * ratio)* ACI 25.4.2.3

= Max (30.0, 667.0 / 1.1 / (36)½ * 0.8 * 1.0 / 2.5 * 1.3 * 1.20 * 0.02) = 30.0 cm

Hooked *Ldh = Max (8 * db, 15 cm, fy / 7.2 / (f'c)½ * (db)^1.5 * ψr * ψc)* = ACI 25.4.3

Max (8 * 1.20, 15 cm, 667.0 / 7.2 / (36.0)½ * (1.20)^1.5 * 1.0 * 0.96) = 19.5 cm

Dev. length at stem side = N.A. (Continuous stem rebars) OK

Dev. length at toe side = *Toe - Cover* = 0.50 * 100 - 2.5 = 47.5 cm > 19.5 cm OK

*As min = 0.0018 * b * t* = 0.0018 * 100.0 * 30.0 = 5.40 cm²/m ACI 7.6.1.1

Min. steel area ratio = *As min / As* = 5.40 / 11.29 = 0.48 < 1.0 OK

*As S&T min = 0.0018 * b * t* = 0.0018 * 100.0 * 30.0 = 5.40 cm²/m ACI 24.4.3.2

Min. steel S&T ratio = *As S&T min / As* = Max(5.40 / 22.58, 5.40 / 22.58) = 0.24 < 1.0 OK

Max. steel area for fy/Es + 0.003 tension strain = 37.44 cm²/m > 11.29 cm²/m OK ACI 21.2.2

*fs = Min (Msvc / (As * j * d) * 10, 0.66 Fy)* = Min (2.4 * 100 / (11.29 * 0.9 * 26.9) * 10, 0.66 * 667.0) = 8.4 MPa

*Smax cracking = Min (38 * 280 / fs - 2.5 Cc, 30 * 280 / fs)* = ACI Table 24.3.2

Min (38 * 280 / 8.4 - 2.5 * 2.5, 30 * 280 / 8.4)) = 995.7 cm

*Smax = Min (Smax cr, 3 * t, 45.7)* = Min (995.7, 3 * 30.0, 45.7) = 45.7 cm >= 10.0 cm OK ACI 7.7.2.3

SHEAR KEY DESIGN (Comb. 1.4D+0.9H)

Shear key depth = 0.0 cm Shear key thickness = 0.0 cm

Passive force = *Lat factor * (Passive1 + Passive2) / 2 * Key* = 0.9 * (125.9 + 125.9) / 2 * 0.0 / 100 = 0.0 KN/m

Shear at crit. section Vu = *Max shear * (Key - d) / Key* = 0.0 * (0.0 - 0.1) / 0.0 = 0.0 KN/m

Arm = *(Passive1 * Key² / 2 + (Passive2 - Passive1) * Key² / 3) / Force*

= (125.9 * 0.00² / 2 + (125.9 - 125.9) * 0.00² / 3) / 0.0 = 0.00 m

Max. moment Mu = 0.0 * 0.00 = 0.0 KN-m/m

Size factor λs = 1.0 for footings ACI 13.2.6.2

Shear strength *φ Vc = φ * 0.66 * λs * ρ⅓ * (f'c)½ * b * d / 10* ACI Table 22.5.5.1

φ Vc = 0.75 * 0.66 * 1.0 * (1.1290)⅓ * (36)½ * 100 * 0.1 / 10 = 1.9 KN/m > 0.0 KN/m OK

At a Glance | Condensed | Detailed | Graph

SHEAR KEY DESIGN (Comb. 1.4D+0.9H)

Shear key depth = 0.0 cm Shear key thickness = 0.0 cm

Passive force = *Lat factor * (Passive1 + Passive2) / 2 * Key* = 0.9 * (125.9 + 125.9) / 2 * 0.0 / 100 = 0.0 KN/m

Shear at crit. section Vu = *Max shear * (Key - d) / Key* = 0.0 * (0.0 - 0.1) / 0.0 = 0.0 KN/m

Arm = *(Passive1 * Key² / 2 + (Passive2 - Passive1) * Key² / 3) / Force*

= (125.9 * 0.00² / 2 + (125.9 - 125.9) * 0.00² / 3) / 0.0 = 0.00 m

Max. moment Mu = 0.0 * 0.00 = 0.0 KN-m/m

Size factor λs = 1.0 for footings ACI 13.2.6.2

Shear strength *φ Vc = φ * 0.66 * λs * ρ⅓ * (fc)½ * b * d / 10* ACI Table 22.5.5.1

φ Vc = 0.75 * 0.66 * 1.0 * (1.1290)⅓ * (36)½ * 100 * 0.1 / 10 = 1.9 KN/m > 0.0 KN/m OK

Use D12 @ 10.0 cm U-bars As = 11.29 cm²/m *ρ = As / b d* = 11.29 / (100 * 0.1) = 1.1290

Bending strength *φ Mn = φ * d² * f'c * q * (1 - 0.59 * q)* q = ρ * fy / f'c = 20.918 ACI 22.2

φ Mn = 0.90 * 0.1² * 36.0 * 20.918 * (1 - 0.59 * 20.918) = 0.1 KN-m/m > Mu = 0.0 KN-m/m OK

*As min = 0.0018 * b * t* = 0.0018 * 100.0 * 0.0 = 0.00 cm²/m ACI 7.6.1.1

Min. steel area ratio = *As min / As* = 0.00 / 11.29 = 0.00 < 1.0 OK

*As S&T = 0.0018 * b * t* = 0.0018 * 100.0 * 0.0 = 0.00 cm²/m ACI 24.4.3.2

Min. steel S&T ratio = *As S&T / As* = Max(0.00 / 22.58, 0.00 / 4.52) = 0.00 < 1.0 OK

Max. steel area for fy/Es + 0.003 tension strain = 10.89 cm²/m 11.29 cm²/m OK ACI 21.2.2

MATERIALS

	Stem	Footing	
Concrete f'c	36.0	36.0	MPa
Rebars fy	667.0	667.0	MPa
Masonry f'm	10.3		MPa

DESIGN CODES

General Analysis	IBC 2018
Concrete Design	ACI 318-19
Masonry Design	TMS 402-16
Load Combinations	ASCE 7-10/16

At a Glance | Condensed | Detailed | Graph

Overturning | Sliding | Bearing | Stem | Footing | Construction

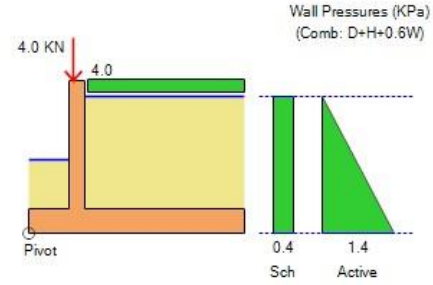

Stability Safety Factors

Overturning 110.58 > 1.50 ✓ (D+H+0.6W)

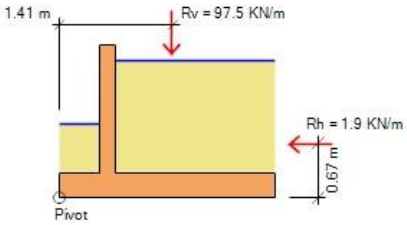

Load Combination:

Controlling


At a Glance
Condensed
Detailed
Graph
Overturning
Sliding
Bearing
Stem
Footing
Construction
Wall Pressures (KPa)
(Comb: D+H+0.6W)
4.0 KN
4.0
125.9
0.4
Sch
1.4
Active
0.1
Water
Stability Safety Factors
Sliding 56.97 > 1.50 ✓ (D+H+0.6W)
1.41 m
Rv = 97.5 KN/m
Passive
= 57.3 KN/m
0.30 m
Rh = 1.9 KN/m
0.67 m
Friction = 48.7 KN/m
Load Combination:
Controlling


At a Glance
Condensed
Detailed
Graph
Overturning
Sliding
Bearing
Stem
Footing
Construction
Wall Pressures (KPa)
(Comb: D+L+0.6H)
8.0 KN
9.0
0.2
Sch
0.8
Active
36.8 KN/m²
45.8 KN/m²
Stability Safety Factors
Bearing 4.18 > 1.00 ✓ (D+L+0.6H)
1.41 m
Rv = 111.5 KN/m
Rh = 1.1 KN/m
0.67 m
R = 111.5 KN/m
e = -0.05 m
Load Combination:
Controlling

At a Glance | Condensed | Detailed | Graph

Overturning | Sliding | Bearing | Stem | Footing | Construction

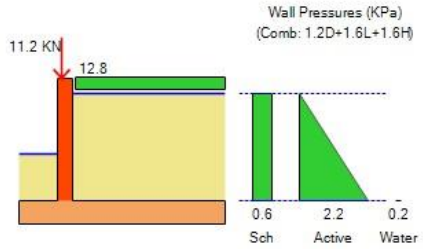

Load Combination:

Controlling

Stem Design Ratios

Flexure	0.02	< 1.00	✓	(1.2D+1.6L+1.6H)
Shear	0.02	< 1.00	✓	(1.2D+1.6L+1.6H)

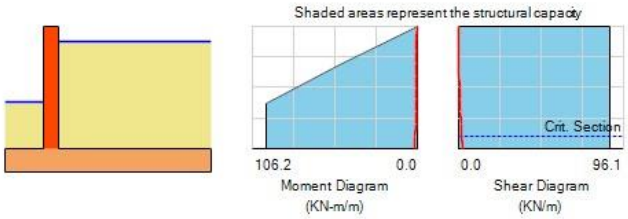

At a Glance | Condensed | Detailed | Graph

Overturning | Sliding | Bearing | Stem | Footing | Construction

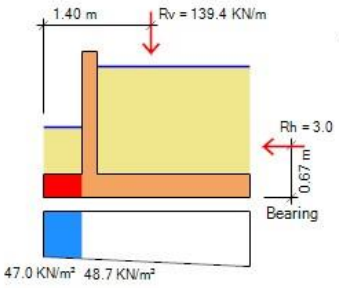

Toe Design Ratios

Flexure	0.02	< 1.00	✓	(1.2D+1.6L+1.6H)
Shear	0.04	< 1.00	✓	(1.2D+1.6L+1.6H)

Load Combination:

Controlling

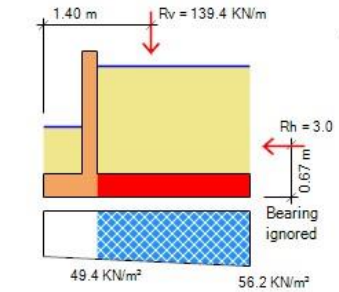

Heel Design Ratios

Flexure	0.61	< 1.00	✓	(1.2D+1.6L+1.6H)
Shear	0.81	< 1.00	✓	(1.2D+1.6L+1.6H)

Load Combination:

Controlling

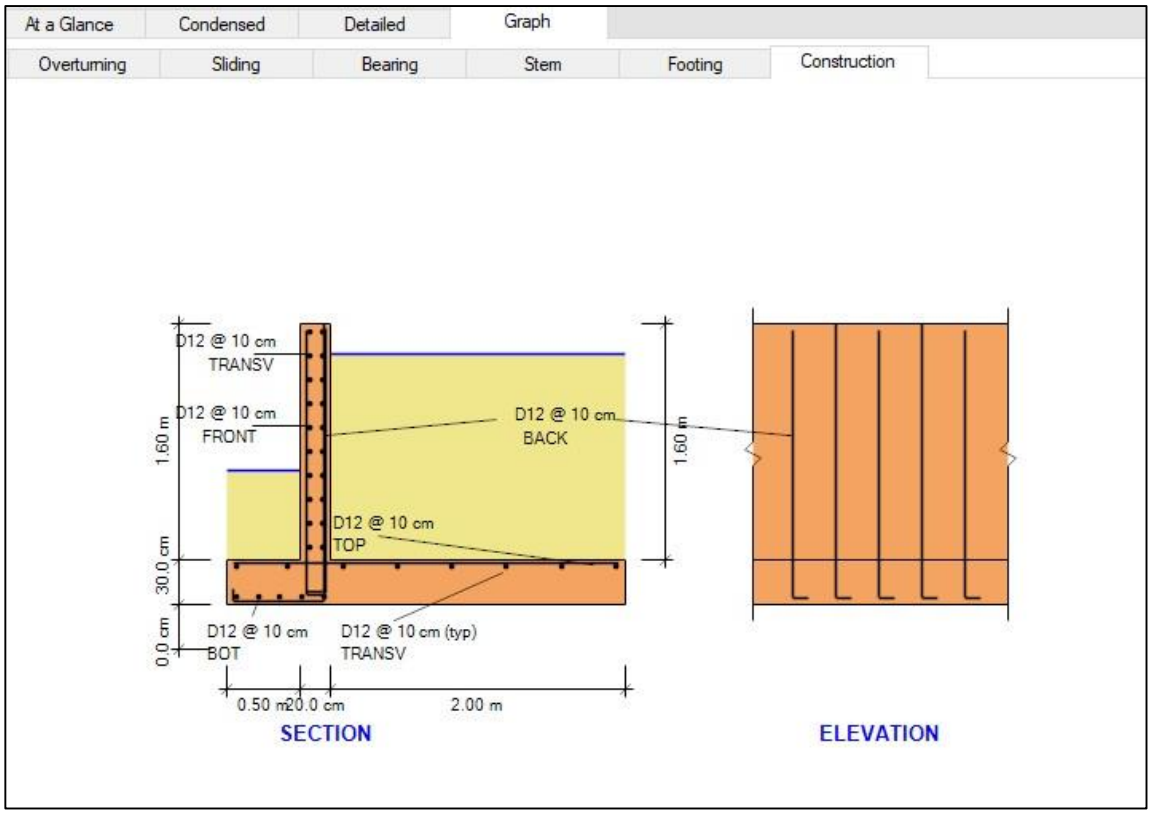
At a Glance
Condensed
Detailed
Graph
Overturning
Sliding
Bearing
Stem
Footing
Construction
D12 @ 10 cm
TRANSV
D12 @ 10 cm
FRONT
D12 @ 10 cm
BACK
D12 @ 10 cm
TOP
D12 @ 10 cm
BOT
D12 @ 10 cm (typ)
TRANSV
1.60 m
30.0 cm
0.0 cm
0.50 m
20.0 cm
2.00 m
1.60 m
SECTION
ELEVATION

الخلاصة

في الآونة الأخيرة، استخدمت مشاريع الهندسة المدنية بشكل متزايد التربة المستقرة ميكانيكيًا (MSE) كبديل فعال للخرسانة المسلحة. يعتمد الاستقرار الداخلي لبنية التربة المسلحة على التفاعلات الميكانيكية بين مادة الحشو والتسليح والواجهة.

وبناء على ذلك يهدف البحث الحالي إلى دراسة سلوك الجدار MSE تحت الحمل الساكن. تتكون منهجية العمل من ثلاثة أجزاء: الجزء الأول ركز على الدراسة الميدانية لقياس توزيع الضغط الجانبي للمنشآت الصغيرة والمتوسطة المستخدمة كجدران استنادية في تقاطع الأم في الحلة–العراق.

بالنسبة لجسر تقاطع الأم فإن منهجية العمل تتكون من جزأين الأول أثناء الإنشاء والثاني أثناء التشغيل. عدد المتحسسات 4 والمسافة بين كل متحسس واخر 50 سم. تم تركيبها أثناء الإنشاء ولكن تم أخذ القراءات على مرحلتين، المرحلة الأولى أثناء بناء الجسر، وتم أخذ القراءات تحت تأثير الأحمال الساكنة، ومن ثم تم أخذ القراءات خلال فترة تشغيل الجسر تحت تأثير الأحمال المرورية الحركية. أظهرت النتائج أن تأثير الضغط الجانبي على جدار MSE يتناقص مع زيادة عمق الجدار.

الجزء الثاني هو محاكاة جدار MSE نموذجا مبسطا تقريبا. يتيح النموذج التحقيق في العديد من المعلمات؛ الشكل المتعرج والشكل المستقيم، لذلك تم بناء واختبار عينتين تقريبًا. أظهرت النتائج التجريبية أن استخدام التسليح بالشرائط المتعرجة يعطي مقاومة أفضل للضغط الجانبي والرأسي مقارنة بالتسليح بالشرائط المستقيمة. والشكل المتعرج يعطي نتائج أفضل من الشكل المستقيم بنسبة 19% في الضغط الجانبي. بينما الشكل المتعرج يعطي نتائج أفضل من الشكل المستقيم بنسبة 60% في الضغط العمودي.

كما أن استخدام التسليح بالشرائط المتعرجة أعطى إزاحة أقل في الجدار MSE مقارنة بالشرائط المستقيمة. بالإضافة إلى أن استخدام نوعي تسليح شرائح التربة أدى إلى تقليل الإزاحة اللاحقة مع العمق. والشكل المستقيم يعطي نتائج أفضل من الشكل المتعرج بنسبة 50% في تقليل الإزاحة.

الجزء الثالث هو نموذج العناصر المحدودة باستخدام برنامج ABAQUS Standard/Explicit 2019 لدراسة السلوك غير الخطي لجدار MSE. أشارت نتائج FEM إلى توافق جيد مع النتائج التجريبية. إن قدرة البرنامج على توسيع الدراسة تعطي المزيد من النتائج في فهم السلوك الفعلي لجدار MSE. في هذه الأطروحة، تم إجراء تحليل حدودي لدراسة مجموعة واسعة من المتغيرات الرئيسية (عرض الشريط وموقع الحمل المطبق). خلاصة القول، أظهر التحقيق البارامتري أن الشريط المستخدم بعرض W قلل من تأثير الإزاحة أفقياً، كما أثر مكان الحمل على السلوك على MSE. العلاقة بين مكان الحمل المطبق وتأثير الإزاحة أفقياً والضغط الجانبي والإجهادات في الشرائح تكون سالبة عندما يكون الحمل قريباً من الجدار يزداد تأثير الإزاحة جانبياً والضغط الجانبي والإجهادات في الشرائح.

جمهورية العراق
وزارة التعليم العالي والبحث العلمي
جامعة بابل
كلية الهندسة
قسم الهندسة المدنية

تفاعل بنية التربة لجدران الأرض المستقرة ميكانيكياً لدعامات الجسر

أطروحة

مقدمة إلى كلية الهندسة في جامعة بابل

كجزء من متطلبات نيل درجة الدكتوراه فلسفة في الهندسة /الهندسة المدنية /إنشاءات

من قبل

ميادة وحيد فلاح كضيب

اشراف

أ.د. هيثم حسن متعب

1445 هـ **2023 م**